PALACKÝ UNIVERSITY IN OLOMOUC

FACULTY OF SCIENCE

Laboratory of Growth Regulators

Ph.D. Thesis

Study of auxin metabolism at the organ level

Author:	**Mgr. Pavel Hladík**
Study programme:	P0511D030004 - Experimental biology
Form:	Daily
Supervisor:	**Prof. Mgr. Ondřej Novák, Ph.D.**
Consultant:	Mgr. Aleš Pěnčík, Ph.D.
Date of submitting:	2024

Bibliografická identifikace

Jméno autora:	Mgr. Pavel Hladík
Název práce:	Studium metabolismu auxinů na orgánové úrovni
Typ práce:	Ph.D.
Pracoviště:	Laboratoř růstových regulátorů
Vedoucí práce:	prof. Ondřej Novák, Ph.D.
Rok obhajoby:	2024
Abstrakt:	Auxiny jsou skupinou fytohormonů regulujících správný růst a vývoj rostlin. Jedním z mechanismů podílejícím se na jejich správné funkci je metabolismus, při kterém vznikají neaktivní konjugáty a degradační produkty. Nicméně tyto metabolické dráhy byly studovány především na kyselině indol-3-yl octové (IAA) a v ostatních endogenních auxinech nejsou dosud objasněny. Tato práce se zabývá objevem nových metabolitů IAA a kyseliny fenyloctové (PAA) za použití kapalinové chromatografie ve spojení s tandemovou hmotnostní spektrometrií. Na základě těchto výsledků bylo poté provedeno metabolické profilování těchto dvou auxinů v rostlinách a jejich orgánech v různých vývojových stádiích. Jelikož enzymy zodpovědné za syntézu PAA konjugátů nejsou téměř popsány, byly provedeny bakteriální enzymatické testy, které vedly k objasnění těchto drah. Další částí této práce byl vývoj extrakčních a analytických metod pro kvantifikaci syntetických derivátů IAA s anti-auxinovou aktivitou. Tyto výsledky by měly přispět k lepšímu porozumění regulace auxinů napříč vyššími rostlinami.
Klíčová slova:	Auxin, kyselina indol-3-yl octová, kyselina fenyloctová, metabolismus, extrakce, LC-MS/MS
Počet stran:	61
Počet příloh:	4
Jazyk:	Anglický

Bibliographical identification

Author's first name and surname:	Mgr. Pavel Hladík
Title of thesis:	Study of auxin metabolism at the organ level
Type of thesis:	Ph.D.
Department:	Laboratory of Growth Regulators
Supervisor:	Prof. Ondřej Novák, Ph.D.
The year of presentation:	2024

Abstract: Auxins are a group of phytohormones regulating plant growth and development. One of the mechanisms involved in regulating their proper function is metabolism, during which inactive conjugates and degradation products are formed. However, these metabolic pathways were extensively studied in indole-3-acetic acid (IAA) and have not yet been elucidated in other endogenous auxins. This thesis focuses on the discovery of new metabolites of IAA and phenylacetic acid (PAA) utilizing liquid chromatography coupled with tandem mass spectrometry. Based on these results, metabolic profiling of these two auxins was then conducted in plants and their organs at various growth stages. Due to the limited information available on the enzymes responsible for the synthesis of PAA conjugates, bacterial enzymatic assays were performed, leading to the clarification of these pathways. Different part of this work focuses on the development of extraction and analytical methods for the quantification of synthetic IAA derivatives with anti-auxin activity. Together, these results aim to improve our understanding of auxin regulation across land plants.

Keywords:	Auxin, indole-3-acetic acid, phenylacetic acid, metabolism, extraction, LC-MS/MS
Number of pages:	61
Number of appendices:	4
Language:	English

Declaration of originality

I, Mgr. Pavel Hladík, hereby declare that the work presented in this thesis is a result of my original research, conducted under the great supervision of prof. Mgr. Ondřej Novák Ph.D. and Mgr. Aleš Pěnčík, Ph.D. using the literature sources listed in the Reference section.

In Olomouc, …….

Mgr. Pavel Hladík

Acknowledgement

First and foremost, I am immensely grateful to my supervisor prof. Mgr. Ondřej Novák, Ph.D. and consultant Mgr. Aleš Pěnčík, Ph.D. for their unwavering guidance, invaluable advice and steadfast support throughout my whole four-year long journey. I extend my heartfelt appreciation to prof. Karin Ljung and her research group from Umeå Plant Science Centre (UPSC), for their warm welcome and generosity, which made me feel at home during my time abroad. I am deeply indebted to my colleagues and technicians from Laboratory of Growth Regulators and Department of Chemical Biology, for their assistance, expertise, and invaluable contributions to this work. Finally, I wish to express my gratitude to my girlfriend, friends, and family for their unwavering encouragement, understanding, and patience during the ups and downs of this Ph.D. journey.

This work was supported by Internal grant agency of Palacký University in Olomouc (IGA_PrF_2024_013).

Content

List of papers 8

Contribution report 9

Abbreviations 10

1 Introduction 12

2 Aims and scope 13

3 Literature review 14

3.1 Plant hormones 14

3.2 Auxin in history 14

3.3 Synthetic auxins 16

3.4 Auxin biological roles 17

3.5 Auxin signalling and perception 19

3.6 Auxin homeostasis 21

3.6.1 IAA biosynthesis 21

3.6.2 PAA biosynthesis 24

3.6.3 IAA metabolism 26

3.6.4 PAA metabolism 29

3.6.5 Auxin transport 30

3.6.6 Auxin localization and regulation 31

3.7 Phytohormone analysis 32

3.7.1 Sample preparation 33

3.7.2 Quantitative analysis 34

3.7.3 Auxin identification 36

4 Material and methods 38

4.1 Chemicals 38

4.2 Plant material and growth conditions 38

4.3 Methods 39

4.3.1 Extraction and purification 39
4.3.2 HPLC-MS/MS 39
5 Survey of results 41
5.1 2-oxindole-3-acetyl-amino acids are an important auxin metabolites in plants 41
5.2 Unravelling novel metabolic pathways in PAA metabolism 43
5.3 Method development for novel synthetic auxin derivatives 46
6 Conclusion and future perspectives 48
7 References 49
8 Supplements 61

List of papers

This thesis summarizes and links the following papers that are referred in the text by Roman numerals I-IV, which are attached at the end of this thesis in the Supplementary section.

I **Hladík P**., Petřík I., Žukauskaitė A., Novák O., Pěnčík A. (2023) Metabolic profiles of 2-oxindole-3-acetyl-amino acid conjugates differ in various plant species. *Front. Plant Sci.* 14, 1217421.

II **Hladík P.**, Brunoni F., Žukauskaitė A., Zatloukal M., Novák O., Pěnčík A. (2024) Phenylacetic acid metabolism in plants: unravelling novel pathways and metabolites by liquid chromatography-mass spectrometry analysis. (In preparation)

III Bieleszová K., **Hladík P.**, Kubala M., Napier R., Brunoni F., Gelová Z., Fiedler L., Kulich L., Strnad M., Doležal K., Novák O., Friml J., Žukauskaitė A. (2024) New fluorescent auxin derivatives: anti-auxin activity and accumulation patterns in *Arabidopsis thaliana*. *Plant Growth Regul.* 102, 589-602.

IV Zhang C., Bieleszová K., Žukauskaitė A., **Hladík P.**, Grúz J., Novák O., Doležal K. (2024) In situ separation and visualization of isomeric auxin derivatives in Arabidopsis by ion mobility mass spectrometry imaging. *Anal Bioanal Chem*. 416(1), 125-139.

Contribution report

I As a first author, P.H. designed and performed all the experiments for auxin identification and metabolite profiling in all plant species. P.H. also wrote the first draft of the manuscript.

II As a first author, P.H. designed and performed all the experiments for auxins identification and metabolite profiling in all plant species. P.H. performed auxin treatment experiments with Arabidopsis mutant lines and kakeimide. P.H. also wrote the first draft of the manuscript.

III As a co-author, P.H. developed extraction and mass spectrometry techniques for newly synthesized fluorescently labelled auxins. P.H. measured experiments with stability of those compounds in plants and also reviewed and edited the manuscript.

IV As a co-author, P.H. developed extraction and mass spectrometry techniques for synthetic auxins. P.H. measured IAA metabolic profiles in plants and reviewed and edited the manuscript.

Abbreviations

1-NAA	1-naphthalene acetic acid
2,4-D	2,4-dichlorophenoxyacetic acid
4-Cl-IAA	4-chloroindole-3-acetic acid
4pTb-MeIAA	methyl 2-indol-3-yl-4-oxo-4-p-tolyl-butanoate
6-OH-IAA-AAs	*N*-(6-hydroxyindol-3-ylacetyl)-amino acids
6-OH-IAA-Phe	*N*-(6-hydroxyindol-3-ylacetyl)-phenylalanine
6-OH-IAA-Val	*N*-(6-hydroxyindol-3-ylacetyl)-valine
7-OH-oxIAA	7-hydroxy-2-oxindole-3-acetic acid
7-OH-OxIAA-glc	7-hydroxy-2-oxindole-3-acetyl-7-*O*-β-D-glucose
AADC	aromatic amino acid decarboxylases
ABCB	ATP-binding cassette-B
ABP1	AUXIN-BINDING PROTEIN 1
AC	adenylate cyclase
AFB	AUXIN SIGNALING F-BOX
AMI	indole-3-acetamide hydrolase
AO	aldehyde oxidases
ARFs	AUXIN RESPONSE FACTORS
ATP	adenosine triphosphate
AUX1/LAX1,2,3	AUXIN RESISTANT 1/LIKE AUX1, 2, 3
Auxinole	4-(2,4-dimethylphenyl)-2-(1H-indol-3-yl)-4-oxobutanoic acid
BBCH	Biologische Bundesanstalt, Bundessortenamt und Chemische Industrie
BP-IAA	4-([1,1'-biphenyl]-4-yl)-2-(1H-indol-3-yl)-4-oxobutanoic acid
cAMP	cyclic adenosine monophosphate
CYP	CYTOCHROME P450
dioxIAA	3-hydroxy-2-oxindole-3-acetic acid
dioxIAA-AAs	3-hydroxy-2-oxindole-3-acetyl amino acids
DAO1	DIOXYGENASE FOR AUXIN OXIDATION 1
DESI-IM-MSI	desorption electrospray ionization with ion mobility mass spectrometry imaging
Dicamba	3,6-dichloro-2-methoxybenzoic acid
DNS	5-(dimethylamino)naphthalene-1-sulfonyl
dSPE	dispersive solid-phase extraction
ER	endoplasmic reticulum
ESI	electrospray ionization
FW	fresh weight
GC	gas chromatography
GC-MS	gas chromatography-mass spectrometry
GH3	GRETCHEN HAGEN 3
HPLC	high performance liquid chromatography
HRMS	high resolution mass spectrometry
IAA-*N*-glc	indole-3-acetyl-*N*-ß-d-glucose
IAA	indole-3-acetic acid
IAA-AAs	indole-3-acetyl-amino acids
IAAld	indole-3-acetaldehyde
IAA-Asp	indole-3-acetyl-aspartate
IAA-Glu	indole-3-acetyl-glutamate
IAA-glc	indole-3-acetyl-1-*O*-ß-d-glucose
IAInos synthase	indole-3-acetyl-1-*O*-ß-d-glucose: myo-inositol indoleacetyl transferase
IAM	indole-3-acetamid
IAMT1	IAA CARBOXYMETHYLTRANSFERASE 1
IAN	indole-3-acetonitrile
IAOx	indole-3-acetaldoxime
IAR3	IAA-ALANINE RESISTANT 3
IBA	indole-3-butyric acid
ILLs	ILR1-LIKE proteins

ILR1	IAA-LEUCINE RESISTANT 1
IPyA	indole-3-pyruvic acid
IS	internal standard
KKI	kakeimide
L-Phe	L-phenylalanine
L-Trp	L-tryptophan
LC	liquid chromatography
LC-MS/MS	liquid chromatography-tandem mass spectrometry
LLE	liquid-liquid extraction
meIAA	indole-3-acetic acid methyl ester
MES17	methylesterase 17
MISPE	molecularly imprinted solid-phase extraction
MRM	multiple reaction monitoring
MS	mass spectrometry
NBD-IAA	nitrobenzoxadiazole-indole-3-acetic acid
NGT1	*N*-glucosyltransferase 1
NIT	nitrilase
oxIAA	2-oxindole-3-acetic acid
oxIAA-AAs	2-oxindole-3-acetyl-amino acids
oxIAA-Asp	2-oxindole-3-acetyl-aspartate
oxIAA-glc	2-oxindole-3-acetyl-1-*O*-ß-d-glucose
oxIAA-Glu	2-oxindole-3-acetyl-glutamate
oxIAA-Leu	2-oxindole-3-acetyl-leucine
oxIAA-Phe	2-oxindole-3-acetyl-phenylalanine
PAA	phenylacetic acid
PAA-AAs	phenylacetyl-amino acids
PAAld	phenylacetaldehyde
PAAS	phenylacetaldehyde synthase
PAA-Asp	phenylacetyl-aspartate
PAA-glc	phenylacetyl-1-*O*-ß-d-glucose
PAA-Glu	phenylacetyl-glutamate
PAA-Leu	phenylacetyl-leucine
PAA-Phe	phenylacetyl-phenylalanine
PAA-Trp	phenylacetyl-tryptophan
PAA-Val	phenylacetyl-valine
PAM	phenylacetamide
PAOx	phenylacetaldoxime
PEA	phenylethylamine
PEO-IAA	2-(1H-Indol-3-yl)-4-oxo-4-phenylbutanoic acid
PINs	PIN proteins
PPA	phenylpyruvate
SKP2A	S-PHASE KINASE-ASSOCIATED PROTEIN 2A
SPE	solid-phase extraction
TAA1	TRYPTOPHAN AMINOTRANSFERASE OF ARABIDOPSIS 1
TARS	TRYPTOPHAN AMINOTRANSFERASE-RELATED
TIR1	TRANSPORT INHIBITOR RESPONSE 1
UGTs	uridine 5'-diphospho-glucuronosyltransferase

1 Introduction

Proper plant growth and development are intricately regulated by a group of bioactive compounds known as plant hormones (phytohormones). These substances function optimally within a narrow concentration range, necessitating strict regulation of their levels in plant cells and organs. This regulation primarily occurs through biosynthesis, metabolism and transport mechanisms.

Among the diverse groups of phytohormones, auxins were the first to be identified owing to their profound effects on plant tropisms. Two essential endogenous auxins are indole-3-acetic acid (IAA) and phenylacetic acid (PAA). These compounds exhibit biological active only in their free, unconjugated form. Enzymatic reactions produce metabolites that serve as temporary storage and transport forms, as well as degradation products. This conversion occurs either through irreversible oxidation of IAA to 2-oxo-indole-3-acetic acid (oxIAA) or reversible conjugation with amino acids and sugars. In the presence of GRETCHEN HAGEN 3 (GH3) family enzymes, IAA and oxIAA form amides, primarily (ox)IAA-aspartate and glutamate. Another important pathway involves reversible glycosylation by the uridine diphosphate glucosyltransferases, UGT84B1 and UGT74D1, resulting in indole-3-acetyl-1-*O*-ß-d-glucose (IAA-glc) and its oxidised form 2-oxindole-3-acetyl-1-*O*-ß-d-glucose (oxIAA-glc), respectively.

In most plant species, the auxin PAA is found at higher levels than IAA. However, the concentration required to induce an auxin response is significantly higher for PAA. Consequently, PAA has received less research attention, and its metabolism remains relatively unexplored. So far, the metabolism of PAA and IAA appears quite similar, as the same enzymes catalyse the synthesis of identical conjugates. Currently, only three metabolites (PAA-aspartate, PAA-glutamate and PAA-tryptophan) have been identified in plants. Although *in vitro* studies have demonstrated the conjugation of PAA with glucose by the enzyme UGT84B1, this compound has not yet been found *in planta*.

Delving deeper into the complex world of phytohormones can uncover their role in plant growth and development. Therefore, this doctoral thesis aims to broaden our understanding of auxin metabolic pathways across various plant species and their organs by sensitive mass spectrometry methods.

2 Aims and scope

In recent years, many new discoveries have been made in the field of auxin metabolism, expanding our knowledge about conjugates and catalysing enzymes. However, most of this research is connected to IAA and *Arabidopsis thaliana* as a model plant. Therefore, this doctoral thesis aims to broaden the understanding of these processes in two endogenous auxins (IAA and PAA) across various land plant species and their organs.

The main aims described in this thesis are as follows:

- Identification of novel IAA and PAA metabolites in plants by liquid chromatography coupled with tandem mass spectrometry (LC-MS/MS).

- Complex IAA and PAA metabolite profiling in various land plant species and their organs by previously developed LC-MS/MS methods.

- Understanding the regulatory mechanism of PAA metabolism by elucidating catalysing enzymes and pathways complementarity.

- Developing extraction and detection methods for newly synthesized synthetic auxins with anti-auxin activity and utilizing this method to measure the uptake and stability of these compounds in plants.

3 Literature review

3.1 Plant hormones

Plant development from seed germination to senescence is controlled by a chemically diverse group of molecules known as plant hormones or phytohormones (Davies, 2010). These compounds can be divided into several groups based on their structure. Among them are “stress” hormones, such as abscisic acid, jasmonates, and salicylic acid, which mainly mediate biotic and abiotic stress responses in various plant organs and tissues. The “growth” hormones are responsible for physiological functions in plant development. Into this group auxins, cytokinins, gibberellins, brassinosteroids and others can be placed. Although it is important to say, that all of them may have a physiological function during plant development and also work as stress signalling molecules. Unlike animal hormones, phytohormones are not synthesized in specific glands, and their specificity of action is much broader (Davies, 2010). Their function can range from activation to inhibition depending on their concentration or interaction with other hormonal groups.

The following chapters will focus on the auxins, including a detailed description of their activity, homeostasis, signal transduction and analytical analysis.

3.2 Auxin in history

The history of the auxin’s discovery begins in the nineteenth century, when Charles Darwin and his son Francis observed the effect of light on the growth of the coleoptiles of the canary grass (*Phalaris canariensis* L.) (Darwin and Darwin, 1880). When the coleoptile was illuminated by light from one side, there was a subsequent bending and growth towards the light. However, when the tip of the coleoptile was covered, this phenomenon did not occur. Based on these results, Charles Darwin formulated a hypothesis which postulates the appearance of a certain signal in the tip of the coleoptile which propagates further to the point of bending.

His work was later followed up by Boysen-Jensen (1911) with an experiment in which he inserted an agar block between the cut tip of the coleoptile and the rest of the plant. Even after the block insertion, the coleoptile bended towards the light, confirming that signal molecules were responsible for the phototropism. He later developed this theory by inserting an impenetrable mica layer into the agar block. When the layer was inserted on the illuminated side, bending occurred, but when inserted on the non-illuminated side, the signal was stopped and no phototropism was observed (Boysen-Jensen, 1913). This diffusive signal was first isolated by Frits Went (1926), who placed freshly cut coleoptile tips of *Avena sativa* on agar blocks for several hours, later attached

them back on the coleoptiles and moved them to the dark. In all these plants, the coleoptiles started to bend, and therefore confirming the existence of the signal molecule.

Thanks to this agar-bending assay, this molecule was first identified in human urine and given the name auxin, based on the Greek word "auxein" meaning to increase or grow (Kögl and Haagen-Smit, 1931). Chemically, auxin indole-3-acetic acid (IAA) was firstly isolated from a fungus – *Rhizopus* in 1935 (Thimann, 1935) and later from a cornmeal in 1942 (Haagen-Smit et al., 1942), which was a first successful isolation from a plant material.

In the following decades, the development of analytical techniques, as thin-layer chromatography or gas chromatography, enabled the identification and quantification of IAA and its precursors and metabolites across plant kingdom (Schneider and Wigthman, 1974). During this time, several other naturally occurring auxins were identified, as 4-chloroindole-3-acetic acid (4-Cl-IAA) and its methylester, which were isolated from an immature seed of pea (Marumo et al., 1968) (Fig. 1). Another compound, which was found to have an auxin activity, was phenylacetic acid (PAA) (Haagen-Smit and Went, 1935). This molecule was firstly isolated from an aqueous extract of etiolated seedlings of *Phaseolus* and later detected in many plant species (Okamoto et al., 1967). Highly discussed naturally occurring auxin is indole-3-butyric acid (IBA), which was believed to be an endogenous compound in many plant species (reviewed in Korasick et al., 2013). However, in more recent studies, the occurrence of this molecule in plants was questioned as multiple laboratories were not able to identify it in samples from *Arabidopsis*, Populus, and wheat (Novák et al., 2012; Frick and Strader, 2018). Important question remains, whether the accumulation of IBA cannot be affected by growth conditions or extraction and purification methods, which is on the other hand unlikely, due to the good recovery of the isotopically labelled IBA internal standard (IS) during these processes (Novák et al., 2012).

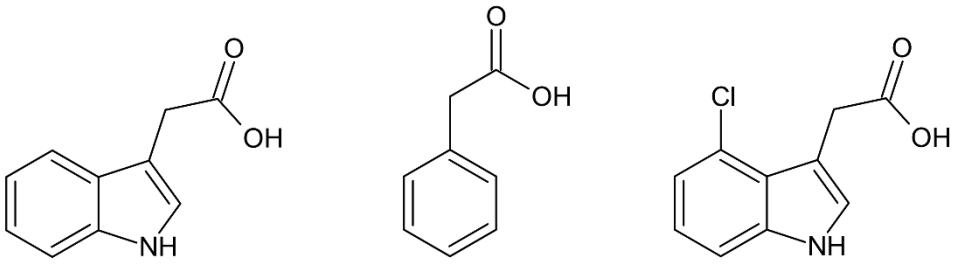

Fig. 1: Structures of endogenous auxins. Abbreviations: 4-Cl-IAA, 4-chloroindole-3-acetic acid; IAA, indole-3-acetic acid; PAA, phenylacetic acid.

3.3 Synthetic auxins

Auxin can be defined by various definitions. In a broader context, auxins are weak organic acids containing an aromatic ring with an attached carboxyl group, which needs to be at a distance of 0.55 Å, in order to be biologically active (Sauer et al., 2013).

Over the past 80 years, significant efforts have been made to improve our understanding of auxin activity through the synthesis of numerous synthetic compounds. Dating back to the 1940s, laboratories have successfully synthesised derivatives of IAA such as 2,4-dichlorophenoxyacetic acid (2,4-D), 3,6-dichloro-2-methoxybenzoic acid (dicamba) and 1-naphthalene acetic acid (1-NAA) (Cobb, 1992) (Fig. 2). These molecules offer advantages over endogenous auxins due to their enhanced stability in the light and within plants, as opposed to the rapid conjugation and degradation typically observed with IAA (Woodward and Bartel, 2005). However, the reduced degradation rate of these synthetic compounds can lead to their accumulation in plants, potentially resulting in toxicity at higher concentrations, as this property has been exploited in herbicide development and agricultural applications (Grossmann, 2010).

Another, different group, forms synthetic auxins with an anti-auxin activity. Among these 4-(2,4-dimethylphenyl)-2-(1H-indol-3-yl)-4-oxobutanoic acid (auxinole), 4-([1,1'-biphenyl]-4-yl)-2-(1H-indol-3-yl)-4-oxobutanoic acid (BP-IAA), and 2-(1H-Indol-3-yl)-4-oxo-4-phenylbutanoic acid (PEO-IAA) were prepared (Hayashi et al., 2012; Žukauskaitė et al., 2023). These molecules competitively bind to the main IAA receptor - TRANSPORT INHIBITOR RESPONSE 1 (TIR1), and therefore reversibly block the IAA signalling pathway (Hayashi et al., 2012).

A completely different approach to synthetic auxin analogues is their fluorescently labelled relatives. These molecules provide an excellent tool for visualising auxin distribution from subcellular compartments to whole plants. To be effective at auxin receptors, these molecules require a planar aromatic ring with an attached carboxyl chain, where the choice of the labelling site, the spacer length and the fluorophore used is crucial (Bieleszová et al., 2019). So far, several fluorophores have been attached to these molecules, such as nitrobenzoxadiazole (NBD) (Hayashi et al., 2014; Bieleszová et al., 2019) or fluorescein isothiocyanate (Sokolowska et al., 2014).

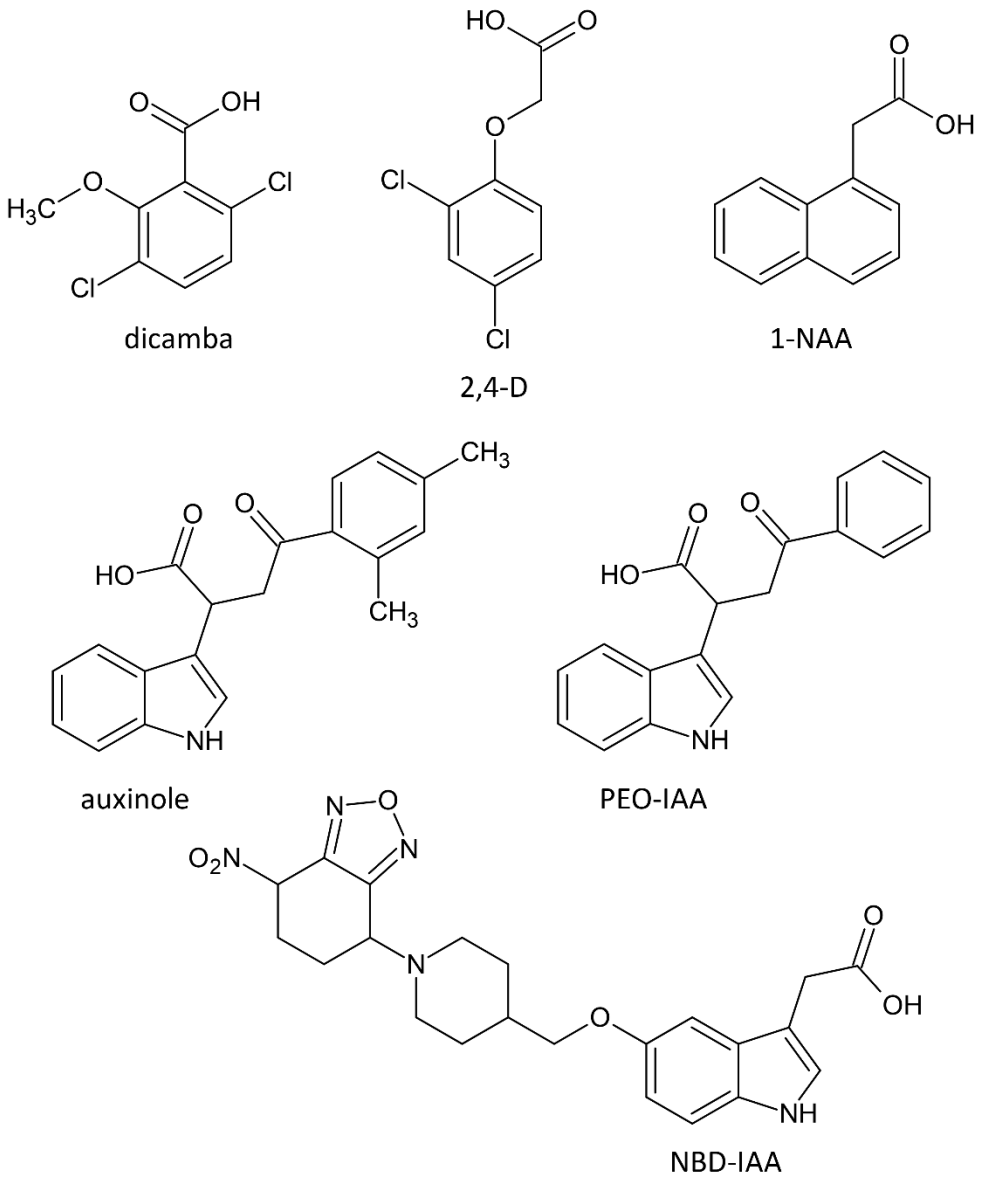

Fig. 2: Structures of synthetic auxins. The first row represents compounds with auxin activity, the second row shows molecules with anti-auxin activity and the third row shows fluorescently labelled auxin derivative NBD-IAA. Abbreviations: 1-NAA, 1-naphthalene acetic acid; 2,4-D, 2,4-dichlorophenoxyacetic acid; Auxinole, 4-(2,4-dimethylphenyl)-2-(1H-indol-3-yl)-4-oxobutanoic; Dicamba, 3,6-dichloro-2-methoxybenzoic acid; NBD-IAA, nitrobenzoxadiazole-indole-3-acetic acid; acid; PEO-IAA, 2-(1H-Indol-3-yl)-4-oxo-4-phenylbutanoic acid.

3.4 Auxin biological roles

Assessing the full effects of auxins during plant development is a challenging task. Auxins, and IAA in particular, affect a wide variety of processes, starting at the cellular level and ending with the whole plant response to an environmental stimulus. To further complicate the tangled web of effects that auxins have on the plant, many of these are influenced by the interaction of auxins with

other phytohormones such as ethylene and cytokinins, which together regulate root architecture and development (Schaller et al., 2015; Liu et al., 2017).

One of the earliest known effects of IAA is its ability to mediate cell growth elongation. Applying exogenous IAA affects stem and coleoptile growth after a short lag phase of 12-15 minutes followed by 15-20 minutes of accelerated growth rate (Fuente and Leopold, 1970). This rapid growth is made possible by the ability of auxin to activate ATPases on a cytoplasm membrane, which cause acidification of the cell's internal environment, by pumping hydrogen ions to the cell. In this acidic environment, proteins that loosen the cell wall are activated, and its subsequent enlargement leads to the activation of potassium channels that diffuse K^+ ions into the cell, thereby raising water uptake and causing cell enlargement by increasing turgor (Majda and Robert, 2018).

Acidic auxin growth, coupled with polar auxin transport, is used in many physiological processes such as phototropism and gravitropism (Davies, 2010). Due to their chemical composition, auxins are capable of moving short distances within plants via polar transport mechanisms. Within the intercellular space, at a slightly acidic pH, big portion of IAA is in its protonated, uncharged state. However, upon entering a cell, where the pH is neutral, IAA is deprotonated and prevented from leaving the cell, unless actively transported by PIN proteins (PINs) or ATP-binding cassette-B (ABCB) auxin exporters (Han et al., 2021). These proteins have the ability to move within the cell, embedding themselves in the cytoplasmic membrane and thereby dictating the direction of auxin flow throughout the plant (Petrášek et al., 2006). Upon exposure to blue light, receptors called phototropins are activated (Huala et al., 1997; Christie et al., 1998), and stimulate the translocation of PIN proteins to the cytoplasmic membrane facing away from the light source, thereby promoting the efflux of IAA towards the basal part of the tissue (Liscum et al., 2014). Consequently, auxins accumulate in the shaded region of the organ and trigger its curvature by acidic auxin-mediated growth. A similar mechanism underlies gravitropism in roots, where the root columella is composed of cells containing starch-filled plastids known as statoliths. These statoliths move across the cell through a gravity manner, eliciting the relocation of PIN proteins in the cytoplasmic membrane (Leitz et al., 2009), and inducing polar auxin transport (Adamowski and Friml, 2015). Overall, auxins regulate many developmental and growth processes including apical dominance, root initiation, leaf senescence and abscission, flowering, and fruit ripening and abscission (as thoroughly reviewed in Davies, 2010).

Auxin is responsible for both developmental processes and responses to biotic or abiotic stress. In mildly elevated temperatures, acclimation responses are governed by a process called thermomorphogenesis (Delker et al., 2022), which is driven by auxin signalling and biosynthesis. Auxin regulates pollen and anther development (Yao et al., 2018), but after passing a critical

temperature threshold, pollen development is disrupted, leading to male sterility possessing a threat to global food supplies (Jing et al., 2023).

High salinity stress alters auxin biosynthesis, transport, and signalling. It has been found that overexpressing auxin biosynthetic genes leads to improved salt tolerance in plants (Kim et al., 2013; Ke et al., 2015). Additionally, suppressing the function of GRETCHEN HAGEN 3 (GH3) enzymes, which are responsible for auxin conjugation with amino acids and therefore its deactivation, also contributes to this improvement (Koochak and Ludwig-Müller, 2021; Casanova-Sáez et al., 2022). In addition, polar auxin transport mediated by auxin transporters is responsible for the root's escape from high salinity concentrations (van den Berg et al., 2016). Similarly, increasing auxin levels during drought stress can enhance resistance (Lee et al., 2012; Kim et al., 2013). To maintain water potential and support main root growth, local auxin maxima are created, supressing cell elongation and arresting the emergence of lateral roots (Korver et al., 2018).

3.5 Auxin signalling and perception

In cells, auxins bind to intracellular receptors to initiate a signal transduction cascade that leads to gene expression. Upon entering the cell, auxins bind to the nuclear TIR1 receptor, which contains AUXIN SIGNALING F-BOX proteins (AFB) (Fig. 3). The AFB proteins then bind with members of the Aux/IAA transcriptional repressor family (Tan et al., 2007). The reaction results in the complex ubiquitination and release of the AUXIN RESPONSE FACTOR (ARFs), which then promote transcription (Korasick et al., 2014).

Several *tir1/afb* genes were identified in plants, mosses, algae, and spermatophytes (Parry et al., 2009). These genes encode TIR1/AFB proteins family that contribute redundantly to various biological processes, such as the regulation of primary and secondary metabolism, seed and root development, cell proliferation, and immunity or stress responses (Du et al., 2022). F-box proteins are subunits of SCF-type ubiquitin protein ligase complexes. These complexes transfer activated ubiquitin from a ubiquitin activating enzyme to target proteins (Smalle and Vierstra, 2004; Leyser, 2018). After auxin binds to the TIR1/AFB receptor, the protein domain II of the Aux/IAA proteins binds across the pocket mouth. This complex is then ubiquitinated and degraded by SFC protein ligase. To make things more complicated, in Arabidopsis, there are a total of 29 Aux/IAAs (Paponov et al., 2008). Calderón Villalobos et al., (2012) found that different TIR1/AFB-Aux/IAA pairs have varying affinities to different auxins, resulting in a wide range of Aux/IAA lifetimes, and therefore various lengths of effect.

The Aux/IAA proteins contain a conserved EAR domain, which recruits corepressors of the TOPLESS family to promoters for chromatin remodelling and stabilizing transcriptional repression

(Szemenyei et al., 2008). The ARF transcription factors mediate the binding to DNA by forming dimers with Aux/IAA proteins (Guilfoyle, 2015). These factors then bind to the auxin responsive elements and prevent gene transcription.

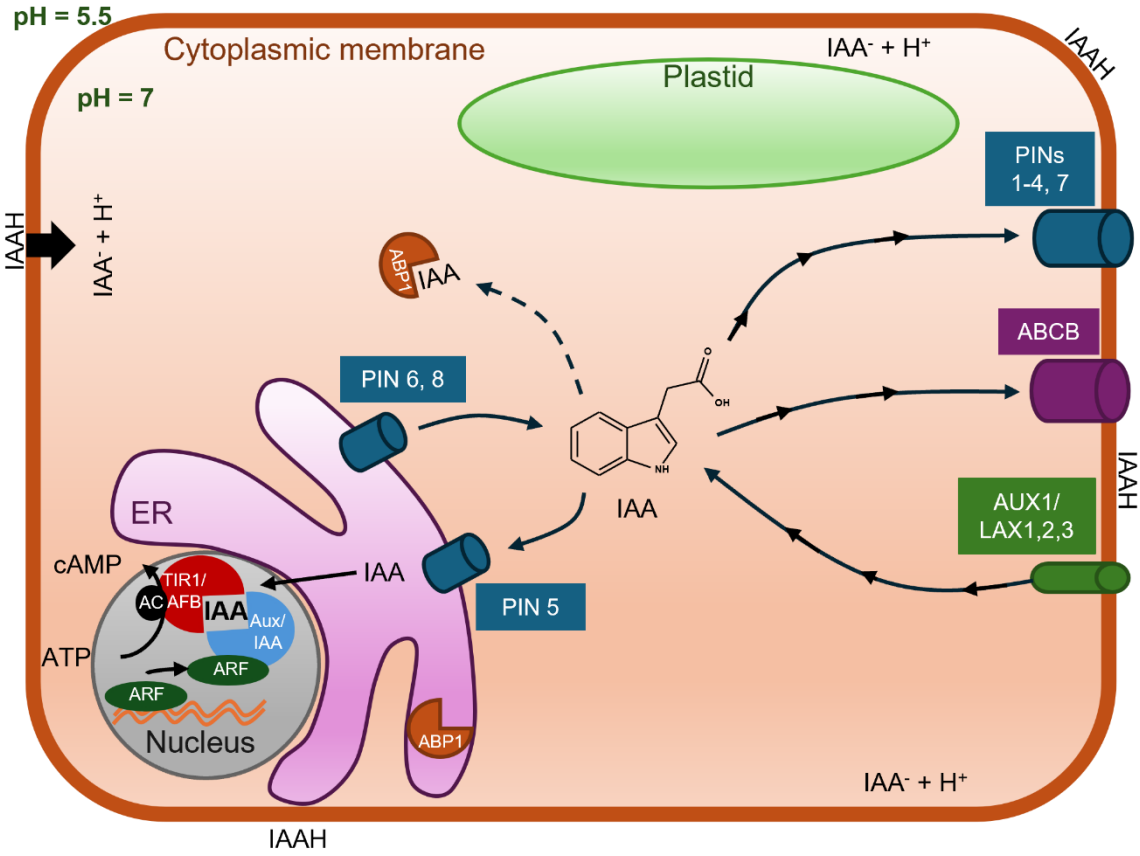

Fig. 3: Scheme of subcellular IAA transport and signalling. Arrows represent IAA transport direction with corresponding transporters. In a nucleus, activated auxin receptor signalling pathway is depicted. Auxin binds to TIR1 receptor, which contains AFB. This complex then reacts with members of the Aux/IAA transcriptional repressor family, which results in the complex ubiquitination and release of the ARFs, which then promote transcription of auxin related genes. Abbreviations: ABCB, ATP-binding cassette-B; ABP1, AUXIN-BINDING PROTEIN 1; AC, adenylate cyclase; AFB, AUXIN SIGNALING F-BOX proteins; ARFs, AUXIN RESPONSE FACTORs; ATP, adenosine triphosphate; AUX1, AUXIN RESISTANT 1; cAMP, cyclic adenosine monophosphate; ER, endoplasmic reticulum; IAA, indole-3-acetic acid; LAX, LIKE AUX; PINs, PIN proteins; TIR 1, TRANSPORT INHIBITOR RESPONSE 1.

Recently, it was discovered that the TIR1/AFB pathway has adenylate cyclase (AC) activity. *In vitro*, auxin stimulates the AC activity of TIR1/AFB receptors, and auxin treatment also steadily increases cAMP levels in roots (Qi et al., 2022). Knockdown mutations in this AC domain arrested AC activity but did not affect TIR1 function towards Aux/IAAs. However, they did affect the TIR1 function in mediating sustained root growth inhibition and auxin-induced transcription (Qi et al., 2022).

Several auxin-related processes occur too rapidly to involve this transcription-regulating pathway. Examples of such rapid processes include rearrangement of the microtubule cytoskeleton (Adamowski et al., 2019), inhibition of PIN endocytic recycling (Paciorek et al., 2005), and alkalization of the apoplast due to Ca^{2+} influx (Monshausen et al., 2011). The fast response reactions were believed to be mediated by the auxin receptor AUXIN-BINDING PROTEIN 1 (ABP1), which is mainly present in the ER and apoplast. This belief was further confirmed by the embryo lethality phenotype of the *abp1*-knockout mutant (Chen et al., 2001). However, later findings have shown that the embryo lethality was not due to the disruption of the *abp1* gene, but rather the neighbouring *bsm* gene (Michalko et al., 2015). This finding has raised serious doubts about the relevance of the ABP1 signalling pathway, which remains under investigation, as these rapid responses have also been shown to be mediated by the TIR1/AFB pathway (Li et al., 2021).

Auxin is also responsible for mediating cell-cycle regulation, as found by Chen et al., (2001). Jurado et al., (2010) proposed the S-PHASE KINASE-ASSOCIATED PROTEIN 2A (SKP2A) receptor as a potential target for this process. This receptor is responsible for the degradation of the transcription factors EF2C and DPB, allowing the cell to transition from G1 to S phase (del Pozo et al., 2006; Jurado et al., 2008). The role of SKP2A, EF2C and DPB in this signalling pathway has been further confirmed by the ubiquitination process that results from the active addition of auxin (Jurado et al., 2010).

3.6 Auxin homeostasis

To ensure proper functioning, it is necessary to maintain auxins within a precise concentration range. Early research in the phytohormonal field has shown that excessive levels of auxins can inhibit growth processes (Thimann, 1937). These concentrations are tightly regulated through various mechanisms, including *de novo* hormone biosynthesis, metabolism, and transport. Endogenous auxins demonstrate biological activity only in their free form with conjugation leading to their rapid deactivation and degradation, facilitating straightforward regulation. The following chapters will provide detailed insights into these processes, with a specific focus on the biosynthesis and metabolism of IAA and PAA.

3.6.1 IAA biosynthesis

The biosynthesis of indole-3-acetic acid (IAA) commences with the amino acid L-tryptophan (L-Trp), which can be indirectly metabolized to IAA through several redundant metabolic pathways. Unlike animals, plants and bacteria are capable of synthesizing aromatic amino acids such as L-Trp, L-phenylalanine (L-Phe), and L-tyrosine via the shikimate pathway (Maeda and Dudareva, 2012).

This pathway is named after the first identified intermediate, shikimate (Bohm, 1965), which is metabolized through other intermediates to chorismate and finally L-Trp (Bentley, 1990) (Fig. 4).

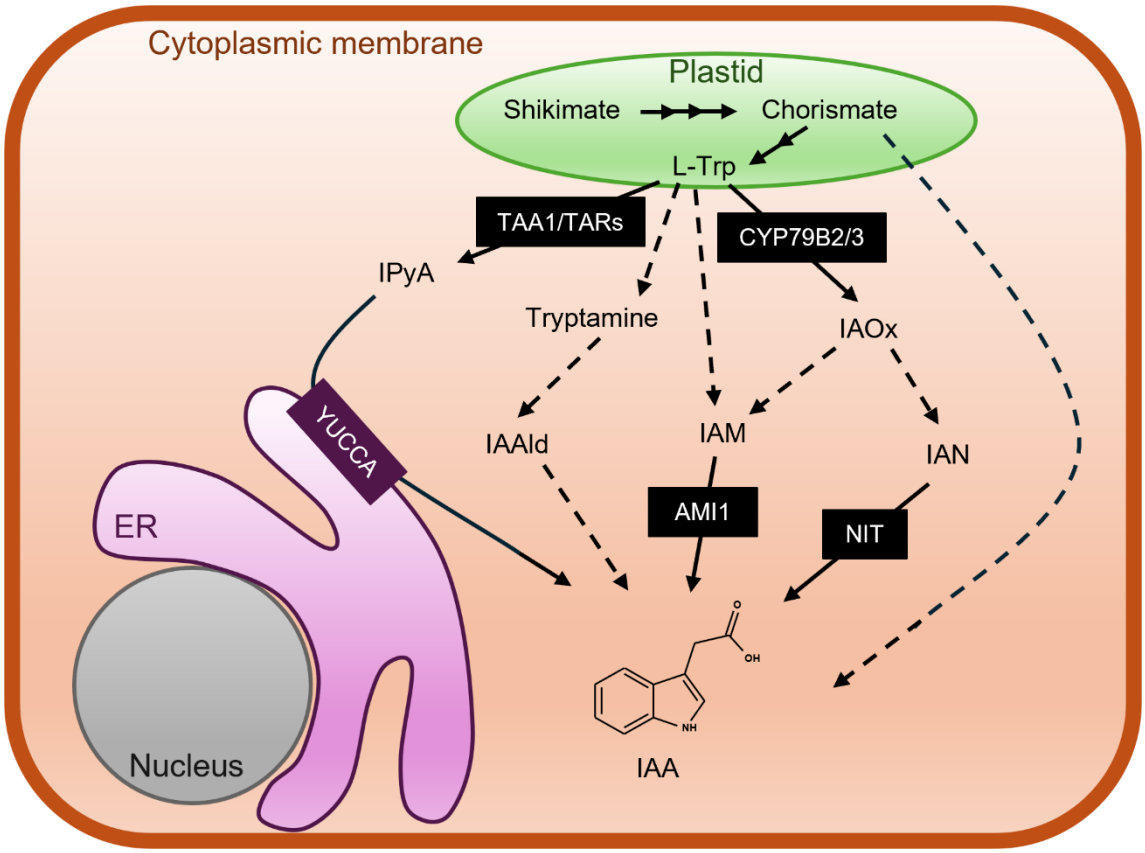

Fig. 4: Scheme of IAA biosynthesis. The solid line arrows represent pathways with discovered enzymes, which are described by a white text in a black or purple box. The dashed arrows represent predicted biosynthetic pathways. Abbreviations: AMI1, indole-3-acetamide hydrolase 1; CYP, CYTOCHROME P450; ER, endoplasmic reticulum; IAA, indole-3-acetic acid; IAAld, indole-3-acetaldehyde; IAM, indole-3-acetamid; IAN, indole-3-acetonitrile; IAOx, indole-3-acetaldoxime; IPyA, indole-3-pyruvic acid; L-Trp, L-tryptophan; NIT, nitrilases; TAA1, TRYPTOPHAN AMINOTRANSFERASE OF ARABIDOPSIS 1; TARs, TRYPTOPHAN AMINOTRANSFERASE-RELATED.

The primary biosynthetic pathway in plants involves the deamination of L-Trp to indole-3-pyruvic acid (IPyA) by TRYPTOPHAN AMINOTRANSFERASE OF ARABIDOPSIS 1/TRYPTOPHAN AMINOTRANSFERASE-RELATED (TAA1/TARs) enzymes. This step is followed by the direct decarboxylation of IPyA to IAA by flavin-containing monooxygenases from the YUCCA family (Mashiguchi et al., 2011). This irreversible reaction is a rate-limiting step in IAA biosynthesis, controlling endogenous levels (Zhao et al., 2001). Studies on *taa1/tars* and *yucaQ* Arabidopsis knockout lines have provided evidence supporting the importance of this pathway, as they exhibit auxin deficient phenotypes (Stepanova et al., 2008; Yamada et al., 2009; Chen et al., 2014).

Another biosynthetic pathway involves conversion of L-Trp to indole-3-acetaldoxime (IAOx) by enzymes from the cytochrome P450 (CYP) family - CYP79B2 and CYP79B3 (Hull et al., 2000;

Mikkelsen et al., 2000). These enzymes were however detected only in the *Brassicaceae* family, and therefore this pathway is only relevant in those species (Sugawara et al., 2009). Although, IAOx is an important precursor of glucosinolates (Sønderby et al., 2010) and camalexin (Nguyen et al., 2022), which serve as a defensive compound, its conversion to IAA is still not completely explained (Casanova-Sáez et al., 2021). An attempt to elucidate this metabolic conversion was performed by Sugawara et al., 2009, who conducted experiments using $^{13}C_6$ labelled IAOx on *cyp79b2 cyp79b3* deficient Arabidopsis mutants. The incorporation of the $^{13}C_6$ label was observed in indole-3-acetamide (IAM), indole-3-acetonitrile (IAN) and IAA, thereby confirming the role of IAOx in IAA synthesis. These mutant lines exhibited significantly reduced endogenous levels of IAN, however, supplementation with IAOx resulted in the rescue of IAN levels, indicating their significant involvement downstream of this metabolic pathway. Furthermore, the conversion of IAN to IAA by nitrilases (NIT) has been demonstrated (Lehmann et al., 2017).

Although the role of IAM in the IAA biosynthetic pathway in plants is not fully understood, it has been well-described in several bacterial species that induce gall tumors on host plants (Thomashow et al., 1984; Manulis et al., 1998). This pathway involves the conversion of L-Trp to IAM by the enzyme L-tryptophan 2-monooxygenase, followed by deamination to IAA by indole-3-acetamide hydrolase (AMI) (Patten et al., 2013). Reports suggesting this IAOx-independent pathway in plants have been supported by the detection of IAM outside the *Brassicaceae* family in multiple studies (Sugawara et al., 2009; Novák et al., 2012). Additionally, plant AMI hydrolases capable of hydrolysing IAM *in vitro* and *in vivo* have been identified in Arabidopsis (Pollmann et al., 2003; Gao et al., 2020).

The last biosynthetic pathway arising from L-Trp is a matter of debate. It involves the conversion of L-Trp to tryptamine, which is then oxidized to indole-3-acetaldehyde (IAAld) and subsequently to IAA (Quittenden et al., 2009). The enzyme responsible for the conversion of IAAld to IAA was initially thought to be ARABIDOPSIS ALDEHYDE OXIDASE 1 (Seo et al., 1998). However, the *aba3* mutant, which is unable to synthesise the cofactor of this enzyme, did not exhibit any auxin-deficient phenotype and did not show accumulation of IAAld (Mashiguchi et al., 2011). Therefore, IAAld was excluded, as an orphan intermediate in auxin biosynthesis (Korasick et al., 2013). Interestingly, this pathway has been overlooked in recent years, as the most recent reviews on auxin biosynthesis completely neglect it (Casanova-Sáez et al., 2021; Solanki and Shukla, 2023).

Although, most of the IAA appears to by synthetized via a L-Trp dependent pathway, there have been reports of L-Trp independent pathway. The initial evidence was presented by Normanly et al., (1993), who observed a higher enrichment of ^{15}N in IAA compared to L-Trp in *trp1-2* mutant grown on media containing ^{15}N labelled L-Trp precursor anthranilate. Subsequent evidence came after discovering, that *ins-1* mutants, bearing null mutation in indole synthase responsible for indole

synthesis from indole-3-glycerol phosphate, exhibited reduced levels of IAA (Wang et al., 2015). However, mutant lines defective further downstream in the L-Trp biosynthetic pathway showed decreased levels of L-Trp levels, but increased levels of IAA (Radwanski et al., 1996). All this work was later critically evaluated, and all these results were questioned, as they could potentially be explained by the L-Trp dependent pathway alone (Nonhebel, 2015).

3.6.2 PAA biosynthesis

The synthesis of phenylacetic acid (PAA) originates from its precursor L-Phe and appears to follow a similar process to that of indole-3-acetic acid (IAA) biosynthesis, although probably catalysed by different enzymes (Fig. 5). Recent research has identified the arogenate dehydratase group as a key regulator of PAA levels in Arabidopsis, highlighting the importance of the L-Phe-dependent synthesis pathway (Aoi et al., 2020a).

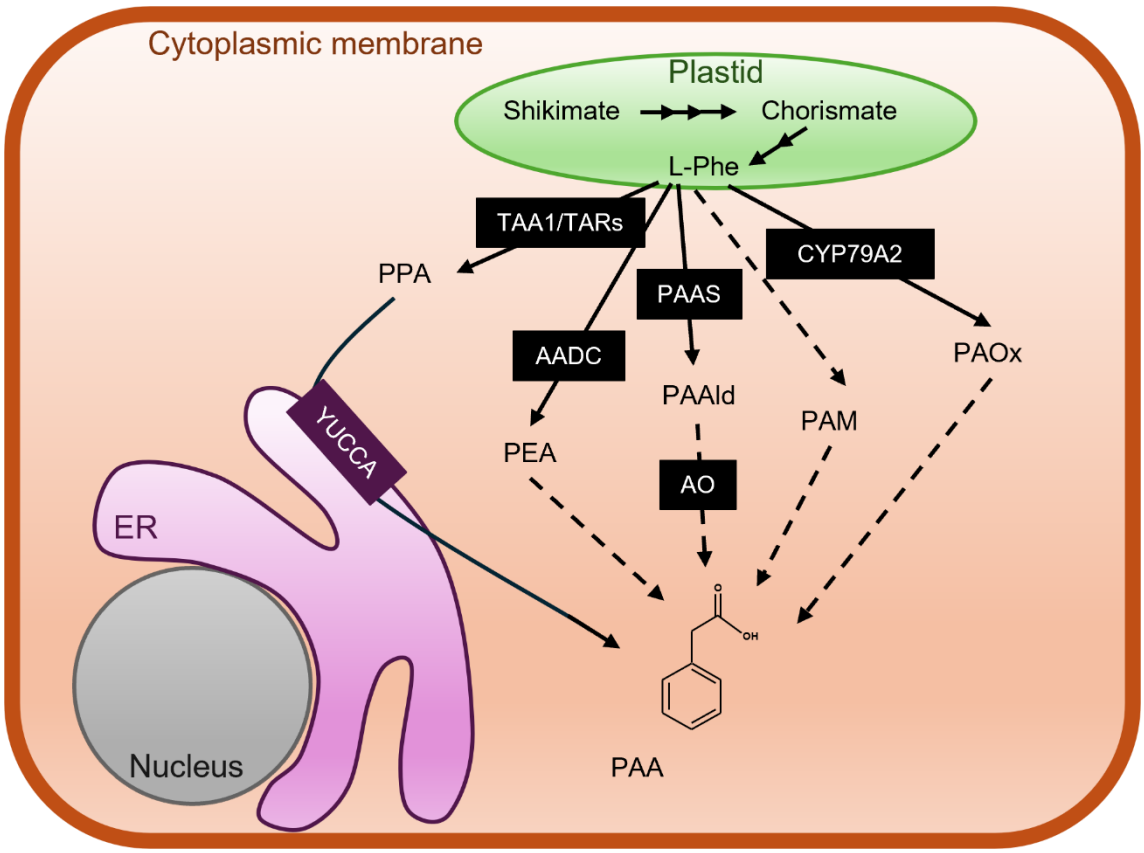

Fig. 5: Scheme of PAA biosynthesis. The solid line arrows represent pathways with discovered enzymes, which are described by a white text in a black or purple box. The dashed arrows represent predicted biosynthetic pathways. Abbreviations: AADC, aromatic amino acid decarboxylases; AO, aldehyde oxidases; CYP, CYTOCHROME P450; ER, endoplasmic reticulum; L-Phe, L-phenylalanine; PAA, phenylacetic acid; PAAld, phenylacetaldehyde; PAAS, phenylacetaldehyde synthase; PAM, phenylacetamide; PAOx, phenylacetaldoxime; PEA, phenylethylamine; PPA, phenylpyruvate; TAA1, TRYPTOPHAN AMINOTRANSFERASE OF ARABIDOPSIS 1; TARs, TRYPTOPHAN AMINOTRANSFERASE-RELATED.

The main biosynthetic pathway involves the reversible conversion of phenylpyruvate (PPA) from L-Phe, followed by its subsequent decarboxylation to produce PAA (Cook et al., 2016). This process is similar to the well-characterised formation of IAA from tryptophan by the *taa1/tars* and *yucca* gene families in Arabidopsis (Mashiguchi et al., 2011). Although the mechanisms behind L-Phe to PAA conversion are not yet fully understood, phenylpyruvate aminotransferase, which was identified in petunia, is a strong candidate enzyme (Cook et al., 2016; Yoo et al., 2013). Furthermore, it has been demonstrated that overexpression of YUCCA enzymes increases endogenous PAA levels. However, in *yuc1 yuc2 yuc6* triple knockdown mutants, no changes in PAA levels were observed, suggesting the presence of alternative biosynthetic pathways in plants (Sugawara et al., 2015). In addition, a small amount of PPA can be produced directly from prephenate, which is the precursor of L-Phe, by prephenate dehydratase, followed by its subsequent metabolism to PAA (Cho et al., 2007).

The secondary biosynthetic pathway involves the conversion of Phe to either phenylacetaldehyde (PAAld) by phenylacetaldehyde synthase (PAAS) (Kaminaga et al., 2006) or to phenylethylamine (PEA) by aromatic amino acid decarboxylases (AADC) (Tieman et al., 2006). Although there is no evidence of PEA being converted to PAAld in plants, amino oxidases responsible for the formation of IAAld from tryptamine are described in the IAA biosynthetic pathway (Quittenden et al., 2009). The final step in the formation of PAA from PAAld is not well characterised, as no amino oxidases (AO) have been found to be active in this reaction (Cook, 2019), except for AO from maize, which can use PAAld as a substrate with very limited activity (Koshiba et al., 1996).

Additionally, a minor, tissue-dependent, and probably stress-activated biosynthetic pathway involves the formation of phenylacetaldoxime (PAOx) from Phe by the enzyme CYP79A2, which is then directly converted to PAA (Perez et al., 2021). Until recently, it was believed that PAOx had to be converted to benzyl glucosinolates before being hydrolysed into free PAA (Urbancsok et al., 2018). However, this step is only possible in the *Brassicaceae* family, as other plants lack the necessary enzymes. Interestingly, direct conversion of PAOx to PAA also occurs in maize, suggesting glucosinolates independent pathway (Perez et al., 2021).

In cell cultures of *Agrobacterium tumefaciens*, it was discovered that the bacterial intermediate phenylacetamide (PAM), which is formed from Phe, can be converted to PAA (Kemper et al., 1985). However, it has never been shown whether this pathway also occurs in plants (Cook, 2019).

3.6.3 IAA metabolism

The majority of IAA in plants exists in its non-active form, which can be categorised into two main groups. The first comprises reversible storage forms, such as esters and amides, or methylated IAA (meIAA) (Fig. 6). The second group consists of oxidised metabolites, which undergo irreversible metabolism leading to their degradation (Casanova-Sáez et al., 2021) (Fig. 6).

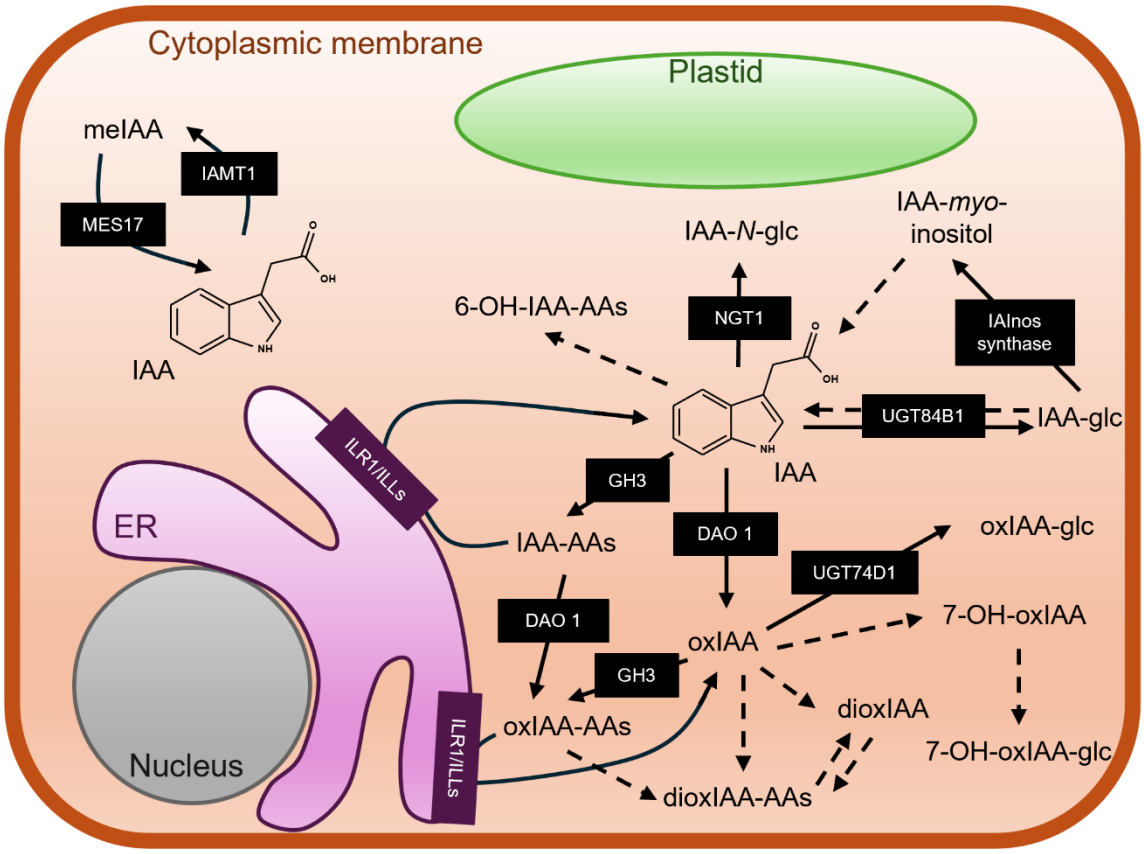

Fig. 6: Scheme of IAA metabolism. The solid line arrows represent pathways with discovered enzymes, which are described by a white text in a black or purple box. The dashed arrows represent predicted metabolism pathways. Abbreviations: 6-OH-IAA-AAs, *N*-(6-hydroxyindol-3-ylacetyl)-amino acids; 7-OH-oxIAA, 7-hydroxy-2-oxindole-3-acetic acid; 7-OH-oxIAA-glc, 7-hydroxy-2-oxindole-3-acetyl-7-*O*-β-D-glucose; DAO1, DIOXYGENASE FOR AUXIN OXIDATION 1; dioxIAA, 3-hydroxy-2-oxindole-3-acetic acid; dioxIAA-AAs, 3-hydroxy-2-oxindole-3-acetyl amino acids; ER, endoplasmic reticulum; GH3, GRETCHEN HAGEN 3; IAA-N-glc, indole-3-acetyl-*N*-ß-d-glucose; IAA, indole-3-acetic acid; IAA-AAs, indole-3-acetyl-amino acids; IAA-glc, indole-3-acetyl-1-*O*-ß-d-glucose; IAInos synthase, indole-3-acetyl-1-*O*-ß-d-glucose: myo-inositol indoleacetyl transferase; IAMT1, IAA CARBOXYMETHYLTRANSFERASE 1; ILLs, ILR1-LIKE proteins; ILR1, IAA-LEUCINE RESISTANT 1; meIAA, indole-3-acetic acid methyl ester; MES17, methylesterase 17; NGT1, N-glucosyltransferase 1; oxIAA, 2-oxindole-3-acetic acid; oxIAA-AAs, 2-oxindole-3-acetyl-amino acids; oxIAA-glc, 2-oxindole-3-acetyl-1-*O*-ß-d-glucose; UGTs, uridine 5'-diphospho-glucuronosyltransferases.

In plants, various types of ester conjugates are formed, including, indole-3-acetyl-1-*O*-ß-d-glucose (IAA-glc), its oxidised form 2-oxindole-3-acetyl-1-*O*-ß-d-glucose (oxIAA-glc), and IAA-*myo*-

inositol (Hall, 1980; Kai et al., 2007a; Pěnčík et al., 2018). These compounds are synthesised by Uridine 5'-diphospho-glucuronosyltransferases (UGTs) such as UGT84B1, UGT74D1, and UGT76E3456 (Jackson et al., 2001; Tanaka et al., 2014; Mateo-Bonmatí et al., 2021). IAA can be initially conjugated to IAA-glc by UGT84B1 (Jackson et al., 2001), followed by its conjugation to IAA–*myo*-inositol via the reversible activity of indole-3-acetyl-1-*O*-ß-d-glucose: myo-inositol indoleacetyl transferase (IAInos synthase) (Kowalczyk et al., 2003). In maize, both of these conjugates can then be hydrolysed back to free IAA (Jakubowska and Kowalczyk, 2005). Additionally, the oxidative metabolite 2-oxindole-3-acetic acid (oxIAA) can be conjugated to oxIAA-glc by the enzyme UGT74D1 (Tanaka et al., 2014; Mateo-Bonmatí et al., 2021), which is a predominant low-molecular-weight conjugate in Arabidopsis (Kai et al., 2007a). Several other esters have been identified in plants, including indole-3-acetyl-*N*-ß-d-glucose (IAA-N-glc), discovered in Scots pine and rice (Ljung et al., 2001a; Kai et al., 2007b), although most of it was bound with aspartate and glutamate. Recently, an enzyme N-glucosyltransferase 1 (NGT1) responsible for IAA-*N*-glc formation from IAA and IAA-amides was discovered in gingko biloba species (Yin et al., 2021).

The alternative metabolic pathway involves the synthesis of amides with amino acids, peptides or proteins. This biochemical reaction is facilitated by a class of enzymes known as GH3. Initially identified in soybean hypocotyls during the 1980s (Hagen and Guilfoyle, 1985), GH3 enzymes have since been observed to be conserved across various plant species (Zhang et al., 2018). The GH3 enzymes are classified into three main groups based on their structural and functional characteristics (Westfall et al., 2010). Group I enzymes conjugate jasmonic acid (Wakuta et al., 2011), group II enzymes regulate IAA metabolism (Staswick et al., 2005), and group III enzymes prefer 4-substituted benzoates (Okrent et al., 2009). In Arabidopsis, there are a total of 19 GH3 enzymes (Zhang et al., 2018), with eight members (GH3.1, GH3.2, GH3.3, GH3.4, GH3.5, GH3.6, GH3.9 and GH3.17) belonging to the second group (Staswick et al., 2005). These enzymes have different affinities for various substrates. For example, GH3.3 and GH3.4 preferentially conjugate IAA with aspartate, GH3.17 predominantly forms indole-3-acetyl-glutamate (IAA-Glu), while GH3.2, GH3.5, and GH3.6 do not display any distinct substrate preferences (Staswick et al., 2005; Brunoni et al., 2019).

Numerous IAA-amino acids (IAA-AAs) conjugates were identified in various plant species. The most common IAA-AAs are indole-3-acetyl-aspartate (IAA-Asp) and IAA-Glu (Kojima et al., 2009; Novák et al., 2012; Pěnčík et al., 2018), while others such as IAA-alanine, glycine, leucine, phenylalanine, tryptophan and valine have also been identified across multiple species (Kowalczyk and Sandberg, 2001; Pěnčík et al., 2009). For a considerable period, IAA-Asp and IAA-Glu were presumed to be non-hydrolysable conjugates because of their higher levels compared to other IAA-AAs, which are convertible back to free IAA through the action of IAA-amino acid amidohydrolases

such as IAA-LEUCINE RESISTANT 1 (ILR1), ILR1-LIKE proteins (ILLs), and IAA-ALANINE RESISTANT 3 (IAR3) (Bartel and Fink, 1995; Davies et al., 1999; LeClere et al., 2002). However, recent evidence has demonstrated that they are also susceptible to hydrolysis, leading to the release of free IAA (Hayashi et al., 2021).

High-molecular-weight conjugates have been identified in the seeds of many plant species, including oat (Percival and Bandurski, 1976), bean (Bialek and Cohen, 1986), pea (Park et al., 2010) and Arabidopsis (Park et el., 2006). In bean seeds, IAA-modified protein 1 has been observed to be bound with IAA, which may serve as an alteration of protein stability or a storage reservoir for free IAA (Walz et al., 2002). Moreover, GH3 enzymes have been implicated in the formation of these IAA-protein conjugates in pea seeds, where they constitute a major portion of the total IAA pool (Park et al., 2010; Ostrowski and Ciarkowska, 2021).

Another metabolic pathway involves the methylation of IAA to meIAA. This conversion is mediated by the enzyme IAA CARBOXYMETHYLTRANSFERASE 1 (IAMT1) (Qin et al., 2005), and results in the formation of a non-polar auxin. This form of auxin can likely be transported independently of a transporter (Li et al., 2008). In comparison to IAA, meIAA is more potent in inhibiting hypocotyl elongation and inducing lateral roots, but weaker in inducing root hairs growth (Li et al., 2008). Additionally, meIAA can be hydrolysed back to release free IAA by methylesterase 17 (MES17) (Yang et al., 2008).

Irreversible auxin deactivation involves oxidative reactions. The primary catabolic pathway entails the oxidation of IAA to oxIAA by the enzyme DIOXYGENASE FOR AUXIN OXIDATION 1(DAO1) (Novák et al., 2012; Pěnčík et al., 2013; Zhao et al., 2013; Porco et al., 2016). Similarly, IAA-AAs can also undergo oxidation by this enzyme to form their oxidative counterparts (Hayashi et al., 2021; Müller et al., 2021). To date, 2-oxindole-3-acetyl-aspartate (oxIAA-Asp) and 2-oxindole-3-acetyl-glutamate (oxIAA-Glu) have been identified in numerous angiosperm plant species (Hayashi et al., 2021; Kim et al., 2021; Isobe and Miyagawa, 2022). This pathway was previously thought to be a distinct branch of IAA oxidation. However, Hayashi et al. (2021) demonstrated that DAO1 primarily oxidizes IAA-AAs to oxIAA-amino acids (oxIAA-AAs), which are then subsequently hydrolysed by ILR1/ILLs to oxIAA. Recently, oxIAA conjugation by GH3 enzymes has been confirmed, but this reaction appears to be species-dependent (Brunoni et al., 2023).

However, the fate of these conjugates remains elusive. Although, the presence of 3-hydroxy-2-oxindole-3-acetic acid (dioxIAA) has been observed in plants (Tsurumi and Wada, 1980; Östin et al., 1992; Isobe and Miyagawa, 2022), the underlying mechanism of this conjugate formation has not yet been described. Similarly, 3-hydroxy-2-oxindole-3-acetylaspartate and glutamate have been identified in plants, and they are believed to be synthesized from IAA-Asp and IAA-Glu (Östin et al., 1992; Isobe and Miyagawa, 2022). Furthermore, an alternative oxidation pathway has been

identified. *In vitro* studies have demonstrated that peroxidases can metabolize IAA, leading to the formation of indole-3-carbinol and oxindole-3-carbinol (BeMiller and Colilla, 1972; Grambow and Langenbeck-Schwich, 1983).

Several other oxidative metabolites have been identified in plants, with particular attention given to 6-hydroxy conjugates, such as *N*-(6-hydroxyindol-3-ylacetyl)-amino acids (6-OH-IAA-AAs). Upon the application of exogenous IAA, the synthesis of *N*-(6-hydroxyindol-3-ylacetyl)-aspartate has occurred in plants (Östin et al., 1998). Similarly, Arabidopsis has been found to contain trace levels of *N*-(6-hydroxyindol-3-ylacetyl)-phenylalanine (6-OH-IAA-Phe) and *N*-(6-hydroxyindol-3-ylacetyl)-valine (6-OH-IAA-Val) (Kai et al., 2007a). These molecules are likely formed through the oxidation of IAA-AAs rather than by conjugating amino acids with 6-OH-IAA. This is demonstrated by their appearance following the supply of radiolabelled IAA-AAs to plants (Östin et al., 1998; Kai et al., 2007a). Furthermore, in maize seedlings, the presence of 7-hydroxy-2-oxindole-3-acetyl-7-*O*-β-D-glucose (7-OH-OxIAA-glc) was shown (Nonhebel and Bandurski, 1984; Nonhebel et al., 1985). Its formation is expected to proceed from oxIAA through 7-hydroxy-2-oxindole-3-acetic acid (7-OH-oxIAA) (Zhang and Peer, 2017).

3.6.4 PAA metabolism

It appears that the metabolic pathways are conserved across all auxins. In the studies focused on PAA metabolism, it was found that these processes are even mediated by the same enzymes (Cook, 2019; Perez et al., 2023). Initial investigations in 2005 revealed that GH3 enzymes, known for their role in forming IAA-amides with amino acids, also demonstrated *in vitro* sensitivity to PAA (Staswick et al., 2005). However, it was not until another decade passed that the first PAA conjugates – phenylacetyl-aspartate (PAA-Asp) and phenylacetyl-glutamate (PAA-Glu) – were discovered (Sugawara et al., 2015). This experiment involved Arabidopsis mutant lines expressing β-estradiol-inducible GH3.9 enzymes, which significantly increased PAA-Glu levels and confirmed GH3 dependent synthesis. A similar experiment was conducted by Westfall et al., (2017) who demonstrated the formation of PAA-Asp in a GH3.5 dependent manner by utilising GH3.5 overexpressing lines. Furthermore, treatment with IAA or PAA led to a decrease in the endogenous concentrations of the other auxin by forming its corresponding aspartate metabolite (Aoi et al., 2020b). Since IAA esterification is an important metabolic pathway in Arabidopsis (Kai et al., 2007a), the activity of UGT84B1 towards PAA was examined, revealing the formation of phenylacetyl-1-*O*-ß-d-glucose (PAA-glc) *in vitro* (Aoi et al., 2020c). However, attempts to identify PAA-glc in Arabidopsis plants were unsuccessful (Aoi et al., 2020c).

Amide conjugation was also found in the other auxins, as GH3.3 did form aspartate conjugates with chlorinated auxins *in vitro* (Walter et al., 2020). Additionally, peroxisomal UDP-glucosyltransferase UGT74E2 did glycosylate IBA in Arabidopsis (Tognetti et al., 2010). Overall, both UGT and GH3 enzymes show a great promiscuity, as aspartate and glutamate metabolites of synthetic auxins 2,4-D and dicamba were also identified (Eyer et al., 2016; Chiu et al., 2018), as well as glucosyl ester of 2,4-D (Eyer et al., 2016).

3.6.5 Auxin transport

The final aspect of homeostatic regulation lies in auxin transport. For proper functionality, auxin must be transported directionally from its site of synthesis to its site of action. Two primary mechanisms govern the transport of IAA. The first involves movement from highly photosynthetic tissues, such as young leaves, to roots, facilitated by an intercellular vascular phloem network (Robert and Friml, 2009). This transport operates at a speed of 1–2.4 cm/h and is energetically neutral due to concentration differentials of IAA between the two ends (Feng et al., 2022).

Secondly, polar auxin transport predominantly occurs in short cell-to-cell distances, with its underlying mechanism elucidated in a preceding chapter (3.4 Auxin biological roles). For this transport, several groups of auxin transporters are needed, including AUXIN RESISTANT 1/LIKE AUX (AUX1/LAX1,2,3), PINs and ABCB (Zažímalová et al., 2010) (Fig. 3).

In most tissues, IAA enters cells through passive diffusion. However, in highly auxin-demanding tissues, AUX1/LAX1,2,3 transporters actively facilitate IAA import into cells (Bennett et al., 1996; Péret et al., 2012). This active IAA import is responsible for root gravitropism, lateral root development, vascular development, and phyllotactic patterning (reviewed in Swarup and Bhosale, 2019).

Among these transporters, PINs are the most extensively studied, comprising eight different types divided into two categories based on the length of the hydrophilic domain. The long PINs 1-4 and 7 mediate the directional efflux of IAA from the cell by embedding into the cytoplasmatic membrane (Petrášek et al., 2006; Wisniewska et al., 2006). Conversely, PINs 5, 6, and 8 facilitate intracellular transport, as they are localized on the endoplasmic reticulum (Mravec et al., 2009; Barbez and Kleine-Vehn, 2013).

ABCB proteins are required for the proper function of PINs (Deslauriers and Spalding, 2021). The use of *twd1* mutants, which prevent several ABCB transporters from reaching the plasma membrane, disrupted polar auxin transport but did not affect PIN polar localisation (Bouchard et al., 2006). Furthermore, mutations in *abcb* genes do not affect PIN protein localisation, however, make it more sensitive to disruption by the detergent Triton X-100 (Titapiwatanakun et al., 2008).

Together, these results suggest a synergistic function of these transporters in directional IAA transport (Deslauriers and Spalding, 2021).

Although the biosynthesis and metabolism of other auxins appear to mirror that of IAA, there are variations in their transport mechanisms. Previous transport studies, which used isotopically labelled $^{14}C_6$ IAA, demonstrated its long-distance polar transport in pea stems (Morris and Johnson, 1987). However, treatment with $^{14}C_6$ PAA did not result in directional transport, with PAA remaining in segments up to 10 mm from the site of application (Morris and Johnson, 1987; Procházka and Borkovec, 1984). Furthermore, the treatment with PAA resulted in the inhibition of IAA transport, as reported by Morris and Johnson, (1987). In contrast, the application of 1-NAA, a polar auxin transport inhibitor, to the tips of maize coleoptiles arrested the basipetal transport of IAA but did not affect the gradient patterns of PAA (Sugawara et al., 2015).

On the contrary, synthetic auxins such as 1-NAA and 2,4-D are transported in plants through auxin carriers. 1-NAA enters cells through passive diffusion and its concentration is regulated by efflux carriers (Delbarre et al., 1996). While it was previously believed that 2,4-D uptake is primarily facilitated by influx transporters and not secreted by efflux transporters (Delbarre et al., 1996), subsequent research has confirmed its active efflux (Hošek et al., 2012).

3.6.6 Auxin localization and regulation

Elucidating auxin signalling and homeostasis facilitates the comprehension of auxin localisation and regulation in plants, from the whole organism down to subcellular compartments. It is widely recognised that high auxin levels negatively regulate biosynthesis (Ljung et al., 2001b). Through a feedback loop, elevated levels of IAA induce the down-regulation of IPyA-related genes (Suzuki et al., 2015). Moreover, an increase in IAA concentrations stimulates the induction of GH3 enzymes, while DAO1 activity remains constant (Mellor et al., 2016; Porco et al., 2016). However, auxin oxidation may contribute to the attenuation of auxin signalling induced by reactive oxygen species (Zhang and Peer, 2017). A similar compensatory mechanism operates between multiple auxins, whereby exogenous treatment with one, results in a concentration decrease of the second in a GH3-dependent manner (Aoi et al., 2020b).

These mechanisms regulate the concentrations of auxin conjugates in tissues. The majority of IAA is synthesised in young, highly photosynthetic active tissues and transported via the phloem to the root tip (Ljung et al., 2001b; Robert and Friml, 2009). Advancements in analytical techniques have facilitated the understanding of these processes through auxin concentration measurements in distinct tissues, as extensively reviewed by Novák et al., (2017). For example, auxin maxima have been pinpointed in quiescent control cells within the meristematic root zone (Petersson et al.,

2009), and analysis of the 0.5 mm region of the youngest leaf apex revealed the highest IAA concentration and capacity for hormone synthesis (Ljung et al., 2001b).

In recent years, there has been significant progress in understanding subcellular auxin organization. Auxin biosynthesis primarily begins in the chloroplasts, where amino acid precursors are synthesised (Ljung, 2013). Within the IPyA biosynthetic pathway, TAA1/TARs enzymes are predominantly localised in the cytoplasm and plasma membrane, respectively (Skalický et al., 2018). Similarly, the YUCCA enzymes are also primarily located in the cytoplasm, although some have been detected on the cytosolic face of the ER membrane (Kriechbaumer et al., 2012). Following *de novo* biosynthesis or entry into the cell, auxins can be transported to the nuclei to bind to the TIR1 receptor or metabolise into inactive forms. It is established that ILR/ILLs are mainly located on the ER membrane (LeClere et al., 2002; Skalický et al., 2018), while GH3 and DAO1 enzymes are likely to be cytosolic (Di Mambro et al., 2019; Porco et al., 2016). Although, previous studies have attempted to measure auxin levels in organelles (Polanská et al., 2007; Ranocha et al., 2013; Skalický et al., 2021), the first comprehensive mapping of auxin distribution was achieved through Fluorescence-Activated Multi-Organelle Sorting in Arabidopsis root-derived cell cultures, revealing the IAA metabolic pool in nuclei, mitochondria, chloroplasts, ER, and vacuoles (Skalický et al., 2023).

3.7 Phytohormone analysis

Since the discovery of auxin, scientists have attempted to measure its concentrations in plants. Initially, auxin bioassays were used for this purpose (Went, 1926). However, this method is not ideal for identifying multiple compounds, lacks accuracy and repeatability, and is time-consuming. As a result, other techniques have been employed (Du et al., 2012). Over the years, immunoassays such as radioimmunoassay or enzyme-linked immunosorbent assays have been popular (Weiler, 1984). However, determining multiple compounds simultaneously has been a challenging task. As a result, chromatographic methods followed by mass spectrometry (MS) analysis have become the standard approach for auxin qualitative and quantitative determination (Du et al., 2012).

Quantifying phytohormone concentrations in plants poses a formidable challenge owing to their low levels, typically ranging pmol-fmol/g fresh weight, while interfering substances are present in much higher concentrations (Tarkowska et al., 2014). Therefore, the extraction and purification processes, along with the use of highly sensitive and selective methods, are critical in the analysis.

3.7.1 Sample preparation

The objective of the sample preparation is to remove interfering compounds and to enhance the concentration of the target analytes. Due to the enzymatic activity and spontaneous oxidation of analytes, sample preparation should be carried out under cold conditions (Porfírio et al., 2016). Typically, plant material is flash-frozen in liquid nitrogen after sampling or subjected to lyophilization (Fu et al., 2011). The process of sample preparation usually involves three main stages: homogenisation, extraction into solution, and purification (Fig. 7).

Sample homogenization is commonly performed under liquid nitrogen by a mortar and a pestle. However, this method often results in significant sample loss. As a result, small sample quantities are typically homogenised in Eppendorf tubes within a bead mill using small zirconium oxide beads (Tarkowská et al., 2014). This method enables simultaneous grinding of multiple samples, thereby reducing time consumption, enhancing yield, and mitigating sample degradation.

To achieve optimal extraction efficiency, solvent with polarity similar to that of analytes should be selected. Auxins, being polar compounds, are easily soluble in water and organic solvents, such as methanol, acetone, dimethyl sulfoxide or basic buffers, as reviewed in Porfírio et al., (2016). Although methanol:water is a prevalent extraction solvent, it may lead to auxin esterification (Barkawi et al., 2010). Conversely, basic buffers like sodium-phosphate buffer does not prevent the enzymatic degradation of IAA (Liang et al., 2012). Therefore, antioxidants such as diethyl dithiocarbamate (Kowalczyk and Sandberg, 2001; Pěnčík et al., 2009) or butylated hydroxytoluene (Quittenden et al., 2009) should be added prior to extraction.

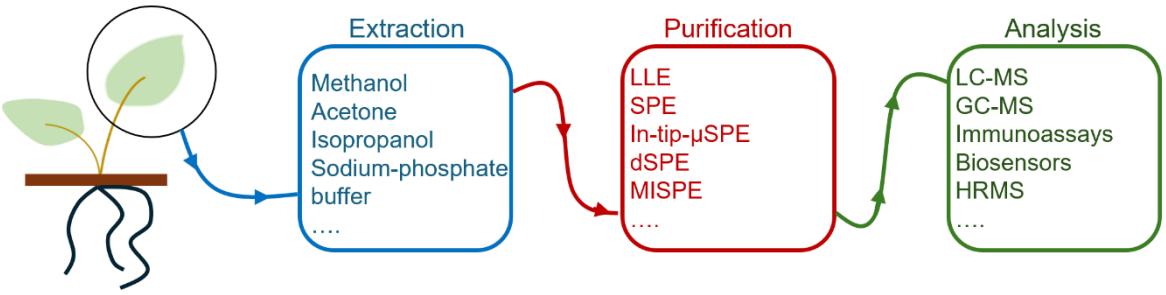

Fig. 7: Scheme of sample preparation and analysis. Plant tissues are harvested and phytohormones extracted in organic or aqueous solutions according to their polarity. Extracts are then purified by a traditional SPE, LLE or by novel miniaturized methods. Prepared samples are then qualitatively or quantitatively analysed. Abbreviations: dSPE, dispersive solid-phase extraction; GC, gas chromatography; HRMS, high resolution mass spectrometry; LC, liquid chromatography; LLE, liquid-liquid extraction; MISPE, molecularly imprinted solid-phase extraction; MS, mass spectrometry; SPE, solid-phase extraction.

Historically, two primary approaches have been employed for auxin purification. The first involves liquid-liquid extraction (LLE), which separates compounds based on their solubility in two

immiscible liquids. However, this method is solvent-intensive and time-consuming, often resulting in low extraction efficiency due to emulsification. Consequently, its popularity in hormone studies has decreased over time (Fu et al., 2011). The second approach is solid-phase extraction (SPE), wherein the analyte is reversibly bound to a solid-phase packed column or cartridge and subsequently released by an elution solvent. Various solid-phase sorbents, ranging from reverse phase to cation/anion exchange, or their combinations, have been utilised, as reviewed in multiple publications (Du et al., 2012; Porfírio et al., 2016; Vrobel and Tarkowski, 2023).

Presently, there is a trend toward miniaturization in a sample preparation. Novel microextraction techniques improve solvent and sample consumption, reduce the number of extraction steps, hasten purification, allow online coupling with analytical instruments, and maintain extraction selectivity and sensitivity (Sajid and Płotka-Wasylka, 2018). For auxin analysis, several techniques based on LLE were employed, such as dispersive liquid-liquid microextraction (Luo et al., 2013) or hollow fiber-based liquid-liquid-liquid microextraction (Wu and Hu, 2009). Numerous other techniques have been derived from SPE, including in-tip micro SPE (Liu et al., 2012; Pěnčík et al., 2018), dispersive solid-phase extraction (dSPE) (Cai et al., 2016), and molecularly imprinted solid-phase extraction (MISPE) (Yan et al., 2012), to name a few.

To enhance extraction recovery, various techniques were employed. Pěnčík et al., (2009) utilised an immunoaffinity columns as an additional step in sample purification following SPE. Conjugates of IAA with bovine serum albumin were used to produce rabbit polyclonal antibodies, which were then immobilized on the surface of the immunoaffinity gel and utilised for sample extract purification. Previously, high performance liquid chromatography (HPLC) was also used as a purification step, although it turned out to be time consuming (Tam et al., 2000; Mravec et al., 2009). Recently, a method for auxin and other phytohormones quantification by liquid-chromatography-tandem mass spectrometry (LC-MS/MS) without purification steps has been developed (Karady et al., 2024), indicating a potential future trend towards abandoning these purification steps through advancements in method sensitivity.

3.7.2 Quantitative analysis

Auxin analysis is predominantly conducted using gas chromatography (GC) and liquid chromatography (LC) coupled to mass spectrometry (MS) due to their high sensitivity and selectivity, making them the gold standard in the field. However, various other analytical methods have also been employed for quantification purposes, including immunoassays (Weiler, 1984), pressurized capillary electrochromatography (Lu et al., 2010), capillary electrophoresis with

electrochemiluminescent detection (Yin et al., 2010), surface plasmon resonance (Wei et al., 2011), and biosensors (Naqvi et al., 2023).

Initially, GC-MS was widely used for plant hormone analysis, wherein samples were separated based on different partition coefficients between the mobile (gaseous) and stationary phases in columns (Wang et al., 2020). However, prior to GC analysis, samples need to be dissolved in the gaseous phase, which poses a challenge for non-volatile auxins and therefore requires a derivatization step. The common derivatization reagent for auxin analysis is diazomethane, yet its toxicity and explosiveness have prompted the exploration of alternative reagents, as comprehensively reviewed in Fu et al. (2011) and Porfírio et al. (2016). Derivatization also serves as a tool for enhancing compound stability, as demonstrated by the derivatization of labile IAA precursors - IPyA and IAAld - using cysteamine (Novák et al., 2012; Pěnčík et al., 2018).

Currently, LC-MS/MS is the most used method for both quantitative and qualitative analysis of auxins due to its efficient separation, rapid speed, and straightforward sample preparation and operation (Vrobel and Tarkowski, 2023). One notable advantage of LC is its ability to directly analyse non-volatile metabolites from the liquid phase without prior derivatization.

The mass spectrometer consists of three main parts: an ion source, a mass analyser and a detector. In phytohormone analysis, electrospray ionization (ESI) is the preferred ionization technique due to its soft ionization and compatibility with polar hormones (Wang et al., 2020). The mass analyser measures the mass-to-charge ratio (m/z) of charged particles (Fu et al., 2011). Advancements in mass spectrometry have led to the use of tandem mass spectrometers for quantitative analysis due to their lower limit of detection and high linearity (Vrobel and Tarkowski, 2023). One such tandem MS is the triple quadrupole, wherein measurement by multiple reaction monitoring (MRM) mode is preferred for auxin analysis (Porfírio et al., 2016). This mode involves selecting a precursor ion in the first quadrupole and further fragmenting it in the collision cell into product ions that pass through the third quadrupole to the analyser (Fu et al., 2011).

For precise quantification of auxin, it is common practice to use the isotope dilution technique (Rittenberg and Foster, 1940). This technique allows for the correction of errors that may arise from sample extraction, purification, and ionization. Therefore, it is necessary to use a chemically and structurally analogous IS to the measured analytes. Typically, stable isotopically labelled IS, such as ^{2}H, ^{13}C, or ^{15}N, are used (Novák et al., 2014). However, when preparing or using these analogues, it is important to consider various factors. These include ensuring a sufficient m/z difference and potential forward shift in retention time in reverse-phase chromatography due to multiple ^{2}H atoms in the molecule (Vrobel and Tarkowski, 2023).

Auxin metabolic profiling is a complex subject due to the wide concentration range of IAA metabolites in plants, different acidity and basicity, and the instability of some metabolites during

sample preparation (Novák et al., 2014). Therefore, methods developed for this profiling must address these issues while maintaining extraction efficiency, analyte recovery, and matrix effect suppression. Several LC-MS/MS methods are currently available to measure the entire low-molecular-weight auxin metabolome from less than 10 mg of plant tissue (Pěnčík et al., 2018; Hayashi et al., 2021). However, to gain a better understanding of auxin metabolism, it is necessary to measure specific parts of plant tissues. This has already been initiated through IAA and oxIAA measurement in various cell types in the root tip (Petersson et al., 2009; Pěnčík et al., 2013) or metabolite profiling in subcellular organelles (Skalický et al., 2023).

3.7.3 Auxin identification

Over the past century significant progress has been made in our understanding of auxin metabolism and biosynthesis. This advancement can be attributed to the discovery of new endogenous auxins and their metabolites. Identification methods have evolved from thin-layer chromatography and electrophoresis to more sensitive mass spectrometry techniques since the initial description of the structure of IAA by Kögl and Haagen-Smit, (1931).

The widespread adoption of GC-MS and LC-MS techniques in in numerous laboratories has enabled simpler identification of auxin metabolites in plants. This typically involves *in vitro* synthesis of predicted metabolites, followed by measurement of these standards and subsequent comparison of chromatograms with those from plant extracts (Plüss et al., 1989; Pěnčík et al., 2009; Sugawara et al., 2015). Kowalczyk and Sandberg, (2001) took an alternative approach by fractionating sample extracts using HPLC and subjecting each sample to full scan analysis. The resulting data were then used as a database for screening indole fragments in mass spectra. Similarly, Kai et al., (2007a) employed the MRM technique to search for oxidative metabolites of IAA in Arabidopsis extracts. The authors initially analysed the mass fragmentation spectra of established compounds and subsequently created a screening technique to detect new amide and oxidative metabolites. They successfully identified 6-OH-IAA-Val and 6-OH-IAA-Phe in plants for the first time. Finally, Kai et al., (2007b) utilised strong alkaline hydrolysis to liberate free IAA from metabolites in a sample extract. It was assumed that all IAA metabolites would produce a quinolinium ion at m/z 130 (in ESI+ ionisation), allowing for the detection of over 20 compounds, including unidentified N-glucosides such as IAA-*N*-glc amides.

In plant metabolomics, there is a current trend towards measuring the entire metabolome through untargeted mass spectrometry analysis (Manickam et al., 2023). This approach enables straightforward metabolite comparison between plant species or tissues, elucidates metabolic plant responses to biotic or abiotic stress, and aids in the identification of novel metabolites and

signalling pathways. High-resolution mass spectrometry has primarily been used as a tool for auxin structural analysis (Revelou et al., 2019), however this approach has already enabled the identification of several brassinosteroids from the plant metabolome (Xin et al., 2016; Xiong et al., 2022). In the future, this methodology could improve our understanding of auxin metabolism and biosynthesis by simple identification of the new compounds. However, the sensitivity of high-resolution mass spectrometers is lower than that of triple quadrupole instruments (Nováková, 2013), making the detection of low-abundance phytohormones challenging.

4 Material and methods

The detailed information about employed methods and equipment parameters is presented in research papers attached in the Supplementary section (*Supplements I – IV*).

4.1 Chemicals

- Plant agar and Murashige & Skoog media were purchased from Duchefa (Haarlem, Netherlands); hypergrade purity methanol and acetonitrile for LC-MS/MS analysis and all other chemicals were purchased from Merck (Darmstadt, Germany), Sigma-Aldrich (MA, USA), and Lach-Ner (Neratovice, Czech Republic).
- Auxin standards and analogues were purchased from OlChemIm (Olomouc, Czech Republic) or synthesized by colleagues from Department of Chemical biology (Faculty of Science, Palacký University in Olomouc) (*Supplement I-IV*). Isotopically labelled auxin standards were purchased from Cambridge Isotope Laboratories, Inc (MA, USA).

4.2 Plant material and growth conditions

- *Arabidopsis thaliana* seeds ecotype Columbia-0 were used as a wild type in all experiments.
- Arabidopsis knockout mutant lines with alterations in auxin metabolism - GH3 sextuple *gh3.1,2,3,4,5,6* (Porco et al., 2016); GH3 octuple *gh3.1,2,3,4,5,6,9,17* (Casanova-Saéz et al., 2022); *ugt74d1* and *ugt84b1* (Mateo-Bonmatí et al., 2021). (*Supplement II*)
- Other cultivated plant species *(Supplements I, II)*: maize (*Zea mays* L.), pea (*Pisum sativum arvense* L.), wheat (*Triticum aestivum* L.), moss (*Physcomitrella patens*), and spruce (*Picea abies* L. Karst).
- Arabidopsis seeds were sterilized in 70% ethanol with the addition of 0.1% Tween 20 for 5 min sown on Murashige & Skoog medium in square agar plates (10 g sucrose, 2.2 g MS medium, 10 g agar, pH 5.7, all amounts are per litre) and cold treated for 4 days prior to germination. The plates were then transferred to a cultivation chamber and vertically placed under long-day conditions (16 h light/8 h dark) at 22 ± 1°C under cool white fluorescent light (maximum irradiance 550 µmol m^{-2} s^{-1}).
- Pea, wheat, and maize seeds were left germinating in wet conditions in the dark for 2, 3, and 4 days, respectively, selected according to their uniformity from a large population, transferred to hydroponic boxes, watered with Hoagland's solution and left growing in the cultivation room (16 h light/8 h dark) at 22 ± 2°C, while changing the solution every 3 days.

- Spruce seeds were soaked in the tap water for 24 h at 4°C and sown in a wet vermiculite. Germination and seedling growth occurred in a growth chamber under long-day conditions (16 h light/8 h dark) at 22 ± 2°C.
- Gametophores from *P. patens* were cultured on round Petri plates (Knop medium, pH 5.8, 1.5% plant agar). The plates with gametophores were transferred to a cultivation chamber and vertically placed under long-day conditions (16 h light/8 h dark) at 22 ± 1°C. Each 3 weeks, gametophores were moved to a fresh medium.
- For auxin metabolite profiling, all plant species were harvested in the growth stage 1.0 according to *Biologische Bundesanstalt, Bundessortenamt und Chemische Industrie* (BBCH) scale (Tottman, 1987; Lancashire et al., 1991; Boyes et al., 2001), except for *P. patens* which was harvested 3 weeks after the last transfer to fresh medium.

4.3 Methods

A detailed description of the applied methods and instruments is given in *Supplements I-IV*.

4.3.1 Extraction and purification

- For auxin metabolite profilling, ≈ 10 mg FW of plant tissues was harvested and extracted in 1 ml of sodium-phosphate buffer (50 mM, pH 7.0, 4°C) containing 0.1% diethyldithiocarbamic acid sodium salt. The extracts were then purified by in-tip µSPE (Pěnčík et al., 2018) (with modifications outlined in *Supplements I and II*) and evaporated to dryness *in vacuo*. To cover analytes lost during sample preparation, a mixture of isotopically labelled standards was added prior to extraction.
- Plant extracts from Arabidopsis tissues for all measured auxin analogues were prepared by an one-step LLE utilizing a water:methanol/acetonitrile:hexane (1:1:1) solution. The water:methanol/acetonitrile fraction was filtered through MicroSpin tubes (0.2 µm, nylon, Chromservis, Czech Republic) and flow-through fraction was then evaporated *in vacuo*. (*supplements III, IV*)

4.3.2 LC-MS/MS

- For measurement of IAA, PAA and their metabolic profiles, a HPLC 1260 Infinity II system and a 6495B Triple Quadrupole LC/MS system equipped with Jet Stream and Dual Ion Funnel systems (Agilent Technologies, CA, USA) were employed. A reverse-phase column (Kinetex C18 100 Å, 50 x 2.1 mm, 1.7 µm; Phenomenex, CA, USA) was used to separate the compounds. The time of

each analysis was 18 min, the flow rate was 0.3 mL/min, and metabolites were eluted with a linear gradient as follows: 0 min – 10% B, 11.5 min – 60% B, 11.75 min – 100% B, 14.75 min – 100% B, 15 min – 10% B. Analytes were detected and quantified using diagnostic MRM transitions of precursor and appropriate product ions. The concentrations of all compounds were then calculated by the isotopic dilution method using corresponding stable isotope labelled standards. LC-MS/MS analysis as well as data processing were performed using Mass Hunter software (Agilent Technologies, CA, USA). (*Supplements I and II*)

- Development of LC-MS/MS method for the analysis of newly synthesized NBD or 5-(dimethylamino)naphthalene-1-sulfonyl (DNS) labelled auxin analogues was performed on an Acquity UPLC® I-Class System (Waters, USA) coupled to a triple quadrupole mass spectrometer Xevo™ TQ-S MS (Waters MS Technologies, UK). A reverse-phase column (Kinetex C18 100 Å, 50 x 2.1 mm, 1.7 µm; Phenomenex, CA, USA) was used for LC compound separation. The mobile phase consisted of acetonitrile (A) and deionized water (B), both with the addition of 0.1% acetic acid. The duration of each analysis was 5.5 min, flow rate 0.3 mL/min and gradient elution as follows: 0 min – 60% B, 3.0 min – 30% B, 4.25 min – 99% B, 4.5 min – 99% B, 5.5 – 60% B. For compound quantification, Arabidopsis extracts were spiked with 1 nmol of NBD- or DNS-labelled conjugates and samples were processed by LLE as described above. To calculate analytes losses and matrix effects, a six-point external calibration curve ranging from 1 fmol to 100 pmol in 10% acetonitrile was measured and the recovery factor of each analyte was calculated. For samples with unknown conjugates levels, dilution and recovery factors were applied and concentration was calculated from an external calibration curve. (*supplement III*)
- Auxinole and methyl 2-(1H-indol-3-yl)-4-oxo-4-p-tolyl-butanoate (4pTb-MeIAA) were measured on a HPLC 1260 Infinity II system and a 6495B Triple Quadrupole LC/MS system (Agilent Technologies, CA, USA). The chromatographic reverse-phase column (Kinetex C18 100 Å, 50 x 2.1 mm, 1.7 µm; Phenomenex, CA, USA) was employed for analytes separation. The analysis time was 13 min, the flow rate was 0.3 mL/min, and the mobile phase consisted of deionized water (A) and methanol (B), both with the addition of 0.1% acetic acid. Gradient elution was set as follows: 0 min – 40% B, 9 min – 95% B, 9.25 min – 99% B, 10 min – 99% B, 10.50 min – 40% B. For metabolites quantification, the same method as described in the previous paragraph was applied. (*Supplement IV*)

5 Survey of results

The methodical part of this work builds upon the results obtained in the master's thesis, where the LC-MS/MS method was developed for measuring the IAA and PAA metabolic profiles (Hladík, 2020). By utilizing this method, we made a groundbreaking discovery: two new oxIAA conjugates, namely 2-oxindole-3-acetyl-leucine (oxIAA-Leu) and 2-oxindole-3-acetyl-phenylalanine (oxIAA-Phe), were identified in plants for the first time. We further measured low-molecular-weight IAA metabolites, with a specific focus on oxIAA conjugates, in the organs of four representative monocotyledonous and dicotyledonous plants at different developmental stages. This investigation aimed to enhance our understanding of auxin metabolism during plant growth (*Supplement I*).

In our exploration of PAA metabolites, we identified four new conjugates: phenylacetyl-leucine (PAA-Leu), phenylacetyl-phenylalanine (PAA-Phe), phenylacetyl-valine (PAA-Val) and PAA-glc (*Supplement II*). The concentrations of these new conjugates with other known PAA metabolites were then screened at the organ level in various plants species. To gain insights into novel PAA metabolic pathways, we concluded feeding experiments with PAA using Arabidopsis mutant lines defective in auxin metabolic regulation. Additionally, we employed kakeimide (KKI), a selective inhibitor of GH3 proteins (Fukui et al., 2022), in conjunction with PAA treatments in Arabidopsis, spruce and moss. These experiments allowed us to monitor metabolic redundancy in other plant species where mutant lines were not available.

Synthetic auxins play a crucial role in auxin homeostasis research. Many of these molecules have anti-auxin activity by binding to the TIR1/AFB receptor, yet they do not trigger typical auxin responses (Hayashi et al., 2012). This group of synthetic auxins includes compounds such as auxinole and its analogues (*Supplement IV*), as well as fluorescently labelled synthetic anti-auxins (*Supplement III*). Notably, these molecules have different chemical structures compared to endogenous auxins, necessitating the development and optimization of novel extraction and MS-based methods. This task was particularly challenging task due to their varying polarity, size and stability. Importantly, the newly developed methods have enabled us to study the stability and uptake of selected synthetic auxins in treated plants (*Supplements III, IV*).

5.1 2-oxindole-3-acetyl-amino acids are important auxin metabolites in plants

Recently, many studies describing the synthesis and hydrolysis of 2-oxindole-3-acetyl-amino acids (oxIAA-AAs) have been published (Hayashi et al., 2021; Müller et al., 2021; Isobe and Miyagawa, 2022). However, their distribution and importance in auxin metabolism have not been determined.

Therefore, we employed a previously developed in-tip µSPE purification method (Pěnčík et al., 2018) and subsequent LC-MS/MS analysis, to quantify oxIAA-AAs in multiple plant species and their organs, and compare their levels with other IAA metabolites. This method was subsequently optimised and validated for full IAA metabolite profiling, including oxIAA-AAs (Hladík, 2020). Due to the low detection limit of the LC-MS/MS method, optimised MRM transitions for oxIAA-Leu and oxIAA-Phe were added (*Supplement I*, Tab. S2) and their occurrence screened in organs of different plant species (*Supplement I*, Fig. 2). Their endogenous concentrations were observed in pea cotyledons and oxIAA-Phe also in maize cotyledons, however both at low levels, corresponding to low abundance of their IAA counterparts (*Supplement I*, Fig. 3) (Kowalczyk and Sandberg, 2001; Pěnčík et al., 2009).

Employing the LC-MS/MS method, we performed profiling of IAA metabolite in roots, shoots and cotyledons of pea, wheat and maize, and only in roots and shoots of Arabidopsis due to the large amount of plant material required and the technical difficulties of cotyledon harvesting (*Supplement I*, Fig. 3). To make the metabolic profile of various species as comparable as possible, we harvested plants at growth stage 1.0, according to the BBCH scale, which was developed to compare between species according to their phenotype (Tottman, 1987; Lancashire et al., 1991; Boyes et al., 2001). All of IAA-AAs and oxIAA-AAs were combined into an appropriate group and their relative (%) abundance to the total IAA pool was calculated. This profiling revealed significant difference in dominant conjugates and metabolic pathways between plant species and even their tissues (*Supplement I*, Fig. 4). In Arabidopsis organs, most of the IAA was found in the form of oxIAA-glc, followed by oxIAA, demonstrating the importance of this pathway. On the other hand, in pea, oxIAA-AAs were completely dominant, as in cotyledons, oxIAA-Asp forms > 99% of the total IAA pool. Furthermore, we quantified the IAA metabolome in seeds of the same species, which were allowed to germinate for 24 hours under wet conditions (Tab. 1). Interestingly, our results indicate higher levels of free IAA in these seeds compared to cotyledons at growth stage 1.0, suggesting a potential contribution of free IAA to seed germination (*Supplement I*, Tab. S5). Conversely, levels of IAA conjugates were lower in seeds, implying that cotyledons may serve as a reservoir for auxin during later developmental stages.

In plants, auxin metabolism is an ever-changing process depending on the development and environmental conditions. To address these changes during plant development, we measured plants and their tissues in the three growth stages 1.0, 1.1 and 1.2 according to BBCH scale. These stages show early seedling development from the first leaf emergence to two fully developed leaves in stage 1.2 (*supplement I*, Fig. S1; Tab. S1). In all crop species, higher auxin concentrations were found in roots compared to shoots at all growth stages (*Supplement I*, Fig. 5). Amide-linked conjugates were more prevailed in earlier stages and steadily decreased, in contrast to oxIAA-glc in

monocots roots, which increased during growth. In conclusion, IAA metabolites levels are strongly dependent on plant development, which contributes to the proper auxin balance.

Tab. 1: IAA metabolite profiles in seeds of maize, wheat, and pea. Levels (pmol/g FW) of IAA, oxIAA and their conjugates with amino acids and glucose were determined in seeds of maize, wheat and pea after being left to germinate in moist conditions for 24 hours. The levels of IAA and oxIAA conjugates with individual amino acids (Asp, Glu, Leu and Phe) were summed up into two corresponding groups IAA-AA and oxIAA-AA, respectively. The distribution (%) of different conjugate classes was calculated as their relative abundance to the total measured IAA metabolite pool (%). All samples were measured in five biological replicates. <LOD, under the limit of detection.

	Maize		**Wheat**		**Pea**	
	(pmol/g)	(%)	(pmol/g)	(%)	(pmol/g)	(%)
IAA	6 858.6	27.31	119.5	63.14	19.2	0.01
IAA-AA	287.8	0.00	30.7	16.24	710.2	0.30
IAA-glc	<LOD	-	<LOD	-	<LOD	-
oxIAA	17 311.9	68.94	39.0	20.62	170.0	0.07
oxIAA-AA	297.0	1.18	<LOD	-	238 191.5	99.62
oxIAA-glc	356.5	1.42	<LOD	-	<LOD	-

More information is provided in *Supplement I* - **Hladík P.**, Petřík I., Žukauskaitė A., Novák O., Pěnčík A. (2023) Metabolic profiles of 2-oxindole-3-acetyl-amino acid conjugates differ in various plant species. *Front. Plant Sci.* **14**, 1217421.

5.2 Unravelling novel metabolic pathways in PAA metabolism

In the field of auxin research, most attention has been dedicated to studying IAA owing to its high activity in auxin bioassays. Nevertheless, emerging evidence suggests that other auxins, such as PAA, which exhibits approximately 10% of the activity of IAA in these tests, may also play crucial roles in plant development. Numerous studies suggest that PAA contributes to processes such as lateral root development, antimicrobial activity and auxin crosstalk (reviewed in Perez et al., 2023). Despite sharing similarities in conjugation pathways with IAA, including involvement of the same enzymes, information regarding PAA metabolism remains limited (Sugawara et al., 2015; Westfall et al., 2017; Aoi et al., 2020c). We therefore aimed to elucidate novel conjugates and metabolic pathways associated with PAA metabolism (Fig. 8).

The extraction and LC-MS/MS methods developed for the profiling of IAA metabolites were also optimized and validated also for PAA metabolite profile (Hladík, 2020). Utilizing this method, we identified four new PAA conjugates: PAA-Leu, PAA-Phe, PAA-Val and PAA-glc (*Supplement II*, Fig. 2; Fig. 3). Although *in vitro* synthesis of PAA-glc has been reported previously (Aoi et al., 2020c), we provide the first evidence of its presence in Arabidopsis and spruce tissues (*Supplement II*, Fig. 2C).

Furthermore, we conducted bacterial enzymatic assays with AtUGT84B1 and AtUGT74D1 expressed in *Escherichia coli* to investigate their conjugation activity towards PAA (*Supplement II*, Fig. 2E). Our findings demonstrate that both enzymes are capable of forming PAA-glc *in vitro*. Finally, this was also confirmed in Arabidopsis *ugt74d1* and *ugt84b1* knockout lines, which exhibited reduced concentrations of PAA-glc compared to wild type Columbia-0 (*Supplement II*, Fig. 2D).

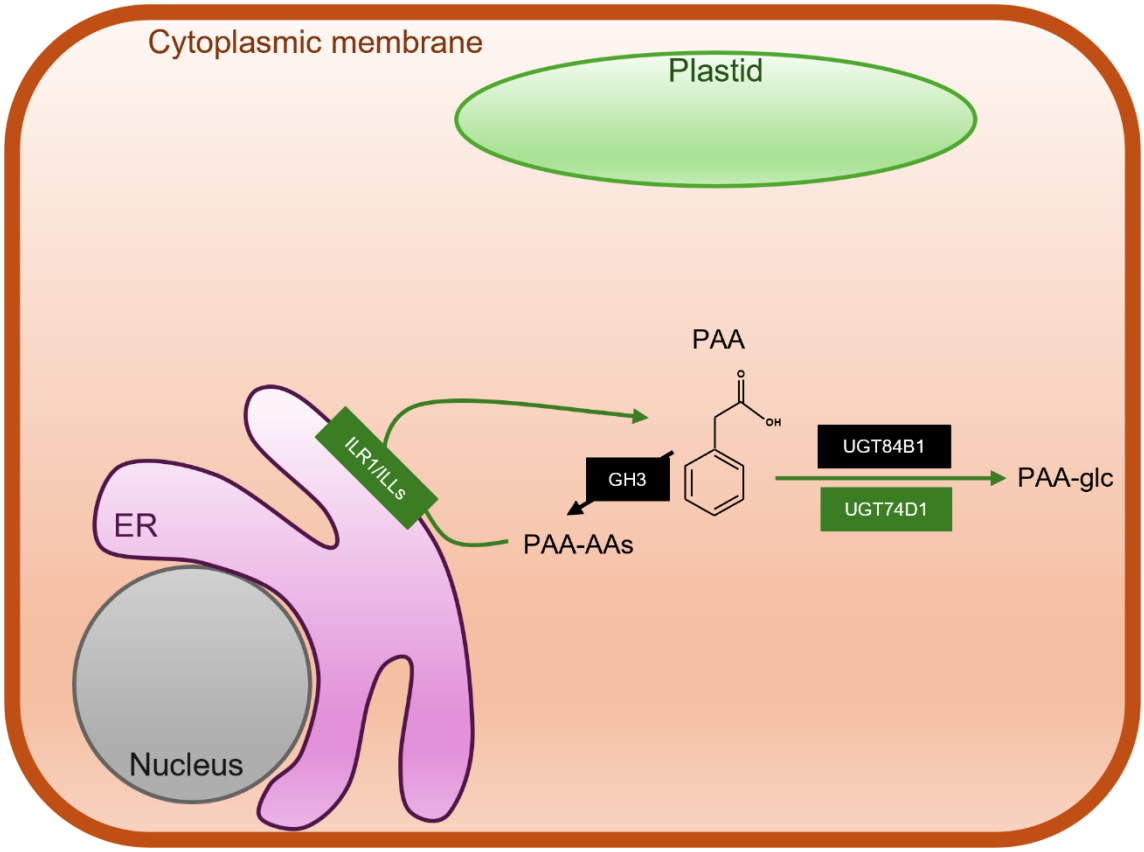

Fig. 8: Scheme of PAA metabolism. Black arrows combined with enzyme names (white text in a black box) represent previously known metabolic pathways. Green arrows and boxes with enzyme names indicate the newly described pathways presented in *Supplement II*. Abbreviations: ER, endoplasmic reticulum; PAA, phenylacetic acid; PAA-AAs, phenylacetyl-amino acids; PAA-glc, phenylacetyl-1-O-ß-d-glucose; UGTs, uridine 5'-diphospho-glucuronosyltransferases.

Similar experiments were also performed for the newly identified PAA-AAs. These metabolites were detected in all pea tissues and also in wheat cotyledons, although at concentrations not surpassing 8 pmol/g FW (*Supplement II*, Fig. 3B). These low concentrations mirror those of their IAA and oxIAA relatives. The potential for their synthesis in Arabidopsis was examined through PAA treatment, revealing their formation even after 30 minutes (*Supplement II*, Fig. 3C). However, their levels did not show significant increases over time, indicating rapid turnover. While the involvement of GH3 enzymes in PAA-Glu and PAA-Asp synthesis has been previously published (Sugawara et al., 2015; Staswick et al., 2017), our study demonstrates that these enzymes also form other PAA-AAs

(*Supplement II*, Fig. 3D). Although the hydrolysis of IAA-AAs back to IAA has been documented (Bartel and Fink, 1995; Hayashi et al., 2021), such a process has not been investigated for PAA-AAs. Utilizing bacterial enzyme assays with AtIAR3, AtILL2, AtILL6 and AtILR1 enzymes cloned in *E. coli*, we confirmed that PAA-Glu, PAA-Leu, PAA-Trp and PAA-Val can serve as substrates for these enzymes and then release free PAA (*Supplement II*, Fig. 3E). Overall, our findings confirm that PAA undergoes metabolic processes similar to IAA.

Previous studies have extensively measured PAA levels in diverse plant species and their tissues (reviewed in Perez et al., 2023), however our understanding of PAA metabolism is largely restricted to Arabidopsis. Therefore, we conducted a comprehensive analysis of known PAA metabolites across six species spanning from Eudicots to Bryophyta (*Supplement II*, Tab. 1). Our findings showed that PAA-AA formation is the dominant metabolic pathway in all species except spruce. Conversely, in spruce, PAA glycosylation emerges as the preferred metabolic pathway.

To further elucidate the complementarity of these two metabolic pathways, we utilised Arabidopsis knockout lines *gh3.1,2,3,4,5,6* and gh3.*1,2,3,4,5,6,9,17*, which lack the formation of amino acid conjugates depending on GH3 activity. It was hypothesised that a metabolic shift towards other conjugates would be induced after PAA treatment. This was successfully observed by blocking PAA-Asp synthesis in both lines, as there was no significant increase after PAA treatment (*Supplement II*, Fig. 4B). However, higher levels of PAA-Glu were detected in *gh3* mutant lines compared to WT Col-0 (*Supplement II*, Fig. 4C). This indicates GH3-independent synthesis of PAA-AA conjugates or the potential that these mutant lines are not null expressing lines, which is consistent with findings regarding IAA conjugates (Casanova-Sáez et al., 2022). Despite the increases in PAA levels, PAA-glc concentrations remained unaltered compared to WT Col-0, suggesting no compensation in Arabidopsis (*Supplement II*, Fig. 4A, 4D). To validate this lack of complementarity in other species, we employed the selective GH3 inhibitor KKI (Fukui et al., 2022). Our results demonstrated a similar trend in spruce and Arabidopsis, with significant differences observed in PAA-AA levels between PAA alone or PAA+KKI treatments. Interestingly, no difference in PAA-glc levels was noted (*Supplement II*, Fig. 5A, B). On the other hand, KKI did not prevent IAA-Asp synthesis in *P. patens*, raising questions about species-specific differences in GH3 enzymes (*Supplement II*, Fig. 5C). Moreover, PAA-glc was not detected in the moss even after PAA treatment, suggesting the inability to synthesize this conjugate. In conclusion, our data contribute to a better understanding of PAA metabolism in plants, but also highlight the potential significance of other as-yet-undiscovered metabolic pathways.

More information is provided in *Supplement II* - **Hladík P.**, Brunoni F., Žukauskaitė A., Zatloukal M., Novák O., Pěnčík A. (2023) Phenylacetic acid metabolism in plants: unravelling novel pathways and metabolites by liquid chromatography-mass spectrometry analysis. (In preparation)

5.3 Method development for novel synthetic auxin derivatives

Over the past decades, numerous synthetic hormone analogues, encompassing agonists, antagonists or fluorescently labelled compounds, have been utilized (Jiang and Asami, 2018). These analogues serve as invaluable tools for investigating auxin distribution and signalling pathways. To facilitate these studies, several novel NBD- or DNS-labelled IAA derivatives were prepared (*Supplement III*). Remarkably, DNS-labelled molecules exhibited the capacity to impede IAA signalling by downregulating the expression of early responsive auxin genes. To validate the uptake of these compounds and their stability in planta, an extraction protocol and an LC-MS/MS method were developed.

The chosen extraction protocol employed LLE with a solvent mixture of water:acetonitrile:hexane (1:1:1) (*Supplement III*, Tab. S2). This extraction method, previously proven to be effective for the extraction of fluorescently labelled auxin analogues (Pařízková et al., 2021), was adapted and optimized for the current study. Subsequently, an LC-MS/MS method was developed involving the optimization of LC and MS conditions for each compound (*Supplement III*, Tab. S1). The efficacy of this method was then demonstrated by measuring the uptake of new fluorescent auxin derivatives by Arabidopsis plants after a 30-min treatment (*Supplement II*, Fig. 7C). Similarly, their stability was assessed after 1, 3 and 6 h of treatment (*Supplement II*, Fig. S1). Overall, these studies revealed a good uptake of all compounds by Arabidopsis roots, albeit with poor stability observed over longer treatment durations, suggesting their suitability for short-term experimental applications.

More information is provided in *Supplement III* - Bieleszová K., **Hladík P.**, Kubala M., Napier R., Brunoni F., Gelová Z., Fiedler L., Kulich L., Strnad M., Doležal K., Novák O., Friml J., Žukauskaitė A. (2024) New fluorescent auxin derivatives: anti-auxin activity and accumulation patterns in *Arabidopsis thaliana*. Plant Growth Regul. 102, 589-602.

The structural similarity of synthetic auxin analogues poses a challenge for their separation and highlights the need for innovative analytical approaches. To address this, we employed desorption electrospray ionization coupled with ion mobility mass spectrometry imaging (DESI-IM-MSI) to visualize and separate selected isomers. Specifically, two isomers, auxinole and 4pTb-MeIAA, were administered to Arabidopsis plants, quantified using DESI-IM-MSI and LC-MS/MS techniques, and the results obtained were compared.

Therefore, we developed and optimized LLE protocols and LC-MS/MS methods for both compounds (*Supplement IV*, Tab. S1; Tab. S2). Subsequently, administered to Arabidopsis plants were treated with auxinole and 4pTb-MeIAA, and their levels were measured using LC-MS/MS or

DESI-MSI with or without ion mobility separation (*Supplement IV,* Fig. 9). Additionally, IAA metabolic profiles were also analysed using these MS-based techniques, with quantification performed either in picomoles per gram fresh weight (pmol/g FW) or by calculating the area under the curve for the chromatographic peaks of each analyte (*Supplement IV*, Tab. S4). These quantitative data were then compared across all three MS methods (*Supplement IV*, Fig. S4). Ultimately, DESI-IM-MSI emerged as a promising technique for isomer separation that offers high spatial resolution imaging of low-molecular-weight compounds from tissues such as Arabidopsis roots.

More information is provided in *Supplement IV* - Zhang C., Bieleszová K., Žukauskaitė A., **Hladík P.**, Grúz J., Novák O., Doležal K. (2024) In situ separation and visualization of isomeric auxin derivatives in Arabidopsis by ion mobility mass spectrometry imaging. Anal Bioanal Chem. 416(1), 125-139.

6 Conclusion and future perspectives

This doctoral thesis aims to broaden our understanding of auxin metabolism in various plant species and their organs. Through the application of LC-MS/MS methods, several novel conjugates of two auxins, IAA and PAA, together with their metabolic pathways, were identified. Additionally, the development of extraction and detection methods for newly synthesized synthetic auxins with anti-auxin activity enabled the measurement of their uptake and stability *in planta*.

The key results obtained in this thesis include the following:

- Utilizing the LC-MS/MS detection methods, novel oxIAA and PAA amino acid conjugates were identified for the first time *in planta*.
- Analysis of auxin metabolic profiles in organs of various plant species at different growth stages facilitated the elucidation of dominant metabolic pathways during seedlings development.
- The enzymes responsible for PAA conjugation with amino acids and glucose *in planta* have been characterised. Moreover, the interrelationship of these metabolic pathways was explored in Arabidopsis, spruce and moss, indicating the potential existence of additional unexplored pathways.
- New extraction and LC-MS/MS methods were developed for NBD- and DNS-labelled auxins with anti-auxins activity and employed to measure their stability and uptake by Arabidopsis roots.
- A new DESI-IM-MSI method was developed for *in situ* imaging of two synthetic auxin isomers, auxinole and 4pTb-MeIAA. Quantitative results were then compared with a conventional LC-MS/MS approach, highlighting the potential of high spatial resolution imaging of low-molecular-weight compounds by the DESI-IM-MSI.

In summary, the results presented in this thesis should help to understand auxin homeostasis in plants as well as their organs and cells. In the future, follow-up experiments could explore whether these novel metabolites and biosynthetic pathways play roles in plant responses to environmental stimuli, such as biotic or abiotic stresses. Additionally, considering the insights gained from measuring PAA metabolism complementarity, further screening for additional PAA conjugates should be performed.

7 References

Adamowski M., Friml J. (2015) PIN-dependent auxin transport: Action, regulation, and evolution. *Plant Cell*. **27**(1), 20–32.

Adamowski M., Li L., Friml J. (2019) Reorientation of Cortical Microtubule Arrays in the Hypocotyl of Arabidopsis thaliana Is Induced by the Cell Growth Process and Independent of Auxin Signaling. *Int J Mol Sci*. **20**(13), 3337.

Aoi Y., Oikawa A., Sasaki R., Huang J., Hayashi K., Kasahara H. (2020a) Arogenate dehydratases can modulate the levels of phenylacetic acid in Arabidopsis. *Biochem Bioph Res Co*. **524**(1), 83–88.

Aoi Y., Tanaka K., Cook S. D., Hayashi K. I., Kasahara H. (2020b) GH3 Auxin-Amido Synthetases Alter the Ratio of Indole-3-Acetic Acid and Phenylacetic Acid in Arabidopsis. *Plant Cell Physiol*. **61**(3), 596–605.

Aoi Y., Hira H., Hayakawa Y., Liu H., Fukui K., Dai X., Tanaka K., Hayashi K., Zhao Y., Kasahara H. (2020c) UDP-glucosyltransferase UGT84B1 regulates the levels of indole-3-acetic acid and phenylacetic acid in Arabidopsis. *Biochem Bioph Res Co*. **532**(2), 244–250.

Barbez E., Kleine-Vehn J. (2013) Divide Et Impera--cellular auxin compartmentalization. *Curr Opin Plant Biol*. **16**(1), 78–84.

Barkawi L. S., Tam Y. Y., Tillman J. A., Normanly J., Cohen J. D. (2010) A high-throughput method for the quantitative analysis of auxins. *Nat Protoc*. **5**(10), 1609–1618.

Bartel B., Fink G. R. (1995) ILR1, an amidohydrolase that releases active indole-3-acetic acid from conjugates. *Science*. **268**(5218), 1745–1748.

BeMiller J. N., Colilla W. (1972) Mechanism of corn indole-3-acetic acid oxidase in vitro. *Phytochemistry*. **11**(12), 3393–3402.

Bennett M. J., Marchant A., Green H. G., May S. T., Ward S. P., Millner P. A., Walker A. R., Schulz B., Feldmann K. A. (1996) Arabidopsis AUX1 gene: a permease-like regulator of root gravitropism. *Science*. **273**(5277), 948–950.

Bentley R. (1990) The shikimate pathway--a metabolic tree with many branches. *Crit Rev Biochem Mol Biol*. **25**(5), 307–384.

Bialek K., Cohen J. D. (1986) Isolation and partial characterization of the major amide-linked conjugate of indole-3-acetic acid from Phaseolus vulgaris L. *Plant Physiol*. **80**, 99–104.

Bieleszová K., Pařízková B., Kubeš M., Husičková A., Kubala M., Ma Q., Sedlářová M., Robert S., Doležal K., Strnad M., Novák O., Žukauskaitė A. (2019) New fluorescently labeled auxins exhibit promising anti-auxin activity. *New Biotechnol*. **48**, 44–52.

Bohm B. A. (1965) Shikimic acid (3,4,5-trihydroxy-1-cyclohexene-1-carboxylic acid). *Chem Rev*. **65**, 435–466.

Bouchard R., Bailly A., Blakeslee J. J., Oehring S. C., Vincenzetti V., Lee O. R., Paponov I., Palme K., Mancuso S., Murphy A. S., Schulz B., Geisler M. (2006) Immunophilin-like TWISTED DWARF1 modulates auxin efflux activities of Arabidopsis P-glycoproteins. *J Biol Chem.* **281**, 30603–30612.

Boyes D. C., Zayed A. M., Ascenzi R., McCaskill A. J., Hoffman N. E., Davis K. R., Görlach J. (2001) Growth stage-based phenotypic analysis of Arabidopsis: a model for high throughput functional genomics in plants. *Plant Cell*. **13**(7), 1499–1510.

Boysen-Jensen P. (1911) La transmission de l'irritation phototropique dans l'avena. *Bulletin Academie des Sciences et Lettres de Montpellier*. **3**, 1–24.

Boysen-Jensen P. (1913) Uber die Leitung des phototropischen Reizes in der Avenakoleoptile. *Berichte der Deutschen Botanischen Gesellschaft*. **31**, 559–566.

Brunoni F., Collani S., Simura J., Schmid M., Bellini C., Ljung K. (2019) A bacterial assay for rapid screening of IAA catabolic enzymes. *Plant Methods*. **15**, 126.

Brunoni F., Pěnčík A., Žukauskaitė A., Ament A., Kopečná M., Collani S., Kopečný D., Novák O. (2023) Amino acid conjugation of oxIAA is a secondary metabolic regulation involved in auxin homeostasis. *New Phytol*. **238**, 2264–2270.

Cai W., Ye T., Wang Q., Cai B., Feng Y. (2016) A rapid approach to investigate spatiotemporal distribution of phytohormones in rice. *Plant Methods*. **12**(1), 47–57.

Calderón Villalobos L. I., Lee S., De Oliveira C., Ivetac A., Brandt W., Armitage L., Sheard L. B., Tan X., Parry G., Mao H., Zheng N., Napier R., Kepinski S., Estelle M. (2012) A combinatorial TIR1/AFB-Aux/IAA co-receptor system for differential sensing of auxin. *Nat Chem Biol*. **8**, 477–485.

Casanova-Sáez R., Mateo-Bonmatí E., Ljung K. (2021) Auxin Metabolism in Plants. *CSH Perspect Biol*. **13**(3), a039867.

Casanova-Sáez R., Mateo-Bonmatí E., Šimura J., Pěnčík A., Novák O., Staswick P., Ljung K. (2022) Inactivation of the entire Arabidopsis group II GH3s confers tolerance to salinity and water deficit. *New Phytol*. **235**, 263–275.

Chen J. G., Ullah H., Young J. C., Sussman M. R., Jones A. M. (2001) ABP1 is required for organized cell elongation and division in Arabidopsis embryogenesis. *Gene Dev*. **15**, 902–911.

Chen Q., Dai X., De-Paoli H., Cheng Y., Takebayashi T., Kasahara H., Kamiya Y., Zhao Y. (2014) Auxin Overproduction in Shoots Cannot Rescue Auxin Deficiencies in Arabidopsis Roots. *Plant Cell Physiol*. **55**(6), 1072–1079.

Chiu L., Heckert M. J., You Y., Albanese N., Fenwick T., Siehl D. L., Castle L. A., Tao Y. (2018) Members of the GH3 Family of Proteins Conjugate 2,4-D and Dicamba with Aspartate and Glutamate. *Plant Cell Physiol*. **59**(11), 2366–2380.

Cho M. H., Corea O. R. A., Yang H., Bedgar D. L., Laskar D. D., Anterola A. M., Moog-Anterola F. A., Hood R. L., Kohalmi S. E., Bernards M. A., Kang C., Davin L. B., Lewis N. G. (2007) Phenylalanine biosynthesis in Arabidopsis thaliana. Identification and characterization of arogenate dehydratases. *J Biol Chem*. **282**(42), 30827–30835.

Christie J. M., Reymond P., Powell G. K., Bernasconi P., Raibekas A. A., Liscum E. a Briggs W. R. (1998) NPH1: a flavoprotein with the properties of a photoreceptor for phototropism. *Science*. **282**, 1698–1701.

Cobb A. H. (1992) Auxin-type herbicides. *Herbicides and Plant Physiology*. Chapman and Hall, London, 82–106.

Cook S. D., Nichols D. S., Smith J., Chourey P. S., McAdam E. L., Quittenden L., Ross J. J. (2016) Auxin biosynthesis: Are the indole-3-acetic acid and phenylacetic acid biosynthesis pathways mirror images? *Plant Physiol*. **171**(2), 1230–1241.

Cook S. D. (2019) An Historical Review of Phenylacetic Acid. *Plant Cell Physiol*. **60**(2), 243–254.

Darwin C., Darwin F. (1880) The power of movement in plants. John Murray, London.

Davies R. T., Goetz D. H., Lasswell J., Anderson M. N., Bartel B. (1999) IAR3 encodes an auxin conjugate hydrolase from Arabidopsis. *Plant Cell*. **11**(3), 365–376.

Davies P. J. (2010) Plant hormones: Biosynthesis, signal transduction, action! - *The plant hormones: Their nature, occurrence and functions.* Springer, New York, USA, 1–15.

del Pozo J. C., Diaz-Trivino S., Cisneros N., Gutierrez C. (2006) The balance between cell division and endoreplication depends on E2FC-DPB, transcription factors regulated by the ubiquitin-SCF^{SKP2A} pathway in Arabidopsis. *Plant Cell*. **18**, 2224–2235.

Delbarre A., Muller P., Imhoff V., Guern J. (1996) Comparison of mechanisms controlling uptake and accumulation of 2,4-dichlorophenoxy acetic acid, naphthalene-1-acetic acid, and indole-3-acetic acid in suspension-cultured tobacco cells. *Planta*. **198**(4), 532–541.

Delker C., Quint M., Wigge P. A. (2022) Recent advances in understanding thermomorphogenesis signaling. *Curr Opin Plant Biol*. **68**, 102231.

Deslauriers S. D., Spalding E. P. (2021) Electrophysiological study of Arabidopsis ABCB4 and PIN2 auxin transporters: Evidence of auxin activation and interaction enhancing auxin selectivity. *Plant Direct*. **5**(11), e361.

Di Mambro R., Svolacchia N., Dello Ioio R., Pierdonati E., Salvi E., Pedrazzini E., Vitale A., Perilli S., Sozzani R., Benfey P.N., Busch W., Costantino P., Sabatini S. (2019) The lateral root cap acts as an auxin sink that controls meristem size. *Curr Biol*. **29**, 1199–1205.

Du F., Ruan G., Liu H. (2012) Analytical methods for tracing plant hormones. *Anal Bioanal Chem*. **403**(1), 55-74.

Du W. C., Lu Y., Li Q., Luo S. X., Shen S. X., Li N., Chen X. P. (2022) TIR1/AFB proteins: Active players in abiotic and biotic stress signaling. *Front Plant Sci*. **13**, 1083409.

Eyer L., Vain T., Pařízková B., Oklešťková J., Barbez E., Kozubíková H., Pospíšil T., Wierzbicka R., Kleine-Vehn J., Fránek M., Strnad M., Robert S., Novák O. (2016) 2,4-D and IAA Amino Acid Conjugates Show Distinct Metabolism in Arabidopsis. *PLoS One*. **11**(7), e0159269.

Feng Y., Bayaer E., Qi Y. (2022) Advances in the Biological Functions of Auxin Transporters in Rice. *Agriculture*. **12**(7), 989.

Frick E. M., Strader L. C. (2018) Roles for IBA-derived auxin in plant development. *J Exp Bot*. **69**(2), 169–177.

Fu J., Sun X., Wang J., Chu J., Yan C. (2011) Progress in quantitative analysis of plant hormones. *Chinese Sci Bull*. **56**, 355–366.

Fuente R. K. D. a Leopold A. C. (1970) Time course of auxin stimulations of growth. *Plant Physiol*. **46**, 186–189.

Fukui K., Arai K., Tanaka Y., Aoi Y., Kukshal V., Jez J. M., Kubeš M. F., Napier R., Zhao Y., Kasahara H., Hayashi K. (2022) Chemical inhibition of the auxin inactivation pathway uncovers the roles of metabolic turnover in auxin homeostasis. *P Natl Acad Sci USA*. **119**, e2206869119.

Gao Y., Dai X., Aoi Y., Takebayashi Y., Yang L., Guo X., Zeng Q., Yu H., Kasahara H., Zhao Y. (2020) Two homologous INDOLE-3-ACETAMIDE (IAM) HYDROLASE genes are required for the auxin effects of IAM in Arabidopsis. J *Genet Genomics*. **47**(3), 157–165.

Grambow H. J., Langenbeck-Schwich B. (1983) The relationship between oxidase activity, peroxidase activity, hydrogen peroxide, and phenolic compounds in the degradation of indole-3-acetic acid in vitro. *Planta*. **157**(2), 132–137.

Grossmann, K. (2010) Auxin herbicides: current status of mechanism and mode of action. *Pest Manag Sci*. **66**, 113–120.

Guilfoyle T. J. (2015) The PB1 domain in auxin response factor and Aux/IAA proteins: a versatile protein interaction module in the auxin response. *Plant Cell*. **27**(1), 33–43.

Haagen-Smit A. J., Went F. W. (1935) A Physiological Analysis of Growth Substances. *P K Akad Wet Amsterd*. **38**, 852–857.

Haagen-Smit A. J., Leech W. D., Bergern W. R. (1942) The estimation, isolation and identification of auxins in plant materials. *Am J Bot*. **29**, 500-506.

Hagen G., Guilfoyle T. J. (1985) Rapid induction of selective transcription by auxins. *Mol Cell Biol*. **5**, 1197–1203.

Hall P. J. (1980) Indole-3-acetyl-myo-inositol in kernels of Oryza sativa. *Phytochemistry*. **19**, 2121–2123.

Han H., Adamowski M., Qi L., Alotaibi S. S., Friml, J. (2021) PIN-mediated polar auxin transport regulations in plant tropic responses. *New Phytol*. **232**, 510–522.

Hayashi K., Neve J., Hirose M., Kuboki A., Shimada Y., Kepinski S., Nozaki H. (2012) Rational Design of an Auxin Antagonist of the SCFTIR1 Auxin Receptor Complex. *ACS Chem Biol*. **7**(3), 590–598.

Hayashi K., Nakamura S., Fukunaga S., Nishimura T., Jenness M. K., Murphy A. S., Motose H., Nozaki H., Furutani M., Aoyama T. (2014) Auxin transport sites are visualized in planta using fluorescent auxin analogs. *P Natl Acad Sci USA*. **111**, 11557–11562.

Hayashi K., Arai K., Aoi Y., Tanaka Y., Hira H., Guo R., Hu Y., Ge C., Zhao Y., Kasahara H., Fukui K. (2021) The main oxidative inactivation pathway of the plant hormone auxin. *Nat Commun*. **12**(1), 6752.

Hladík P. (2020) Studium nových metabolických drah auxinů v rostlinách. Master thesis. University of Palacký in Olomouc, Faculty of Science. Available from: https://theses.cz/id/a44ieq/.

Hošek P., Kubeš M., Laňková M., Dobrev P. I., Klíma P., Kohoutová M., Petrášek J., Hoyerová K., Jiřina M., Zažímalová E. (2012) Auxin transport at cellular level: new insights supported by mathematical modelling. *J Exp Bot*. **63**(10), 3815–3827.

Huala E., Oeller P. W., Liscum E., Han I.-S., Larsen E. a Briggs W. R. (1997) NPH1: a protein kinase with a putative redox-sensing domain. *Science*. **278**, 2120- 2123.

Hull A. K., Vij R., Celenza J. L. (2000) Arabidopsis cytochrome P450s that catalyze the first step of tryptophan-dependent indole-3-acetic acid biosynthesis. *P Natl Acad Sci USA*. **97**, 2379–2384.

Isobe T., Miyagawa H. (2022) Facilitation of auxin biosynthesis and metabolism by salt stress in rice plants. *Biosci Biotech Bioch*. **86**(7), 824–831.

Jackson R. G., Lim E.-K., Li Y., Kowalczyk M., Sandberg G., Hoggett J., Ashford D. A., Bowles D. J. (2001) Identification and biochemical characterization of an Arabidopsis indole-3-acetic acid glucosyltransferase. *J Biol Chem*. **276**, 4350–4356.

Jakubowska A., Kowalczyk S. (2005) A specific enzyme hydrolyzing 6-O(4-O)-indole-3-ylacetyl-beta-D-glucose in immature kernels of Zea mays. *J Plant Physiol*. **162**(2), 207–213.

Jiang K, Asami T. (2018) Chemical regulators of plant hormones and their applications in basic research and agriculture. *Biosci Biotech Bioch*. **82**(8), 1265–1300.

Jing H., Wilkinson E. G., Sageman-Furnas K., Strader L. C. (2023) Auxin and abiotic stress responses. *J Exp Bot*. **74**(22), 7000–7014.

Jurado S., Díaz-Triviño S., Abraham Z., Manzano C., Gutierrez C., del Pozo C. (2008) SKP2A, an F-box protein that regulates cell division, is degraded via the ubiquitin pathway. *Plant J*. **53**, 828–841.

Jurado S., Abraham Z., Manzano C., López-Torrejón G., Pacios L. F. a Del Pozo J. C. (2010) The Arabidopsis cell cycle F-box protein SKP2A binds to auxin. *Plant Cell*. **22**, 3891–3904.

Kai K., Horita J., Wakasa K., Miyagawa H. (2007a) Three oxidative metabolites of indole-3-acetic acid from Arabidopsis thaliana. *Phytochemistry*. **68**(12), 1651–1663.

Kai K., Wakasa K., Miyagawa H. (2007b) Metabolism of indole-3-acetic acid in rice: Identification and characterization of N-β-d-glucopyranosyl indole-3-acetic acid and its conjugates. *Phytochemistry*. **68**(20), 2512–2522.

Kaminaga Y., Schnepp J., Peel G., Kish C. M., Ben-Nissan G., Weiss D., Orlova I., Lavie O., Rhodes D., Wood K., Porterfield D. M., Cooper A. J. L., Schloss J. V., Pichersky E., Vainstein A., Dudareva N. (2006) Plant Phenylacetaldehyde Synthase Is a Bifunctional Homotetrameric Enzyme That Catalyzes Phenylalanine Decarboxylation and Oxidation. *J Biol Chem*. **281**(33), 23357–23366.

Karady M., Hladík P., Cermanová K., Jiroutová P., Antoniadi I., Casanova-Sáez R., Ljung K., Novák O. (2024) Profiling of 1-aminocyclopropane-1-carboxylic acid and selected phytohormones in Arabidopsis using liquid chromatography-tandem mass spectrometry. *Plant Methods*. **20**, 41.

Ke Q., Wang Z., Ji C. Y., Jeong J. C., Lee H. S., Li H., Xu B., Deng X., Kwak S. S. (2015) Transgenic poplar expressing Arabidopsis YUCCA6 exhibits auxin-overproduction phenotypes and increased tolerance to abiotic stress. *Plant Physiol Bioch*. **94**, 19–27.

Kemper E., Wafenschmidt S., Weiler E. W., Rausch T., Schröder J. (1985) T-DNA-encoded auxin formation in crown-gall cells. *Planta* **163**, 257–262.

Kim J. I., Baek D., Park H. C., Chun H. J., Oh D. H., Lee M. K., Cha J. Y., Kim W. Y., Kim M. C., Chung W. S., Bohnert H. J., Lee S. Y., Bressan R. A., Lee S. W., Yun D. J. (2013) Overexpression of Arabidopsis YUCCA6 in potato results in high-auxin developmental phenotypes and enhanced resistance to water deficit. *Mol Plant*. **6**(2), 337–349.

Kim R., Osako Y., Yamane H., Tao R., Miyagawa H. (2021) Quantitative analysis of auxin metabolites in lychee flowers. *Biosci Biotech Bioch*. **85**(3), 467–475.

Kögl F., Haagen-Smit A. J. (1931) I. Mitteilung uber pflanzliche wachstumsstoffe. Uber die vhemie des euchsstoffs. *Proceedings Koninklijke Nederlandse Akademie van Wetenschappen* **34**, 1411–1416.

Kojima M., Kamada-Nobusada T., Komatsu H., Takei K., Kuroha T., Mizutani M., Ashikari M., Ueguchi-Tanaka M., Matsuoka M., Suzuki K., Sakakibara H. (2009) Highly sensitive and high-throughput analysis of plant hormones using MS-probe modification and liquid chromatography-tandem mass spectrometry: an application for hormone profiling in Oryza sativa. *Plant Cell Physiol*. **50**, 1201–1214.

Koochak H., Lüdwig-Muller J. (2021) Physcomitrium patens mutants in auxin conjugating GH3 proteins show salt stress tolerance but auxin homeostasis is not involved in regulation of oxidative stress factors. *Plants*. **10**, 1398.

Korasick D. A., Enders T. A., Strader L. C. (2013) Auxin biosynthesis and storage forms. *J Exp Bot*. **64**(9), 2541–2555.

Korasick D. A., Westfall C. S., Lee S. G., Nanao M. H., Dumas R., Hagen G., Guilfoyle T. J., Jez J. M., Strader L. C. (2014) Molecular basis for AUXIN RESPONSE FACTOR protein interaction and the control of auxin response repression. *P Natl Acad Sci USA*. **111**(14), 5427–5432.

Korver R. A., Koevoets I. T., Testerink C. (2018) Out of Shape During Stress: A Key Role for Auxin. *Trends Plant Sci*. **23**(9), 783–793.

Koshiba T., Saito E., Ono N., Yamamoto N., Satô M. (1996) Purification and Properties of Flavin- and Molybdenum-Containing Aldehyde Oxidase from Coleoptiles of Maize. *Plant Physiol*. **110**(3), 781–789.

Kowalczyk M., Sandberg G. (2001) Quantitative analysis of indole-3-acetic acid metabolites in Arabidopsis. *Plant Physiol*. **127**(4), 1845–1853.

Kowalczyk S., Jakubowska A., Zielińska E., Bandurski R. S. (2003) Bifunctional indole-3-acetyl transferase catalyses synthesis and hydrolysis of indole-3-acetyl-myo-inositol in immature endosperm of Zea mays. *Physiol Plantarum*. **119**, 165–174.

Kriechbaumer V., Wang P., Hawes C., Abell B.M. (2012) Alternative splicing of the auxin biosynthesis gene YUCCA4 determines its subcellular compartmentation. *Plant J*. **70**, 292–302.

Lancashire P. D., Bleiholder H., Boom P. V. D., Langeluddeke P., Stauss R., Weber E., Witzenberger A. (1991) A uniform decimal code for growth stages of crops and weeds. *Ann Appl Biol*. **11**, 561–601.

LeClere S., Tellez R., Rampey R. A., Matsuda S. P., Bartel B. (2002) Characterization of a family of IAA-amino acid conjugate hydrolases from Arabidopsis. *J Biol Chem*. **277**(23), 20446–20452.

Lee M., Jung J. H., Han D. Y., Seo P. J., Park W. J., Park C. M. (2012) Activation of a flavin monooxygenase gene *YUCCA7* enhances drought resistance in Arabidopsis. *Planta*. **235**, 923–938.

Lehmann T., Janowitz T., Sánchez-Parra B., Alonso M. P., Trompetter I., Piotrowski M., Pollmann S. (2017) Arabidopsis NITRILASE 1 Contributes to the Regulation of Root Growth and Development through Modulation of Auxin Biosynthesis in Seedlings. *Front Plant Sci*. **24**, 8–36.

Leitz G., Kang B. H., Schoenwaelder M. E. A. (2009) Statolith sedimentation kinetics and force transduction to the cortical endoplasmic reticulum in gravity-sensing Arabidopsis columella cells. *Plant Cell*. **21**(3), 843–860.

Leyser O. (2018) Auxin signaling. *Plant physiol*. **176**(1), 465–479.

Li L., Hou X., Tsuge T., Ding M., Aoyama T., Oka A., Gu H., Zhao Y., Qu L. J. (2008) The possible action mechanisms of indole-3-acetic acid methyl ester in Arabidopsis. *Plant Cell Rep*. **27**, 575–584.

Li L., Verstraeten I., Roosjen M., Takahashi K., Rodriguez L., Merrin J., Chen J., Shabala L., Smet W., Ren H., Vanneste S., Shabala S., De Rybel B., Weijers D., Kinoshita T., Gray W.M., Friml J. (2021) Cell surface and intracellular auxin signalling for H+ fluxes in root growth. *Nature*. **599**(7884), 273–277.

Liang Y., Zhu X., Wu T., Zhao M., Liu H. (2012) Rapid and sensitive detection of auxins and flavonoids in plant samples by high-performance liquid chromatography coupled with tandem mass spectrometry. *J Sep Sci*. **35**(19), 2559–2566.

Liscum E., Askinosie S. K., Leuchtman D. L., Morrow J., Willenburg K. T., Coats D. R. (2014) Phototropism: growing towards an understanding of plant movement. *Plant Cell*. **26**(1), 38–55.

Liu X., Hegeman A. D., Gardner G. a Cohen J. D. (2012) Protocol: high-throughput and quantitative assays of auxin and auxin precursors from minute tissue samples. *Plant Methods*. **8**, 31.

Liu J., Moore S., Chen C., Lindsey K. (2017) Crosstalk Complexities between Auxin, Cytokinin, and Ethylene in Arabidopsis Root Development: From Experiments to Systems Modeling, and Back Again. *Mol Plant*. **10**(12), 1480–1496.

Ljung K., Östin A., Lioussanne L., Sandberg G. (2001a) Developmental regulation of indole-3-acetic acid turnover in Scots pine seedlings. *Plant Physiol*. **125**(1), 464–475.

Ljung K., Bhalerao R. P., Sandberg G. (2001b) Sites and homeostatic control of auxin biosynthesis in Arabidopsis during vegetative growth. *Plant J*. **28**, 465–474.

Ljung K. (2013) Auxin metabolism and homeostasis during plant development. *Development*. **140**(5), 943–950.

Lu Q., Zhang L., Chen L., Lu M., Tong P., Chen G. (2010) Simultaneous analysis of endogenetic and ectogenic plant hormones by pressurized capillary electrochromatography. *J Sep Sci*. **33**(4-5), 651–657.

Luo S. S., Lin L., Wang X. W., Zou S. C., Luan T. G. (2013) Determination of phytohormones in plant extracts using in-matrix ethyl chloroformate derivatization and DLLME-GC-MS. *LCGC Europe*. **26**(6), 310.

Maeda H., Dudareva H. (2012) The Shikimate Pathway and Aromatic Amino Acid Biosynthesis in Plants. *Annu Rev Plant Biol*. **63**, 73–105.

Majda M., Robert S. (2018) The Role of Auxin in Cell Wall Expansion. *Int J Mol Sci*. **19**(4), 951.

Manickam S., Rajagopalan V. R., Kambale R., Rajasekaran R., Kanagarajan S., Muthurajan R. (2023) Plant Metabolomics: Current Initiatives and Future Prospects. *Curr Issues Mol Biol*. **45**(11), 8894-8906.

Manulis S., Haviv-Chesner A., Brandl M. T., Lindow S. E., Barash I. (1998) Differential involvement of indole-3-acetic acid biosynthetic pathways in pathogenicity and epiphytic fitness of Erwinia herbicola pv. gypsophilae. *Mol Plant Microbe In*. **11**, 634–642.

Marumo S., Hattori H., Abe H., Munakata K. (1968) Isolation of 4-chloroindolyl-3-acetic acid from immature seeds of Pisum sativum. *Nature*. **219**(5157), 959–960.

Mashiguchi K., Tanaka K., Sakai T., Sugawara S., Kawaide H., Natsume M., Hanada A., Yaeno T., Shirasu K., Yao H., McSteen P., Zhao Y., Hayashi K., Kamiya Y., Kasahara H. (2011) The main auxin biosynthesis pathway in Arabidopsis. *P Natl Acad Sci USA*. **108**(45), 18512–18517.

Mateo-Bonmatí E., Casanova-Sáez R., Šimura J., Ljung K. (2021) Broadening the roles of UDP-glycosyltransferases in auxin homeostasis and plant development. *New Phytol*. **232**(2), 642–654.

Mellor N., Band L. R., Pěnčík A., Novák O., Rashed A., Holman T., Wilson M. H., Voß U., Bishopp A., King J. R., Ljung K., Bennett M. J., Owen M. R. (2016) Dynamic regulation of auxin oxidase and conjugating enzymes AtDAO1 and GH3 modulates auxin homeostasis. *P Natl Acad Sci USA*. **113**(39), 11022–11027.

Michalko J., Dravecká T., Bollenbach T., Friml J. (2015) Embryo-lethal phenotypes in early abp1 mutants are due to disruption of the neighboring BSM gene. *F1000Res*. **4**, 1104.

Mikkelsen M. D., Hansen C. H., Wittstock U., Halkier B. A. (2000) Cytochrome P450 CYP79B2 from Arabidopsis catalyzes the conversion of tryptophan to indole-3-acetaldoxime, a precursor of indole glucosinolates and indole-3-acetic acid. *J Biol Chem*. **275**(43), 33712–33717.

Monshausen G. B., Miller N. D., Murphy A. S., Gilroy S. (2011) Dynamics of auxin-dependent Ca2+ and pH signaling in root growth revealed by integrating high-resolution imaging with automated computer vision-based analysis. *Plant J*. **65**, 309–318.

Morris, D. A., Johnson, C. F. (1987) Regulation of auxin transport in pea (Pisum sativum L.) by phenylacetic acid: Inhibition of polar auxin transport in intact plants and stem segments. *Planta*. **172**(3), 408–416.

Mravec J., Skůpa P., Bailly A., Hoyerová K., Křeček P., Bielach A., Petrášek J., Zhang J., Gaykova V., Stierhof Y. D., Dobrev P. I., Schwarzerová K., Rolčík J., Seifertová D., Luschnig C., Benková E., Zažímalová E., Geisler M., Friml J. (2009) Subcellular homeostasis of phytohormone auxin is mediated by the ER-localized PIN5 transporter. *Nature*. **459**, 1136–1140.

Müller K., Dobrev P. I., Pěnčík A., Hošek P., Vondráková Z., Filepová R., Malínská K., Brunoni F., Helusová L., Moravec T., Retzer K., Harant K., Novák O., Hoyerová K., Petrášek J. (2021) DIOXYGENASE FOR AUXIN OXIDATION 1 catalyzes the oxidation of IAA amino acid conjugates. *Plant Physiol*. **187**(1), 103–115.

Naqvi S. M. Z. A., Zhang Y., Tahir M. N., Ullah Z., Ahmed S., Wu J., Raghavan V., Abdulraheem M. I., Ping J., Hu X. (2023) Advanced strategies of the in-vivo plant hormone detection. *TrAC Trends Anal Chem*. **166**, 117186.

Nguyen N. H., Trotel-Aziz P., Clément C., Jeandet P., Baillieul F., Aziz A. (2022) Camalexin accumulation as a component of plant immunity during interactions with pathogens and beneficial microbes. *Planta*. **255**(6), 116.

Nonhebel H. M., Bandurski R. S. (1984) Oxidation of indole-3-acetic acid and oxindole-3-acetic acid to 2,3-dihydro-7-hydroxy-2-oxo-1H indole-3acetic acid-7'-O-beta-D-glucopyranoside in Zea mays seedlings. *Plant Physiol*. **76**, 979–983.

Nonhebel H. M., Kruse L. I., Bandurski R. S. (1985) Indole-3-acetic acid catabolism in Zea mays seedlings. Metabolic conversion of oxindole3-acetic acid to 7-hydroxy-2-oxindole-3-acetic acid 7'-O-beta-Dglucopyranoside. *J Biol Chem*. **260**, 12685–12689.

Nonhebel H. M. (2015) Tryptophan-Independent Indole-3-Acetic Acid Synthesis: Critical Evaluation of the Evidence. *Plant Physiol*. **169**(2), 1001 –1005.

Normanly J., Cohen J. D., Fink G. R. (1993) Arabidopsis thaliana auxotrophs reveal a tryptophan-independent biosynthetic pathway for indole-3-acetic acid. *P Natl Acad Sci USA*. **90**(21), 10355–10359.

Novák O., Hényková E., Sairanen I., Kowalczyk M., Pospíšil T., Ljung K. (2012) Tissue-specific profiling of the Arabidopsis thaliana auxin metabolome. *Plant J*. **72**, 523–536.

Novák O., Pěnčík A., Ljung K. (2014) Auxin and Its Role in Plant Development: Identification and Profiling of Auxin and Auxin Metabolites. Springer-Verlag Wien, Austria, 39–60.

Novák O., Napier R., Ljung K. (2017) Zooming In on Plant Hormone Analysis: Tissue- and Cell-Specific Approaches. *Annu Rev Plant Biol*. **68**, 323–348.

Nováková L. (2013) Challenges in the development of bioanalytical liquid chromatography–mass spectrometry method with emphasis on fast analysis. *J Chromatogr A*. **1292**, 25–37.

Okamoto T., Koizumi T., Isogai Y. (1967) Studies on Plant Growth Regulators. II. Isolation of Indole-3-Acetic Acid, Phenylacetic Acid, and Several Plant Growth Inhibitors from Etiolated Seedlings of Phaseolus. *Chem Pharm Bull*. **15**, 159–163.

Okrent R. A., Brooks M. D., Wildermuth M. C. (2009) Arabidopsis GH3.12 (PBS3) conjugates amino acids to 4-substituted benzoates and is inhibited by salicylate. *J Biol Chem*. **284**(15), 9742–9754.

Östin A., Monteiro A. M., Crozier A., Jensen E., Sandberg G. (1992) Analysis of Indole-3-Acetic Acid Metabolites from Dalbergia dolichopetala by High Performance Liquid Chromatography-Mass Spectrometry. *Plant Physiol*. **100**(1), 63–68.

Östin A., Kowalyczk M., Bhalerao R. P., Sandberg G. (1998) Metabolism of indole-3-acetic acid in Arabidopsis. *Plant Physiol*. **118**, 285–296.

Ostrowski M., Ciarkowska A., (2021) Pea GH3 acyl acid amidosynthetase conjugates IAA to proteins in immature seeds of Pisum sativum L. – A new perspective on formation of high-molecular weight conjugates of auxin. *J Plant Physiol*. **256**, 153312.

Paciorek T., Zažímalová E., Ruthardt N., Petrášek J., Stierhof Y., Kleine-Vehn J., Morris D. A., Emans N., Jürgens G., Geldner N., Friml J. (2005) Auxin inhibits endocytosis and promotes its own efflux from cells. *Nature*. **435**, 1251–1256.

Paponov I. A., Paponov M., Teale W., Menges M., Chakrabortee S., Murray J. A., Palme K. (2008) Comprehensive transcriptome analysis of auxin responses in Arabidopsis. *Mol Plant*. **1**, 321–337.

Pařízková B., Žukauskaitė A., Vain T., Grones P., Raggi S., Kubeš M. F., Kieffer M., Doyle S. M., Strnad M., Kepinski S., Napier R., Doležal K., Robert S., Novák O. (2021) New fluorescent auxin probes visualise tissue-specific and subcellular distributions of auxin in Arabidopsis. *New Phytol*. **230**(2), 535–549.

Park S., Cohen J. D., Slovin J. P. (2006) Strawberry fruit protein with a novel indole-acyl modification. *Planta*. **224**, 1015–1022.

Park S., Ozga J. A., Cohen J. D., Reinecke D. M. (2010) Evidence of 4-Cl-IAA and IAA bound to proteins in pea fruit and seeds. *J Plant Growth Regul*. **29**(2), 184–193.

Parry G., Calderon-Villalobos L. I., Prigge M., Peret B., Dharmasiri S., Itoh H., Lechner E., Gray W. M., Bennett M., Estelle M. (2009) Complex regulation of the TIR1/AFB family of auxin receptors. *P Natl Acad Sci USA*. **106**, 22540–22545.

Patten C. L., Blakney A. J. C., Coulson T. J. D. (2013) Activity, distribution and function of indole-3-acetic acid biosynthetic pathways in bacteria. *Crit Rev Microbiol*. **39**(4), 395–415.

Pěnčík A., Rolčík J., Novák O., Magnus V., Barták P., Buchtík R., Salopek-Sondi B., Strnad M. (2009) Isolation of novel indole-3-acetic acid conjugates by immunoaffinity extraction. *Talanta*. **80**(2), 651–655.

Pěnčík A., Simonovik B., Petersson S. V., Henyková E., Simon S., Greenham K., Zhang Y., Kowalczyk M., Estelle M., Zažímalová E., Novák O., Sandberg G., Ljung K. (2013) Regulation of auxin homeostasis and gradients in Arabidopsis roots through the formation of the indole-3-acetic acid catabolite 2-oxindole-3-acetic acid. *Plant Cell*. **25**(10), 3858–3870.

Pěnčík A., Casanova-Sáez R., Pilarová V., Žukauskaite A., Pinto R., Micol J. L., Ljung K., Novák O. (2018) Ultra-rapid auxin metabolite profiling for high-throughput mutant screening in Arabidopsis. *J Exp Bot*. **69**, 2569–2579.

Percival F. W., Bandurski R. S. (1976) Esters of indole-3-acetic Acid from Avena seeds. *Plant Physiol*. **58**(1), 60–67.

Péret B., Swarup K., Ferguson A., Seth M., Yang Y., Dhondt S., James N., Casimiro I., Perry P., Syed A., Yang H., Reemmer J., Venison E., Howells C., Perez-Amador M. A., Yun J., Alonso J., Beemster G. T., Laplaze L., Murphy A., Bennett M. J., Nielsen E., Swarup R. (2012) AUX/LAX genes encode a family of auxin influx transporters that perform distinct functions during *Arabidopsis* development. *Plant Cell*. **24** (7), 2874–2885.

Perez V. C., Dai R., Bai B., Tomiczek B., Askey B. C., Zhang Y., Rubin G. M., Ding Y., Grenning A., Block A. K., Kim, J. (2021) Aldoximes are precursors of auxins in Arabidopsis and maize. *New Phytol*. **231**(4), 1449–1461.

Perez V. C., Zhao H., Lin M., Kim J. (2023) Occurrence, Function, and Biosynthesis of the Natural Auxin Phenylacetic Acid (PAA) in Plants. *Plants (Basel)*. **12**(2), 266.

Petersson S. V., Johansson A. I., Kowalczyk M., Makoveychuk A., Wang J. Y., Moritz T., Grebe M., Benfey P. N., Sandberg G., Ljung K. (2009) An auxin gradient and maximum in the Arabidopsis root apex shown by high-resolution cell-specific analysis of IAA distribution and synthesis. *Plant Cell*. **21**(6), 1659–1668.

Petrášek J., Mravec J., Bouchard R., Blakeslee J. J., Abas M., Seifertová D., Wisniewska J., Tadele Z., Kubeš M., Covanová M., Dhonukshe P., Skupa P., Benková E., Perry L., Křeček P., Lee O. R., Fink G. R., Geisler M., Murphy A. S., Luschnig C., Zažímalová E., Friml J. (2006) PIN proteins perform a rate-limiting function in cellular auxin efflux. *Science*. **312**(5775), 914–918.

Plüss R., Jenny T., Meier H. (1989) IAA-induced adventitious root formation ingreenwood cuttings of Populus tremula and formation of 2-indolone-3-acetylasparticacid, a new metabolite of exogeneously applied indole-3-acetic acid. *Physiol Plantarum*. **75**, 89–96.

Polanská L., Vičánková A., Nováková M., Malbeck J., Dobrev P. I., Brzobohatý B., Vaňková R., Macháčková I. (2007) Altered cytokinin metabolism affects cytokinin, auxin, and abscisic acid contents in leaves and chloroplasts, and chloroplast ultrastructure in transgenic tobacco. *J Exp Bot*. **58**, 637–649.

Pollmann S., Neu D., Weiler E. W. (2003) Molecular cloning and characterization of an amidase from *Arabidopsis thaliana* capable of converting indole-3-acetamide into the plant growth hormone, indole-3-acetic acid. *Phytochemistry*. **62**, 293–300.

Porco S., Pěnčík A., Rashed A., Voß U., Casanova-Sáez R., Bishopp A., Golebiowska A., Bhosale R., Swarup R., Swarup K., Peňáková P., Novák O., Staswick P., Hedden P., Phillips A. L., Vissenberg K., Bennett M. J., Ljung K. (2016) Dioxygenase-encoding AtDAO1 gene controls IAA oxidation and homeostasis in Arabidopsis. *P Natl Acad Sci USA*. **113**(39), 11016–11021.

Porfírio S., Gomes da Silva M. D. R., Peixe A., Cabrita M. J., Azadi P. (2016) Current analytical methods for plant auxin quantification-A review. *Anal Chim Acta*. **902**, 8–21.

Procházka S., Borkovec V. (1984) Transport and regulative properties of phenylacetic acid. *Biol Plantarum*. **26**(5), 358–363.

Qi L., Kwiatkowski M., Chen H., Hoermayer L., Sinclair S., Zou M., Del Genio C. I., Kubeš M. F., Napier R., Jaworski K., Friml J. (2022) Adenylate cyclase activity of TIR1/AFB auxin receptors in plants. *Nature*. **611**, 133–138.

Qin G., Gu H., Zhao Y., Ma Z., Shi G., Yang Y., Pichersky E., Chen H., Liu M., Chen Z., Qu L. J. (2005) An indole-3-acetic acid carboxyl methyltransferase regulates Arabidopsis leaf development. *Plant Cell*. **17**, 2693–2704.

Quittenden L. J., Davies N. W., Smith J. A., Molesworth P. P., Tivendale N. D., Ross, J. J. (2009) Auxin Biosynthesis in Pea: Characterization of the Tryptamine Pathway. *Plant Physiol*. **151**(3), 1130.

Radwanski E. R., Barczak A. J., Last R. L. (1996) Characterization of tryptophan synthase alpha subunit mutants of Arabidopsis thaliana. *Mol Gen Genet*. **253**(3), 353-361.

Ranocha P., Dima O., Nagy R., Felten J., Corratgé-Faillie C., Novák O., Morreel K., Lacombe B., Martinez Y., Pfrunder S., Jin X., Renou J., Thibaud J., Ljung K., Fischer U., Martinoia E., Boerjan W., Goffner D. (2013) Arabidopsis WAT1 is a vacuolar auxin transport facilitator required for auxin homoeostasis. *Nat Commun*. **4**, 2625.

Revelou M., Kokotou M. G., Constantinou-Kokotou V. (2019) Identification of Auxin Metabolites in Brassicaceae by Ultra-Performance Liquid Chromatography Coupled with High-Resolution Mass Spectrometry. *Molecules*. **24**(14), 2615.

Rittenberg D., Foster L. (1940) A new procedure for quantitative analysis by isotope dilution, with application to the determination of amino acids and fatty acids. *J Biol Chem*. **133**, 727–744.

Robert H. S., Friml J. (2009) Auxin and other signals on the move in plants. *Nat Chem Biol*. **5**(5), 325–332.

Sajid M., Płotka-Wasylka J. (2018) Combined extraction and microextraction techniques: Recent trends and future perspectives. *TrAC Trends Anal Chem*. **103**, 74–86.

Sauer M., Robert S., Kleine-Vehn J. (2013) Auxin: simply complicated. *J Exp Bot*. **64**(9), 2565–2577.

Schaller G. E., Bishopp A., Kieber J. J. (2015) The yin-yang of hormones: cytokinin and auxin interactions in plant development. Plant Cell. **27**(1), 44–63.

Schneider E. A., Wightman F. (1974) Metabolism of auxin in higher plants. *Ann Rev Plant Physio*. **25**, 487–513.

Seo M., Akaba S., Oritani T., Delarue M., Bellini C., Caboche M., Koshiba T. (1998) Higher activity of an aldehyde oxidase in the auxin-overproducing *superroot1* mutant of *Arabidopsis thaliana*. *Plant Physiol*. **116**, 687–693.

Skalický V., Kubeš M., Napier R., Novák O. (2018) Auxins and cytokinins-the role of subcellular organization on homeostasis. *Int J Mol Sci*. **19**, 3115.

Skalický V., Vojtková T., Pěnčík A., Vrána J., Juzoń K., Koláčková V., Sedlářová M., Kubeš M. F., Novák O. (2021) Auxin metabolite profiling in isolated and intact plant nuclei. *Int J Mol Sci*. **22**, 12369.

Skalický V., Antoniadi I., Pěnčík A., Chamrád I., Lenobel R., Kubeš M. F., Zatloukal M., Žukauskaitė A., Strnad M., Ljung K., Novák O. (2023) Fluorescence-activated multi-organelle mapping of subcellular plant hormone distribution. *Plant J*. **116**(6), 1825–1841.

Smalle J., Vierstra R. D. (2004) The ubiquitin 26S proteasome proteolytic pathway. *Annu Rev Plant Biol*. **55**, 555–590.

Sokolowska K., Kizinska J., Szewczuk Z., Banasiak A. (2014) Auxin conjugated to fluorescent dyes - a tool for the analysis of auxin transport pathways. *Plant Biol*. **16**, 866–877.

Solanki M., Shukla L. I. (2023) Recent advances in auxin biosynthesis and homeostasis. *3 Biotech*. **13**(9), 290.

Sønderby I. E., Geu-Flores F., Halkier B. A. (2010) Biosynthesis of glucosinolates – gene discovery and beyond. *Trends Plant Sci*. **15**(5), 283–290.

Staswick P. E., Serban B., Rowe M., Tiryaki I., Maldonado M. T., Maldonado M. C., Suza W. (2005) Characterization of an Arabidopsis enzyme family that conjugates amino acids to indole-3-acetic acid. *Plant Cell*. **17**(2), 616–627.

Staswick P., Rowe M., Spalding E. P., Splitt B. L. (2017) Jasmonoyl-L-Tryptophan Disrupts IAA Activity through the AUX1 Auxin Permease. *Front Plant Sci*. **8**, 736.

Stepanova A. N, Robertson-Hoyt J., Yun J., Benavente L. M., Xie D., Doležal K., Schlereth A., Jürgens G., Alonso J. M. (2008) TAA1-Mediated Auxin Biosynthesis Is Essential for Hormone Crosstalk and Plant Development. *Cell*. **133**(1), 177–191.

Sugawara S., Hishiyama S., Jikumaru Y., Hanada A., Nishimura T., Koshiba T., Zhao Y., Kamiya Y., Kasahara H. (2009) Biochemical analyses of indole-3-acetaldoxime-dependent auxin biosynthesis in Arabidopsis. *P Natl Acad Sci USA*. **106**(13), 5430–5435.

Sugawara S., Mashiguchi K., Tanaka K., Hishiyama S., Sakai T., Hanada K., Kinoshita-Tsujimura K., Yu H., Dai X., Takebayashi Y., Takeda-Kamiya N., Kakimoto T., Kawaide H., Natsume M., Estelle M., Zhao Y., Hayashi K., Kamiya Y., Kasahara H. (2015) Distinct Characteristics of Indole-3-Acetic Acid and Phenylacetic Acid, Two Common Auxins in Plants. *Plant Cell Physiol*. **56**(8), 1641–1654.

Suzuki M., Yamazaki C., Mitsui M., Kakei Y., Mitani Y., Nakamura A., Ishii T., Soeno K., Shimada Y. (2015) Transcriptional feedback regulation of YUCCA genes in response to auxin levels in Arabidopsis. *Plant Cell Rep*. **34**, 1343–1352.

Swarup R., Bhosale R. (2019) Developmental Roles of AUX1/LAX Auxin Influx Carriers in Plants. *Front Plant Sci*. **10**, 1306.

Szemenyei H., Hannon M., Long J. A. (2008) TOPLESS mediates auxin-dependent transcriptional repression during Arabidopsis embryogenesis. *Science*. **319**, 1384–1386.

Tam Y. Y., Epstein E., Normanly J. (2000) Characterization of auxin conjugates in Arabidopsis. Low steady-state levels of indole-3-acetyl-aspartate, indole-3-acetyl-glutamate, and indole-3-acetyl-glucose. *Plant Physiol*. **123**(2), 589–596.

Tan X., Calderon-Villalobos L. I. A., Sharon M., Zheng C., Robinson C. V., Estelle M., Zheng N. (2007) Mechanism of auxin perception by the TIR1 ubiquitin ligase. *Nature*. **446**, 640–645.

Tanaka K., Hayashi K., Natsume M., Kamiya Y., Sakakibara H., Kawaide H., Kasahara H. (2014) UGT74D1 catalyzes the glucosylation of 2-oxindole-3-acetic acid in the auxin metabolic pathway in Arabidopsis. *Plant Cell Physiol*. **55**, 218–228.

Tarkowská D., Novák O., Floková K., Tarkowski P., Turečková V., Grúz J., Rolčík J., Strnad M. (2014) Quo vadis plant hormone analysis? *Planta*. **240**(1), 55–76.

Thimann K. V. (1935) On the plant growth hormone produced by *Rhizopus suinus. J Biol Chem*. **109**, 279–291.

Thimann K. V. (1937) On the Nature of Inhibitions Caused by Auxin. *Am J Bot*. **24**(7), 407–412.

Thomashow L. S., Reeves S., Thomashow M. F. (1984) Crown gall oncogenesis: evidence that a T-DNA gene from the Agrobacterium Ti plasmid pTiA6 encodes an enzyme that catalyzes synthesis of indoleacetic acid. *P Natl Acad Sci USA*. **81** 5071–5075.

Tieman D., Taylor M., Schauer N., Fernie A. R., Hanson A. D., Klee H. J. (2006) Tomato aromatic amino acid decarboxylases participate in synthesis of the flavor volatiles 2-phenylethanol and 2-phenylacetaldehyde. *P Natl Acad Sci USA*. **103**(21), 8287.

Titapiwatanakun B., Blakeslee J. J., Bandyopadhyay A., Yang H., Mravec J., Sauer M., Cheng Y., Adamec J., Nagashima A., Geisler M., Sakai T., Friml J., Peer W. A., Murphy A. S. (2008) ABCB19/PGP19 stabilises PIN1 in membrane microdomains in Arabidopsis. *Plant J*. **57**, 27–44.

Tognetti V. B., Van Aken O., Morreel K., Vandenbroucke K., van de Cotte B., De Clercq I., Chiwocha S., Fenske R., Prinsen E., Boerjan W., Genty B., Stubbs K. A., Inzé D., Van Breusegem F. (2010) Perturbation of indole-3-butyric acid homeostasis by the UDP-glucosyltransferase UGT74E2 modulates Arabidopsis architecture and water stress tolerance. *Plant cell*. **22**, 2660–2679.

Tottman D. R. (1987) The decimal code for the growth stages of cereals, with illustrations. *Ann Appl Biol*. **110**, 441–454.

Tsurumi S., Wada S. (1980) Metabolism of indole-3-acetic acid and natural occurrence of dioxindole-3-acetic acid derivatives in Vicia roots. *Plant Cell Physiol*. **21**(8), 1515–1525.

Urbancsok J., Bones A. M., Kissen R. (2018) Benzyl Cyanide Leads to Auxin-Like Effects Through the Action of Nitrilases in Arabidopsis thaliana. *Front Plant Sci*. **9**, 1240.

van den Berg T., Korver R. A., Testerink C., Ten Tusscher K. H. (2016) Modeling halotropism: a key role for root tip architecture and reflux loop remodeling in redistributing auxin. *Development*. **143**, 3350–3362.

Vrobel O., Tarkowski P. (2023) Can plant hormonomics be built on simple analysis? A review. *Plant Methods*. **19**, 107.

Wakuta S., Suzuki E., Saburi W., Matsuura H., Nabeta K., Imai R., Matsui H. (2011) OsJAR1 and OsJAR2 are jasmonyl-L-isoleucine synthases involved in wound- and pathogen-induced jasmonic acid signalling. *Biochem Bioph Res Co*. **409**(4), 634–639.

Walter A., Caputi L., O'Connor S., van Pée K. H., Ludwig-Müller J. (2020) Chlorinated Auxins-How Does *Arabidopsis Thaliana* Deal with Them? *Int J Mol Sci*. **21**(7), 2567.

Walz A., Park S., Slovin J. P., Ludwig-Müller J., Momonoki Y. S., Cohen J. D. (2002) A gene encoding a protein modified by the phytohormone indoleacetic acid. *P Natl Acad Sci USA*. **99**, 1718–1723.

Wang B., Chu J., Yu T., Xu Q., Sun X., Yuan J., Xiong G., Wang G., Wang Y., Li J. (2015) Tryptophan-independent auxin biosynthesis contributes to early embryogenesis in Arabidopsis. *P Natl Acad Sci USA*. **112**(15), 4821–4826.

Wang L., Zou Y., Kaw H. Y., Wang G., Sun H., Cai L., Li C., Meng L. Y., Li D. (2020) Recent developments and emerging trends of mass spectrometric methods in plant hormone analysis: a review. *Plant Methods*. **16**, 16–54.

Wei C., Zhou H., Chen C., Li Z., Zhou J. (2011) On-Line Monitoring 1H-Indole-3-Acetic Acid in Plant Tissues Using Molecular Imprinting Monolayer Techniques on a Surface Plasmon Resonance Sensor. *Anal Lett*. **44**(18), 2911–2921.

Weiler E. W. (1984) Immunoassay of Plant Growth Regulators. *Ann Rev Plant Physiol*. **35**, 85–95.

Went F. W. (1926) On growth accelerating substances in the coleoptile of Avena sativa. *Proceedings Koninklijke Nederlandse Akademie van Wetenschappen* **30**, 10–19.

Westfall C. S., Herrmann J., Chen Q., Wang S., Jez J. M. (2010) Modulating plant hormones by enzyme action: The GH3 family of acyl acid amido synthetases. *Plant Signal Behav*. **5**, 1607–1612.

Westfall C. S., Sherp A. M., Zubieta C., Alvarez S., Schraft E., Marcellin R., Ramirez L., Jez, J. M. (2017) Arabidopsis thaliana GH3.5 acyl acid amido synthetase mediates metabolic crosstalk in auxin and salicylic acid homeostasis. *P Natl Acad Sci USA*. **113**(48), 13917–13922.

Wisniewska J., Xu J., Seifertová D., Brewer P. B., Ruzicka K., Blilou I., Rouquié D., Benková E., Scheres B., Friml J. (2006) Polar PIN localization directs auxin flow in plants. *Science*. **312**(5775), 883.

Woodward A. W., Bartel B. (2005) Auxin: regulation, action, and interaction. Ann Bot. **95**, 707–735.

Wu Y., Hu B. (2009) Simultaneous determination of several phytohormones in natural coconut juice by hollow fiber-based liquid-liquid-liquid microextraction-high performance liquid chromatography. J Chromatogr A. **1216**(45), 7657–7663.

Xin P., Yan J., Li B., Fang S., Fan J., Tian H., Shi Y., Tian W., Yan C., Chu J. (2016) A comprehensive and effective mass spectrometry-based screening strategy for discovery and identification of new brassinosteroids from rice tissues. *Front Plant Sci*. **7**, 233601.

Xiong C. F., Bai Y. L., Yin X. M., Ye T. T., Feng Y. Q. (2022) Use of chemical labeling-assisted liquid chromatography-mass spectrometry for discovering derivatives of brassinosteroids. *J Chromatogr A*. **1685**, 463639.

Yamada M., Greenham K., Prigge M. J., Jensen P. J., Estelle M. (2009) The TRANSPORT INHIBITOR RESPONSE2 gene is required for auxin synthesis and diverse aspects of plant development. *Plant Physiol*. **151**(1), 168–179.

Yan H., Wang F., Han D., Yang G. (2012) Simultaneous determination of four plant hormones in bananas by molecularly imprinted solid-phase extraction coupled with high performance liquid chromatography. *Analyst*. **137**(12), 2884–2890.

Yang Y., Xu R., Ma C. J., Vlot A. C., Klessig D. F., Pichersky E. (2008) Inactive methyl indole-3-acetic acid ester can be hydrolyzed and activated by several esterases belonging to the AtMES esterase family of Arabidopsis. *Plant Physiol*. **147**, 1034–1045.

Yao X., Tian L., Yang J., Zhao Y. N., Zhu Y. X., Dai X., Zhao Y., Yang Z. N. (2018) Auxin production in diploid microsporocytes is necessary and sufficient for early stages of pollen development. *PLoS Genet*. **14**(5), e1007397.

Yin Q., Zhang J., Wang S., Cheng J., Gao H., Guo C., Ma L., Sun L., Han X., Chen S., Liu A. (2021) N-glucosyltransferase GbNGT1 from ginkgo complements the auxin metabolic pathway. *Hortic Res*. **8**(1), 229.

Yin X. B., Guo J. M., Wei W. (2010) Dual-cloud point extraction and tertiary amine labeling for selective and sensitive capillary electrophoresis-electrochemiluminescent detection of auxins. *J Chromatogr A*. **1217**(8), 1399–1406.

Yoo H., Widhalm J. R., Qian Y., Maeda H., Cooper B. R., Jannasch A. S., Gonda I., Lewinsohn E., Rhodes D., Dudareva N. (2013) An alternative pathway contributes to phenylalanine biosynthesis in plants via a cytosolic tyrosine:phenylpyruvate aminotransferase. *Nat Commun*. **4**, 2833.

Zažímalová E., Murphy A. S., Yang H., Hoyerová K., Hošek P. (2010) Auxin transporters-why so many? *Cold Spring Harb Perspect Biol.* **2**, 1552–1563.

Zhang J., Peer W. A. (2017) Auxin homeostasis: the DAO of catabolism. *J Exp Bot*. **68**(12), 3145–3154.

Zhang C., Zhang L., Wang D., Ma H., Liu B., Shi Z., Ma X., Chen Y., Chen Q. (2018) Evolutionary History of the Glycoside Hydrolase 3 (GH3) Family Based on the Sequenced Genomes of 48 Plants and Identification of Jasmonic Acid-Related GH3 Proteins in Solanum tuberosum. *Int J Mol Sci*. **19**(7), 1850.

Zhao Y., Christensen S. K., Fankhauser C., Cashman J. R., Cohen J. D., Weigel D., Chory J. (2001) A role for flavin monooxygenase-like enzymes in auxin biosynthesis. *Science*. **291**(5502), 306–309.

Zhao Z., Zhang Y., Liu X., Zhang X., Liu S., Yu X., Ren Y., Zheng X., Zhou K., Jiang L., Guo X., Gai Y., Wu C., Zhai H., Wang H., Wan J. (2013) A role for a dioxygenase in auxin metabolism and reproductive development in rice. *Dev Cell*. **27**, 113–122.

Žukauskaitė A., Saiz-Fernández I., Bieleszová K., Iškauskienė M., Zhang C., Smýkalová I., Dzedulionytė K., Kubeš M. F., Sedlářová M., Pařízková B., Pavlović I., Vain T., Petřík I., Malinauskienė V., Šačkus A., Strnad M., Robert S., Napier R., Novák O., Doležal K. (2023) New PEO-IAA-Inspired Anti-Auxins: Synthesis, Biological Activity, and Possible Application in Hemp (*Cannabis Sativa* L.) Micropropagation. *J Plant Growth Regul*. **42**, 7547–7563.

8 Supplements

Supplement I

Hladík P., Petřík I., Žukauskaitė A., Novák O., Pěnčík A. (2023) Metabolic profiles of 2-oxindole-3-acetyl-amino acid conjugates differ in various plant species. *Front. Plant Sci.* 14, 1217421.

Supplement II

Hladík P., Brunoni F., Žukauskaitė A., Zatloukal M., Novák O., Pěnčík A. (2024) Phenylacetic acid metabolism in plants: unravelling novel pathways and metabolites by liquid chromatography-mass spectrometry analysis. (In preparation)

Supplement III

Bieleszová K., **Hladík P.**, Kubala M., Napier R., Brunoni F., Gelová Z., Fiedler L., Kulich L., Strnad M., Doležal K., Novák O., Friml J., Žukauskaitė A. (2024) New fluorescent auxin derivatives: anti-auxin activity and accumulation patterns in Arabidopsis thaliana. *Plant Growth Regul.* 102, 589-602.

Supplement IV

Zhang C., Bieleszová K., Žukauskaitė A., **Hladík P.**, Grúz J., Novák O., Doležal K. (2024) In situ separation and visualization of isomeric auxin derivatives in Arabidopsis by ion mobility mass spectrometry imaging. *Anal Bioanal Chem.* **416**(1), 125-139.

Supplement I

Supplement II

Supplement III

Supplement IV

Hladík P., Petřík I., Žukauskaitė A., Novák O., Pěnčík A. (2023) Metabolic profiles of 2-oxindole-3-acetyl-amino acid conjugates differ in various plant species. *Front. Plant Sci.* 14, 1217421.

frontiers | Frontiers in Plant Science

TYPE Original Research
PUBLISHED 18 July 2023
DOI 10.3389/fpls.2023.1217421

OPEN ACCESS

EDITED BY
Simon Scofield,
Cardiff University, United Kingdom

REVIEWED BY
Nathan Tivendale,
University of Western Australia, Australia
Atsushi Okazawa,
Osaka Metropolitan University, Japan
Walter Dewitte,
Cardiff University, United Kingdom

*CORRESPONDENCE
Aleš Pěnčík
alespencik@seznam.cz

RECEIVED 05 May 2023
ACCEPTED 28 June 2023
PUBLISHED 18 July 2023

CITATION
Hladík P, Petřík I, Žukauskaitė A, Novák O and Pěnčík A (2023) Metabolic profiles of 2-oxindole-3-acetyl-amino acid conjugates differ in various plant species. *Front. Plant Sci.* 14:1217421. doi: 10.3389/fpls.2023.1217421

Metabolic profiles of 2-oxindole-3-acetyl-amino acid conjugates differ in various plant species

Pavel Hladík[1], Ivan Petřík[1], Asta Žukauskaitė[2], Ondřej Novák[1] and Aleš Pěnčík[1]*

[1]Laboratory of Growth Regulators, Institute of Experimental Botany, The Czech Academy of Sciences & Faculty of Science, Palacký University, Olomouc, Czechia, [2]Department of Chemical Biology, Faculty of Science, Palacký University, Olomouc, Czechia

Auxins are a group of phytohormones that play a key role in plant growth and development, mainly presented by the major member of the family - indole-3-acetic acid (IAA). The levels of free IAA are regulated, in addition to *de novo* biosynthesis, by irreversible oxidative catabolism and reversible conjugation with sugars and amino acids. These conjugates, which serve as inactive storage forms of auxin and/or degradation intermediates, can also be oxidized to form 2-oxindole-3-acetyl-1-O-ß-D-glucose (oxIAA-glc) and oxIAA-amino acids (oxIAA-AAs). Until now, only oxIAA conjugates with aspartate and glutamate have been identified in plants. However, detailed information on the endogenous levels of these and other putative oxIAA-amino acid conjugates in various plant species and their spatial distribution is still not well understood but is finally getting more attention. Herein, we identified and characterized two novel naturally occurring auxin metabolites in plants, namely oxIAA-leucine (oxIAA-Leu) and oxIAA-phenylalanine (oxIAA-Phe). Subsequently, a new liquid chromatography–tandem mass spectrometry method was developed for the determination of a wide range of IAA metabolites. Using this methodology, the quantitative determination of IAA metabolites including newly characterized oxIAA conjugates in roots, shoots and cotyledons of four selected plant models - *Arabidopsis thaliana*, pea (*Pisum sativum* L.), wheat (*Triticum aestivum* L.) and maize (*Zea mays* L.) was performed to compare auxin metabolite profiles. The distribution of various groups of auxin metabolites differed notably among the studied species as well as their sections. For example, oxIAA-AA conjugates were the major metabolites found in pea, while oxIAA-glc dominated in Arabidopsis. We further compared IAA metabolite levels in plants harvested at different growth stages to monitor the dynamics of IAA metabolite profiles during early seedling development. In general, our results show a great diversity of auxin inactivation pathways among angiosperm plants. We believe that our findings will greatly contribute to a better understanding of IAA homeostasis.

KEYWORDS

auxin metabolism, auxin conjugates, HPLC-MS/MS, indole-3-acetic acid, 2-oxindole-3-acetic acid, catabolism, quantitative analysis

Introduction

The plant hormone auxin is involved in many growth and developmental processes. For the regular control of these processes, it is necessary to create local auxin gradients within cells and organs, which are mainly regulated by biosynthesis, polar transport, and metabolism. Although auxin metabolic pathways and endogenous levels of individual metabolites are well characterised in Arabidopsis, auxin biosynthesis and metabolism are diverse among the plant kingdom (Matsuda et al., 2005; Kai et al., 2007b; Sugawara et al., 2015; Brunoni et al., 2020; Brunoni et al., 2023). However, a full understanding of the biochemical processes in economically important crop plants is needed to better prepare for the ever-increasing demands. The Poaceae is the most agriculturally grown plant family. Maize, rice and wheat are the world's most important source of food, with more than 600 million tons each being harvested annually (Shewry, 2009). Unfortunately, increasingly demanding growth conditions caused by climate change are reducing their yield. Another highly cultivated family is the Fabaceae, which are able to process nitrogen from the atmosphere through their symbiosis with nitrogen-fixing bacteria (Broughton et al., 2003). Pea, an important member of this family is used as a model plant since the beginning of the genetics research and was also used in the early auxin research to confirm its role in apical dominance (reviewed in Smýkal, 2014). Elucidation of auxin metabolic pathways in these species should lead to a better understanding of plant growth and adaptation to extreme conditions.

The most important auxin indol-3-acetic acid (IAA) can form biologically inactive metabolites via an amide bond with amino acids, peptides, and proteins or through an ester bond with glucose, inositol, and glucan (reviewed in Seidel et al., 2006; Normanly, 2010; Ludwig-Müller, 2011; Casanova-Sáez et al., 2021). In Arabidopsis, amide conjugates constitute 78% to 90% of the total IAA pool (Tam et al., 2000; Ljung et al., 2002), whereas in monocots IAA predominantly exists in the form of IAA esters (Ludwig-Müller, 2011). For example, in rice seeds, esters constitute 68% to 70% of the total IAA pool (Bandurski and Schulze, 1977). The conjugation of IAA with amino acids is mediated by a group of GRETCHEN HAGEN 3 (GH3) enzymes (Staswick et al., 2005). The most abundant IAA amino acid conjugates indole-3-acetyl-aspartic acid (IAA-Asp) and indole-3-acetyl-glutamic acid (IAA-Glu) have been determined in a number of plant species such as Arabidopsis (Östin et al., 1998; Novák et al., 2012), rice (Matsuda et al., 2005) or spruce (Brunoni et al., 2020). Indole-3-acetyl-alanine, indole-3-acetyl-leucine (IAA-Leu) (Kowalczyk and Sandberg, 2001) and indole-3-acetyl-tryptophan (Staswick, 2009) have been also detected in Arabidopsis. Furthermore, endogenous levels of IAA conjugates with glycine, phenylalanine (IAA-Phe) and valine were determined in seeds of *Helleborus niger* (Pěnčík et al., 2009). Besides conjugation, IAA may be inactivated by oxidation to 2-oxindole-3-acetic acid (oxIAA). Until recently, this mechanism was considered to be the main catabolic pathway of IAA (Östin et al., 1998; Woodward and Bartel, 2005; Pěnčík et al., 2013). Oxidized IAA can be further glucosylated to 2-oxindole-3-acetate-glucosyl ester (oxIAA-glc) (Tanaka et al., 2014).

There is also evidence of oxidation of IAA-Asp to 2-oxindole-3-aspartic acid (oxIAA-Asp). Application of exogenous IAA to branches of aspen (*Populus tremula* L.) led to an increase in IAA-Asp concentration and later formation of oxIAA-Asp (Plüss et al., 1989). Arabidopsis plants supplemented with exogenous IAA accumulated endogenous IAA-Asp, IAA-Glu, and oxIAA-Asp, while formation of oxIAA-Glu was not observed (Östin et al., 1998). When feeding Arabidopsis with deuterium-labeled IAA-Valine and IAA-Phe, the formation of oxIAA-Valine and oxIAA-Phe was confirmed, but no endogenous levels were detected (Kai et al., 2007a). Recent research revealed that DIOXYGENASE FOR AUXIN OXIDATION 1 (DAO1) is responsible for the conversion of IAA-Asp to oxIAA-Asp in Arabidopsis (Müller et al., 2021). oxIAA-Asp can be further converted to corresponding high molecular weight oxIAA-peptides (Riov and Bangerth, 1992) or 3-hydroxy-oxIAA (Tsurumi and Wada, 1986; Hayashi et al., 2021). So far, only oxIAA-Asp and oxIAA-Glu have been determined as endogenous metabolites in Arabidopsis (Hayashi et al., 2021), oxIAA-Asp in roots of rice (Isobe and Miyagawa, 2022), lychee leaves, flowers (Kim et al., 2021) and ovaries (Osako et al., 2022), while oxIAA-Glu was also detected in lychee leaves (Kim et al., 2021). In rice, oxIAA-Glu was not detected in the tissue, but it was present in hydroponic medium after stress treatment, thus suggesting its formation in rice (Isobe and Miyagawa, 2022). For a long time, the GH3-mediated conjugation and irreversible oxidation of IAA by DAO1 were believed to be two parallel pathways of auxin inactivation. Hayashi et al. (2021) showed that in Arabidopsis DAO1 preferably oxidizes IAA-amino acid conjugates IAA-Asp and IAA-Glu into oxIAA-Asp and oxIAA-Glu, respectively, which are subsequently hydrolysed by IAA-Leu-Resistance1/Arabidopsis ILR1-Like hydrolases (ILR1/ILL) to inactive oxIAA. Both mechanisms therefore contribute to the same auxin inactivation pathway (Figure 1). Recently, oxIAA conjugation mediated by GH3 enzymes has also been confirmed, however, its contribution to IAA homeostasis is species-dependent (Brunoni et al., 2023).

Auxins are present in plants in trace amounts, making their quantitative and qualitative analysis very challenging (Fu et al.,

Abbreviations: BBCH, Biologische Bundesanstalt, Bundessortenamt und Chemische Industrie scale; DAO1, DIOXYGENASE FOR AUXIN OXIDATION 1; GH3, GRETCHEN HAGEN 3; HPLC, high-performance liquid chromatography; HPLC-MS/MS, high-performance liquid chromatography with tandem electrospray mass spectrometry; IAA, indole-3-acetic acid; IAA-AA, indole-3-acetyl-amino acid; IAA-Asp, indole-3-acetyl-aspartic acid; IAA-glc, indole-3-acetyl-1-O-ß-D-glucose; IAA-Glu, indole-3-acetyl-glutamic acid; IAA-Leu, indole-3-acetyl-leucine; IAA-Phe, indole-3-acetyl-phenylalanine; ILR1/ILL, IAA-Leu-Resistance1/Arabidopsis ILR1-Like hydrolases; in-tip μSPE, micro-scale in-tip solid-phase extraction; oxIAA, 2-oxindole-3-acetic acid; oxIAA-AA, 2-oxindole-3-acetyl-amino acid; oxIAA-Asp, 2-oxindole-3-acetyl-aspartic acid; oxIAA-glc, 2-oxindole-3-acetyl-1-O-ß-D-glucose; oxIAA-Glu, 2-oxindole-3-acetyl-glutamic acid; oxIAA-Leu, 2-oxindole-3-acetyl-leucine; oxIAA-Phe, 2-oxindole-3-acetyl- phenylalanine; PCA, principal component analysis; UGT84B1/UGT74D1, UDP-glucosyltransferase 84B1/74D1.

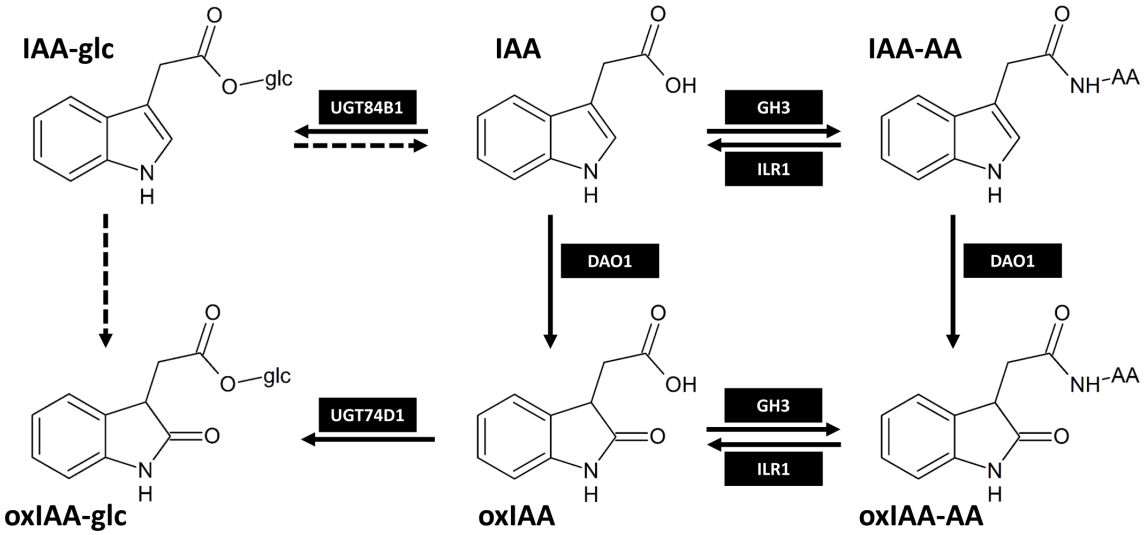

FIGURE 1
The main IAA inactivation pathways in Arabidopsis thaliana as proposed by Tanaka et al., 2014; Hayashi et al., 2021; Müller et al., 2021 and Brunoni et al., 2023. Dashed arrows represent metabolic steps that are still not fully described. IAA-AA and oxIAA-AA represent amide-linked conjugates with amino acids. The enzymes responsible for IAA metabolism shown in black boxes are as follows: DAO1, DIOXYGENASE FOR AUXIN OXIDATION 1; GH3, GRETCHEN HAGEN 3; UGT84B1/UGT74D1, UDP-glucosyltransferase 84B1/74D1; ILR1, IAA-Leu-Resistance 1.

2011; Du et al., 2012; Porfírio et al., 2016). Many solvents are used for extraction, such as organic solvents or aqueous buffers (reviewed in Du et al., 2012). Recently, sample purification by solid-phase extraction (SPE) has become the most used method of auxin purification with the tendency to minimize the amount of solvents and analytes (Liu et al., 2007; Liu et al., 2012; Novák et al., 2012; Porfírio et al., 2016; Pěnčík et al., 2018; Wang et al., 2020). Until now, a wide range of sorbents have been used for purification: reverse phase columns C18 (Rolčík et al., 2005; Tivendale et al., 2012), and HLB (Novák et al., 2012), poly (styrene-divinylbenzene) copolymer SDB-XC (Pěnčík et al., 2018) or mixed-mode ion-exchange polymeric sorbents (Dobrev et al., 2005; Izumi et al., 2009). Gas chromatography and high-performance liquid chromatography (HPLC) are the most widely used methods for auxin detection (Porfírio et al., 2016). Modern methods provide fast and efficient separation of several classes of phytohormones (Šimura et al., 2018; Široká et al., 2022). Examples given are nanoflow capillary liquid chromatography (Izumi et al., 2009) or ultra-high performance liquid chromatography using sub-2 µm particles and higher pressure tolerance (1000 bar versus 500 bar for HPLC), which together allow more efficient and faster separation of substances (Novák et al., 2008; Kojima et al., 2009). For auxin analysis, the combination of high-performance liquid chromatography with tandem mass spectrometry (HPLC-MS/MS) is currently the most used method (Kai et al., 2007a; Novák et al., 2012; Sugawara et al., 2015; Pěnčík et al., 2018).

Although some oxIAA-amino acids have been identified in plants, information about their occurrence in various plant species and distribution within individual plant organs is still under-investigated. In this study, we identified two novel oxIAA amide conjugates oxIAA-Leu and oxIAA-Phe and performed tissue-specific quantitative determination of four 2-oxindole-3-acetic acid amides: oxIAA-Asp, oxIAA-Glu, oxIAA-Leu and oxIAA-Phe using optimised protocol combining micro-scale in-tip solid-phase extraction (in-tip µSPE) with HPLC-MS/MS. In order to uncover the diversity of IAA metabolism, we further analysed IAA metabolite profiles of four representative angiosperm plant models - *Arabidopsis thaliana*, pea (*Pisum sativum* L.), wheat (*Triticum aestivum* L.) and maize (*Zea mays* L.) at multiple growth stages according to the Biologische Bundesanstalt, Bundessortenamt und Chemische Industrie (BBCH) scale (Tottman, 1987; Lancashire et al., 1991; Boyes et al., 2001).

Materials and methods

Reagents and standards

The standards for IAA and indole-$^{13}C_6$-labeled IAA were purchased from Merck (Germany). Standards for IAA-Asp, IAA-Glu, IAA-Leu, IAA-Phe, oxIAA, and $^{13}C_6$-[benzene ring]-IAA-Asp, [$^{13}C_6$]IAA-Glu and [$^{13}C_6$]oxIAA were purchased from OlChemIm (Czech Republic). IAA-glc, oxIAA-glc, [$^{13}C_6$]IAA-glc, [$^{13}C_6$] oxIAA-glc, oxIAA-Asp, oxIAA-Glu, oxIAA-Leu, oxIAA-Phe, oxIAA-[$^{13}C_4$,^{15}N]Asp, oxIAA-[$^{13}C_5$,^{15}N]Glu were synthesised in accordance to (Kai et al., 2007a; Kai et al., 2007c) with minor modifications. Plant agar and Murashige & Skoog media were purchased from Duchefa; methanol for HPLC analysis and all other chemicals were purchased from Merck (Germany) and Lach-Ner (Czech Republic).

Plant material and growth conditions

Arabidopsis seeds (ecotype Col-0) were sterilized with 70% ethanol with the addition of 0.1% Tween 20 for 5 minutes, sown on Murashige & Skoog square agar plates (10 g sucrose, 4.4 g MS medium, 10 g agar per liter, pH 5.7) and cold treated for 4 days prior to germination. The plates were then transferred to a cultivation chamber and vertically placed under long-day conditions (16 h light/8 h dark) at 22 ± 1°C under cool white fluorescent light (maximum irradiance 550 µmol m^{-2} s^{-1}). The seedlings were harvested at different growth stages according to the BBCH scale (Table S1; Figure S1). Shoots and roots were separated and weighed in five replicates, homogenized and immediately frozen in liquid nitrogen, and stored at -80°C until extraction.

Pea (*Pisum sativum arvense* L.), wheat (*Triticum aestivum* L.), and maize (*Zea mays* L.) seeds were left germinating in the dark for two, three and four days, respectively, selected according to their uniformity from a large population, transferred to hydroponic boxes, watered with Hoagland's solution and left growing in the cultivation room (16 h light/8 h dark) at 22 ± 2°C. Three to five plants per growth stage were harvested (Table S1; Figure S1). Shoots, roots, and cotyledons were separated and weighed in five replicates, homogenized and immediately frozen in liquid nitrogen, and stored at -80°C until extraction.

Extraction and purification of auxins

Frozen samples containing 10 mg of fresh weight (pea, maize, wheat, Arabidopsis shoot) or 3 mg (Arabidopsis root) were extracted in 1 ml (500 µl for Arabidopsis root samples) of ice-cold Na-phosphate buffer (50 mM, pH 7.0, 4°C) containing 0.1% diethyldithiocarbamic acid sodium salt. A mixture of stable isotope-labeled internal standards ([$^{13}C_6$]IAA, [$^{13}C_6$]IAA-Asp, [$^{13}C_6$]IAA-glc, [$^{13}C_6$]IAA-Glu, [$^{13}C_6$]oxIAA, oxIAA-[$^{13}C_4$,^{15}N]Asp, [$^{13}C_6$]oxIAA-glc, oxIAA-[$^{13}C_5$,^{15}N]Glu) was added to each sample in amount of 5 pmol each (2.5 pmol for Arabidopsis roots). Due to the high concentration of oxIAA-Asp in pea seeds, five replicates were diluted in an ice-cold Na-phosphate buffer by one hundred (10 µl of sample to 990 µl of Na-phosphate buffer) and then 5 pmol of internal standards were added as described above. All samples were then homogenized using a MM400 bead mill (Retsch GmbH, Germany) at a frequency of 27 Hz for 10 minutes after adding three zirconium oxide beads. Extracted samples were incubated at 4°C with continuous shaking for 15 minutes and then centrifuged (15 minutes, 206 642 g, 4°C). From each sample, 200 µl of Na-phosphate buffer was transferred to clean microtubes, pH adjusted to 2.7 by 0.1 M hydrochloric acid and purified using in-tip µSPE (Pěnčík et al., 2018) with two types of extraction sorbents (three layers of each): HLB AttractSPE™ (Affinisep, France) and SDB-XC Empore™ (3M, USA). Briefly, multi-StageTip microcolumns were activated by 50 µl of acetone (centrifugation 10 minutes, 3 846 g, 8°C), 50 µl of methanol (10 minutes, 3 846 g, 8°C), and 50 µl of water (15 minutes, 4 654 g, 8°C). The acidified samples were then applied to activated microcolumns (centrifugation 30 minutes, 16 961 g, 8°C), washed by 50 µl of 0.1% acetic acid (20 minutes, 9 846 g, 8°C) and eluted with 50 µl of 80% methanol (20 minutes, 8 653 g, 8°C). After elution, the samples were evaporated to dryness *in vacuo*, and stored at -20°C until HPLC-MS/MS analysis.

For optimization of in-tip µSPE method, three types of extraction sorbents (SDB-XC Empore™, HLB AttractSPE™, and C18 Empore™) and their combinations were tested. For the single sorbent, five layers of HLB or SDB-XC were applied to the StageTip microcolumn. For multiple sorbent combinations, three layers of each sorbent were used. To compare extraction recovery of each microcolumn, 200 µl of acidified Na-phosphate buffer containing 2 pmol of unlabeled standards (IAA, IAA-Asp, IAA-glc, IAA-Glu, oxIAA, oxIAA-Asp, oxIAA-glc, oxIAA-Glu, oxIAA-Leu, oxIAA-Phe) was applied to activated microcolumns, washed and eluted as mentioned above. The samples were then evaporated to dryness *in vacuo* and stored at -20°C until HPLC-MS/MS analysis. Finally, process efficiency of each sorbent was expressed as a percentage recovery and calculated as the ratio of the peak area of an unlabeled analyte spiked before µSPE to the peak area of the neat solution (Matuszewski et al., 2003).

Quantification of IAA metabolites

The evaporated samples were dissolved in 30 µl of 10% methanol prior to HPLC-MS/MS analysis using a 1290 Infinity LC system and a 6490 Triple Quadrupole LC/MS system equipped with Jet Stream and Dual Ion Funnel systems (Agilent Technologies, CA, USA). The chromatographic reverse-phase column (Kinetex C18 100A, length 50 mm, diameter 2.1 mm, particle size 1.7 µm; Phenomenex, CA, USA) was used for the separation of individual analytes by HPLC. The mobile phase consisted of deionized water (A) and methanol (B) with the addition of 0.1% acetic acid. The time of each analysis was 18 min, flow rate 0.3 ml/min and IAA metabolites were eluted using gradient elution as follows: 0 min – 10% B, 11.5 min – 60% B, 11.75 min – 100% B, 14.75 min – 100% B, 15 min – 10% B. For IAA-glc quantification in Arabidopsis, different type of column (Kinetex C18 100A, length 150 mm, diameter 2.1 mm, particle size 1.7 µm; Phenomenex, CA, USA) was used with the identical chromatographic conditions as described above. During analysis, the samples were stored in an autosampler at 4°C, a column tempered at 40°C and 10 µl of each sample was injected.

Individual analytes were detected by the MS instrument combining positive and negative ESI mode (+/-) with optimised conditions as follows: nebulizer pressure, 25 psi; drying gas flow and temperature, 14 l/min and 130°C; sheath gas flow and temperature, 12 l/min and 400°C; capillary voltage, 2.8 kV in positive mode and 3.0 kV in negative mode; nozzle voltage, 0 V. Analytes were detected and quantified using diagnostic multiple reaction monitoring (MRM) transitions of precursor and appropriate product ions using optimal collision energies and 50 ms dwell time (Table S2). For data interpretation, Mass Hunter software (Agilent Technologies, CA, USA) was used.

Method validation

Seven-day-old pea and wheat seedlings were harvested, weighed, and immediately frozen in liquid nitrogen, and stored at -80°C until extraction. Samples of 10 mg of FW were extracted in 1 ml of Na-phosphate buffer (50 mM, pH 7.0, 4°C, 0.1% diethyldithiocarbamic acid sodium salt) as previously described. After centrifugation, the samples were diluted to 5 ml with Na-phosphate buffer and each sample divided into doses of 200 µl (15 samples per plant). Subsequently, in five replicates, samples were supplemented with 1 pmol, 10 pmol or without unlabeled standards (IAA, IAA-Asp, IAA-glc, IAA-Glu, oxIAA, oxIAA-Asp, oxIAA-glc, oxIAA-Glu, oxIAA-Leu, oxIAA-Phe) and 5 pmol of internal stable isotope-labeled standards ([$^{13}C_6$]IAA, [$^{13}C_6$]IAA-Asp, [$^{13}C_6$]IAA-Glu, [$^{13}C_6$]IAA-glc, [$^{13}C_6$]oxIAA, oxIAA-[$^{13}C_4$,^{15}N]Asp, [$^{13}C_6$]oxIAA-glc, oxIAA-[$^{13}C_5$,^{15}N]Glu). All samples were then acidified and purified by in-tip µSPE method as described above. Finally, concentrations of all analytes were quantified by HPLC-MS/MS using a standard isotope dilution method. To calculate the accuracy of the method, the deviation of the determined analyte concentration (after subtraction of endogenous level) from its nominal level (known amount of analyte standard added to sample) was divided by the nominal level and expressed as percentage bias. Method precision was calculated as the relative standard deviation of determined levels.

Data analysis

Multivariate data analysis was performed using SIMCA 17 software (Sartorius Stedim Data Analytics, Umeå, Sweden). Dataset containing endogenous concentrations (pmol/g FW) was log transformed, centered and scaled using unit-variance scaling method. Values under limit of detection (LOD) were replaced with 0.95-fold of respective LOD value. Principal component analysis (PCA) was calculated for description of data structure. All PCA models were cross-validated to assess model reliability. Variables with no or neglectable effect in score plot were excluded.

Results

Development and validation of oxIAA-amino acids profiling method

Solid phase extraction is becoming the most widely used method for the purification of phytohormones. In the last decade, there has been a trend towards minimal use of solvents, which has led to the development of new solid phase microextraction such as in-tip µSPE, which was first used for cytokinin analysis (Svačinová et al., 2012) and later for auxin purification (Liu et al., 2012; Pěnčík et al., 2018). We adopted the in-tip µSPE purification protocol described by Pěnčík et al. (2018) to achieve the highest possible extraction efficiency for all IAA metabolites including novel oxIAA-AA conjugates. The recovery rate of analytes was tested using three types of extraction sorbents and their combination: SDB-XC Empore™, HLB AttractSPE™, and C18 Empore™. The recoveries of added auxin standards in acidified Na-phosphate buffer applied onto microcolumns are summarized in Figure S2. The single-StageTips filled with HLB or SDB-XC sorbents recovered 49 ± 9% and 59 ± 11% of auxin compounds, respectively. In good agreement with previously published data (Pěnčík et al., 2018), multi-StageTips C18/SDB-XC also showed high extraction yields (mean recovery 60 ± 11%). Under our experimental conditions, the HLB/SDB-XC microcolumns combined hydrophilic-lipophilic balance/polymer-based sorbents provided the highest recoveries ranging from 47% to 89% across all analytes (Figure S2). Importantly, oxIAA-AA conjugates were efficiently retained on HLB/SDB-XC sorbents with recovery rates ranging from 47 ± 14% (oxIAA-Asp) to 76 ± 5% (oxIAA-Leu). According to our findings, a combination of HLB/SDB-XC sorbents was used to isolate oxIAA-AA conjugates from the studied plant material.

All auxin metabolites were analysed by LC-MS/MS method using electrospray ionization in positive and negative modes. MRM transitions and collision energies were optimised for all analytes and their corresponding stable isotope labelled internal standards (Table S2). Confirmation of the newly identified metabolites in pea cotyledons was performed based on comparisons to the retention times of a synthetic oxIAA-AA reference standard (Figure 2). Importantly, two chromatographic peaks were detected due to the optical activity of investigated compounds at position three in the oxindole molecule, 8.9/9.5 min for oxIAA-Leu and 9.3/9.8 min for oxIAA-Phe. Moreover, each sample extract (Arabidopsis, wheat and pea) was spiked with a mixture of oxIAA-Leu and oxIAA-Phe at known levels (0, 1.0 and 10.0 pmol). These results also confirmed the detection of two chromatographic peaks of both new amino acid conjugates. Representative MRM chromatograms of the spiked Arabidopsis samples are shown in Figure 2.

For method validation, 18-point calibration curves ranging from 45 amol to 90 pmol were constructed and the LOD (S/N ratio > 3) as well as the dynamic linear range were calculated (Table S2). For newly identified metabolites, the linear range stretched from 9 fmol to 90 pmol, and for the other compounds, the linear range started even at 90 amol. Finally, a spiking experiment with authentic standards of auxin metabolites was performed. Wheat and pea extracts were used for method validation as representatives of monocots and dicots, respectively. A standard mixture containing 1 or 10 pmol of individual authentic standards was added to extracts containing 2 mg of plant material (homogenized whole plants) and their recovery was calculated after subtraction of endogenous levels (Matuszewski et al., 2003). The method accuracy (percentage deviation from the accepted reference value, % bias) and method precision (relative standard deviation of determined levels, RSD) were then calculated (Table S3). Mean method accuracy was 15 ± 12% bias for pea samples and 19 ± 15% bias for extracts prepared from wheat seedlings. Method precisions of all analytes were below 14% RSD for both tested matrices (Table S3). Overall, our results showed that the method has good linearity, high sensitivity and sufficient precision and accuracy, and thus the levels of auxin metabolites were finally determined.

10.3389/fpls.2023.1217421

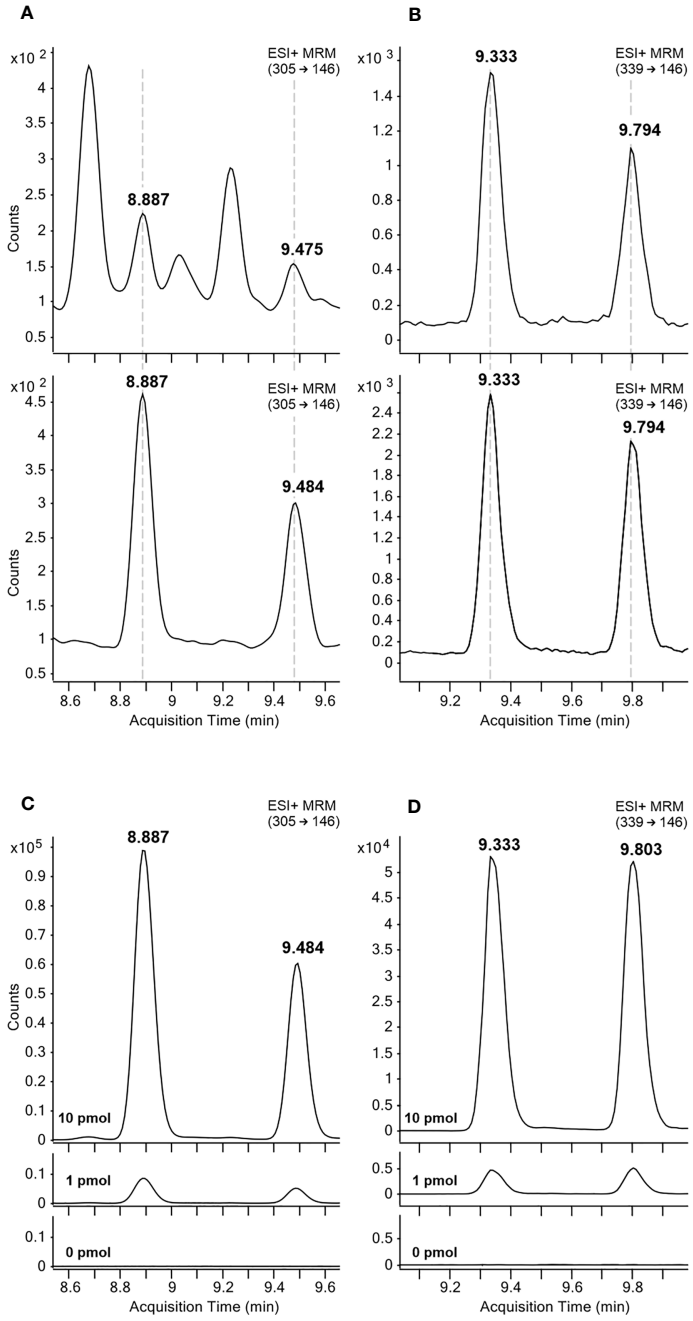

FIGURE 2
Representative MRM chromatograms of oxIAA-Leu **(A, C)** and oxIAA-Phe **(B, D)**. The retention times of oxIAA-Leu **(A)** and oxIAA-Phe **(B)** in pea cotyledons extracts containing 2 mg FW of the tissue (upper) and 5 fmol (oxIAA-leu) or 50 fmol (oxIAA-Phe) of synthetic reference standards (lower). Arabidopsis extracts spiked with 1 or 10 pmol of oxIAA-Leu **(C)** and oxIAA-Phe **(D)** synthetic standards.

Quantification of oxIAA-amino acid conjugates

Endogenous levels of oxIAA-AAs were determined in roots, cotyledons and shoots of three crop species (maize, pea, and wheat), and in shoots and roots of Arabidopsis (Figure 3; Table S4). In order to obtain comparable data, all species were harvested at the same growth stage 1.0 (Table S1; Figure S1).

Conjugates of oxIAA with Asp and Glu were determined in all four analysed species, but the levels varied greatly depending on the species and particular part of the plant. In general, oxIAA-Asp was found to be the most abundant oxIAA conjugate in pea tissues, for example concentrations close to 300 nmol·g^{-1} FW in cotyledons (Table S4). In contrast, oxIAA-Glu was the major oxIAA-AA conjugate in Arabidopsis. The determined levels of oxIAA-Glu were 81/92 pmol·g^{-1} FW in Arabidopsis shoots/roots,

10.3389/fpls.2023.1217421

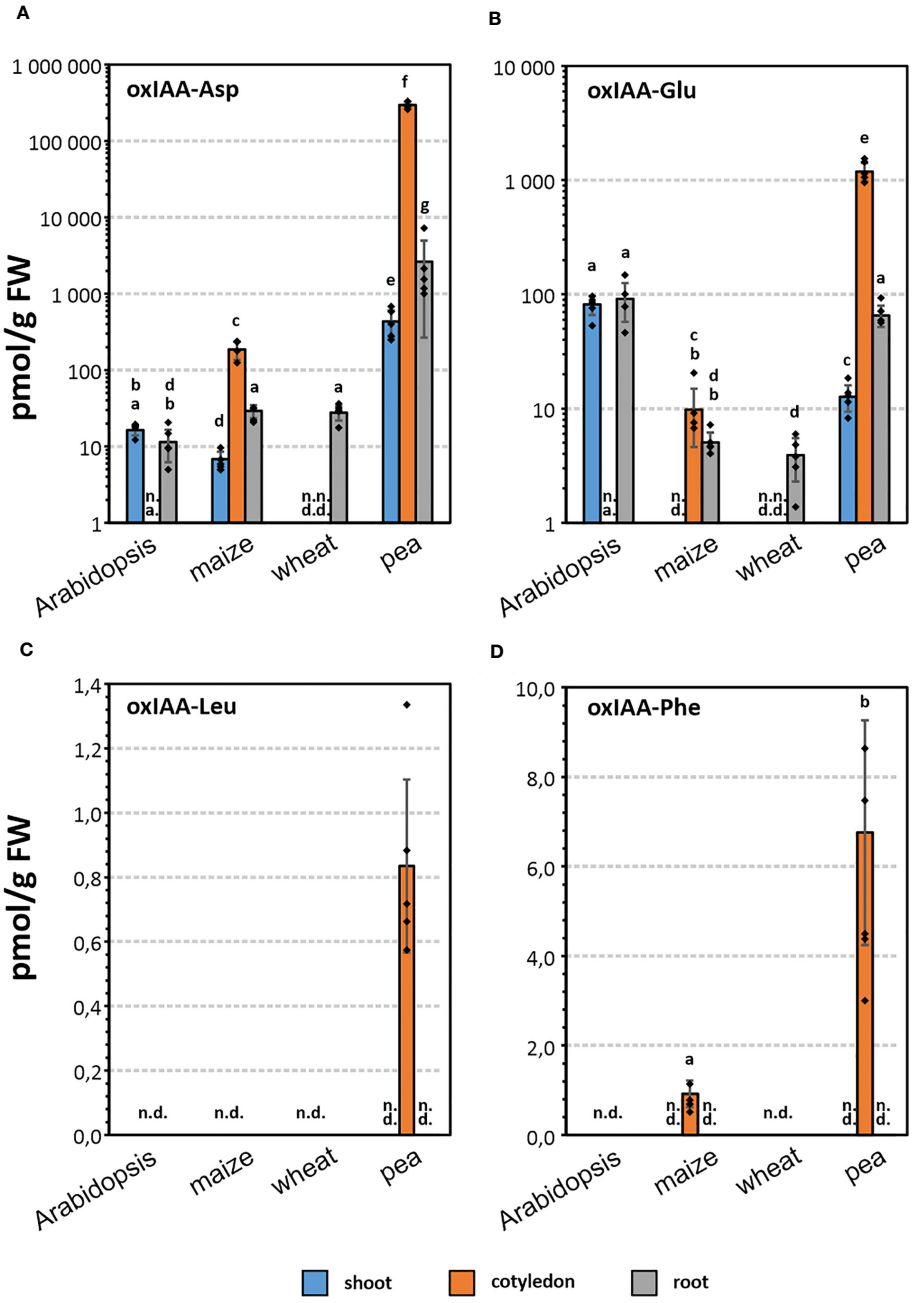

FIGURE 3
Endogenous levels (pmol · g^{-1} FW) of oxIAA-Asp **(A)**, oxIAA-Glu **(B)**, oxIAA-Leu **(C)** and oxIAA-Phe **(D)** in root, shoot, and cotyledon of maize, wheat, pea, and root and shoot of Arabidopsis. Levels of oxIAA-Asp and oxIAA-Glu are shown on a logarithmic scale. The error bars indicate the standard deviations of five replicates (mean ± SD, n=5). One-way ANOVA and Tukey's post hoc test were applied to log-transformed data to assess the differences between groups. Different letters (a-g) indicate significant differences at the 5% level of significance. n.d., not detected; n.a., not analysed.

while oxIAA-Asp was detected in lower quantities (16/11 pmol·g^{-1} FW). In both members of the Poaceae family, wheat and maize, oxIAA conjugates with Asp and Glu were partially determined. No oxIAA-Glu was detected in maize shoot samples (Figures 3B). Moreover, both amino acid conjugates were below the limit of detection in wheat shoots and cotyledons. Interestingly, endogenous levels of oxIAA-Asp showed similar pattern in maize tissues compared to pea samples, but at picomolar levels (Figure 3A).

The newly identified metabolites, oxIAA-Leu and oxIAA-Phe, were detected only in cotyledon samples, oxIAA-Phe in maize and both conjugates in pea (Figures 3C, D). Importantly, these Leu and Phe conjugates were much less abundant compared to oxIAA-Asp or oxIAA-Glu. Pea cotyledons contained 7 pmol·g^{-1} of oxIAA-Phe and

less than 1 pmol·g^{-1} of oxIAA-Leu, similar to oxIAA-Phe level in maize cotyledons (Table S4).

Metabolite profiles of IAA and oxIAA conjugates in different plant species

Full auxin metabolite profiles including free IAA, oxIAA and their low-molecular-weight conjugates with amino acids and glucose were determined in the same four plant models at growth stage 1.0. The levels of IAA and oxIAA conjugates with individual amino acids (Asp, Glu, Leu and Phe) were summed up into two corresponding groups IAA-AA and oxIAA-AA, respectively. The contributions of different conjugate classes as well as glucosyl esters were calculated as their relative abundances to the total pool of IAA metabolites (Figure 4; Table S5). Overall, the relative distribution of auxin metabolites differed notably within studied species as well as within the individual plant parts.

The dominant conjugate in Arabidopsis was oxIAA-glc taking 81% (shoots) and 68% (roots) of all measured metabolites, while IAA-glc and amino acid conjugates of both IAA and oxIAA, as well as free IAA, were found to have a minor representation in Arabidopsis. The second most abundant metabolite was oxIAA, which took 15% of the IAA metabolite pool in the shoots and 23% in the roots (Figure 4A).

FIGURE 4
Relative distribution of auxin metabolites in Arabidopsis **(A)**, pea **(B)**, maize **(C)** and wheat **(D)** plants at 1.0 growth stage. IAA-AA represents a sum of IAA-Asp, IAA-Glu, IAA-Leu, and IAA-Phe relative abundances; oxIAA-AA represents a sum of oxIAA-Asp, oxIAA-Glu, oxIAA-Leu, and oxIAA-Phe relative abundances. Non-oxidized forms of IAA are shown in shades of blue and oxidized forms in yellow shades. All samples were measured in five replicates. R, Roots; S, Shoots; C, cotyledons.

In contrast, the major auxin metabolites in pea were oxIAA-AA conjugates, accounting for 53% in shoots and 58% in roots. IAA-AAs were the second most abundant conjugates in pea shoots (22%) and roots (15%). In cotyledons, oxIAA-AAs were fully dominant, taking 99% of all auxin metabolites (Figure 4B). Similar profiles of auxin metabolites were observed in maize and wheat. In both species, oxIAA was major metabolite in shoots (79% in maize; 88% in wheat). In other parts, oxIAA was also the most abundant inactive auxin metabolite; only free IAA had a greater proportion in maize roots and wheat cotyledons. Amide conjugates of oxIAA were also present in maize and wheat, but occupied a relatively minor part of the total auxin metabolite profile (Figures 4C, D).

Spatiotemporal dynamics of auxin metabolites distribution during early plant development

We further investigated the distribution of IAA and its metabolites during the early development of Arabidopsis, pea, maize and wheat. Therefore, different plant parts such as roots, shoots (all species) and cotyledons (only crop species) were sampled at different growth stages. The first analysed stage was 1.0, in which the first leaf emerges from the coleoptile in grains, or cotyledons are fully unfolded in pea and Arabidopsis. The following stages were 1.1 and 1.2, in which the first and second leaf are fully developed and unfolded (Figure S1). However, the stage 1.1 is not differentiated in Arabidopsis as first two leaves develop simultaneously.

Principal component analysis (PCA) was used to observe the variability in auxin metabolite content. As already indicated in Figure 4, the significant differences of the relative distribution of auxin metabolites between plant species was observed. Therefore, each species was evaluated in individual PCA model to describe the distribution of metabolites in roots and shoots and growth stages (Figure 5, complete dataset provided as Supplementary Table 6). The most complex patterns found in this study were later analysed using additional PCA to describe changes in the development of individual plant parts (Figure 6).

In Arabidopsis, only stages 1.0 and 1.2 were analysed. At stage 1.0 the cotyledons are completely opened, while stage 1.2 is defined by fully developed first two true leaves (Boyes et al., 2001). A more pronounced stage-dependent alteration of auxin metabolome was observed in shoots, where auxin metabolite content was higher at the early stage (1.0) and dropped during seedling development up to stage 1.2 (Figure 5A). This trend was observed not only in auxin metabolites, but also in free active IAA. Interestingly, there were no significant changes in auxin metabolome in the roots during development. Regardless of the stages, oxIAA-glc levels were much higher in shoots, compared to roots. Pea roots contained a higher concentration of auxin metabolites than shoots at all growth stages (Figure 5B). The roots at stage 1.0 were characterised by the highest content of oxIAA-Asp and oxIAA-Glu, the concentrations of which gradually decreased until stage 1.2. A similar trend was observed in the shoots, where the highest levels of all IAA and oxIAA conjugates were determined at stage 1.0. The levels of conjugates dropped towards later stages, while oxIAA showed a maximum at middle stage 1.1 (Figure 6A). In maize and wheat, higher concentrations were also observed in roots compared to shoots throughout the development period. In maize, the two earlier stages were associated with higher levels of oxIAA, while the last stage was characterized by the accumulation of oxIAA-glc in roots (Figure 5C). With the increasing stage of development, the concentration of amino acid conjugates of both IAA and oxIAA decreased in wheat roots, while oxIAA and oxIAA-glc levels have changed in the opposite manner (Figures 5D, 6B).

Discussion

Auxin metabolism is a complex process, which is still not very well understood. Several mechanisms of IAA inactivation and degradation have been described so far. One of the most intensively studied and best characterised mechanisms of IAA inactivation is the conjugation with amino acids mediated by GH3 enzyme family (Staswick et al., 2005). The amides of IAA can be then irreversibly oxidized by DAO1 to form oxIAA-AAs (Müller et al., 2021). Hayashi et al. (2021) revealed that in Arabidopsis, oxIAA-AAs are hydrolysed by amido hydrolases to oxIAA, which is then possibly further oxidized to 3-hydroxy-oxIAA (dioxIAA). According to the newly proposed model of auxin metabolism, conjugation with amino acids and oxidation of indole ring contribute to the same pathway, in which oxIAA-AAs serve as intermediates (Figure 1). This pathway involving oxIAA-AAs is proposed as a main route of IAA inactivation and is therefore a key mechanism contributing to auxin homeostasis in Arabidopsis (Hayashi et al., 2021). Interestingly, it was recently shown that the GH3-ILR1-DAO pathway does not operate in non-flowering plants (Brunoni et al., 2020; Brunoni et al., 2023). Apart from Arabidopsis, endogenous levels of oxIAA-Asp and oxIAA-Glu were recently determined in lychee (Kim et al., 2021; Osako et al., 2022), oxIAA-Asp also in rice (Isobe and Miyagawa, 2022). However, there is no evidence about their endogenous levels and distribution in other plant species. Furthermore, the occurrence of oxIAA conjugates with other amino acids was not yet reported.

In our study, we focused on investigating the abundance and distribution of oxIAA amino acid conjugates (oxIAA-Asp/Glu/Leu/Phe) in Arabidopsis and three important crop species: maize, pea and wheat. Therefore, we utilized an optimised analytical method combining micro-scale purification with LC-MS/MS. For the isolation of oxIAA amino acid conjugates, we adopted the μSPE protocol previously developed for the purification IAA metabolites (Pěnčík et al., 2018). To maximise the yield of the purification step, we compared the recoveries of oxIAA-AAs as well as other IAA metabolites using various types of SPE sorbents and their combinations. Finally, we used multi-μSPE columns assembled from a combination of HLB and SDB-XC sorbents, which provided the highest overall extraction yield of all tested sorbents (Figure S2). The accuracy and precision of the analytical method was then tested by quantifying known amounts of authentic standards added to pea and wheat extracts. Overall, the method validation demonstrated good applicability of the new protocol for the quantitative analysis of auxin metabolites in distinct plant

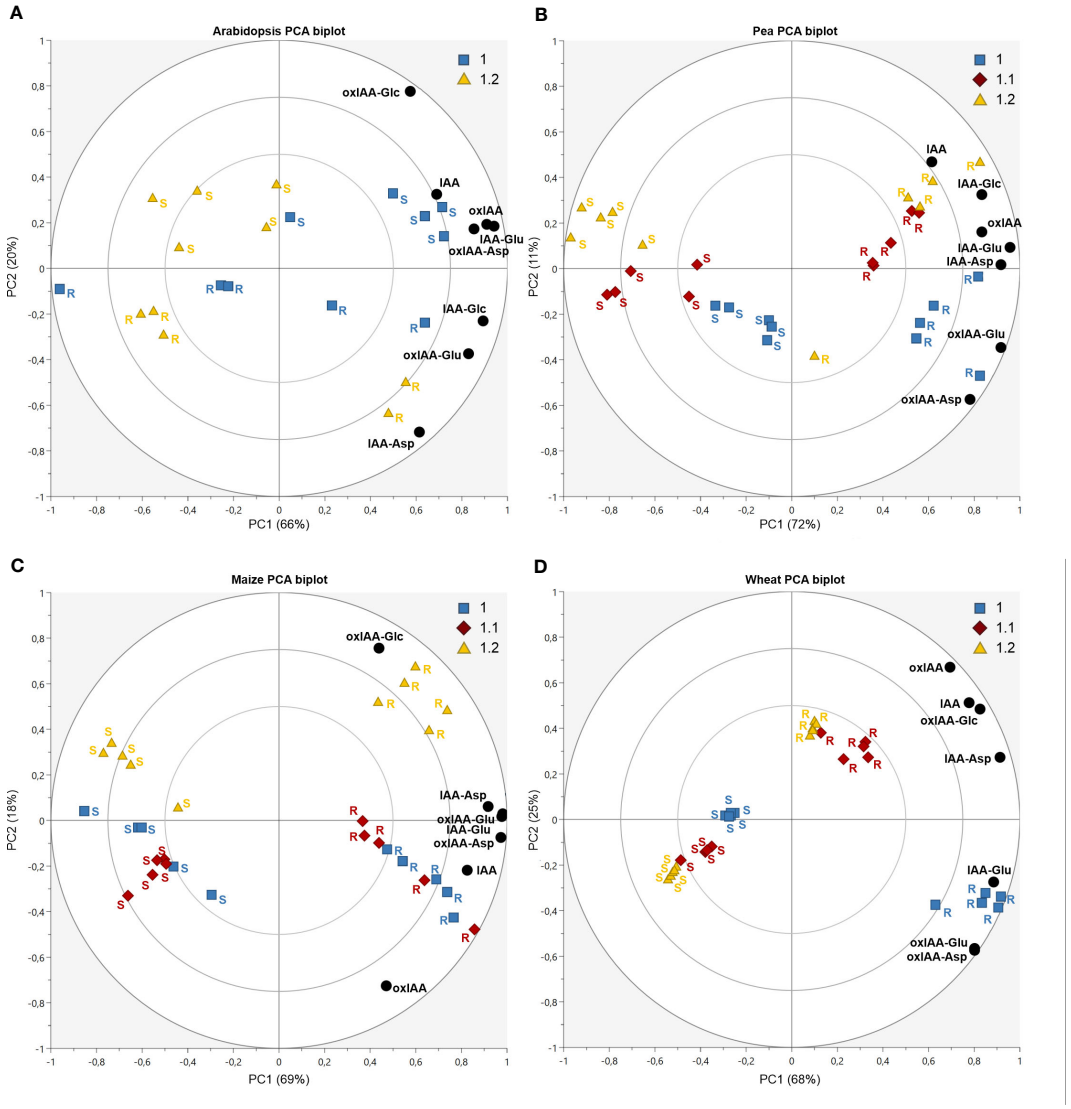

FIGURE 5
Auxin metabolites distribution dynamics during plant development in Arabidopsis **(A)**, pea **(B)**, maize **(C)** and wheat **(D)**. Each figure displays a PCA biplot, axes PC1 and PC2 express correlation-scaled loadings as concentration of metabolites (black circles) and correlation-scaled scores as samples of root (R) and shoot (S) at growth stages 1.0 (blue squares), 1.1 (red diamonds) and 1.2 (yellow triangles).

matrices (Table S3). Unsatisfactory method accuracy (up to 48% bias) was achieved only for oxIAA-Leu and oxIAA-Phe, for which corresponding isotopically labelled standards are still missing. Unfortunately, the close-eluting internal standard oxIAA-[$^{13}C_5$,^{15}N]Glu was not able to fully compensate for analytes losses during sample processing and subsequent LC-MS/MS analysis. Importantly, the reduced accuracy was mainly detected in wheat samples in which the two novel naturally occurring auxin metabolites were not detected (Figures 3C, D).

The optimised and validated analytical method was then utilized for determination of oxIAA amino acid conjugates in Arabidopsis and three crop species: pea, maize and wheat. In Arabidopsis, oxIAA-Asp and oxIAA-Glu were determined in comparable levels in both roots and shoots. According to previously performed quantification (Hayashi et al., 2021), oxIAA-Glu was the most abundant conjugate in Arabidopsis, in contrast to other studied species, where oxIAA-Asp dominated throughout all seedling parts. In crop species, oxIAA conjugates were mainly accumulated in cotyledons, except for wheat, in which oxIAA conjugates were detected only in roots. While oxIAA-Asp and oxIAA-Glu were found in all studied species, oxIAA-Leu was detected only in pea cotyledons, as well as oxIAA-Phe, which was additionally detected in cotyledons of maize. Kai et al. (2007a) previously observed formation of oxIAA-Phe in Arabidopsis after administration of IAA-Phe. However, here we report for the first time oxIAA conjugates with Leu and Phe as endogenous plant metabolites.

The endogenous content of oxIAA amino acid conjugates was then evaluated in the context of overall auxin metabolome. In accordance with previous studies (Kai et al., 2007a; Pěnčík et al., 2018), oxIAA-glc was determined as a major auxin metabolite in Arabidopsis, followed by oxIAA, while amide-linked conjugates occupied relatively minor part of the total pool (Figure 4A). In

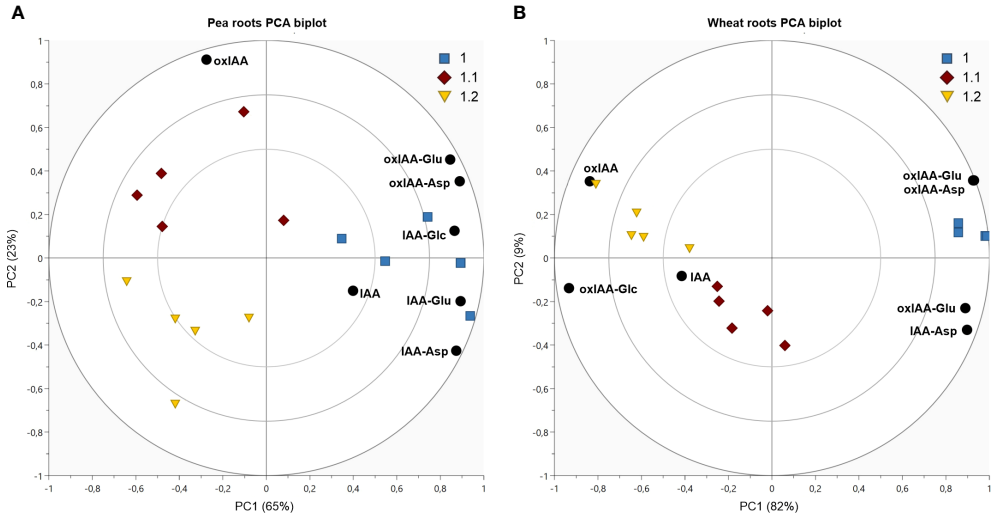

FIGURE 6
Dynamics of auxin metabolites distribution in pea shoots **(A)** and wheat roots **(B)**. Both figures display PCA biplot, axes PC1 and PC2 express correlation-scaled loadings as concentration of metabolites (black circles) and correlation-scaled scores as samples at growth stages 1.0 (blue squares), 1.1 (red diamonds) and 1.2 (yellow triangles).

strong contrast to Arabidopsis, surprisingly no oxIAA-glc was detected in pea, whereas oxIAA amino acids represented the dominant class of metabolites in both roots and shoots. In pea cotyledons, they even made over 99% of total auxin metabolite content (Figure 4B). Our results are consistent with previous findings that the majority of IAA in pea is present as low or high molecular weight amide conjugates (Bandurski and Schulze, 1977). Interestingly, IAA-glc was below the limit of detection in all sections of maize and wheat seedling (Figures 4C, D). Nevertheless, IAA esters were found to be the main conjugated auxin form in seeds of both crops, as well as in vegetative tissue in case of maize (Bandurski and Schulze, 1977). Most likely, a major part of ester-linked auxin is represented by high molecular weight conjugates or indole-3-acetyl-*myo*-inositol, which was reported to serve as an important storage form of auxin in maize seeds (Nowacki and Bandurski, 1980).

Plant development is an ever-changing process controlled by phytohormones, the levels of which are being strictly regulated by *de novo* biosynthesis and metabolism during the entire period of plant growth. Therefore, we addressed the changes in concentrations and distribution of auxin and its metabolites within the seedling at early growth stages as defined by BBCH scale (Lancashire et al., 1991). During seedling development, the levels of auxin metabolites, including oxIAA-Asp and oxIAA-Glu, dropped in Arabidopsis shoots between stage 1.0, when the shoot is constituted of the hypocotyl and fully developed cotyledons, and stage 1.2, already having first pair of true leaves fully developed (Figure 5A). Interestingly, Ljung et al. (2001) showed that IAA levels in cotyledons and hypocotyls are relatively low and constant during early seedling development, while its content was dramatically higher in first two developing true leaves and decreased dramatically during following leaf expansion. Furthermore, high IAA levels were strongly correlated with high cell division rates in Arabidopsis leaves. It can be assumed that seedling at stage 1.0 already comprise primordia of the first pair of true leaves, in which the cells divide intensively and thus accumulate high levels of auxin. The change in auxin metabolite levels between growth stages 1.0 and 1.2 that we observed is most likely a consequence of the decrease in IAA concentration during true leaves development. In agreement with our results, a reduction of IAA metabolite levels during early Arabidopsis development was previously observed in one- or two-week-old seedlings (Tam et al., 2000; Kai et al., 2007a).

Consistently in all crops, higher concentrations of all metabolites were found in roots at all analysed growth stages (Figures 5B-D). A similar distribution was previously observed in another important crop, rice (*Oryza sativa* L.), where IAA amino acid conjugates (Matsuda et al., 2005; Kai et al., 2007b), as well as oxIAA-Asp, dioxIAA-Asp and dioxIAA-Glu (Isobe and Miyagawa, 2022) were determined at higher levels in roots compared to aerial parts. Like Arabidopsis, the levels of IAA metabolites also depended on growth stage in crop species. As a common trend across all three crop species, amide-linked conjugates were the most abundant at the earliest stage and decreased during the growth towards later stages. A very pronounced correlation between oxIAA-amino acids content and growth stage was observed in pea, where the levels of oxIAA-Asp and oxIAA-Glu were the highest at stage 1.0 and declined towards the stage 1.2 in both roots and shoots (Figures 5B, 6A). Interestingly, oxIAA-glc displayed the opposite pattern to amide-linked conjugates in the roots of both monocots, as it accumulated mainly at the stage 1.2.

In summary, we performed a comprehensive profiling of auxin metabolites in Arabidopsis and three crop plant models (pea, maize and wheat) using an optimised and validated micro-scale purification protocol combined with LC-MS/MS method. The novel approach is suitable for profiling of broad range of auxin metabolites in various plant models. We also identified new endogenous auxin metabolites (oxIAA-Leu and oxIAA-Phe) in maize and pea cotyledons. Our findings showed that auxin

metabolite profiles differed between species and individual parts of the seedling (root, shoot and cotyledon). Moreover, the levels of auxin metabolites also strongly depended on the growth stage of the seedling, suggesting an important role of IAA metabolism in maintaining the phytohormonal balance during plant development.

Data availability statement

The original contributions presented in the study are included in the article/Supplementary Material. Further inquiries can be directed to the corresponding author.

Author contributions

ON and AP conceived the project. PH and AP performed method development and optimization. PH grew and sampled the plants. PH conducted the purification and quantification of auxin metabolites. AZ synthesized all new oxIAA conjugates standards. PH, IP, ON and AP analysed and interpreted the data. PH prepared the manuscript draft. PH, ON and AP wrote the article with input from all authors. All authors contributed to the article and approved the submitted version.

Funding

The work was financially supported by the Ministry of Education, Youth and Sports of the Czech Republic (European Regional Development Fund-Project "Plants as a tool for sustainable global development" No. CZ.02.1.01/0.0/0.0/16_019/0000827). PH was supported by the Internal Grant of Palacký University Olomouc IGA_PrF_2023_031.

Acknowledgments

The authors would like to thank Ota Blahoušek for the graphic editing of the figures.

Conflict of interest

The authors declare that the research was conducted in the absence of any commercial or financial relationships that could be construed as a potential conflict of interest.

Publisher's note

Supplementary material

The Supplementary Material for this article can be found online at: https://www.frontiersin.org/articles/10.3389/fpls.2023.1217421/full#supplementary-material

SUPPLEMENTARY TABLE 6
Source dataset for the PCA analysis (Figures 5, 6).

References

Bandurski, R. S., and Schulze, A. (1977). Concentration of indole-3-acetic acid and its derivatives in plants. *Plant Physiol.* 60, 211–213. doi: 10.1104/PP.60.2.211

Boyes, D. C., Zayed, A. M., Ascenzi, R., McCaskill, A. J., Hoffman, N. E., Davis, K. R., et al. (2001). Growth stage-based phenotypic analysis of Arabidopsis: a model for high throughput functional genomics in plants. *Plant Cell* 13 (7), 1499–1510. doi: 10.1105/TPC.010011

Broughton, W. J., Hernández, G., Blair, M., Beebe, S., Gepts, P., and Vanderleyden, J. (2003). Beans (*Phaseolus* spp.) – model food legumes. *Plant Soil* 252, 55–128. doi: 10.1023/A:1024146710611/METRICS

Brunoni, F., Collani, S., Casanova-Sáez, R., Šimura, J., Karady, M., Schmid, M., et al. (2020). Conifers exhibit a characteristic inactivation of auxin to maintain tissue homeostasis. *New Phytol.* 226, 1753–1765. doi: 10.1111/NPH.16463

Brunoni, F., Pěnčík, A., Žukauskaitė, A., Ament, A., Kopečná, M., Collani, S., et al. (2023). Amino acid conjugation of oxIAA is a secondary metabolic regulation involved in auxin homeostasis. *New Phytol.* 238 (6), 2264–2270. doi: 10.1111/nph.18887

Casanova-Sáez, R., Mateo-Bonmatí, E., and Ljung, K. (2021). Auxin metabolism in plants. *Cold Spring Harb. Perspect. Biol.* 13 (3), a039867. doi: 10.1101/CSHPERSPECT.A039867

Dobrev, P. I., Havlíček, L., Vagner, M., Malbeck, J., and Kamínek, M. (2005). Purification and determination of plant hormones auxin and abscisic acid using solid phase extraction and two-dimensional high performance liquid chromatography. *J. Chromatogr. A* 1075 (1-2), 159–166. doi: 10.1016/J.CHROMA.2005.02.091

Du, F., Ruan, G., and Liu, H. (2012). Analytical methods for tracing plant hormones. *Anal. Bioanal. Chem.* 403, 55–74. doi: 10.1007/S00216-011-5623-X

Fu, J., Sun, X., Wang, J., Chu, J., and Yan, C. (2011). Progress in quantitative analysis of plant hormones. *Chin. Sci. Bull.* 56, 355–366. doi: 10.1007/S11434-010-4243-8/METRICS

Hayashi, K., Arai, K., Aoi, Y., Tanaka, Y., Hira, H., Guo, R., et al. (2021). The main oxidative inactivation pathway of the plant hormone auxin. *Nat. Commun.* 12, 6752. doi: 10.1038/s41467-021-27020-1

Isobe, T., and Miyagawa, H. (2022). Facilitation of auxin biosynthesis and metabolism by salt stress in rice plants. *Biosci. Biotech. Bioch.* 86 (7), 824–831. doi: 10.1093/bbb/zbac070

Izumi, Y., Okazawa, A., Bamba, T., Kobayashi, A., and Fukusaki, E. (2009). Development of a method for comprehensive and quantitative analysis of plant hormones by highly sensitive nanoflow liquid chromatography–electrospray ionization-ion trap mass spectrometry. *Anal. Chim. Acta* 648, 215–225. doi: 10.1016/J.ACA.2009.07.001

Kai, K., Horita, J., Wakasa, K., and Miyagawa, H. (2007a). Three oxidative metabolites of indole-3-acetic acid from Arabidopsis thaliana. *Phytochemistry* 68, 1651–1663. doi: 10.1016/J.PHYTOCHEM.2007.04.030

Kai, K., Nakamura, S., Wakasa, K., and Miyagawa, H. (2007c). Facile preparation of deuterium-labeled standards of indole-3-acetic acid (IAA) and its metabolites to quantitatively analyze the disposition of exogenous IAA in *Arabidopsis thaliana*. *Biosci. Biotech. Bioch.* 71 (8), 23, 1946–1954. doi: 10.1271/bbb.70151

Kai, K., Wakasa, K., and Miyagawa, H. (2007b).). metabolism of indole-3-acetic acid in rice: identification and characterization of N-β-d-glucopyranosyl indole-3-acetic acid and its conjugates. *Phytochemistry* 68, 2512–2522. doi: 10.1016/J.PHYTOCHEM.2007.05.040

Kim, R., Osako, Y., Yamane, H., Tao, R., and Miyagawa, H. (2021). Quantitative analysis of auxin metabolites in lychee flowers. *Biosci. Biotech. Bioch.* 85 (3), 467–475. doi: 10.1093/bbb/zbaa083

Kojima, M., Kamada-Nobusada, T., Komatsu, H., Takei, K., Kuroha, T., Mizutani, M., et al. (2009). Highly sensitive and high-throughput analysis of plant hormones using MS-probe modification and liquid chromatography-tandem mass spectrometry: an application for hormone profiling in Oryza sativa. *Plant Cell Physiol.* 50 (7), 1201–1214. doi: 10.1093/PCP/PCP057

Kowalczyk, M., and Sandberg, G. (2001). Quantitative analysis of indole-3-acetic acid metabolites in Arabidopsis. *Plant Physiol.* 127, 1845–1853. doi: 10.1104/PP.010525

Lancashire, P. D., Bleiholder, H., Boom, P. V. D., Langeluddeke, P., Stauss, R., Weber, E., et al. (1991). A uniform decimal code for growth stages of crops and weeds. *Ann. App. Biol.* 11, 561–601. doi: 10.1111/J.1744-7348.1991.TB04895.X

Liu, X., Hegeman, A. D., Gardner, G., and Cohen, J. D. (2012). Protocol: high-throughput and quantitative assays of auxin and auxin precursors from minute tissue samples. *Plant Methods* 8 (1), 31. doi: 10.1186/1746-4811-8-31

Liu, H., Li, Y., Luan, T., Lan, C., and Shu, W. (2007). Simultaneous determination of phytohormones in plant extracts using SPME and HPLC. *Chromatographia* 66, 515–520. doi: 10.1365/S10337-007-0350-3

Ljung, K., Bhalerao, R. P., and Sandberg, G. (2001). Sites and homeostatic control of auxin biosynthesis in Arabidopsis during vegetative growth. *Plant J.* 28 (4), 465–474. doi: 10.1046/j.1365-313x.2001.01173.x

Ljung, K., Hul, A., Kowalczyk, M., Marchant, A., Celenza, J., Cohen, J., et al. (2002). Biosynthesis, conjugation, catabolism and homeostasis of indole-3-acetic acid in Arabidopsis thaliana. *Plant Mol. Biol.* 50, 309–332. doi: 10.1023/A:1016024017872

Ludwig-Müller, J. (2011). Auxin conjugates: their role for plant development and in the evolution of land plants. *J. Exp. Bot.* 62, 1757–1773. doi: 10.1093/jxb/erq412

Matsuda, F., Miyazawa, H., Wakasa, K., and Miyagawa, H. (2005). Quantification of indole-3-acetic acid and amino acid conjugates in rice by liquid chromatography–electrospray ionization–tandem mass spectrometry. *Biosci. Biotech. Bioch.* 69, 778–783. doi: 10.1271/BBB.69.778

Matuszewski, B. K., Constanzer, M. L., and Chavez-Eng, C. M. (2003). Strategies for the assessment of matrix effect in quantitative bioanalytical methods based on HPLC-MS/MS. *Anal. Chem.* 75 (13), 3019–3030. doi: 10.1021/ac020361s

Müller, K., Dobrev, P. I., Pěnčík, A., Hošek, P., Vondráková, Z., Filepová, R., et al. (2021). DIOXYGENASE FOR AUXIN OXIDATION 1 catalyzes the oxidation of IAA amino acid conjugates. *Plant Physiol.* 187 (1), 103–115. doi: 10.1093/PLPHYS/KIAB242

Normanly, J. (2010). Approaching cellular and molecular resolution of auxin biosynthesis and metabolism. *Cold Spring Harb. Perspect. Biol.* 2, 1594–1594. doi: 10.1101/CSHPERSPECT.A001594

Novák, O., Hauserová, E., Amakorová, P., Doležal, K., and Strnad, M. (2008). Cytokinin profiling in plant tissues using ultra-performance liquid chromatography–electrospray tandem mass spectrometry. *Phytochemistry* 69, 2214–2224. doi: 10.1016/J.PHYTOCHEM.2008.04.022

Novák, O., Hényková, E., Sairanen, I., Kowalczyk, M., Pospíšil, T., and Ljung, K. (2012). Tissue specific profiling of the Arabidopsis thaliana auxin metabolome. *Plant J.* 72, 523–536. doi: 10.1111/J.1365-313X.2012.05085.X

Nowacki, J., and Bandurski, R. S. (1980). *Myo*-inositol esters of indole-3-acetic acid as seed auxin precursors of zea mays l. *Plant Physiol.* 65 (3), 422–427. doi: 10.1104/pp.65.3.422

Osako, Y., Yamane, H., Kim, R., Miyagawa, H., and Tao, R. (2022). Characterization of auxin metabolism in the ovaries of the lychee (*Litchi chinensis*) 'Salathiel'. *J. Hortic.* 91 (3), 302–311. doi: 10.2503/hortj.UTD-352

Östin, A., Kowalyczk, M., Bhalerao, R. P., and Sandberg, G. (1998). Metabolism of indole-3-acetic acid in Arabidopsis. *Plant Physiol.* 118, 285–296. doi: 10.1104/PP.118.1.285

Pěnčík, A., Casanova-Sáez, R., Pilařová, V., Žukauskaite, A., Pinto, R., Micol, J. L., et al. (2018). Ultra-rapid auxin metabolite profiling for high-throughput mutant screening in Arabidopsis. *J. Exp. Bot.* 69, 2569–2579. doi: 10.1093/JXB/ERY084

Pěnčík, A., Rolčík, J., Novák, O., Magnus, V., Barták, P., Buchtík, R., et al. (2009). Isolation of novel indole-3-acetic acid conjugates by immunoaffinity extraction. *Talanta* 80, 651–655. doi: 10.1016/J.TALANTA.2009.07.043

Pěnčík, A., Simonovik, B., Petersson, S. V., Henyková, E., Simon, S., Greenham, K., et al. (2013). Regulation of auxin homeostasis and gradients in Arabidopsis roots through the formation of the indole-3-acetic acid catabolite 2-oxindole-3-acetic acid. *Plant Cell* 25 (10), 3858–3870. doi: 10.1105/TPC.113.114421

Plüss, R., Jenny, T., and Meier, H. (1989). IAA-induced adventitious root formation in greenwood cuttings of *Populus tremula* and formation of 2-indolone-3-acetylaspartic acid, a new metabolite of exogeneously applied indole-3-acetic acid. *Physiol. Plantarum* 75, 89–96. doi: 10.1111/J.1399-3054.1989.TB02068.X

Porfirio, S., Gomes da Silva, M. D. R., Peixe, A., Cabrita, M. J., and Azadi, P. (2016). Current analytical methods for plant auxin quantification – a review. *Anal. Chim. Acta* 902, 8–21. doi: 10.1016/J.ACA.2015.10.035

Riov, J., and Bangerth, F. (1992). Metabolism of auxin in tomato fruit tissue: formation of high molecular weight conjugates of oxindole-3-acetic acid via the oxidation of indole-3- acetylaspartic acid. *Plant Physiol.* 100, 1396–1402. doi: 10.1104/PP.100.3.1396

Rolčík, J., Řečinská, J., Barták, P., Strnad, M., and Prinsen, E. (2005). Purification of 3-indolylacetic acid by solid phase extraction. *J. Sep. Sci.* 28 (12), 1370–1374. doi: 10.1002/JSSC.200500189

Seidel, C., Walz, A., Park, S., Cohen, J. D., and Ludwig-Müller, J. (2006). Indole-3-acetic acid protein conjugates: novel players in auxin homeostasis. *Plant Biol.* 8 (3), 340–345. doi: 10.1055/S-2006-923802

Shewry, P. R. (2009). Wheat. *J. Exp. Bot.* 60, 1537–1553. doi: 10.1093/JXB/ERP058

Šimura, J., Antoniadi, I., Široká, J., Tarkowská, D., Strnad, M., Ljung, K., et al. (2018). Plant hormonomics: multiple phytohormone profiling by targeted metabolomics. *Plant Physiol.* 177 (2), 476–489. doi: 10.1104/pp.18.00293

Široká, J., Brunoni, F., Pěnčík, A., Mik, V., Žukauskaitė, A., Strnad, M., et al. (2022). High-throughput interspecies profiling of acidic plant hormones using miniaturised sample processing. *Plant Methods* 18, 122. doi: 10.1186/s13007-022-00954-3

Smýkal, P. (2014). Pea (Pisum sativum L.) in biology prior and after mendel's discovery. *Czech J. Genet. Plant Breed.* 50 (2), 52–64. doi: 10.17221/2/2014-CJGPB

Staswick, P. E. (2009). The tryptophan conjugates of jasmonic and indole-3-acetic acids are endogenous auxin inhibitors. *Plant Physiol.* 150, 1310–1321. doi: 10.1104/PP.109.138529

Staswick, P. E., Serban, B., Rowe, M., Tiryaki, I., Maldonado, M. T., Maldonado, M. C., et al. (2005). Characterization of an Arabidopsis enzyme family that conjugates amino acids to indole-3-acetic acid. *Plant Cell* 17, 616–627. doi: 10.1105/TPC.104.026690

Sugawara, S., Mashiguchi, K., Tanaka, K., Hishiyama, S., Sakai, T., Hanada, K., et al. (2015). Distinct characteristics of indole-3-acetic acid and phenylacetic acid, two common auxins in plants. *Plant Cell Physiol.* 56, 1641–1654. doi: 10.1093/PCP/PCV088

Svačinová, J., Novák, O., Plačková, L., Lenobel, R., Holík, J., Strnad, M., et al. (2012). A new approach for cytokinin isolation from Arabidopsis tissues using miniaturized purification: pipette tip solid-phase extraction. *Plant Methods* 8 (1), 17. doi: 10.1186/1746-4811-8-17/FIGURES/5

Tam, Y. Y., Epstein, E., and Normanly, J. (2000). Characterization of auxin conjugates in Arabidopsis. low steady-state levels of indole-3-acetyl-aspartate, indole-3-acetylglutamate, and indole-3-acetyl-glucose. *Plant Physiol.* 123, 589–596. doi: 10.1104/PP.123.2.589

Tanaka, K., Hayashi, K., Natsume, M., Kamiya, Y., Sakakibara, H., Kawaide, H., et al. (2014). UGT74D1 catalyzes the glucosylation of 2-oxindole-3-acetic acid in the auxin metabolic pathway in Arabidopsis. *Plant Cell Physiol.* 55, 218–228. doi: 10.1093/PCP/PCT173

Tivendale, N. D., Davidson, S. E., Davies, N. W., Smith, J. A., Dalmais, M., Bendahmane, A. I., et al. (2012). Biosynthesis of the halogenated auxin, 4-chloroindole-3-acetic acid. *Plant Physiol.* 159 (3), 1055–1063. doi: 10.1104/pp.112.198457

Tottman, D. R. (1987). The decimal code for the growth stages of cereals, with illustrations. *Ann. Appl. Biol.* 110, 441–454. doi: 10.1111/J.1744-7348.1987.TB03275.X

Tsurumi, S., and Wada, S. (1986). Dioxindole-3-acetic acid conjugates formation from indole-3- acetylaspartic acid in vicia seedlings. *Plant Cell Physiol.* 27, 1513–1522. doi: 10.1093/OXFORDJOURNALS.PCP.A077252

Wang, L., Zou, Y., Kaw, H. Y., Wang, G., Sun, H., Cai, L., et al. (2020). Recent developments and emerging trends of mass spectrometric methods in plant hormone analysis: a review. *Plant Methods* 16, 54. doi: 10.1186/S13007-020-00595-4

Woodward, A. W., and Bartel, B. (2005). Auxin: regulation, action, and interaction. *Ann. Bot.* 95, 707–735. doi: 10.1093/AOB/MCI083

Supplementary Material

Metabolic profiles of 2-oxindole-3-acetyl-amino acid conjugates differ in various plant species

Pavel Hladík, Ivan Petřík, Asta Žukauskaitė, Ondřej Novák, Aleš Pěnčík*

***Correspondence:** Corresponding Author: alespencik@seznam.cz

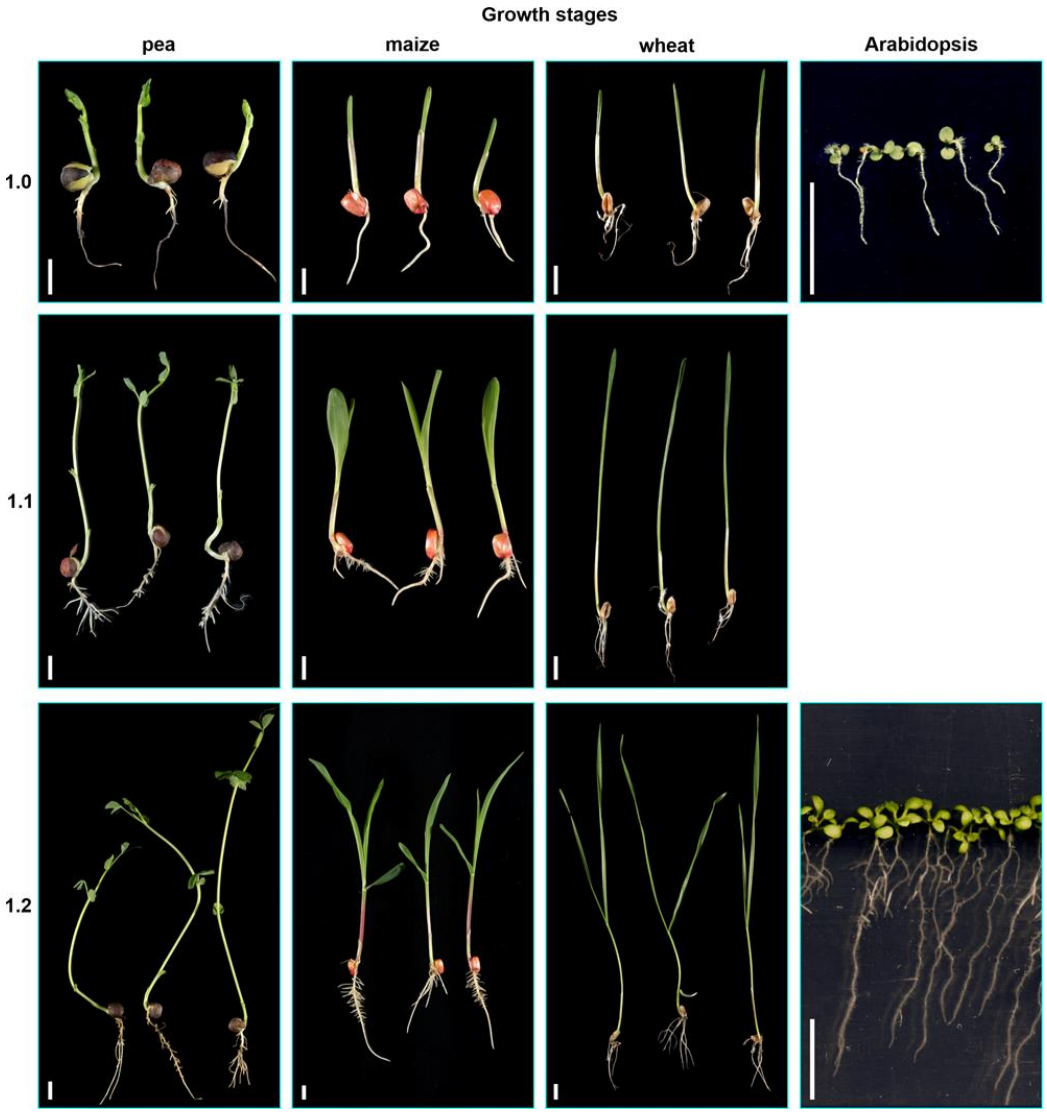

Supplementary Figure 1: Plant growth stages according to BBCH scale.
At stage 1.0, the cotyledons are fully unfolded in pea (A) and Arabidopsis (D), or the first leaf emerges from the coleoptile in maize (B) and wheat (C). The following stage 1.1 shows first leaf fully unfolded in pea (or first tendril developed) (E), maize (F) and wheat (G). At the last stage 1.2, two leaves are fully developed and unfolded in pea (or second tendril developed) (H), maize (I), wheat (J) and Arabidopsis (K). Scale bars indicate 1 cm.

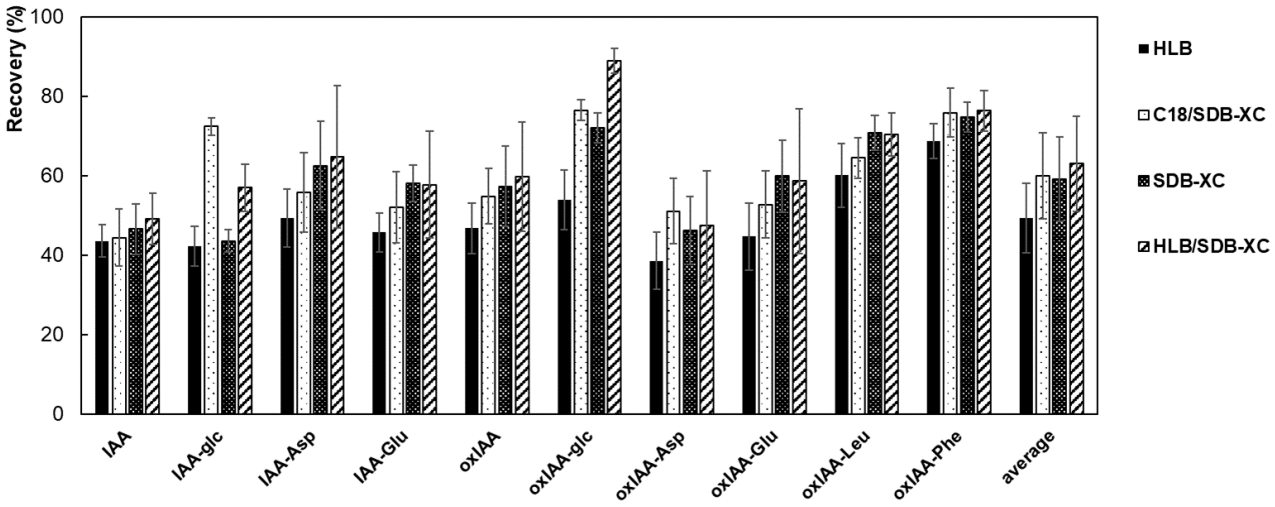

Supplementary Figure 2: In-tip μSPE sorbents optimization.
Recoveries (%) of unlabelled auxin standards (2 pmol added to extraction solvent) were calculated as a recovery of metabolite initial amounts. For all analytes, two types of extraction sorbents (SDB-XC Empore^{TM} and HLB AttractSPE^{TM}) or two multi-StageTips microcolumns (C18/SDB-XC and HLB/SDB-XC) were tested and then average recoveries were calculated. All sorbents' combinations were analysed in four replicates and error bars indicate standard deviations of the means (mean ± SD, n=4).

Supplementary Table 1: Age of plants harvested at different growth stages.
On the dedicated days after planting, four to six plants per species were harvested at the growth stages 1.0, 1.1, and 1.2 of the BBCH scale. For Arabidopsis, stage 1.1 is not differentiated as the first two leaves develop simultaneously.

Growth stages	**Arabidopsis**	**Maize**	**Pea**	**Wheat**
		(days)		
1.0	7	7	9	5
1.1	-	9	12	7
1.2	10	11	14	10

Supplementary Table 2: Conditions of HPLC-MRM-MS method.
Diagnostic MRM transitions and collision energies (CE) were optimised for all auxin metabolites and corresponding internal standards. In addition, retention time (RT), limit of detection (LOD), linear range and linearity (coefficient of determination, R^2) were also measured. Analytes were detected by the MS instrument combining positive and negative ESI mode (+/–) with optimised conditions as follows: nebulizer pressure, 25 psi; drying gas flow and temperature, 14 l/min and 130 °C; sheath gas flow and temperature, 12 l/min and 400 °C; capillary voltage, 2.8 kV in positive mode and 3.0 kV in negative mode; nozzle voltage, 0 V.

Analyte	**RT** (min)	**ESI**	**MRM**	**IS**	**IS MRM**	**CE** (V)	**LOD** (fmol)	**Linear range** (pmol)	R^2
IAA	5.6	+	176>130	[$^{13}C_6$]IAA	182>136	24	0.045	$9*10^{-5}$ - 90	0.9989
IAA-Asp	3.7	+	291>130	[$^{13}C_6$]IAA-Asp	297>136	36	0.45	$9*10^{-4}$ - 90	0.9992
IAA-Glu	4.4	+	305>130	[$^{13}C_6$]IAA-Glu	311>136	24	0.45	$4.5*10^{-4}$ - 90	0.9992
IAA-Leu	10.3	+	289>130	[$^{13}C_6$]IAA-Glu	311>136	36	0.9	$9*10^{-4}$ - 90	0.9980
IAA-Phe	10.7	+	323>130	[$^{13}C_6$]IAA-Glu	311>136	38	4.5	$4.5*10^{-3}$ - 90	0.9990
IAA-glc	4.2	–	336>174	[$^{13}C_6$]IAA-glc	342>180	8	90	$9*10^{-2}$ - 90	0.9988
oxIAA	3.9	+	192>146	[$^{13}C_6$]oxIAA	198>152	12	0.9	$9*10^{-4}$ - 90	0.9938
oxIAA-Asp	2.4; 2.7	+	307>146	oxIAA-[$^{13}C_4$,^{15}N]Asp	312>146	26	4.5	$9*10^{-3}$ - 90	0.9976
oxIAA-Glu	3.0; 3.3	+	321>146	oxIAA-[$^{13}C_5$,^{15}N]Glu	327>146	30	4.5	$9*10^{-3}$ - 90	0.9982
oxIAA-Leu	8.9; 9.5	+	305>146	oxIAA-[$^{13}C_5$,^{15}N]Glu	327>146	30	0.45	$9*10^{-4}$ - 90	0.9974
oxIAA-Phe	9.3; 9.8	+	339>146	oxIAA-[$^{13}C_5$,^{15}N]Glu	327>146	30	4.5	$9*10^{-3}$ - 90	0.9974
oxIAA-glc	3.2	–	352>190	[$^{13}C_6$]oxIAA-Glc	358>196	8	0.45	$4.5*10^{-4}$ - 90	0.9987

Supplementary Table 3: Method validation.
Method accuracy (% BIAS) and method precision (% RSD) were determined by spiking experiment. Briefly, samples were extracted in 1 ml of Na-phosphate buffer with 10 mg of pea or wheat homogenized plants, diluted to 5 ml with Na-phosphate buffer and each sample aliquoted into 200 µl doses (total 15 samples per plant). To each sample, 5 pmol of stable isotope-labelled standards were added. Subsequently, the samples were supplemented with unlabelled standards (1 or 10 pmol). The samples were then purified by in-tip µSPE method and the concentrations of each analyte were determined by HPLC-MS/MS using isotope dilution method. A set of plant extracts were also processed without the addition of unlabelled standards, and endogenous levels of auxin metabolites were subtracted before calculating the validation parameters. All samples were analysed in five replicates.

Analyte	**Pea**				**Wheat**			
	1 pmol		10 pmol		1 pmol		10 pmol	
	BIAS (%)	RSD (%)	BIAS (%)	RSD (%)	BIAS (%)	RSD (%)	BIAS (%)	RSD (%)
IAA	5.7	4.8	14.0	7.3	16.2	6.3	14.1	2.6
IAA-Asp	16.3	13.8	7.5	6.1	24.5	4.5	8.5	4.4
IAA-Glu	31.8	6.1	0.1	4.3	33.6	4.1	2.6	3.5
IAA-Leu	36.4	2.8	21.7	7.9	30.4	2.7	17.2	2.3
IAA-Phe	29.1	4.2	11.5	4.2	18.5	0.7	3.3	1.4
IAA-glc	0.2	1.0	0.5	2.0	17.9	8.4	17.6	3.0
oxIAA	29.1	11.6	1.9	4.4	23.7	10.4	19.7	2.1
oxIAA-Asp	19.0	6.9	3.0	4.0	6.4	1.2	4.0	6.1
oxIAA-Glu	2.0	3.1	0.2	4.0	3.0	3.5	0.6	2.3
oxIAA-Leu	35.3	2.3	27.0	8.1	48.2	3.1	44.4	3.7
oxIAA-Phe	25.4	3.5	20.6	6.6	45.2	5.8	43.4	4.5
oxIAA-glc	21.2	3.5	7.4	4.3	11.2	6.8	0.3	5.3

Supplementary Table 4: Quantification of oxIAA-amino acid conjugates.
Four oxIAA-AAs were quantified (pmol/g FW ± SD; n=5) in roots, shoots and cotyledons of pea, wheat and maize, and roots and shoots of Arabidopsis. <LOD, under the limit of detection.

		oxIAA-Asp	**oxIAA-Glu**	**oxIAA-Leu**	**oxIAA-Phe**
		(pmol/g FW ± SD)			
Arabidopsis	shoot	16.3 ± 2.4	81.3 ± 15.3	<LOD	<LOD
	root	11.4 ± 5.2	91.5 ± 34.2	<LOD	<LOD
Maize	shoot	6.8 ± 1.7	<LOD	<LOD	<LOD
	cotyledon	186.7 ± 51.2	9.8 ± 5.2	<LOD	0.9 ± 0.3
	root	29.1 ± 5.7	5.1 ± 1.1	<LOD	<LOD
Wheat	shoot	<LOD	<LOD	<LOD	
	cotyledon	<LOD	<LOD	<LOD	<LOD
	root	27.8 ± 5.9	3.9 ± 1.6	<LOD	<LOD
Pea	shoot	436.0 ± 168.9	12.7 ± 3.3	<LOD	<LOD
	cotyledon	296 480.2 ± 27 479.2	1 194.2 ± 221.2	0.8 ± 0.3	6.8 ± 2.5
	root	2 618.2 ± 2 350.7	65.6 ± 13.7	<LOD	<LOD

Supplementary Table 5: IAA metabolite profiles in Arabidopsis, maize, wheat, and pea.
Free IAA, oxIAA and their low-molecular-weight conjugates with amino acids and glucose were determined (pmol/g FW) in the four plant models at development stage 1.0. The levels of IAA and oxIAA conjugates with individual amino acids (Asp, Glu, Leu and Phe) were summed up into two corresponding groups IAA-AA and oxIAA-AA, respectively. The distribution (%) of different conjugate classes was calculated as their relative abundance to the total measured IAA metabolite pool (%). All samples were measured in five biological replicates. <LOD, under the limit of detection.

		IAA		**IAA-AA**		**IAA-glc**		**oxIAA**		**oxIAA-AA**		**oxIAA-glc**	
		(pmol/g)	(%)	(pmol/g)	(%)	(pmol/g)	(%)	(pmol/g)	(%)	(pmol/g)	(%)	(pmol/g)	(%)
Arabidopsis	shoot	104.4	0.86	69.5	0.6	157.9	1.3	1 863.0	15.3	97.7	0.8	9 869.6	81.2
	root	58.8	1.65	40.0	1.1	94.7	2.7	835.7	23.5	102.9	2.9	2 421.9	68.1
Maize	shoot	16.7	14.19	1.5	1.3	<LOD	-	93.0	78.8	6.8	5.7	<LOD	-
	cotyledon	2 638.2	24.42	76.2	0.7	<LOD	-	7 006.8	64.8	197.9	1.8	885.8	8.2
	root	159.5	49.64	16.6	5.2	<LOD	-	111.0	34.5	34.2	10.6	<LOD	-
Wheat	shoot	18.3	10.33	2.4	1.3	<LOD	-	156.7	88.3	<LOD	-	<LOD	-
	cotyledon	70.0	40.00	43.9	25.1	<LOD	-	61.2	34.9	<LOD	-	<LOD	-
	root	73.9	11.56	127.5	19.9	<LOD	-	220.1	34.4	31.7	5.0	186.1	29.1
Pea	shoot	84.3	10.04	181.3	21.6	53.5	6.4	71.9	8.6	448.6	53.4	<LOD	-
	cotyledon	14.5	0.005	818.8	0.3	<LOD	-	1 412.3	0.5	297 723.7	99.3	<LOD	-
	root	900.0	19.55	667.1	14.5	69.1	1.5	282.4	6.1	2 683.8	58.3	<LOD	-

Supplement I

Supplement II

Supplement III

Supplement IV

Hladík P., Brunoni F., Žukauskaitė A., Zatloukal M., Novák O., Pěnčík A. (2024) Phenylacetic acid metabolism in plants: unravelling novel pathways and metabolites by liquid chromatography-mass spectrometry analysis. (In preparation)

Phenylacetic acid metabolism in land plants: unravelling novel pathways and metabolites by liquid chromatography-mass spectrometry analysis

Pavel Hladík[1], Federica Brunoni[1], Asta Žukauskaitė[2], Marek Zatloukal[2], Ondřej Novák[1], and Aleš Pěnčík[1,*]

[1]*Laboratory of Growth Regulators, Institute of Experimental Botany, The Czech Academy of Sciences & Faculty of Science, Palacký University - Olomouc (Czech Republic)*
[2]*Department of Chemical Biology and Genetics, Centre of the Region Haná for Biotechnological and Agricultural Research, Faculty of Science, Palacký University - Olomouc (Czech Republic)*
** Corresponding author*

Abstract

Maintaining optimal levels of biologically active phytohormone is essential for facilitating growth and developmental processes in plants. In the regulation of intracellular auxin homeostasis, its inactivation via conjugation plays a pivotal role. While significant progress has been made in understanding the conjugation and metabolism of indole-3-acetic acid (IAA), little is known about the regulatory pathways governing the metabolism of another auxin, phenylacetic acid (PAA). Here, we present a comprehensive investigation aimed at elucidating PAA metabolism in land plants. We conducted thorough screening of PAA metabolites using HPLC-MS/MS, resulting in the identification of four novel metabolites: phenylacetyl-leucine (PAA-Leu), phenylacetyl-phenylalanine (PAA-Phe), phenylacetyl-valine (PAA-Val), and phenylacetyl-glucose (PAA-glc). The formation of these novel conjugates was verified by PAA feeding experiments. Comprehensive LC-MS profiling revealed significant differences in PAA conjugate distribution across the studied species, indicating a great diversity of auxin metabolic pathways in land plants. *In vitro* enzymatic assays and together with mutant analysis were employed to investigate the interplay within PAA metabolic pathways in maintaining PAA homeostasis.

Keywords

auxin, phenylacetic acid, metabolism, conjugation, phytohormone homeostasis, glucosyl ester, Gretchen Hagen 3, HPLC-MS/MS, plant hormone, metabolite profiling

Introduction

Auxins are a class of phytohormones that are essential for coordinating plant growth and development. Indole-3-acetic acid (IAA) has been extensively investigated due to its diverse physiological impacts. Phenylacetic acid (PAA), another constituent of the auxin family, has recently gained attention due to its potential significance in plant physiology and auxin signalling pathways. Although PAA is more prevalent than IAA in many plant species, its physiological roles and regulatory mechanisms are not yet fully understood (Wightman & Lighty, 1982; Sugawara et al., 2015, Cook, 2019). The auxin activity of PAA has been estimated to be less than 10% of that of IAA by three typical auxin tests: cylinder test, oat bending test and the pea test (Haagen-Smit & Went, 1935). However, its main activity appears to be in lateral roots induction and in root growth promotion (reviewed in Cook, 2019; Perez et al., 2023). Additionally, PAA has antimicrobial properties, exhibiting both anti-fungal and anti-bacterial activities (Kawazu et al., 1996; Liu et al., 2014; Zhang et al., 2022). Plants increase PAA production when attacked by herbivores, which has been observed to provide protection against fungal pathogens when applied exogenously (Perez et al., 2023). However, the exact biological function of PAA in plant defence mechanisms is still unclear and requires further evidence (Kunkel & Harper, 2018).

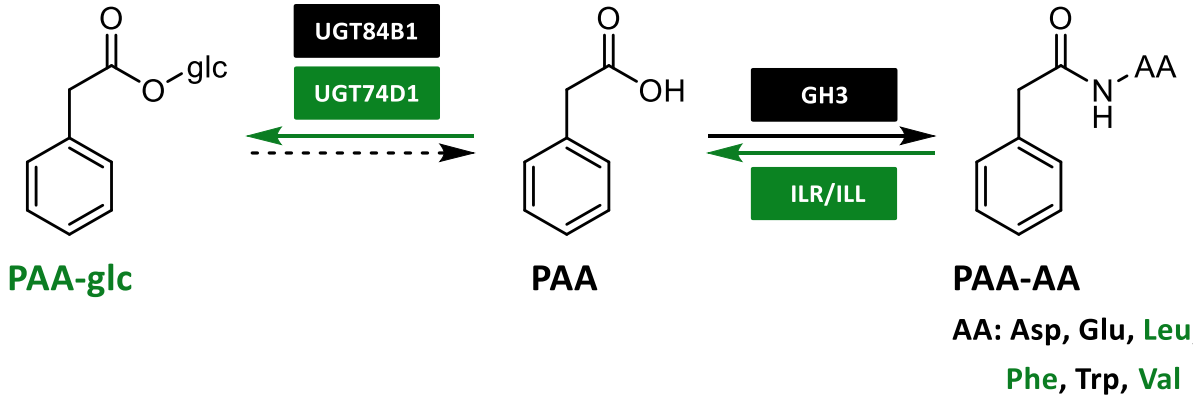

Figure 1: Scheme of PAA metabolism. *Newly identified pathways and conjugates are highlighted in green. Dashed arrow represents putative metabolic step that is still not fully characterised. AA, amino acid; GH3, GRETCHEN HAGEN 3; ILR/ILL, IAA-LEUCINE RESISTANT 1/ILR1-LIKE proteins; PAA, phenylacetic acid; PAA-glc- PAA-glucose.*

The conjugation pathways of PAA appear to be mirror images of those of IAA, as both compounds undergo the analogous conjugation processes mediated by identical enzymes. Initial investigations in 2005 revealed that GRETCHEN HAGEN 3 (GH3) proteins, which are known for their role in forming IAA-amides with amino acids (IAA-AAs), also exhibit *in vitro* sensitivity to PAA (Staswick et al., 2005). Subsequently, the first two conjugates PAA-aspartate (PAA-Asp) and PAA-glutamate (PAA-Glu) were identified utilizing transgenic *Arabidopsis thaliana* plants expressing β-estradiol-inducible YUCCA enzymes, which led to the increase of endogenous levels of PAA-Glu by 14 to 41-fold and PAA-Asp levels by 1.6 to 3.8-fold (Sugawara et al., 2015). The confirmation of GH3 enzyme

involvement in this synthesis has been provided by β-estradiol-inducible GH3.9 transgenic plants, which increased endogenous PAA-Glu levels in Arabidopsis by 13-fold (Sugawara et al., 2015). Confirmation of GH3 enzyme involvement was further demonstrated in GH3.5 overexpressing plants. In these plants, levels of PAA decreased by up to 5-fold, while the concentration of PAA-Asp increased by 15 to 70-fold (Westfall et al., 2017). Additionally, experiments involving wild-type plants treated with both IAA and PAA revealed that the application of one auxin decreased the concentration of the other, leading to increased levels of their respective aspartate metabolites in a GH3-dependent manner (Aoi et al., 2020a). Other IAA metabolites conjugated with amino acids have also been detected in plants (Kowalczyk & Sandberg, 2001; Pěnčík et al., 2009; Staswick, 2009), their concentrations are typically much lower than those of IAA-aspartate and IAA-glutamate, likely due to rapid conversion to free IAA mediated by enzymes such as IAA-LEUCINE RESISTANT 1 (ILR1), ILR1-LIKE proteins (ILLs), and IAA-ALANINE RESISTANT 3 protein (IAR3) (Bartel & Fink, 1995; Davies et al., 1999; LeClere et al., 2002), or through oxidation to oxIAA-amino acids (oxIAA-AAs) (Hladík et al., 2023). Notably, from this group, only PAA-Trp was identified in Arabidopsis at concentrations 17-fold higher than its IAA counterpart, suggesting its potential significance in plant physiology (Staswick et al., 2017).

An alternative pathway in auxin metabolism involves the formation of glucosides catalysed by the enzymes UGT74D1 and UGT84B1 (Jackson et al., 2001; Mateo-Bonmatí et al., 2021). In *in vitro* experiments, both IAA and PAA have been shown to serve as substrates for UGT84B1. However, only IAA glucose ester (IAA-glc) has been detected *in vivo* (Aoi et al., 2020b; Grubb et al., 2004). IAA methylation, mediated by the IAA CARBOXYMETHYLTRANSFERASE 1 (IAMT1) enzyme, has been demonstrated in plants (Qin et al., 2005). However, overexpression of the IAMT1 enzyme in Arabidopsis did not lead to a reduction in PAA levels, suggesting that PAA methylation may not occur in plants, despite its observation in *Escherichia coli* (E. coli) (Takubo et al., 2020). Until now, all these experiments have only been conducted in Arabidopsis, so it is unclear if the same results can be replicated in other plant species.

Recent years have witnessed new discoveries in PAA metabolism. However, our understanding of how PAA is metabolized in plants remains incomplete. In this study, we confirmed the formation of PAA glucose ester (PAA-glc) *in planta* for the first time and identified three novel endogenous amino acid conjugates phenylacetyl-leucine (PAA-Leu), phenylacetyl-phenylalanine (PAA-Phe) and phenylacetyl-valine (PAA-Val). Additionally, we conducted quantitative profiling of range of PAA metabolites across a spectrum of model plant species, spanning from Bryophyta to Angiosperms. This analysis was carried out using an optimized high-performance liquid chromatography-tandem mass spectrometry (HPLC-MS/MS). To elucidate PAA metabolic pathways, we further performed bacterial enzyme assays to investigate the formation and turnover of PAA conjugates *in vitro*. Subsequently, PAA feeding experiments on Arabidopsis mutant lines, spruce and *Physcomitrium* revealed PAA metabolic pathways *in planta*.

Materials and Methods

Reagants and standards

Plant agar and Murashige & Skoog media were purchased from Duchefa (Haarlem, Netherlands). Hypergrade purity methanol for HPLC-MS/MS analysis and all other chemicals, were purchased from Lach-Ner (Neratovice, Czech Republic), Merck KGaA (Darmstadt, Germany), and Sigma-Aldrich (St. Louis, MA, USA). Standards for PAA and $^{13}C_6$-labeled PAA were purchased from Merck KGaA (Darmstadt, Germany). IAA-glc and [$^{13}C_6$]IAA-glc were synthesised in accordance to (Kai et al., 2007a; Kai et al., 2007b) with minor modifications. Standards for [$^{13}C_6$]PAA-Asp and [$^{13}C_6$]PAA-Glu were prepared according to the method of Dr. Volker Magnus (Ruder Boškovič Institute Zagreg Croatia) for the preparation of auxine-amino acids conjugates via "active ester" reactive intermediate. The two step method consists in esterification of [$^{13}C_6$]-phenylacetic acid with *N*-hydroxysuccinimide at presence of *N,N′*-dicyclohexylcarbodiimide (DCC) as a peptide coupling agent in ethyl acetate to give [$^{13}C_6$]-phenylacetic acid-*N*-succinimide ester and subsequent reaction of ester with sodium salt of corresponding amino acid (L-Asp or L-Glu) in dioxan/water. Final conjugates were purified by crystallization or column chromatography. PAA-glc was synthesized via a direct Mitsunobu glycosylation of PAA with unprotected glucose, adopting reaction conditions from Takeuchi et al., (2020).

Plant material and growth conditions

Arabidopsis thaliana seeds ecotype Columbia 0 (Col-0) were used as wild type for all the experiments. Knockout mutant lines *gh3.1,2,3,4,5,6* (*gh3sex*; Porco et al., 2016), *ugt74d1* and *ugt84b1* (Mateo-Bonmatí et al., 2021) were obtained from prof. Karin Ljung (Umeå Plant Science Centre, Sweden). *Arabidopsis thaliana* (L.), maize (*Zea mays* L.), pea (*Pisum sativum arvense* L.), and wheat (*Triticum aestivum* L.) were cultivated as previously published in Hladík et al., (2023). Gametophores from *Physcomitrium patens* and spruce (*Picea abies* L. Karst) plants were cultivated as described in Brunoni et al., (2023a). All the plants were harvested (≈ 10 mg/FW) at growth stage 1.0 according to the Biologische Bundesanstalt, Bundessortenamt und Chemische Industrie (BBCH) scale (Tottman, 1987; Lancashire et al., 1991; Boyes et al., 2001) (except *Physcomitrium,* which was harvested three weeks after the last gametophores transfer to fresh medium).

Feeding experiments

For PAA treatments, seven days after germination (DAG) Arabidopsis seedlings (Col-0 and *gh3sex*) grown under the same conditions as described above, were harvested, washed in ultrapure water and transferred to liquid medium (½ MS medium, 1% sucrose, pH 5.7) supplemented with 20 µM PAA. Plants were then shaken gently in the dark at 22°C and harvested after 0.5, 1 and 3 h. For kakeimide (KKI) treatments, seven DAG Arabidopsis seedlings, 14 DAG spruce plants and *Physcomitrium*

gametophores were transferred to sterile liquid ½ MS medium for 1, 6 and 24 h, depending on the species, according to Fukui et al., (2022) and Brunoni et al., (2023a) and then supplemented with 5 μM PAA, 50 μM KKI or a combination of 5 μM PAA with 50 μM KKI. Mock-treated Arabidopsis, moss and spruce plants were used as controls. Plants were then harvested in five biological replicates per time point (≈ 10 mg/FW), immediately snap frozen in liquid nitrogen and stored at -80°C.

Cloning, protein production, and bacterial enzyme assay

Escherichia coli BL21 (DE3) strains expressing recombinant AtGH3s, AtUGTs, and AtILR1/ILLs used in this work were previously generated (Brunoni et al., 2019; 2023b). Recombinant protein production and enzymatic assay of AtGH3s, AtUGTs, and AtILR1/ILLs were performed as described previously by Brunoni et al., (2019; 2023a; 2023b). For the amino acid conjugation assay, 500 μL of clarified cell lysate from AtGH3.6- or AtGH3.17-producing bacterial cultures was incubated with GH3 cofactors and with or without 0.1 mM PAA. For the glucose conjugation assay, 500 μL of clarified cell lysate from AtUGT84B1- or AtUGT74D1-producing bacterial cultures was incubated with UGT cofactors and with or without 0.1 mM PAA/IAA. For the hydrolysis assay, 500 μL of clarified cell lysate from AtILL2-, AtILL6-, AtILR1-, or AtIAR3-producing bacterial cultures was incubated with 1 mM MgCl 2 and 0.1 mM PAA-Leu, PAA-Trp, PAA-Val or PAA-Glu. GFP-producing bacterial cultures were used as negative controls. The enzymatic activity of the recombinant proteins was tested for 5 hours at 30°C with constant shaking at 50 rpm in darkness and repeated in three biological replicates.

PAA conjugate profiling

Extraction and purification of PAA conjugates followed the methodology described by Hladík et al., (2023) with modifications. Samples containing ≈ 10 mg of fresh weight tissue were extracted in 1 mL of an ice-cold sodium phosphate buffer supplemented with 0.1% diethyldithiocarbamic acid sodium salt. A mixture of isotopically labelled internal standards (IS) was added to the samples, including [$^{13}C_6$]PAA (10 pmol), [$^{13}C_6$]PAA-Asp (5 pmol), [$^{13}C_6$]PAA-Glu (5 pmol). The samples were homogenised using a MM400 bead mill (Retsch GmbH, Haan, DE) with three zirconium oxide beads. The samples were then incubated on a rotary shaker (15 min, 27 rpm, 4°C) and then centrifuged (10 min, 206 642 g, 4°C). From the supernatant, 200 μL were acidified with 1M HCl to pH 2.7 and subjected to purification by in-tip micro solid-phase extraction (in-tip μSPE) utilizing a combination of HLB AttractSPE™ (Affinisep, Le Houlme, France) and SDB-XC Empore™ (3M, MN, USA) sorbents. The multi-StageTip microcolumns were activated sequentially with 50 μL of acetone (centrifugation 10 min, 3 846 g, 8°C), 50 μL of methanol (10 min, 3 846 g, 8°C), and 50 μL of water (15 min, 4 654 g, 8°C). The acidified samples were then applied to the activated microcolumns (30 min, 16 961 g, 8°C), washed with 50 μL of 0.1% acetic acid (20 min, 9 846 g, 8°C), and eluted with 50 μL of 80% methanol (20 min, 8 653 g, 8°C). After elution, samples were evaporated to dryness under vacuum and stored at -20°C until HPLC-MS/MS analysis.

Evaporated samples were reconstituted in 30 µL of 10% methanol prior to analysis on an HPLC-MS/MS system consisting of a 1260 Infinity LC II system (Agilent Technologies, Santa Clara, CA, USA) equipped with a reversed-phase chromatographic column (Kinetex C18 100 Å, 50 x 2.1 mm, 1.7 µm; Phenomenex, CA, USA) and coupled to a 6495B Triple Quadrupole LC/MS system (Agilent Technologies, CA, USA). Mobile phase consisted of deionised water (A) and methanol (B) supplemented with 0.1% acetic acid. The chromatographic analysis was carried out for 18 min at a flow rate of 0.3 ml/min and the elution of auxin metabolites was achieved using a gradient elution programme: 0 min - 10% B, 11.5 min - 60% B, 11.75 min - 99% B, 14.75 min - 99% B, 15 min - 10% B. During analysis, samples were stored in an autosampler at 4°C, with the column maintained at 40°C, and 10 µL of each sample was injected.

Individual analytes were detected using the MS instrument operating in negative electrospray ionisation (ESI-) modes with optimised parameters: nebuliser pressure at 25 psi, drying gas flow rate and temperature set at 14 L/min and 130°C respectively, sheath gas flow rate and temperature set at 12 L/min and 400°C respectively, capillary voltage set at 2.8 kV in positive mode and 3.0 kV in negative mode, and nozzle voltage maintained at 0 V. The measured analytes were detected and quantified by diagnostic multiple reaction monitoring (MRM) transitions of precursor and appropriate product ions using optimal collision energies and a dwell time of 50 ms, as described in **Tab. S1**. Raw data analysis was performed using Mass Hunter software (Agilent Technologies, CA, USA).

The method was validated as described in Hladík et al., (2023). Arabidopsis and pea plants were harvested at the growth stage 1.0 and spiked by 0, 1, and 10 pmol of authentic PAA standards (0, 10, and 50 pmol for PAA-glc), and 5 pmol of IS ([$^{13}C_6$]PAA, [$^{13}C_6$]PAA-Asp, [$^{13}C_6$]PAA-Glu). All samples were then extracted and purified as described above and measured by HPLC-MS/MS. After the measurement, analytes accuracy (percentage bias) and precision (relative standard deviation in %) was calculated (**Tab. S2; Tab. S3).**

Statistical analysis

All analyses were performed using R statistical software (version 4.3.2; R Core Team, 2021) within the RStudio environment (version 2023.12.0.369; Posit team, 2023). The following packages were used for statistical analysis and graph generation: dplyr (Wickham et al., 2023a), ggplot2 (Wickham, 2016), ggbreak (Xu et al., 2021), multcomp (Hothorn at el., 2008), multcompview (Graves et al., 2019) and readxl (Wickham & Bryan, 2023b).

One-way ANOVA was used to assess differences between control and experimental variants. Significant differences detected at the 95% confidence level were subjected to Tukey's post-hoc test. Values under limit of detection (LOD) were replaced with 0.66-fold of respective LOD value. For data visualisation, box-and-whisker plots were generated showing the median (centre line), upper and lower quartiles (box limits) and maximum and minimum values, with individual dots representing each biological replicate.

Results

LC-MS determination of PAA conjugates

To determine PAA conjugates, we adopted and modified a method previously developed and applied for profiling IAA metabolites (Hladík et al., 2023). The method combined microscale sample extraction and purification with detection by LC-MS/MS with optimised conditions for each compound as detailed in **Tab. S1**. For method validation, we constructed 15-point calibration curves ranging from 9 amol to 90 pmol and calculated the limit of detection (LOD) (S/N ratio > 3) as well as the dynamic linear range (**Tab. S1**). Subsequently, a spiking experiment was conducted using authentic standards of PAA conjugates. The average method accuracy, determined from extracts prepared from Arabidopsis and pea seedlings spiked with 1 or 10 pmol of unlabeled standards, exhibited a bias of 13% (**Tab. S2; Tab. S3**). Similarly, the average method precision (RSD) was less than 11% for both matrices, indicating sufficient precision and accuracy of quantitative determination of PAA metabolites in both tested matrices.

PAA-glc is an endogenous PAA metabolite synthesized by UGT84B1 and UGT74D1 glucosyltransferases

Having a dependable analytical method, we systematically screened for PAA conjugates across various species of land plants. Remarkably, we uncovered the presence of endogenous PAA-glc, a compound previously undetected in plants, within three species: Arabidopsis, pea and spruce. To ensure the identity of endogenous PAA-glc, we compared its chromatographic retention times from Arabidopsis and spruce extracts with that of synthetic PAA-glc standard (**Fig. 2A**). Subsequently, to further confirm the formation of PAA-glc *in planta*, we treated Arabidopsis seedlings with 20 µM PAA and PAA-glc levels were subsequently determined after 30-, 60-, and 180-minutes intervals (**Fig. 2B**). Notably, the concentration of PAA-glc progressively increased from ≈180 pmol*g^{-1} to 40 nmol*g^{-1} FW after 180 min of treatment, demonstrating the *de novo* synthesis of PAA-glc in response to exogenous application of PAA.

The quantitative tissue-specific analysis revealed highest levels of PAA-glc in spruce shoots (almost 760 pmol*g^{-1} FW). The levels around 270 pmol*g^{-1} FW were determined in spruce and Arabidopsis roots. Pea and Arabidopsis shoots contained 95 and 80 pmol*g^{-1} FW, respectively. In other tissues and species (maize, wheat, and *Physcomitrium patens*) PAA-glc was not detected (**Fig. 2C, Tab. 1**).

The glucosyltransferase UGT84B1 has been identified as responsible for the formation of IAA-glc and PAA-glc *in vitro* (Aoi et al., 2020b). Similarly, UGT74D1 has been linked to the formation of oxIAA-glc (Mateo-Bonmatí et al., 2021), although its involvement in PAA metabolism hasn't been explored. To investigate whether these enzymes are involved in PAA-glc formation in plants, we explored PAA-glc content in Arabidopsis knockout lines *ugt84b1* and *ugt74d1*. Remarkably, we observed significantly lower levels of PAA-glc in both mutants compared to Col-0 (**Figure 2D**). Additionally, we tested the

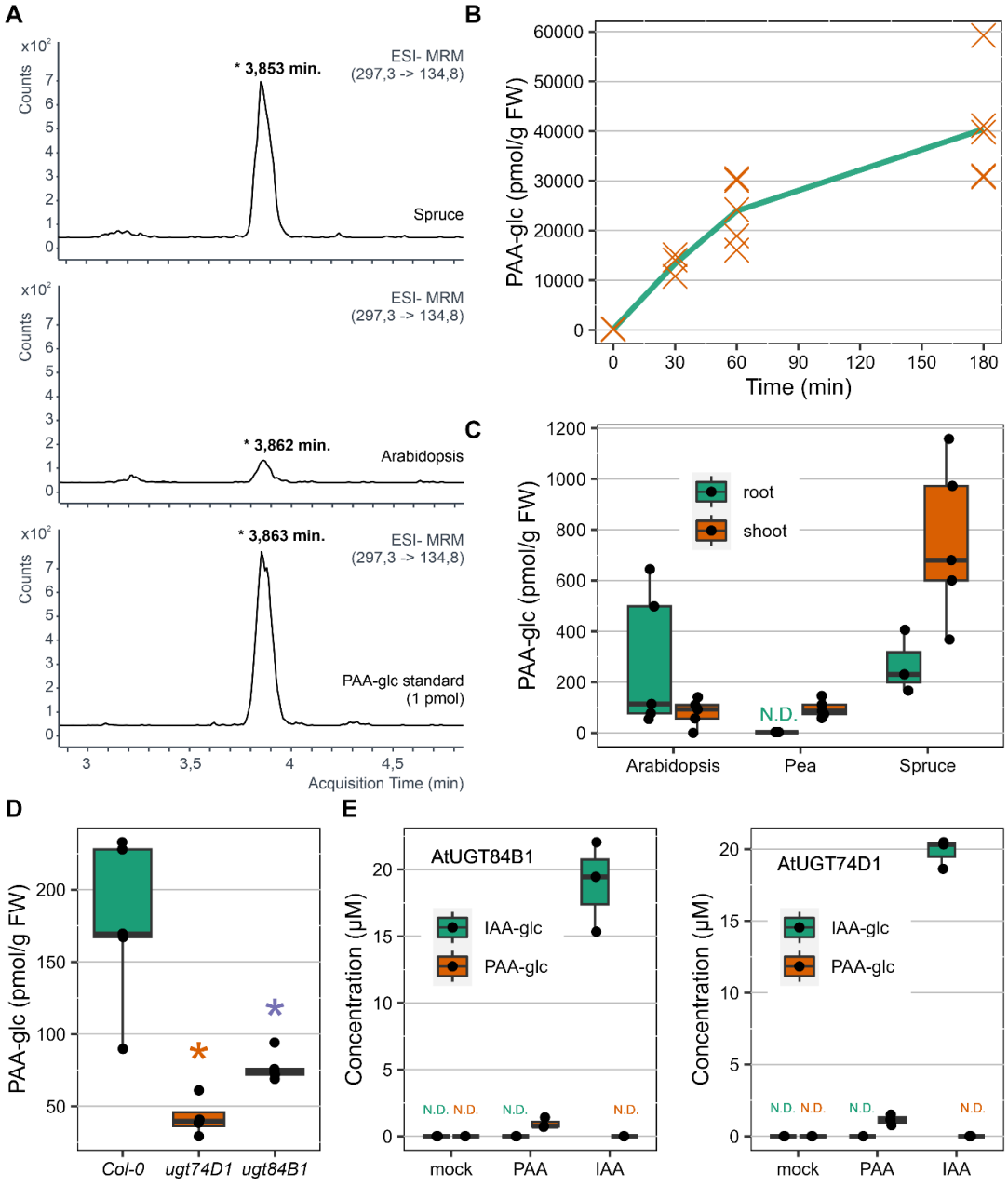

Figure 2: Presence and formation of PAA-glc in plants*. Representative MRM chromatograms of Arabidopsis and spruce extracts compared with the chromatogram of 1 pmol of synthetic PAA-glc standard (A). The concentration (pmol*g^{-1} FW) of PAA-glc after treatment of Arabidopsis with 20 µM PAA for 30, 60 and 180 minutes (B). Each orange cross represents an individual biological replicate (n=5). The endogenous levels of PAA-glc (pmol*g^{-1} FW) in roots and shoots of Arabidopsis, pea and spruce (C). The levels of PAA-glc (pmol*g^{-1} FW) in Col-0, ugt74d1 and ugt84b1 knockout Arabidopsis lines (D). The analysis of IAA-glc and PAA-glc synthesized by a recombinant AtUGT84B1 and AtUGT47D1 produced by a bacterial assay (E). The cell lysate was incubated with 0.1 mM IAA or PAA and UGT cofactors for 5 h at 30°C. Cell lysate without treatment was used as a mock sample. The box plots show the upper and lower quartiles, with horizontal lines indicating medians, and each dot representing a single biological replicate. Statistically significant differences are indicated by asterisks, as determined by Student's t-test ($P \leq 0.05$). All plant profiling was performed in five biological replicates (n=5) and bacterial enzyme assays in three biological replicates (n=3). N.D., not detected.*

conjugation activity of these enzymes by producing them in E. coli and using a bacterial assay designed to study various IAA catabolic enzymes (Brunoni et al., 2019; Brunoni et al., 2023a). Both UGT84B1 and UGT74D1 showed the capability to produce IAA-glc and PAA-glc after exposure to 0.1 μM IAA and PAA, respectively (**Fig. 2E**). Although the activity of both glucosyltransferases towards PAA was only about 5% compared to IAA, the experiment together with mutant analysis clearly demonstrated involvement of UGT84B1 and UGT74D1 in PAA glucosylation.

Exploring novel PAA amide conjugates, their enzymatic synthesis and break down

Conjugates of IAA with various amino acids have been previously determined in plants. However, PAA linked with Asp, Glu and Trp are the only known amide conjugates present in plants (Sugawara et al., 2015; Staswick et al., 2017). In this study, in addition to identifying PAA-glc, we uncovered three previously unreported amide conjugates (PAA-Leu, PAA-Phe, and PAA-Val) in pea and wheat. The verification of newly identified endogenous conjugates relied on comparing their chromatographic retention times to those of synthetic standards, as shown for PAA-Phe in **Fig. 3A**. While endogenous steady state levels of PAA-Leu, PAA-Phe and PAA-Val in Arabidopsis were below the detection limits, feeding plants with 20 μM PAA promoted their *de novo* synthesis, resulting in detectable endogenous concentrations ranging from 0.5 to 1 pmol*g^{-1} FW after just 30 minutes (**Fig. 3B**).

PAA-Leu, PAA-Phe, PAA-Val and PAA-Trp were then quantified in different tissues of various plant species, with detectable concentrations observed only in pea and wheat (**Fig. 3C**). The conjugates were present predominantly in cotyledons, suggesting a storage function. Pea cotyledon contained all four conjugates in concentrations ranging from 0.5 to 8 pmol*g^{-1} FW. PAA-Phe, PAA-Val and PAA-Leu were detected in roots, and PAA-Phe, PAA-Val were also found in shoots, all in concentrations below 2 pmol*g^{-1} FW. All of them were identified in wheat cotyledon at concentrations not exceeding 2 pmol*g^{-1} FW.

It was anticipated that GH3 enzymes would be responsible for their formation. Bacterial enzymatic assays were performed with recombinant AtGH3.6 and AtGH3.17 enzymes cloned in E. coli (**Fig. 3D**). In presence of 0.1 μM PAA, both enzymes formed all tested PAA amino acids. Enzyme AtGH3.6 predominantly conjugates PAA to PAA-Asp. Similarly, enzyme AtGH3.17 prefers Glu as a substrate for conjugation with PAA. Both enzymes formed all conjugates, however, their activity towards other amino acids was much lower and not preferential.

In a light of recent findings demonstrating the hydrolysis of IAA-amino acids to free IAA (Hayashi et al., 2021; Brunoni et al., 2023a), we investigated whether this phenomenon extends to PAA-AAs. To assess this, we conducted experiments using bacterial assays with AtILL2, AtILL6, AtILR1, or AtIAR3 enzymes, incubating them with 0.1 mM PAA-Leu, PAA-Val, PAA-Trp, or PAA-Glu and quantifying the formation of PAA (**Fig. 3E**). The control group consisted of GFP-producing bacteria. The results suggest that AtIAR3 favours PAA-Glu/-Leu/-Val as substrates, while AtILL6 does not exhibit any clear

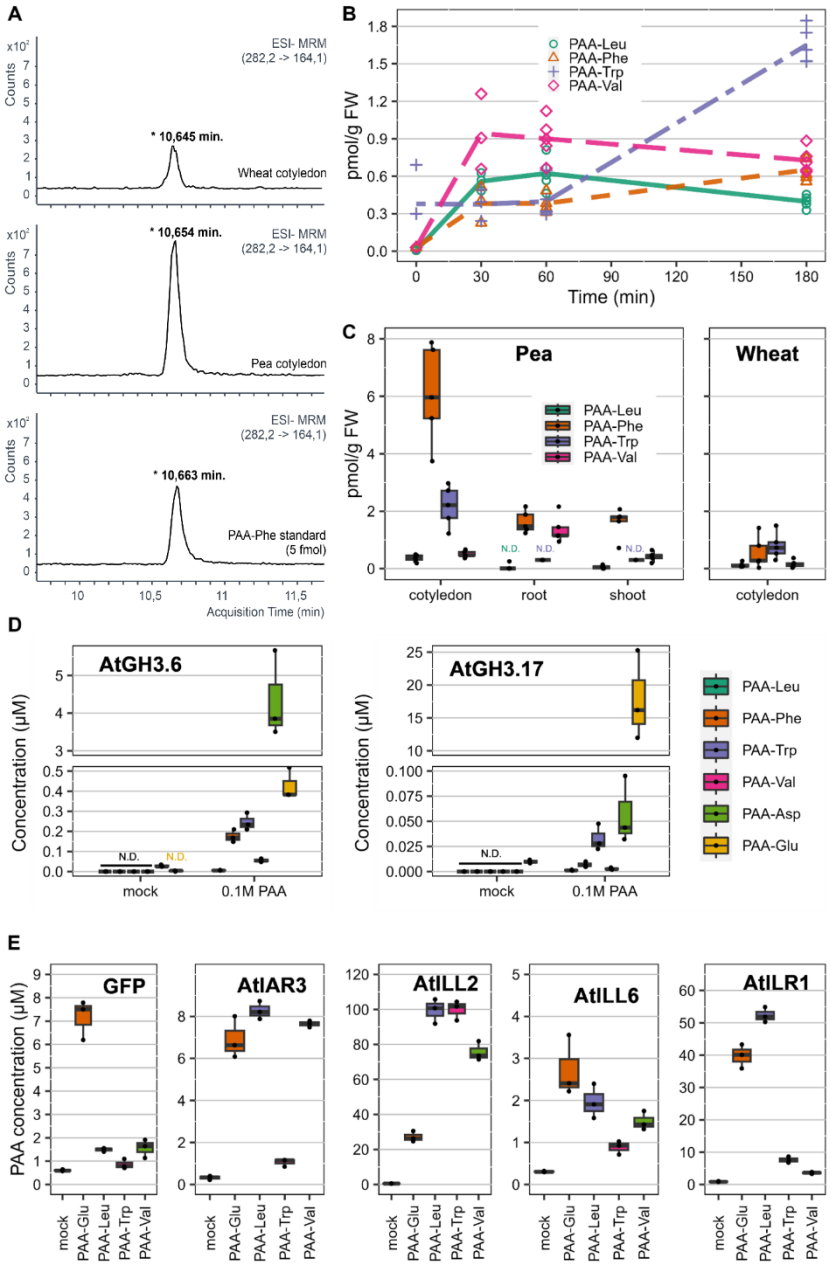

Figure 3: PAA amide conjugates abundance, formation and hydrolysis. *The chromatograms of pea and wheat cotyledon extracts compared with the chromatogram of PAA-Phe standard (A). The concentration levels (pmol*g^{-1} FW) of PAA-Leu, PAA-Phe, PAA-Trp and PAA-Val were measured in Arabidopsis seedlings after treatment with 20 µM PAA for 30, 60 and 180 minutes (B). Each sign in a specific colour represents an individual biological replicate (n=5). The quantification of PAA-Leu, PAA-Phe, PAA-Trp and PAA-Val (pmol*g^{-1} FW) was carried out in pea cotyledons, roots, and shoots, as well as in wheat cotyledons (C). The analysis of PAA-AAs synthesized by recombinant AtGH3.6 and AtGH3.17 in the bacterial assay. The cell lysate was incubated with 0.1 mM PAA and GH3 cofactors for 5 h at 30°C, and the formation of PAA-AAs was determined. As a control, cell lysate without PAA treatment was used (D). The hydrolysis of PAA-AAs to PAA was examined using a bacterial assay with recombinant AtIAR3, AtILL2, AtILL6 and AtILR2 (E). The lysate was incubated with 0.1 mM PAA-Leu, PAA-Trp, PAA-Val and PAA-Glu for 5 hours at 30°C, and the levels of PAA were measured. A negative control was performed using GFP-producing bacteria, and a mock was performed using cell lysate without treatment. The box plots display medians as horizontal lines, upper and lower quartiles as boxes, and each dot represents a single biological replicate. All plant profiling was performed in five biological replicates (n=5) and bacterial enzyme assays in three biological replicates (n=3). N.D., not detected.*

substrate preference. However, the concentration of PAA formed by these enzymes is comparable to the GFP control, indicating that they may not significantly contribute to hydrolysis of PAA conjugates. AtILL2 shows a pronounced preference for PAA-Leu/-Trp/-Val, while AtILR1prefererably hydrolysed PAA-Glu and PAA-Leu. Overall, our findings demonstrate the capability of ILR/ILL proteins to hydrolyse PAA conjugates *in vitro*.

Profiling PAA conjugates in land plants

While previous studies have extensively examined PAA levels across various plant species and tissues (reviewed in Perez et al., 2023), information regarding its conjugate levels are limited predominantly to Arabidopsis (Sugawara et al., 2015, Aoi et al., 2020a). Therefore, we conducted a thorough tissue-specific profiling encompassing high-abundance PAA conjugates, namely PAA-Asp, PAA-Glu and PAA-glc across diverse plant species of land plants (**Table 1**). Intriguingly, we observed significant variations in the PAA conjugate profile among species and even within tissues.

Table 1: PAA conjugate levels in various plant species*. PAA conjugates were quantified (pmol*g^{-1} FW ± SD; n=5) in roots, shoots and cotyledons of pea, wheat and maize, roots and shoots of Arabidopsis and spruce, and gametophores of Physcomitrium patens. <LOD, under the limit of detection.*

Species	Tissue	PAA	PAA-Asp	PAA-Glu	PAA-glc
		*Mean ± SD (pmol*g^{-1}FW)*			
Arabidopsis thaliana	shoot	310.18 ± 23.25	581.03 ± 156.00	507.41 ± 130.00	80.21 ± 54.10
	root	590.80 ± 273.62	1,896.87 ± 906.75	1,928.48 ± 868.86	277.82 ± 273.96
Maize (*Zea mays*)	shoot	<LOD	9.11 ± 2.56	10.18 ± 2.45	<LOD
	cotyledon	422.34 ± 59.50	25.41 ± 21.87	<LOD	<LOD
	root	185.05 ± 21.43	50.83 ± 7.29	99.54 ± 27.47	<LOD
Wheat (*Triticum aestivum*)	shoot	492.95 ± 98.83	16.91 ± 2.18	<LOD	<LOD
	cotyledon	695.43 ± 504.86	432.38 ± 277.06	16.71 ± 11.46	<LOD
	root	340.98 ± 112.34	523.48 ± 345.26	<LOD	<LOD
Pea (*Pisum sativum*)	shoot	1,113.51 ± 304.78	1,444.72 ± 466.83	54.06 ± 7.77	95.20 ± 34.25
	cotyledon	310.19 ± 62.28	37,077.09 ± 12,823.16	1719.90 ± 413.77	<LOD
	root	1,344.98 ± 169.59	1,095.36 ± 990.75	272.08 ± 53.63	<LOD
Spruce (*Picea abies*)	shoot	36.64 ± 13.17	1.62 ± 0.67	5.83 ± 0.34	755.73 ± 311.91
	root	76.47 ± 18.58	1.94 ± 0.36	2.12 ± 0.24	267.79 ± 124.22
Physcomitrium patens	-	82.56 ± 36.08	1.82 ± 0.32	27.33 ± 3.46	<LOD

Remarkably, spruce and *Physcomitrium* exhibited lower levels of free PAA and PAA-Asp compared to all angiosperm representatives. Additionally, spruce represented the only species where the predominant conjugate was PAA-glc, accounting for around 95% of the entire PAA pool in shoots.

Among other species, amide conjugates were more abundant. In *Physcomitrium*, the concentrations of PAA-Glu were more than 10 times higher than PAA-Asp, unlike in all other species. In both monocotyledonous species, maize and wheat, the majority of free PAA was contained in the cotyledons. PAA-glc was not detected in these species. In *Arabidopsis*, the majority of the PAA conjugates was present in roots, primarily in the form of PAA-AAs, although notable levels of free PAA and PAA-glc were also detected. In pea, PAA-Asp was the predominant storage form in, with concentrations reaching approximately 40 nmol/g in cotyledons. Overall, it appears that pea stores a considerable amount of PAA in amide forms.

Metabolic pathways of PAA display only partial functional redundancy

Understanding the redundancy within metabolic pathways is crucial for understanding how plants control hormone homeostasis. Previous studies have demonstrated the presence of functional redundancy within pathways of IAA metabolism (Porco et al., 2016, Mellor et al., 2016). Here, we aimed to investigate the dynamic changes in PAA and its conjugates in response to perturbations in specific metabolic pathways, shedding light on the mechanisms governing PAA homeostasis.

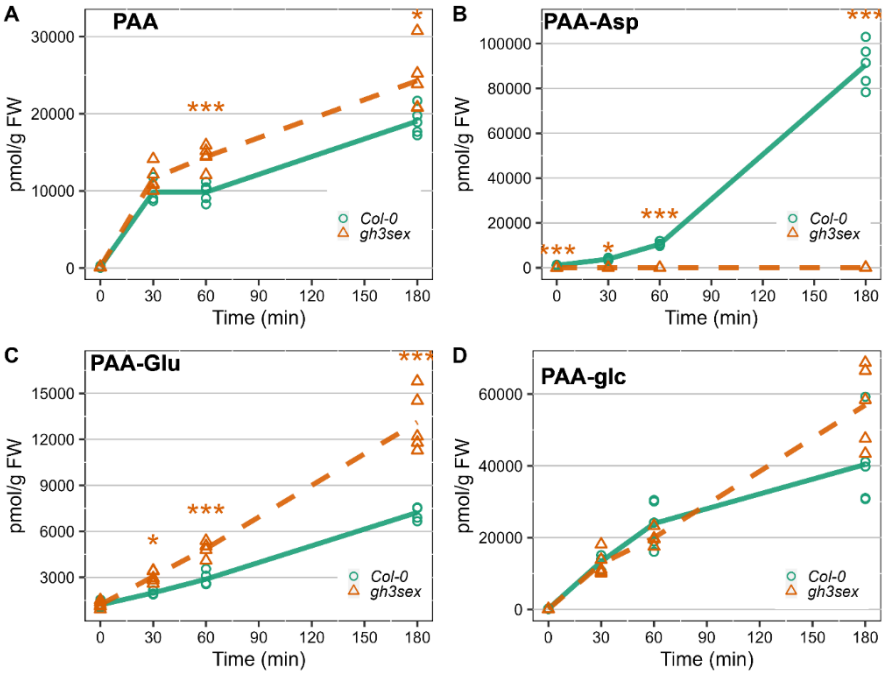

Figure 4: PAA metabolism in Arabidopsis gh3.1-6 knockout mutant*. Arabidopsis line gh3.1,2,3,4,5,6 (gh3sex and Columbia (Col-0) were treated with 20 µM PAA for 30, 60, and 180 minutes. The concentrations levels (pmol*g^{-1} FW) of PAA (A), PAA-Asp (B), PAA-Glu (C) and PAA-glc (D) were measured in those four time points. Each sign in a specific colour represents an individual biological replicate (n=5). Asterisks indicate statistically significant differences between the Col-0 and mutant line in one time point, as determined by Student's t-test (*, $P \leq 0.05$; **, $P \leq 0.01$; ***, $P \leq 0.001$). The colour of the asterisk corresponds to the mutant line that is significantly different from Col-0.*

Arabidopsis mutant *gh3sex*, deficient in GH3-dependent PAA-AAs synthesis, weas treated with 20 µM PAA for 30, 60 and 180 min, and the levels of PAA conjugates were compared with concentration in wild type (Col-0). The PAA levels immediately increased after treatment, suggesting rapid uptake of exogenously applied PAA by the plant (**Fig. 4A**). Subsequent analysis at 60 minutes post-treatment revealed significant differences in PAA concentrations between the mutant lines and Col-0, indicating disruptions in PAA metabolism. Notably, the levels of PAA-Asp were significantly reduced in the mutant throughout the duration of the experiment **(Fig. 4B)**, highlighting the dominant role of AtGH3.1-6 enzymes in conjugation of PAA with Asp. The PAA-Glu levels were elevated in *gh3sex* mutant at 60- and 180-min post-treatment (**Fig. 4C**). The increase in PAA-Glu levels in mutant could be attributed to compensatory mechanisms and functional redundancy of GH3 proteins. Measurement of PAA-glc levels did not reveal any significant differences between wild-type and mutant (**Fig. 4D)**.

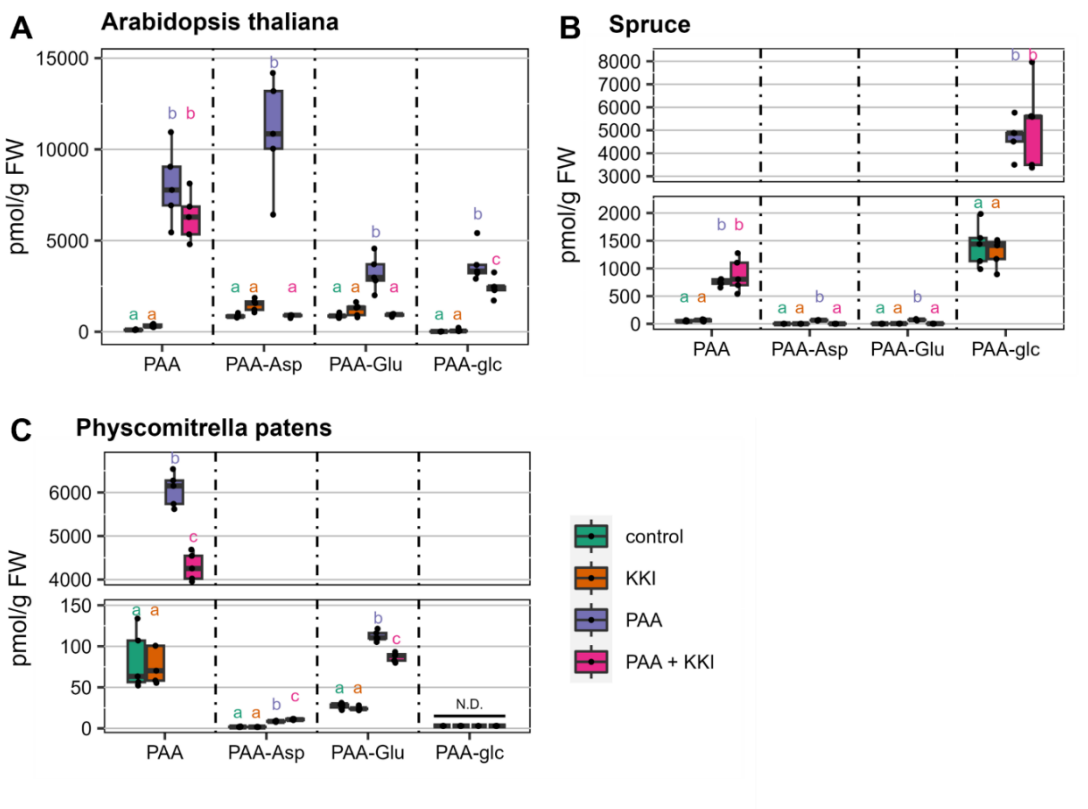

Figure 5: PAA metabolism after PAA and kakeimide (KKI) co-treatment in various plant species*. Arabidopsis thaliana (A), spruce (B) and Physcomitrium p. (C) were treated with 50 µM KKI, 5 µM PAA or their combination for 1, 6 or 24 hours respectively, with time depending on the species. The concertation (pmol*g^{-1} FW) of PAA, PAA-Asp, PAA-Glu and PAA-glc was measured after the treatment. As a control, mock treated samples were used. The box plots display medians as horizontal lines, upper and lower quartiles as boxes, and each dot represents a single biological replicate (n=5). One-way ANOVA and Tukey's post hoc test were applied to assess the differences between treatment groups. Different letters (a-c) indicate significant differences at the 5% level of significance (P ≤ 0.05). The colour of the letters corresponds with the colour of the boxplot. N.D., not detected.*

To compare PAA metabolism across phylogenetically diverse plant species, we employed the synthetic GH3 inhibitor KKI, known for inhibiting the formation of IAA-AAs (Fukui et al., 2022). Anticipating a similar function in PAA metabolism, we investigated its effects in Arabidopsis, spruce and *Physcomitrium*, by treating them with 50 μM KKI, 5 μM PAA, or a combination of both.

In Arabidopsis, co-treatment with PAA and KKI resulted in reduced levels of PAA-Asp and PAA-Glu compared to PAA treatment alone, confirming the activity of KKI in inhibiting PAA-AAs formation. Interestingly, levels of free PAA remained unchanged between the two treatments (**Fig. 5A**). In spruce, the treatment with PAA confirmed predominant role of glukosylation in PAA metabolism. In agreement to Arabidopsis, KKI inhibited the GH3-mediated formation of both amide conjugates (**Fig. 5B).** Interestingly, in *Physcomitrium*, only formation of PAA-Glu was blocked by KKI in co-treatment with PAA, while PAA-Asp level was elevated (**Fig. 5C**). Notably, the formation of PAA-glc was not observed even after PAA treatment, suggesting that glucosylation does not occur in PAA metabolism in *Physcomitrium*.

Discussion

Metabolism plays a pivotal role in maintaining auxin homeostasis, by ensuring optimal levels of biologically active hormone within the plant. While extensive research governing IAA metabolism has been done in previous years (Brunoni et al., 2020; Hayashi et al., 2021; Mateo-Bonmatí et al., 2021; Müller et al., 2021; Brunoni et al., 2023a; Hladík et al., 2023), the inactivation pathways of PAA remain largely uncharacterised. Thus far only PAA-Asp, PAA-Glu and PAA-Trp were identified in Arabidopsis (Sugawara et al., 2015; Staswick et al., 2017). However, there is no evidence about other conjugates or metabolic pathways, as oxidation of the phenyl ring is unlikely and the formation of glucosyl ester (PAA-glc) have only been demonstrated *in vitro* (Aoi et al., 2020b).

In our study we aim to broaden the understanding of PAA metabolism by investigating novel conjugates and metabolic pathways (**Fig. 1**). To achieve this, we employed HPLC-MS/MS, optimized and validated for quantitative analysis of wide range of PAA conjugates (**Tab. S1; Tab. S2; Tab. S3**). Relatively lower method accuracy (more than 20% BIAS) was obtained for PAA-Val and PAA-glc when quantified in pea, probably due to the absence of corresponding isotopically labelled internal standard. [$^{13}C_6$]PAA-Glu, used as reference standard for these conjugates, did not completely compensated for losses during purification and ionization of the molecules.

As a result of comprehensive multi-species screen, we confirmed occurrence of four novel PAA conjugates (PAA-glc, PAA-Leu, PAA-Phe and PAA-Val) in different plant species. The identity of endogenous conjugates was confirmed by comparison of their retention times with that of synthetic standards under the same chromatographic conditions (**Fig. 2A, Fig. 3A**). PAA-glc was found in Arabidopsis, pea and spruce, in concentrations ranging from 50 to 1000 pmol*g^{-1} FW, with the highest levels observed in spruce shoots (**Fig. 2C)**. However, even these high levels were close to the limit of detection of our method, likely due to poor ionisation of the molecule. It is plausible that PAA-glc may

also be present in other studied species, however below the limit of detection. Presence of newly identified amide conjugates, PAA-Leu, PAA-Phe and PAA-Val was observed only in pea and wheat in low concentrations ranging from 0.5 to 8 pmol*g^{-1} FW (**Fig. 3C)**. These findings align with the low levels of IAA and oxIAA conjugates with amino acids other than Asp and Glu quantified previously in various plants (Kowalczyk & Sandberg, 2001; Pěnčík et al., 2009; Hladík et al., 2023). While Staswick et al., (2017) observed high levels of PAA-Trp (approximately 30 pmol*g^{-1} FW) in Arabidopsis tissue, under our experimental conditions PAA-Trp was not detected in Arabidopsis, being only determined in pea and wheat cotyledons. Although PAA conjugates with Leu, Phe, Trp and Val were not found in Arabidopsis, the capability of Arabidopsis GH3 proteins to catalyse their synthesis *in vitro* was proved by bacterial enzymatic assay (**Fig. 3D**). To further validate the formation of newly identified metabolites *in planta*, we conducted feeding experiments by administering exogenous PAA to Arabidopsis seedlings. This led to rapid synthesis of PAA-glc (**Fig. 2B**) as well as all three novel amide conjugates (**Fig. 3B**), underscoring the role of these conjugates in maintaining PAA homeostasis.

Formation of PAA-glc by enzyme UGT84B1 was already showed *in vitro* (Aoi at el., 2020a). However, other glucosyltransferases can also be involved in formation of IAA/oxIAA-glucosyl esters, such as UGT74D1 (Jackson et al., 2001; Mateo-Bonmatí et al., 2021). Thus, we tested the conjugation activity of this protein in bacterial assay designed to study IAA enzymatic inactivation (Brunoni et al., 2019; Brunoni et al., 2023a) and proved the capability of AtUGT74D1 to produce PAA-glc **(Fig. 2E)**. Additionally, we quantified PAA-glc in *ugt84b1* and *ugt74d1* knockouts and demonstrated involvement of both proteins in formation of PAA-glc *in planta* **(Fig. 2D)**.

The GH3-mediated formation of IAA amide conjugates is well described mechanism (Staswick et al., 2005; Zhang et al., 2018). The role of GH3s in PAA metabolism was also indicated for PAA-Asp and PAA-Glu formation (Sugawara et al., 2015; Westfall et al., 2017; Aoi et al., 2020a). To investigate the role of GH3s in formation of other PAA-AAs, we performed bacterial enzyme assays with AtGH3.6 and AtGH3.17 **(Fig. 3D).** Results indicated that both GH3 proteins are capable of synthesizing all tested PAA conjugates, with AtGH3.6 displaying a preference for Asp and AtGH3.17 for Glu as substrates, aligning with previous assays with IAA conjugation (Brunoni et al., 2019). Furthermore, we investigated the putative hydrolysis of PAA-AAs by ILR/ILL amidohydrolases **(Fig. 3E)**, as previously described for IAA conjugates (Bartel & Fink, 1995; Davies et al., 1999; LeClere et al., 2002; Hayashi et al., 2021). Bacterial enzyme assays with AtILL2, AtILL6, AtILR1, and AtIAR3 revealed that PAA-AAs can be hydrolysed into free PAA, indicating storage function of PAA amino acid conjugates.

To elucidate evolutionary aspects of PAA metabolism, we conducted profiling of PAA and its major conjugates, PAA-Asp, PAA-Glu and PAA-glc across a spectrum of phylogenetically diverse land plants. Our study encompassed representatives such as the moss *Physcomitrium*, spruce as a representative of gymnosperm trees, dicots represented by Arabidopsis and pea, and two monocots, maize and wheat (**Tab. 1**).

According to our findings, PAA levels largely align with previous studies, revealing consistent PAA levels in Arabidopsis and pea tissues (Wightman & Lighty, 1982; Sugawara et al., 2015). Notably, comparison with our previous IAA quantifications (Hladík et al., 2023) as well as with earlier reports indicates significantly higher PAA levels in most plant species and tissues. PAA conjugate profiling revealed PAA-AAs as major metabolites across all studied plants except spruce, where PAA-glc concentrations were notably higher compared to PAA amides. This finding, together with results obtained from PAA feeding experiment **(Fig. 5B)**, suggests that glucosylation serves as the preferred pathway for PAA inactivation in spruce. Remarkably, the exceptionally high PAA-AAs concentrations in pea mirror elevated levels of IAA-AAs and oxIAA-AAs in pea tissues (Hladík et al., 2023), suggesting analogous metabolic regulation of both auxins. Similarly, the abundance of PAA-glc corresponds to elevated levels of IAA-glucosyl ester in spruce (Brunoni et al., 2020). Although PAA conjugation pathways share similarities with those of IAA, the oxidation to oxIAA that serves as an degradation mechanism of IAA and IAA-AAs (Hayashi et al., 2021), represents notable difference between IAA and PAA metabolism. OxIAA and its glucose ester are considerably more abundant among IAA metabolites (Kai et al., 2007a; Pěnčík et al., 2018; Hladík et al., 2023). In contrast, PAA-Asp and PAA-Glu exhibit substantially higher accumulation compared to IAA amide conjugates and represent predominant PAA metabolites in Arabidopsis (**Tab. 1**).

To investigate putative functional redundancy in PAA inactivation between GH3s and UGTs, we explored PAA metabolism using GH3-deficient Arabidopsis mutant and synthetic GH3 inhibitor KKI (Fukui et al., 2022). Following the application of PAA, the synthesis of PAA-Asp was dramatically reduced in *gh3.1-6* (**Fig. 4**). This reduction was partially compensated by an increased conjugation of PAA to Glu. Notably, the deficiency in GH3-mediated conjugation was not compensated by glucosylation, mirroring observations seen with IAA (Porco et al., 2016). This observation was further confirmed by the co-treatment of Arabidopsis, spruce and *Physcomitrium* with PAA and KKI, where no metabolic compensation between GH3s and UGTs was observed **(Fig. 5)**.

In conclusion, our investigation of PAA metabolism has provided valuable insights into the metabolic pathways governing PAA homeostasis in land plants. It appears that there may be other metabolic pathways of PAA that have yet to be discovered, as many have been found in bacteria (Schneider et al., 1997; Navarro-Llorens et al., 2005; Teufel et al., 2010). However, through the identification of novel PAA conjugates and the elucidation of metabolic pathways, we have expanded our understanding of the mechanisms maintaining PAA homeostasis and demonstrated the complexity and species-specific nature of PAA metabolism.

References

Aoi Y, Tanaka K, Cook SD, Hayashi KI, Kasahara H. 2020a. GH3 Auxin-Amido Synthetases Alter the Ratio of Indole-3-Acetic Acid and Phenylacetic Acid in Arabidopsis. *Plant & Cell Physiology* **61**(3): 596–605.

Aoi Y, Hira H, Hayakawa Y, Liu H, Fukui K, Dai X, Tanaka K, Hayashi KI, Zhao Y, Kasahara H. 2020b. UDP-glucosyltransferase UGT84B1 regulates the levels of indole-3-acetic acid and phenylacetic acid in Arabidopsis. *Biochemical and Biophysical Research Communications* 532(2):244-250.

Bartel B, Fink GR. 1995. ILR1, an amidohydrolase that releases active indole-3-acetic acid from conjugates. *Science* **268**(5218): 1745–1748.

Boyes DC, Zayed AM, Ascenzi R, McCaskill AJ, Hoffman NE, Davis KR, Görlach J. 2001. Growth stage-based phenotypic analysis of Arabidopsis: a model for high throughput functional genomics in plants. *The Plant Cell* **13**(7): 1499-510.

Brunoni F, Collani S, Šimura J, Schmid M, Bellini C, Ljung K. 2019. A bacterial assay for rapid screening of IAA catabolic enzymes. *Plant Methods,* **15**(1): 1-10.

Brunoni F, Collani S, Casanova-Sáez R, Šimura J, Karady M, Schmid M, Ljung K, Bellini C. 2020. Conifers exhibit a characteristic inactivation of auxin to maintain tissue homeostasis. *New Phytologist* **226**: 1753-1765.

Brunoni F, Pěnčík A, Žukauskaitė A, Ament A, Kopečná M, Collani S, Kopečný D, Novák O. 2023a. Amino acid conjugation of oxIAA is a secondary metabolic regulation involved in auxin homeostasis. *New Phytologist* **238**: 2264-2270.

Brunoni F, Široká J, Mik V, Pospíšil T, Kralová M, Ament A, Pernisová M, Karady M, Htitich M, Ueda M et al. 2023b. Conjugation of cis-OPDA with amino acids is a conserved pathway affecting cis-OPDA homeostasis upon stress responses. *bioRxiv*. doi:10.1101/2023.07.18.549545

Cook SD. 2019. An Historical Review of Phenylacetic Acid. *Plant & Cell Physiology* **60**(2): 243–254.

Davies RT, Goetz DH, Lasswell J. Anderson MN, Bartel B. 1999. IAR3 encodes an auxin conjugate hydrolase from Arabidopsis. *The Plant Cell* **11**(3): 365–376.

Fukui K, Arai K, Tanaka Y, Aoi Y, Kukshal V, Jez JM, Kubeš MF, Napier R, Zhao Y, Kasahara H et al. 2022. Chemical inhibition of the auxin inactivation pathway uncovers the roles of metabolic turnover in auxin homeostasis. *Proc Natl Acad Sci U S A* **119**(32): e2206869119.

Graves S, Piepho H, Selzer L, Dorai-Raj S. 2019. multcompView: Visualizations of Paired Comparisons. R package version 0.1-8/r26, URL https://R-Forge.R-project.org/projects/multcompview.

Grubb CD, Zipp BJ, Ludwig-Müller J, Masuno MN, Molinski TF, Abel S. 2004. Arabidopsis glucosyltransferase UGT74B1 functions in glucosinolate biosynthesis and auxin homeostasis. *The Plant Journal: For Cell and Molecular Biology* **40**(6): 893–908.

Haagen-Smit SAJ, Went FW. 1935. A physiological analysis of growth substance. *Proceedings Koninklijke Nederlandse Akademie van Wetenschappen* **38**: 852-857.

Hayashi K, Arai K, Aoi Y, Tanaka Y, Hira H, Guo R, Hu Y, Ge C, Zhao Y, Kasahara H et al. 2021. The main oxidative inactivation pathway of the plant hormone auxin. *Nature Communication* **12**(1): 6752.

Hladík P, Petřík I, Žukauskaitė A, Novák O, Pěnčík A. 2023. Metabolic profiles of 2-oxindole-3-acetyl-amino acid conjugates differ in various plant species. *Frontiers in Plant Science* **14**: 1217421.

Hothorn T, Bretz F, Westfall P. 2008. Simultaneous Inference in General Parametric Models. *Biometrical Journal* **50**(3): 346-363.

Jackson RG, Lim EK, Li Y, Kowalczyk M, Sandberg G, Hogget J, Ashford DA, Bowles DJ. 2001. Identification and biochemical characterization of an Arabidopsis indole-3-acetic acid glucosyltransferase. *The Journal of Biological Chemistry* **276**(6): 4350–4356.

Kai K, Horita J, Wakasa K, Miyagawa H. 2007a. Three oxidative metabolites of indole-3-acetic acid from Arabidopsis thaliana. *Phytochemistry* **68**: 1651-1663.

Kai K, Nakamura S, Wakasa K, Miyagawa H. 2007b. Facile preparation of deuterium-labeled standards of indole-3-acetic acid (IAA) and its metabolites to quantitatively analyze the disposition of exogenous IAA in *Arabidopsis thaliana*. *Biosci. Biotech. Bioch.* **71** (8): 1946–1954.

Kawazu K, Zhang H, Yamashita H, Kanzaki H. 1996. Relationship between the pathogenicity of the pine wood nematode, Bursaphelenchus xylophilus, and phenylacetic acid production. *Bioscience, Biotechnology, and Biochemistry* **60**: 1413–1415.

Kowalczyk M, Sandberg G. 2001. Quantitative analysis of indole-3-acetic acid metabolites in Arabidopsis. *Plant Physiology* **127**(4): 1845–1853.

Kunkel BN, Harper CP. 2018. The roles of auxin during interactions between bacterial plant pathogens and their hosts. *Journal of Experimental Botany* **69**(2): 245-254.

Lancashire PD, Bleiholder H, Boom PVD, Langeluddeke P, Stauss R, Weber E, Witzenberger A. 1991. A uniform decimal code for growth stages of crops and weeds. *Annals of Applied Biology* **11**: 561-601.

LeClere S, Tellez R, Rampey RA, Matsuda, SPT, Bartel B. 2002. Characterization of a family of IAA-amino acid conjugate hydrolases from Arabidopsis. *The Journal of Biological Chemistry* **277**(23): 20446–20452.

Liu P, Cheng Y, Yang M, Liu Y, Chen K, Long C, Deng X. 2014. Mechanisms of Action for 2-Phenylethanol Isolated from Kloeckera Apiculata in Control of Penicillium Molds of Citrus Fruits. *BMC Microbiology* **14**: 242.

Mateo-Bonmatí E, Casanova-Sáez R, Šimura J, Ljung K. 2021. Broadening the roles of UDP-glycosyltransferases in auxin homeostasis and plant development. *New Phytologist* **232**: 642-654.

Mellor N, Band LR, Pěnčík A, Novák O, Rashed A, Holman T, Wilson MH, Voß U, Bishopp A, King JR et al. 2016. Dynamic regulation of auxin oxidase and conjugating enzymes AtDAO1 and GH3 modulates auxin homeostasis. *Proc Natl Acad Sci U S A* **113**(39): 11022-7.

Müller K, Dobrev PI, Pěnčík A, Hošek P, Vondráková Z, Filepová R, Malínská K, Brunoni F, Helusová L, Moravec T et al. 2021. DIOXYGENASE FOR AUXIN OXIDATION 1 catalyzes the oxidation of IAA amino acid conjugates. *Plant Physiology* **187**(1): 103–115.

Navarro-Llorens JM, Patrauchan MA, Stewart GR, Davies JE, Eltis LD, Mohn WW. 2005. Phenylacetate catabolism in Rhodococcus sp. strain RHA1: a central pathway for degradation of aromatic compounds. *Journal of Bacteriology* **187**: 4497–4504.

Pěnčík A, Rolčík J, Novák O, Magnus V, Barták P, Buchtík R, Salopek-Sondi B, Strnad M. 2009. Isolation of novel indole-3-acetic acid conjugates by immunoaffinity extraction. *Talanta* **80**(2): 651–655.

Pěnčík A, Casanova-Sáez R, Pilařová V, Žukauskaite A, Pinto R, Micol JL, Ljung K, Novák O. 2018. Ultra-rapid auxin metabolite profiling for high-throughput mutant screening in Arabidopsis. *Journal of Experimental Botany* **69**: 2569-2579.

Perez VC, Zhao H, Lin M, Kim J. 2023. Occurrence, Function, and Biosynthesis of the Natural Auxin Phenylacetic Acid (PAA) in Plants. *Plants* **12**: 266.

Porco S, Pěnčík A, Rashed A, Voss U, Casanova-Saez R, Bishopp A, Golebiowska A, Bhosale R, Swarup R, Swarup K et al. 2016. Dioxygenase-encoding AtDAO1 gene controls IAA oxidation and homeostasis in Arabidopsis. *Proc. Natl. Acad. Sci. USA* **113**: 11016–11021.

Posit team. 2023. RStudio: Integrated Development Environment for R. Posit Software, PBC, Boston, MA. URL http://www.posit.co/.

Qin G, Gu H, Zhao Y, Ma Z, Shi G, Yang Y, Pichersky E, Chen H, Liu M, Chen Z et al. 2005. An Indole-3-Acetic Acid Carboxyl Methyltransferase Regulates Arabidopsis Leaf Development. *The Plant Cell* **17**(10): 2693.

R Core Team. 2021. R: A language and environment for statistical computing. R Foundation for Statistical Computing, Vienna, Austria. URL https://www.R-project.org/.

Schneider S, Mohamed ME-S, Fuchs G. 1997. Anaerobic metabolism of L-phenylalanine via benzoyl-CoA in the denitrifying bacterium Thauera aromatica. *Archives of Microbiology* **168**: 310–320.

Staswick PE, Serban B, Rowe M, Tiryaki I, Maldonado MT, Maldonado MC, Suza W. 2005. Characterization of an Arabidopsis enzyme family that conjugates amino acids to indole-3-acetic acid. *The Plant Cell* **17**(2): 616–627.

Staswick PE. 2009. The Tryptophan Conjugates of Jasmonic and Indole-3-Acetic Acids Are Endogenous Auxin Inhibitors. *Plant Physiology* **150**(3): 1310–1321.

Staswick PE, Rowe M, Spalding EP, Splitt BL. 2017. Jasmonoyl-L-tryptophan disrupts IAA activity through the AUX1 auxin permease. *Frontiers in Plant Science* **8**: 736.

Sugawara S, Mashiguchi K, Tanaka K, Hishiyama S, Sakai T, Hanada K, Kinoshita-Tsujimura K, Yu H, Dai X, Takebayashi Y et al. 2015. Distinct Characteristics of Indole-3-Acetic Acid and Phenylacetic Acid, Two Common Auxins in Plants. *Plant and Cell Physiology* **56**(8): 1641–1654.

Takeuchi H, Fujimori Y, Ueda Y, Shibayama H, Nagaishi M, Yoshimura T, Sasamori T, Tokitoh N, Furuta T, Kawabata T. 2020 Solvent-Dependent Mechanism and Stereochemistry of Mitsunobu Glycosylation with Unprotected Pyranoses. *Organic Letters* **22** (12): 4754-4759.

Takubo E, Kobayashi M, Hirai S, Aoi Y, Ge C, Dai X, Fukui K, Hayashi K, Zhao, Y et al. 2020. Role of Arabidopsis INDOLE-3-ACETIC ACID CARBOXYL METHYLTRANSFERASE 1 in auxin metabolism. *Biochemical and Biophysical Research Communications* **527**(4), 1033–1038.

Teufel R, Mascaraque V, Ismail W, Voss M, Perera J, Eisenreich W, Haehnel W, Fuchs G. 2010. Bacterial phenylalanine and phenylacetate catabolic pathway revealed. *Proc. Natl. Acad. Sci. USA* **107**: 14390–14395.

Tottman DR. 1987. The decimal code for the growth stages of cereals, with illustrations. *Annals of Applied Biology* **110**: 441-454.

Westfall CS, Sherp AM, Zubieta C, Alvarez S, Schraft E, Marcellin R, Ramirez L, Jez JM. 2017. Arabidopsis thaliana GH3.5 acyl acid amido synthetase mediates metabolic crosstalk in auxin and salicylic acid homeostasis. *Proc. Natl. Acad. Sci. USA* **113**(48): 13917–13922.

Wickham H. 2016. *ggplot2: Elegant Graphics for Data Analysis*. New York, USA: Springer-Verlag.

Wickham H, François R, Henry L, Müller K, Vaughan D. 2023a. dplyr: A Grammar of Data Manipulation. R package version 1.1.4, URL https://CRAN.R-project.org/package=dplyr.

Wickham H, Bryan J. 2023b. readxl: Read Excel Files. R package version 1.4.3, URL https://CRAN.R-project.org/package=readxl.

Wightman F, Lighty DL. 1982. Identification of phenylacetic acid as a natural auxin in the shoots of higher plants. *Physiologia Plantarum* **55**: 17–24.

Xu S, Chen M, Feng T, Zhan L, Zhou L, Yu G. 2021. Use ggbreak to effectively utilize plotting space to deal with large datasets and outliers. *Frontiers in Genetics* **12**:774846.

Zhang C, Zhang L, Wang D, Ma H, Liu B, Shi Z, Ma X, Chen Y, Chen Q. 2018. Evolutionary History of the Glycoside Hydrolase 3 (GH3) Family Based on the Sequenced Genomes of 48 Plants and Identification of Jasmonic Acid-Related GH3 Proteins in Solanum tuberosum. *International Journal of Molecular Sciences* **19**(7): 1850.

Zhang H, Cheng Q, Wang X, Jia W, Xie J, Fan G, Han C, Zhao X. 2022. Selenium Improved Phenylacetic Acid Content in Oilseed Rape and Thus Enhanced the Prevention of Sclerotinia sclerotiorum by Dimethachlon. *Journal of Fungi* **8**(11): 1193.

Supplementary Material

***Supplementary table 1: Conditions and parameters of HPLC-MS/MS method**. For each PAA metabolite and its corresponding internal standard (IS) diagnostic MRM transition and collision energies (CE) were optimized. Additionally, retention time (RT), limit of detection (LOD), linear range and coefficient of determination (R^2) were measured and calculated. Analytes were detected by the MS instrument with optimised conditions as described: nebulizer pressure, 25 psi; drying gas flow and temperature, 14 l/min and 130 °C; sheath gas flow and temperature, 12 l/min and 400 °C; capillary voltage, 3.0 kv; nozzle voltage, 0 V.*

Compound	MRM transition	IS	MRM transition	CE (V)	retention time (min)	LOD (pmol)	linear range (pmol)	R^2
PAA	135.1 > 91.0	[$^{13}C_6$]PAA	141.1 > 97	2	5	$4.5*10^{-2}$	$4.5*10^{-2}$ - 90	0.9965
PAA-Asp	250.1 > 132.0	[$^{13}C_6$]PAA-Asp	256.2 > 132	10	2.9	$4.5*10^{-3}$	$4.5*10^{-3}$ - 90	0.9973
PAA-glc	297.3 > 91.0	[$^{13}C_6$]PAA-Glu	270.2 > 146	19	3.4	$4.5*10^{-2}$	$9.0*10^{-2}$ - 90	0.9904
PAA-Glu	264.1> 146.0	[$^{13}C_6$]PAA-Glu	270.2 > 146	12	3.7	$9.0*10^{-2}$	$9.0*10^{-2}$ - 90	0.996
PAA-Leu	248.2 > 130.1	[$^{13}C_6$]PAA-Glu	270.2 > 146	12	10.1	$9.0*10^{-5}$	$9.0*10^{-5}$ - 9	0.9985
PAA-Phe	282.2 > 164.1	[$^{13}C_6$]PAA-Glu	270.2 > 146	14	10.5	$4.5*10^{-4}$	$4.5*10^{-4}$ - 9	0.998
PAA-Trp	321.2 > 203.1	[$^{13}C_6$]PAA-Glu	270.2 > 146	14	10.1	$4.5*10^{-3}$	$4.5*10^{-3}$ - 9	0.9974
PAA-Val	234.1 > 116.1	[$^{13}C_6$]PAA-Glu	270.2 > 146	12	8.2	$4.5*10^{-4}$	$4.5*10^{-4}$ - 9	0.9983

***Supplementary table 2: Method validation in Arabidopsis extract**. Validation was performed as described in Hladík et al., 2023. Method precision (% BIAS) and method accuracy (% RSD) were determined by spiking experiment. Briefly, samples were extracted in 1 mL of Na-phosphate buffer with 10 mg of pea or wheat homogenized plants, diluted to 5 mL with Na-phosphate buffer and each sample aliquoted into 200 µL doses (total 15 samples per plant). To each sample, 5 pmol of stable isotope-labelled standards were added. Subsequently, the samples were supplemented with unlabelled standards (1 or 10 pmol). The samples were then purified by in-tip µSPE method, and the concentrations of each analyte were determined by HPLC-MS/MS using isotope dilution method. A set of plant extracts were also processed without the addition of unlabelled standards, and endogenous levels of auxin metabolites were subtracted before calculating the validation parameters. All samples were analysed in five replicates.*

Analyte	1 pmol			10 pmol		
	pmol	BIAS (%)	RSD (%)	pmol	BIAS (%)	RSD (%)
PAA	1.2 ± 0.42	**-15**	**37**	10.1 ± 0.68	**-1**	**7**
PAA-Asp	1.1 ± 0.11	**-7**	**10**	10.2 ± 0.30	**-2**	**3**
PAA-Glu	1.0 ± 0.15	**5**	**16**	9.6 ± 0.14	**4**	**1**
PAA-Val	0.9 ± 0.03	**8**	**3**	10.6 ± 0.34	**-6**	**3**
PAA-Leu	1.0 ± 0.05	**1**	**5**	11.3 ± 0.29	**-13**	**3**
PAA-Phe	1.0 ± 0.05	**3**	**5**	10.9 ± 0.33	**-9**	**3**
PAA-Trp	0.9 ± 0.03	**7**	**3**	11.1 ± 0.47	**-11**	**4**
PAA-glc*	8.5 ± 2.06	**15**	**24**	48.3 ± 1.54	**3**	**5**

* PAA-glc was spiked with 10 and 50 pmol

***Supplementary table 3: Method validation in pea extract**. Validation was performed as described in Hladík et al., 2023. Method precision (% BIAS) and method accuracy (% RSD) were determined by spiking experiment. Briefly, samples were extracted in 1 mL of Na-phosphate buffer with 10 mg of pea or wheat homogenized plants, diluted to 5 mL with Na-phosphate buffer and each sample aliquoted into 200 µL doses (total 15 samples per plant). To each sample, 5 pmol of stable isotope-labelled standards were added. Subsequently, the samples were supplemented with unlabelled standards (1 or 10 pmol). The samples were then purified by in-tip µSPE method, and the concentrations of each analyte were determined by HPLC-MS/MS using isotope dilution method. A set of plant extracts were also processed without the addition of unlabelled standards, and endogenous levels of auxin metabolites were subtracted before calculating the validation parameters. All samples were analysed in five replicates.*

Analyte	**1 pmol**			**10 pmol**		
	pmol	BIAS (%)	RSD (%)	pmol	BIAS (%)	RSD (%)
PAA	1.2 ± 0.17	**-17**	**14**	8.3 ± 0.16	**17**	**2**
PAA-Asp	1.0 ± 0.12	**-2**	**12**	9.5 ± 0.39	**5**	**4**
PAA-Glu	1.0 ± 0.07	**2**	**7**	9.4 ± 0.29	**6**	**3**
PAA-Val	0.7 ± 0.03	**29**	**4**	7.5 ± 0.53	**25**	**7**
PAA-Leu	1.0 ± 0.04	**-5**	**4**	10.6 ± 0.62	**-6**	**6**
PAA-Phe	1.0 ± 0.07	**0**	**7**	10.6 ± 0.49	**-6**	**5**
PAA-Trp	0.9 ± 0.06	**12**	**6**	10.3 ± 0.80	**-3**	**8**
PAA-glc*	8.2 ± 0.40	**18**	**5**	36.7 ± 2.32	**27**	**6**

* PAA-glc was spiked with 10 and 50 pmol

Supplement I

Supplement II

Supplement III

Supplement IV

Bieleszová K., **Hladík P.**, Kubala M., Napier R., Brunoni F., Gelová Z., Fiedler L., Kulich L., Strnad M., Doležal K., Novák O., Friml J., Žukauskaitė A. (2023) New fluorescent auxin derivatives: anti-auxin activity and accumulation patterns in *Arabidopsis thaliana*. *Plant Growth Regul.* 416(1), 125-139.

Plant Growth Regulation (2024) 102:589–602
https://doi.org/10.1007/s10725-023-01083-0

ORIGINAL PAPER

New fluorescent auxin derivatives: anti-auxin activity and accumulation patterns in *Arabidopsis thaliana*

Kristýna Bieleszová[1] · Pavel Hladík[2] · Martin Kubala[3] · Richard Napier[4] · Federica Brunoni[2] · Zuzana Gelová[5] · Lukáš Fiedler[5] · Ivan Kulich[5] · Miroslav Strnad[2] · Karel Doležal[1,2] · Ondřej Novák[2] · Jiří Friml[5] · Asta Žukauskaitė[1]

Received: 18 July 2023 / Accepted: 14 September 2023 / Published online: 13 October 2023

Abstract

Auxin belongs among major phytohormones and governs multiple aspects of plant growth and development. The establishment of auxin concentration gradients, determines, among other processes, plant organ positioning and growth responses to environmental stimuli.

Herein we report the synthesis of new NBD- or DNS-labelled IAA derivatives and the elucidation of their biological activity, fluorescence properties and subcellular accumulation patterns *in planta*. These novel compounds did not show auxin-like activity, but instead antagonized physiological auxin effects. The DNS-labelled derivatives **FL5** and **FL6** showed strong anti-auxin activity in roots and hypocotyls, which also occurred at the level of gene transcription as confirmed by quantitative PCR analysis. The auxin antagonism of our derivatives was further demonstrated in vitro using an SPR-based binding assay. The NBD-labelled compound **FL4** with the best fluorescence properties proved to be unsuitable to study auxin accumulation patterns *in planta*. On the other hand, the strongest anti-auxin activity possessing compounds **FL5** and **FL6** could be useful to study binding mechanisms to auxin receptors and for manipulations of auxin-regulated processes.

Keywords Anti-auxin · *Arabidopsis* · Fluorescent label · Biological activity · Indole-3-acetic acid (IAA), Transport inhibitor response 1 (TIR1)

Introduction

Phytohormones regulate plant growth, development, and responses to both internal and external stimuli *via* a complex network of signalling pathways (Hemelíková et al. 2021; Friml 2022). The structures and main roles of classical phytohormones have been known for decades. Combining this knowledge with synthetic chemistry has allowed the creation of a wide array of synthetic phytohormone analogues including agonists, antagonists, or caged and labelled derivatives. These compounds can be used to manipulate plant growth or serve as powerful tools for obtaining new insights into the modes of action of phytohormones (Rigal et al. 2014; Jiang and Asami 2018; Hemelíková et al. 2021).

Auxin is a key phytohormone, which controls cell division, elongation and differentiation, tropic responses, etc. (Woodward and Bartel 2005). The canonical/transcriptional auxin signalling pathway relies on the action of three main protein families: (i) Transport Inhibitor Response 1/Auxin Signalling F-box proteins (TIR1/AFBs) (Dharmasiri et

Communicated by J. Celenza.

✉ Asta Žukauskaitė
asta.zukauskaite@upol.cz

[1] Department of Chemical Biology, Faculty of Science, Palacký University, Šlechtitelů 27, Olomouc CZ-78371, Czech Republic

[2] Laboratory of Growth Regulators, Faculty of Science, Palacký University & Institute of Experimental Botany, The Czech Academy of Sciences, Šlechtitelů 27, Olomouc CZ-78371, Czech Republic

[3] Department of Experimental Physics, Faculty of Science, Palacký University, 17. listopadu 12, Olomouc CZ-77146, Czech Republic

[4] School of Life Sciences, University of Warwick, Coventry CV47AL, UK

[5] Institute of Science and Technology Austria, Am Campus 1, Klosterneuburg 3400, Austria

al. 2005b; Mockaitis and Estelle 2008; Caumon and Vernoux 2023), (ii) the Aux/IAA transcriptional co-repressors (Remington et al. 2004; Overvoorde et al. 2005), and (iii) Auxin Response Factors (ARFs) (Okushima et al. 2005; Guilfoyle and Hagen 2007). Under low cellular levels of auxin, Aux/IAAs repress the ARF-dependent transcription of auxin-responsive genes. On the other hand, under higher concentrations, auxins enable the interaction of domain II of Aux/IAA transcriptional co-repressors with TIR1/AFB F-box proteins. This leads to Aux/IAA ubiquitination by the Skp1-Cullin-F-box $(SCF)^{TIR1/AFB}$ E3 ligase and to Aux/IAA targeting for degradation. Degradation of Aux/IAAs derepresses ARF proteins, which allows them to modulate the transcription of auxin-responsive genes (Santner et al. 2009). Recently, auxin perception was shown to stimulate the production of a second messenger known from animals, cyclic adenosine monophosphate (cAMP), and TIR1/AFB receptors have been demonstrated to possess adenylate cyclase activity (Qi et al. 2022). Besides TIR1/AFBs, Auxin-binding Protein 1 (ABP1) and its plasma membrane-localized partner, Transmembrane Kinase 1 (TMK1), have been reported to be required for an auxin-induced ultrafast global phospho-response, activation of plasma-membrane H^+-ATPases and acceleration of cytoplasmic streaming (Friml et al. 2022).

Besides indole-3-acetic acid (IAA) and other naturally occurring auxins (Sauer et al. 2013), numerous synthetic compounds with auxin-like activities have been identified (Jiang and Asami 2018). For instance, dichlorophenoxyacetic acid (2,4-D), 3,6-dichloro-2-methoxybenzoic acid (dicamba), etc., inhibit plant growth, and induce senescence and tissue decay in sensitive dicots, making synthetic auxins applicable as plant growth regulators and herbicides (Grossmann 2010; Todd et al. 2020). On the other hand, 4-(2,4-dimethylphenyl)-2-(1*H*-indol-3-yl)-4-oxobutanoic acid (auxinole), 2-(1*H*-indol-3-yl)-4-oxo-4-phenylbutanoic acid (PEO-IAA), or 4-([1,1'-biphenyl]-4-yl)-2-(1*H*-indol-3-yl)-4-oxobutanoic acid (BP-IAA) and its methoxy derivatives possess anti-auxin activity (Hayashi et al. 2012; Žukauskaitė et al. 2023). These derivatives found use in both agriculture and basic plant science to study various biological phenomena (Rigal et al. 2014; Jiang and Asami 2018). Auxinole has been demonstrated to block auxin-induced Ca^{2+} signalling in root cells (Dindas et al. 2018), to decrease auxin-mediated increase in the density of actin filaments in root epidermal cells (Scheuring et al. 2016) and to accelerate petal abscission (Liang et al. 2020). PEO-IAA suppresses root gravitropism and enhances root phototropism (Kimura et al. 2018), and causes chromatin loosening upon application to proliferating plant cells (Hasegawa et al. 2018). The agricultural potential of anti-auxins has also been demonstrated; PEO-IAA was reported to improve grain yield in rice (Tamaki et al. 2015), while both PEO-IAA and BP-IAA derivatives improve in vitro propagation of *Cannabis sativa* L. (Smýkalová et al. 2019; Šenkyřík et al. 2023; Žukauskaitė et al. 2023).

Auxin-sensitive reporter lines such as DR5::GUS, DR5::GFP or DII::VENUS are widely used to study dynamic auxin distribution in plant tissues (Pařízková et al. 2017). However, such auxin-sensitive reporter lines are limited to several model species and, even then, only semi-quantitative in vivo imaging of local substrate concentrations can be achieved (Geisler 2018; Balcerowicz et al. 2021). The recently developed genetically encoded AuxSen biosensor is based on auxin binding to a tryptophan repressor (TrpR), which enables quantitative Förster resonance energy transfer (FRET)-based in vivo visualization of auxin (Herud-Sikimić et al. 2021). As an alternative, efforts have been made to develop fluorescently labelled phytohormones (Lace and Prandi 2016). However, even if the selected fluorescent label is relatively small, its attachment might change the biological activity of the phytohormone due to alterations in hydrophobicity/hydrophilicity, solubility, charge, etc. Therefore, when developing fluorescently labelled compounds, it is essential to optimally choose the labelling site, the fluorophore and the type of linker for preservation of biological activity as well as fluorescence properties (Shani et al. 2013; Prandi et al. 2014; Malachowska-Ugarte et al. 2015).

Materials and methods

Synthesis of compounds

Detailed synthetic procedures and spectral data of the compounds are described in Supplementary Information.

Investigation of fluorescence properties

Absorption spectra

Absorption spectra of 2 µM solutions of NBD-labelled compound **FL4** and DNS-labelled compounds **FL5**, **FL6** in methanol were recorded on a SP-UV1100 spectrometer (DLAB Scientific) in a quartz cuvette with 1 cm optical path, and a pure solvent was used as a reference. The spectra were measured in the 250–550 nm interval with 1 nm step and 2 nm bandpass. The extinction coefficient ε(λ) was calculated from the formula:

$$\epsilon(\lambda) = \frac{A(\lambda)}{cl}$$

where A(λ) is the estimated absorbance, c is the sample concentration and l is the optical path.

Steady-state fluorescence spectra

Steady-state excitation and emission spectra of 2 µM solutions of compounds **FL4**, **FL5** and **FL6** in methanol were recorded on a Fluorolog-3 fluorometer (Jobin-Yvon, France) in a quartz cuvette with 1 cm optical path (both in excitation and emission). The absorbance of the sample at the excitation wavelength should be below 0.05 in all cases, and therefore the inner-filter effect could be neglected. Emission spectra for NBD-labelled compound **FL4** were recorded with excitation at 480 nm, bandpasses in both the excitation and emission monochromator were set to 3 nm, the spectra were scanned with 1 nm steps and integration time 0.5 s per data point at 22 °C. Emission spectra for DNS-labelled compounds **FL5** and **FL6** were recorded with excitation at 360 nm, bandpasses in both the excitation and emission monochromator were set to 2 nm, the spectra were scanned with 1 nm steps and integration time 0.2 s per data point at 22 °C.

Quantum yield (QY) estimation

Emission spectra were acquired under conditions described above. For NBD-labelled compound **FL4** and DNS-labelled derivatives **FL5** and **FL6** fluorescence intensity was integrated in the 485–700 nm and 370–700 nm intervals, respectively, and the quantum yield (QY) was calculated from the formula:

$$QY = \frac{\epsilon_S}{\epsilon}\frac{F}{F_S}\frac{n^2}{n_S^2}QY_S$$

where for NBD-labelled compound **FL4** ε, F and n refer to the extinction coefficient at 480 nm, integrated fluorescence intensity and refractive index, respectively, the subscript „S" refers to the standard (1 nM fluorescein in 0.1 M NaOH, $QY_S = 0.95$) (Brannon and Magde 1978), while for DNS-labelled compounds **FL5** and **FL6** ε, F and n refer to the extinction coefficient at 360 nm, integrated fluorescence intensity and refractive index, respectively, the subscript „S" refers to the standard (2.5 µM quinine sulphate in 0.05 M H_2SO_4, $QY_S = 0.60$) (Suzuki et al. 2009).

Biological activity evaluation

Plant growth conditions

Prior to use, all *Arabidopsis thaliana* seeds were sterilized in 70% ethanol with 0.1% Tween-20 solution for 10 min (2×) and rinsed with 96% ethanol for 10 min. After 2 days of stratification (4 °C in dark), seeds were germinated on sterile ½ MS medium (2.2 g/L Murashige and Skoog medium, 1% sucrose, 0.5 g/L MES PUFFERAN and 0.7% agar, pH 5.6) in a growth chamber under long-day light conditions (22 °C/20 °C, 16 h light/8 h dark, 100 µmol m^{-2} s^{-1}) in a vertical position for indicated time.

Effects of synthesized compounds on auxin signalling in DR5::GUS *Arabidopsis thaliana* transgenic plants

Five-day-old seedlings of *Arabidopsis thaliana* seeds expressing DR5::GUS (Ulmasov et al. 1997) in the Col-0 background were incubated in 24-well plates containing 1 mL of ½ MS liquid medium supplemented with 0.5% DMSO as a blank control, 1 µM IAA as a positive control or derivatives **FL1-6** either on their own at 20 µM concentration or at 5, 10 and 20 µM with 1 µM IAA. The compounds were applied for 5 h. Seedlings were then incubated in 500 µL of GUS staining solution (Na-phosphate buffer, pH 7.0: 4.7 g of $NaH_2PO_4 . H_2O$, 9.6 g of $Na_2HPO_4 . 2\ H_2O$ was dissolved in 500 mL of distilled water to give 200 mM stock solution. Fifty mL of Na-phosphate buffer were supplemented with 0.08 g $K_3[Fe(CN)_6]$, 0.12 g $K_4[Fe(CN)_6]$, 50 µL 0.1% Triton and 50 mg of X-Gluc dissolved in 500 µl of DMSO) (Žukauskaitė et al. 2023) at 37 °C in the dark for 30 min. To stop the staining reaction, seedlings were transferred to 500 µL of 70% ethanol and kept overnight. Roots were cleared with HCG-2 solution (120 g chloral hydrate, 90 mL water, 30 mL glycerol) (Ma et al. 2020). GUS expression was evaluated using an inverted light microscope (Olympus IX51) with a transmission light mode under phase contrast. Experimental set up involved 10× objective.

Effects of synthesized compounds on root growth and auxin signalling in DR5::LUC *Arabidopsis thaliana* transgenic plants

Five-day-old *Arabidopsis thaliana* seedlings expressing DR5::LUC (Moreno-Risueno et al. 2010) in the Col-0 background (10–15 seedlings per treatment) were transferred to plates containing sterile ½ MS supplemented with 0.3% DMSO as a blank control, 0.1 µM IAA as positive control or compounds **FL4**, **FL5** and **FL6** at a final concentration of 10 µM with or without 0.1 µM IAA. Immediately, treated plates were placed on a flatbed scanner (Epson, model: V370 Photo). Samples were automatically scanned in the 8-bit grayscale mode and at 800 dpi every 10 min using the AutoIt program for 6 h. Afterwards, the shoots were cut off and roots were collected in 2 mL Eppendorf tubes (with 2 iron beads inside) and flash-frozen in liquid nitrogen. Samples were ground with Retsch mill and then 700 µL of

Cell Culture Lysis reagent (CCLR, 5× diluted in water) was added. Then the samples were mixed, centrifuged and left for 2 min on ice. Subsequently, 100 µL of lysate was transferred to a microtiter plate and assayed with a luminometer (BioTek Synergy H1 Plate Reader) using Luciferase Assay Reagent II (LAR II), Stop & Glo® (S&G) Reagent. Values presented are means ± S.E. from 3 biological replicates. Root growth was evaluated in ImageJ.

Effects of synthesized compounds on the elongation of hypocotyl segments and auxin signalling in DR5::LUC *Arabidopsis thaliana* transgenic plants

The elongation experiment was done as described previously (Fendrych et al. 2016; Li et al. 2018). Plates with *Arabidopsis thaliana* seeds expressing DR5::LUC (Moreno-Risueno et al. 2010) in the Col-0 background on sterile ½ MS medium were placed vertically under light for 6 h in a growth chamber at 21 °C. Plates were wrapped with aluminium foil and grown for 3 days vertically at 21 °C.

Petri dishes with 5 mL of depletion media (10 mM KCl, 1 mM MES, adjusted to pH 6 by KOH, 1.5% phytagel, MiliQ water as solvent) were prepared. After solidification, cellophane foil was placed on the surface and damped with liquid depletion medium solution.

Petri dishes with three-day-old seedlings were unwrapped and seedlings with similar hypocotyl length were selected. Decapitation was done by cutting seedlings on the surface of the agar right below the apical hook and above the shoot-root junction to get a hypocotyl segment. For each treatment 6–8 segments were prepared. The segments were transferred onto the cellophane foil on the depletion plate and kept in darkness for 30–60 min to deplete endogenous auxin. Subsequently, hypocotyl segments were transferred onto a treatment plate with the depletion medium supplemented with 0.3% DMSO as a blank control, 0.5 µM IAA as positive control and **FL4**, **FL5** or **FL6** at a final concentration of 50 µM with or without 0.5 µM IAA. The treatment plates were placed on a flatbed scanner (Epson, model: V370 Photo) and wet black filter paper was placed inside the lid of the dish to improve the contrast of the image. The samples were scanned in the 8-bit grayscale mode automatically using the AutoIt program and at 1200 dpi every 20 min for 3 h. Afterwards, hypocotyl segments were collected in 2 mL Eppendorf tubes (with 2 iron beads inside) and flash-frozen in liquid nitrogen. Samples were ground with Retsch mill and then 700 µL of Cell Culture Lysis reagent (CCLR, 5× diluted in water) was added. The samples were mixed, centrifuged and left on ice for 2 min. Subsequently, 100 µL of lysate was transferred to a microtiter plate and assayed with a luminometer (BioTek Synergy H1 Plate Reader) using Luciferase Assay Reagent II (LAR II), Stop & Glo® (S&G) Reagent. Values presented are means ± S.E. from 3 biological replicates. Hypocotyl elongation was evaluated in ImageJ.

qPCR analysis

Five-day-old seedlings of *Arabidopsis thaliana* wild-type Col-0 were transferred to ½ MS liquid medium supplemented with 0.3% DMSO as a blank control, 1 µM IAA as a positive control or **FL5** and **FL6** at 20 µM concentration with or without 1 µM IAA. After 3 h seedlings were harvested by flash-freezing in liquid nitrogen. Samples were ground to fine powder in liquid nitrogen using pestle and mortar.

Total RNA was extracted using the Spectrum™ Plant Total RNA Kit, and DNA-free™ Kit was used to remove contaminating DNA. Two µg total RNA was reverse transcribed to cDNA using Oligo$(dT)_{18}$ primer and RevertAid H Minus Reverse Transcriptase. Real-time qPCR analysis was performed using a SYBR® Select Master Mix on a Bio-Rad CFX96 Touch Real-Time PCR Detection System. The three-step cycling programme was as follows: 95 °C for 2 min, followed by 40 cycles at 95 °C for 5 s, 60.5 °C for 20 s and 72 °C for 10 s. Melting curve analysis was conducted between 75 and 95 °C. Transcript levels of four auxin-responsive genes, *Lateral organ boundaries-domain 29 - LBD29* (AT3G58190), *Indole-3-acetic acid inducible 5 - IAA5* (AT1G15580), *GRETCHEN HAGEN 3.3 - GH3.3* (AT2G23170), *Auxin response factor 19 - ARF19* (AT1G19220) were quantified, and *beta-tubulin 2 - TUB2* (AT5G62690) was used as an internal reference gene. The primer pairs used for qPCR were: *LBD29* forward 5'- GCCACAGAGAGTAGTTACCAC-3' and reverse 5'-TCACGAGAAGGAGATGTAGCC-3'; *IAA5* forward 5'-CGGCGAAAAAGAGTCAAGTTGTG-3' and reverse 5'-TTTGGTCCGTTCGAGACTGTTC-3'; *GH3.3* forward 5'-ACAATTCCGCTCCACAGTTC-3' and reverse 5'-ACGAGTTCCTTGCTCTCCAA-3'; *ARF19* forward 5'-TGGGAAGAGTTTGTGAACTGC-3' and reverse 5'-TGTACTTTCCAAGCATTTCCG-3'; *TUB2* forward 5'-GAGCCTTACAACGCTACTCTGTCTGTC-3' and reverse 5'-ACACCAGACATAGTAGCAGAAATCAAG-3'. The relative transcript abundance was calculated after normalizing with *TUB2*. Expression levels were calculated using the ΔΔCt method (Pfaffl 2001). Values presented are means ± S.E. from three biological replicates.

SPR assay

Surface plasmon resonance (SPR) assay was done in accordance with the previously described protocol (Lee et al. 2014). TIR1 was expressed in insect cell culture

using a recombinant baculovirus. The construct contained sequences for three affinity tags: 10 His, green fluorescent protein (GFP) and FLAG. Protein purified using the His tag was used for SPR assays by passing it over a streptavidin chip loaded with biotinylated IAA7 degron peptide in the absence or presence of IAA and test compounds **FL5** and **FL6** and auxinole as anti-auxin control.

Hepes-buffered saline with 10 mM Hepes, 3 mM EDTA, 150 mM NaCl and 0.05% Tween 20 was used as the SPR buffer. Compounds were premixed with the protein and the binding experiments were run at a flow rate of 30 µl min^{-1} using 2 min of injection time and 4 min of dissociation time. Data from a control channel (a mutated IAA7 peptide) and from a buffer-only run supplemented with DMSO (final 1%) were subtracted from each sensogram following the standard double reference subtraction protocol.

Uptake quantification in *Arabidopsis thaliana* seedlings using LC-MS/MS

Five-day-old seedlings of *Arabidopsis thaliana* wild-type Col-0 were transferred to plates containing sterile ½ MS solid media supplemented with 0.3% DMSO as a blank control, or compounds **FL4**, **FL5** and **FL6** at 10 µM concentration. The seedlings were harvested after 1, 3 and 6 h.

To compare the uptake of compound **FL4** and its controls, **CTRL1** and **CTRL2**, five-day-old seedlings were transferred to sterile ½ MS liquid media supplemented with 0.3% DMSO as a blank control, or compounds **FL4**, **CTRL1** and **CTRL2** at 10 µM concentration. The seedlings were harvested after 30 min.

Immediately after harvest, samples were flash-frozen in liquid nitrogen and divided into five (long feeding) or six (short feeing) biological replicates with ≈10 mg of plant material each. All the samples were purified by liquid-liquid extraction using combination of acetonitrile/H_2O/hexane (1/1/1) in the 900 µL total volume. Three ceria-stabilized zirconium oxide beads were added, and samples were homogenized by MixerMill MM 301 bead mill (Retsch GmBH, Germany) for 10 min at a frequency 27 Hz. Extracts were then incubated at 4 °C shaking continuously for 15 min and centrifuged (15 min, 23 000 g, 4 °C). The acetonitrile/H_2O phase was transferred to MicroSpin tubes (0.2 µm, nylon, Chromservis s.r.o.®, Czech Republic), centrifuged for 10 min (12 000 g, 4 °C) and flow-through fraction was evaporated to dryness under vacuum.

The evaporated samples were dissolved in 50 µl of 10% acetonitrile prior to LC-MS/MS analysis using an Acquity UPLC® System (Waters, USA) coupled to a triple quadrupole mass spectrometer Xevo™ TQ MS (Waters MS Technologies, UK). Chromatographic reverse-phase column (Kinetex C18 100 A, length 50 mm, diameter 2.1 mm, particle size 1.7 µm; Phenomenex, USA) was used for UHPLC separation. The mobile phase consisted of acetonitrile (A) and deionized water (B), both with the addition of 0.1% acetic acid. Time of each analysis was 5.5 min, flow rate 0.3 mL/min and gradient elution as follows: 0 min – 60% B, 3.0 min – 30% B, 4.25 min – 99% B, 4.5 min – 99% B, 5.5 – 60% B. During the analysis, samples were stored in an autosampler at 4 °C, 2 µl of each sample were injected and column tempered at 30 °C.

The eluate was introduced into the electrospray ion source of a tandem MS analyser in positive mode (ESI+) using these optimized conditions: source/desolvation temperature 150/600°C; cone/desolvation gas flow, 150/1000 L/h; capillary voltage, 1 kV; cone voltage, 20 V; collision gas flow, 0.14 mL/min. Analytes were measured in multiple reaction monitoring (MRM) mode with optimized conditions as described in Supplementary Table S1 and data interpreted in MassLynx v4.2 software (Waters MS Technologies, UK).

For compound quantification, samples with known compounds concentration were prepared and their recovery factor was calculated. Three replicates of seven-day-old *Arabidopsis thaliana* seedlings were harvested (≈10 mg per sample) and flash-frozen in liquid nitrogen. To each sample 1 nmol of **FL4**, **FL5**, **FL6**, **CTRL1** and **CTRL2** was added and samples were processed by LLE as described above. To calculate for analytes loses and matrix effects, six points external calibration curve ranging from 1 fmol to 100 pmol in 10% acetonitrile was measured, and recovery factor was calculated from the samples (Supplementary Table S2). For real samples, concentration was calculated from an external calibration curve after application of dilution and recovery factors.

Accumulation of the fluorescently labelled derivatives in *Arabidopsis* root cells

Five-day-old seedlings of *Arabidopsis thaliana* wild-type Col-0 or marker lines: p24δ5-RFP (endoplasmic reticulum marker) (Montesinos et al. 2012), Wave lines 22R/SYP32 (Golgi apparatus marker) (Geldner et al. 2009) were incubated in 24-well plates containing 1 mL of ½ MS liquid media supplemented with fluorescent compounds **FL4** and **CTRL1** at a final concentration of 10 µM for 10–20 min, while 9R/VAMP711 seedlings (Geldner et al. 2009) were treated with **FL4**, **CTRL1** and **CTRL2** at a final concentration of 2 µM for 3 h. Plants were subsequently visualized using a confocal microscope (ZEISS LSM 800 and LSM 900). Experimental set up involved 10× – 100× objective.

Results and discussion

Synthesis of the compound library

The planar aromatic ring and a carboxyl group side chain are regarded to be essential for auxin activity; while the amino group of the IAA indole ring is involved in the hydrogen bonding with the amide group of Leu439 in TIR1 receptor (Tan et al. 2007). To ensure selective alkylation of IAA molecule at the α-position, carboxylic acid and amino groups of commercially available indole-3-acetic acid were protected as methyl esters in accordance with the procedure published by Hayashi et al. (Hayashi et al. 2012). The *tert*-butyl (iodoalkyl)carbamates **2a-d** were prepared from aliphatic amino alcohols *via* Boc-protection of amino group, followed by iodination of hydroxyl group with slight changes to the procedure published by Ensch et al. (Ensch and Hesse 2002). Subsequently, α-alkylation of IAA dimethyl ester **1** was investigated (Fig. 1). Synthesis was done with slight changes to the procedure published by Chen et al. (Chen et al. 2013). IAA dimethyl ester **1** was treated with sodium hydride and linkers **2a-d** in dimethylformamide at 0 °C and the mixture was stirred at room temperature for 3 h resulting in **3a-d** in 19–48% yield. Fluorescent labelling with 4-chloro-7-nitrobenzofurazan (NBD) or 5-(dimethylamino)naphthalene-1-sulfonyl (DNS, Dansyl) chloride was performed adopting procedures published by Bieleszová et al. (Bieleszová et al. 2019) and Saura et al. (Saura et al. 2015). Linker-tagged IAA double methyl ester derivatives **3a-d** were treated with trifluoroacetic acid in dichloromethane at room temperature for 30 min, affording free amines. The latter were treated with triethylamine and NBD- or DNS-chloride in acetonitrile at room temperature for 3 h. This led to the formation of NBD- and DNS-labelled IAA dimethyl esters **4a-d** and **4e-f** in 57–77% and 27–31% overall yield, respectively. The full deprotection of fluorescently labelled IAA dimethyl esters **4a-f** was performed similarly to the procedure published by Bieleszová et al. (Bieleszová et al. 2019). Compounds **4a-f** were dissolved in methanol, treated with 1 M lithium hydroxide solution and stirred at 50 °C for 4 h. Subsequent acidification with 1 M potassium hydrogen sulfate solution led to the formation of final products **5a-f** in 28–52% yield, which were designated as **FL1-6**. Detailed procedures for the synthesis of the compounds are available in Supplementary Information.

Determination of biological activity

First of all, the ability of fluorescently labelled auxin derivatives **FL1-6** to affect auxin signalling was evaluated using the *Arabidopsis* transgenic line DR5::GUS (Ulmasov et al. 1997), in which the expression of the β-glucuronidase

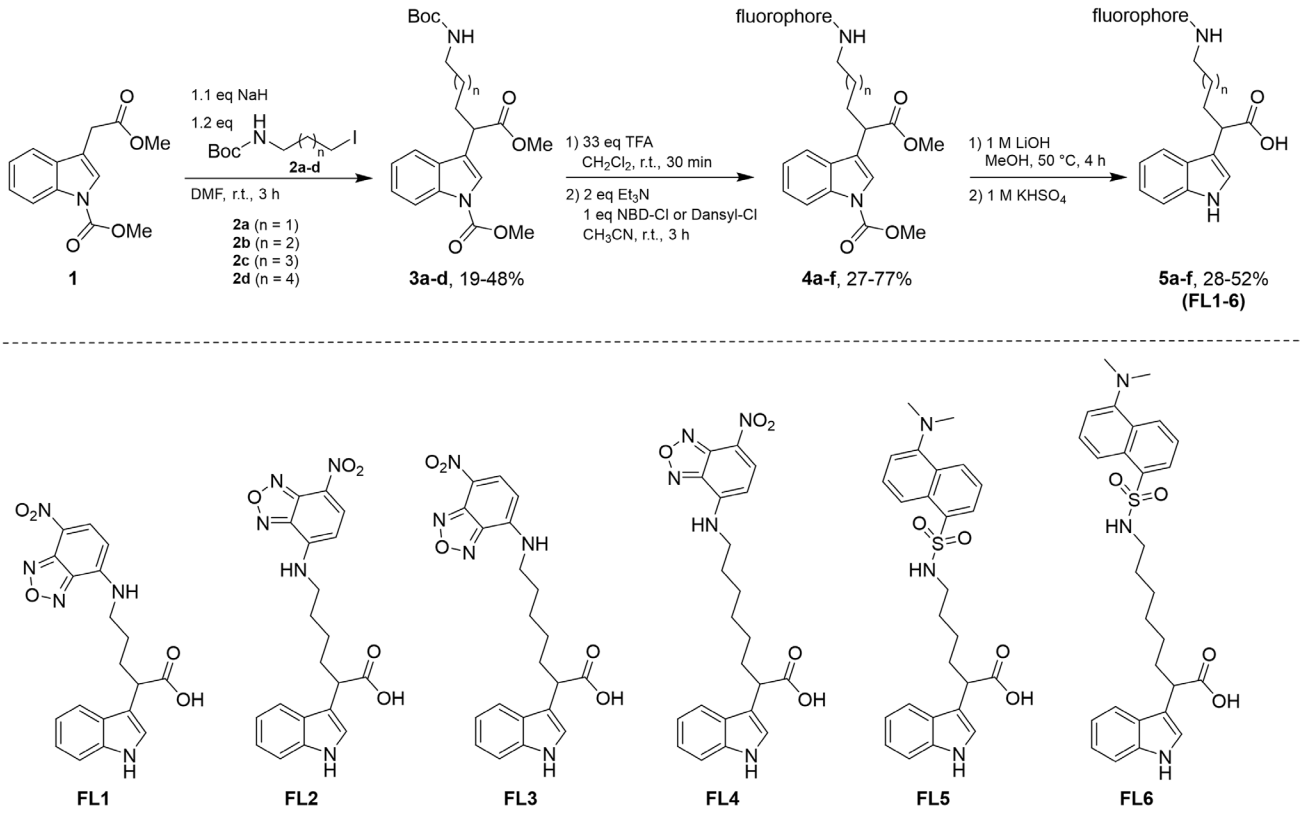

Fig. 1 Synthesis and structures of fluorescently labelled IAA derivatives **5a-f** designated as **FL1-6**

(GUS) reporter gene is controlled by the synthetic auxin-inducible DR5 promoter. Thus, in contrast to 1 µM IAA treatment, where the roots were stained completely, in control plants the blue staining was visible only in the root tip, corresponding to the accumulation of endogenous auxins (Fig. 2a). Compounds **FL1-6**, despite being IAA

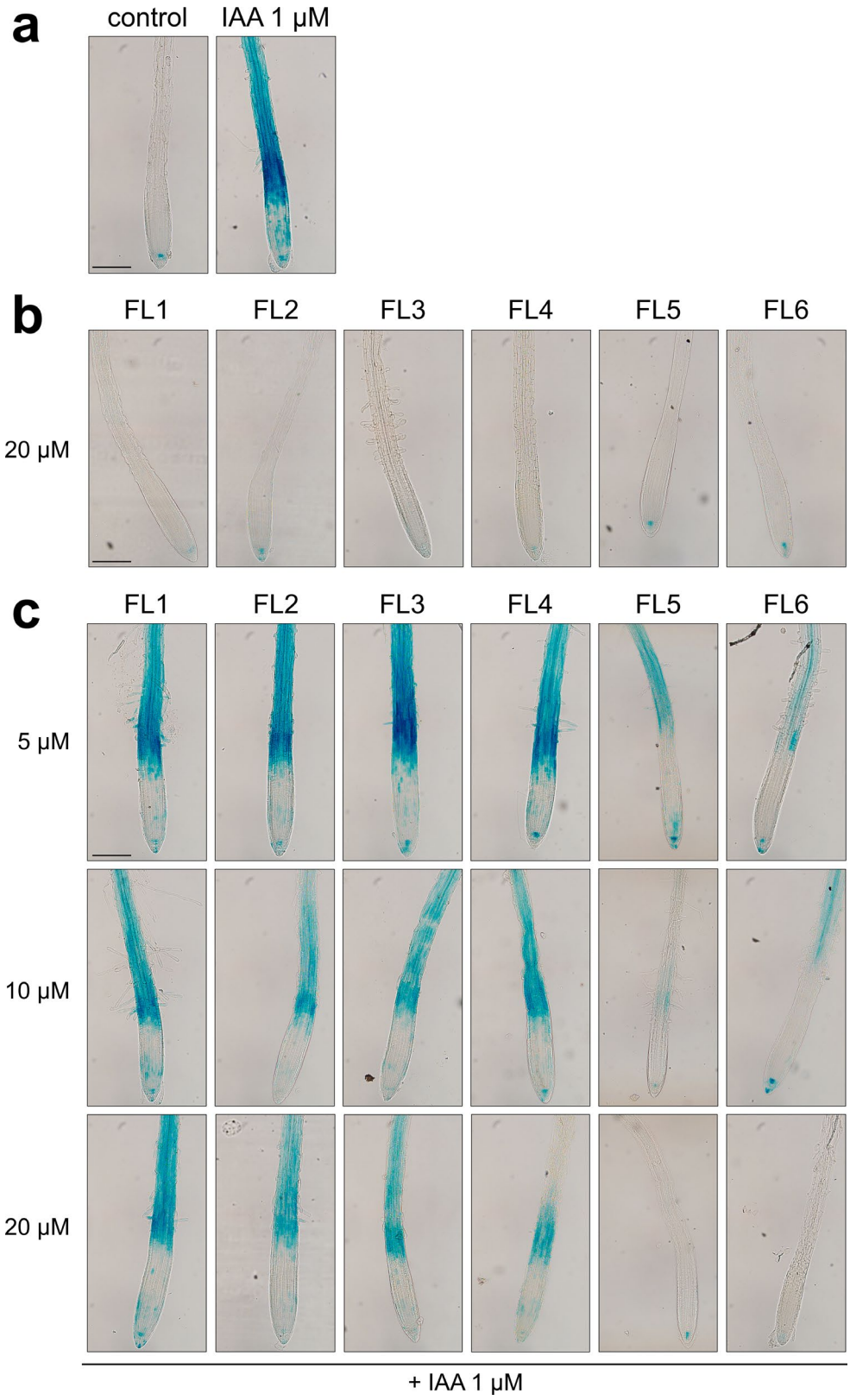

Fig. 2 The effect of compounds **FL1-6** on GUS expression in the DR5::GUS transgenic plants of *Arabidopsis thaliana*. Five-day-old seedlings were treated with 1 µM IAA (**a**), and with compounds 20 µM **FL1-6** for 5 h (**b**). Five-day-old seedlings were co-treated with compounds **FL1-6** at given concentrations (5, 10 and 20 µM) and 1 µM IAA for 5 h (**c**). Figures were chosen as representatives from three independent biological repetitions. Scale bars represents 200 µm

derivatives, did not show auxin activity, manifested by the lack of GUS staining even at 20 µM concentration (Fig. 2b). In contrast, when co-applied with 1 µM IAA (Fig. 2c), some of the fluorescently labelled compounds blocked auxin-induced DR5::GUS expression in a dose-dependent manner, similarly to known anti-auxins (Hayashi et al. 2012). The DNS-labelled compounds **FL5** and **FL6** completely inhibited DR5::GUS expression induced by 1 µM IAA at 20 µM concentration, thus showing the strongest inhibitory effect. Conversely, the longest linker-possessing NBD-labelled compound **FL4** showed weak anti-auxin activity at 20 µM concentration and was not able to completely inhibit effect of 1 µM IAA (Fig. 2c).

Based on the results from DR5::GUS assay, the most active compounds **FL4**, **FL5** and **FL6** were selected for the investigation of their uptake and stability dynamics in vivo by ultra-high performance liquid chromatography coupled with tandem mass spectrometry (UHPLC-MS/MS), to determine the duration over which these compounds can be utilized in *in planta* experiments. Plants were transferred to solid medium treated with 10 µM concentration of **FL4**, **FL5** or **FL6** and subsequently harvested at three time points. After 1 h treatment, all three compounds **FL4**, **FL5** and **FL6** were detected in plants at a similar concentration (Supplementary Figure S1). Compared to **FL5** and **FL6**, for which the concentration within the first 3 h stayed almost unchanged, the concentration of **FL4** after 3 h was decreased approximately 2-fold, indicating its rapid metabolism or degradation. After 6 h the concentration of all three compounds in plants was drastically reduced (Supplementary Figure S1), indicating that the compounds should be primarily used in short term experiments.

Consequently, **FL4**, **FL5** and **FL6** were further examined for their biological activity in short term assays. For this purpose the transgenic line DR5::LUC (Moreno-Risueno et al. 2010) was employed, which possesses a synthetic auxin-responsive promoter DR5 driving the expression of the firefly luciferase enzyme. In this transgenic line, auxin response is determined by the luminescence intensity of luciferase. Thus, to confirm anti-auxin activity of the compounds, we checked whether treatment with the compounds will lead to a decrease in the nuclear auxin response in IAA co-treated DR5::LUC plants (Moreno-Risueno et al. 2010; Fendrych et al. 2018). Similarly to DR5::GUS results, auxin-induced DR5::LUC response was strongly antagonized by DNS-labelled derivatives **FL5** and **FL6**, showing their inhibitory effect on auxin signalling (Fig. 3a). Moreover, treatment of hypocotyl segments prepared from etiolated DR5::LUC

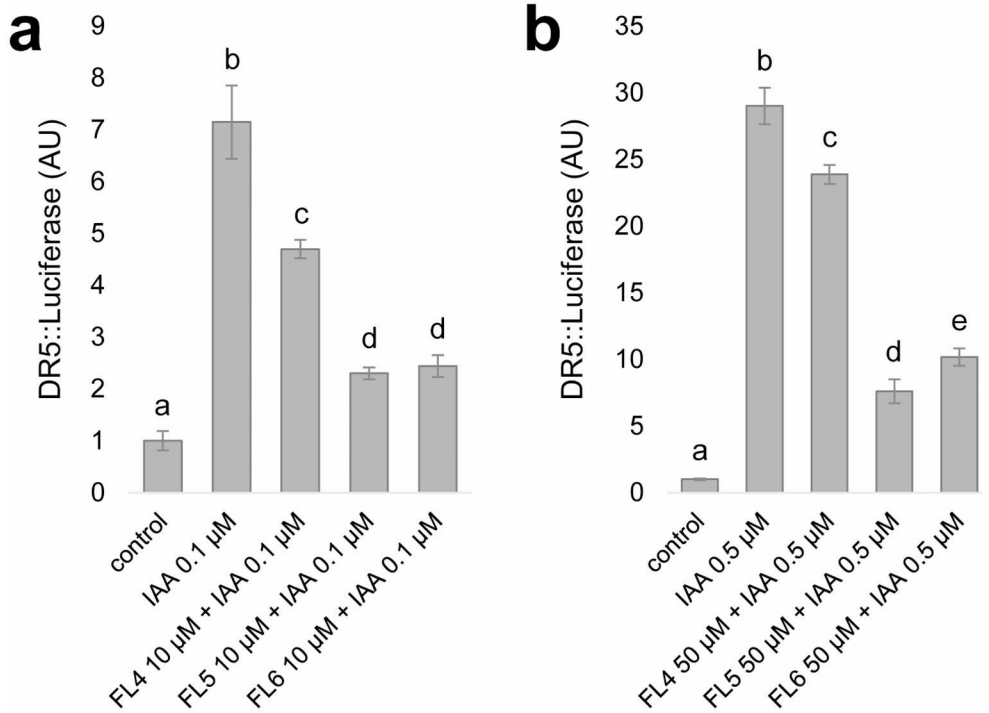

Fig. 3 The effect of compounds **FL4**, **FL5** and **FL6** on luciferase activity in roots and hypocotyl segments of DR5::LUC transgenic plants of *Arabidopsis thaliana*. Five-day-old seedlings were transferred to plates with media containing 0.3% DMSO as a blank control, 0.1 µM IAA as positive control or 10 µM **FL4**, **FL5** and **FL6** with 0.1 µM IAA for 6 h. The luminescence intensity in the roots was quantified (**a**). Hypocotyl segments from three-day-old dark-grown plants were transferred onto a treatment plate with the depletion medium supplemented with 0.3% DMSO as a blank control, 0.5 µM IAA as positive control or compounds **FL4**, **FL5** and **FL6** at final concentration of 50 µM with 0.5 µM IAA for 3 h. The luminescence intensity in the hypocotyls was quantified (**b**). Results are averages from three independent repetitions. Values are means ± S.E. Different letters indicate statistically significant differences between treatments according to Wilcoxon test after Kruskal-Wallis analysis ($P < 0.05$)

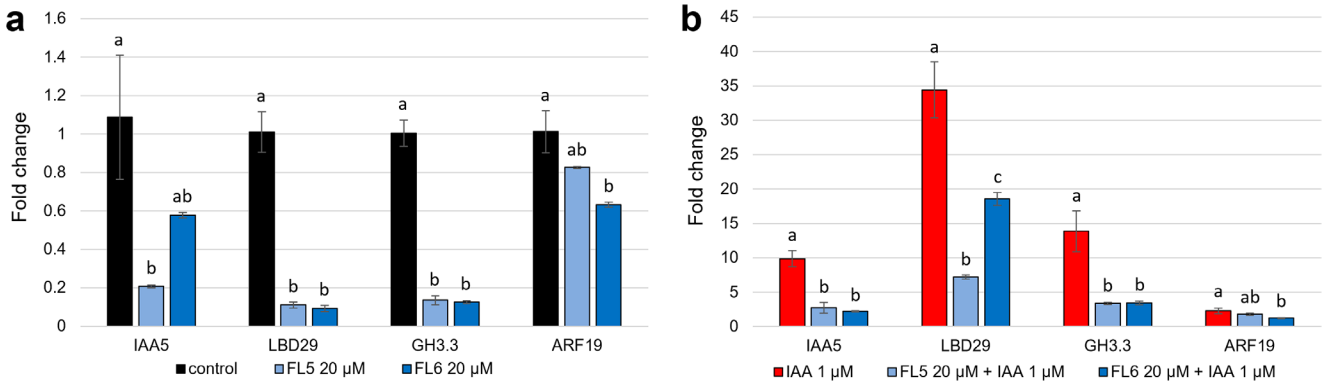

Fig. 4 Transcriptional response of auxin-responsive genes to treatment with compounds **FL5** and **FL6**. Five-day-old seedlings were treated with compounds **FL5** and **FL6** at 20 µM alone (**a**) or in co-treatment with 1 µM IAA (**b**) for 3 h. Transcript levels of four early auxin-responsive genes, *LBD29*, *IAA5*, *GH3.3*, *ARF19* were quantified by real-time PCR and fold change was calculated *via* the comparative cycle threshold (Ct) method and values were normalised based on expression of the *TUB2* gene. Values are means ± S.E. from three biological repetitions. Different letters indicate statistically significant differences between compounds and control (**a**) or between compounds and IAA (**b**), according to Tukey's test after ANOVA ($P < 0.05$)

transgenic plants of *Arabidopsis thaliana* with IAA and DNS-labelled derivatives **FL5** or **FL6** resulted in a significant decrease in luminescence intensity, compared to plants treated with 0.5 µM IAA alone, proving their strong anti-auxin activity also in this tissue (Fig. 3b). The decrease in luminescence intensity in both roots and hypocotyl segments was milder in the case of treatment with **FL4**.

Subsequently, a qPCR analysis of four early auxin-responsive genes, *IAA5*, *LBD29*, *GH3.3* and *ARF19* (Paponov et al. 2008), upon treatment with the most active compounds **FL5** and **FL6** at 20 µM concentration alone or in combination with 1 µM IAA was performed. Compounds **FL5** and **FL6** did not induce the expression of auxin-responsive genes, which further corroborates our initial observation that these compounds do not possess auxin activity (Fig. 4a). In co-treatment with IAA, the compounds suppressed expression of auxin-inducible genes, confirming their anti-auxin activity (Fig. 4b). Moreover, the compounds were also able to inhibit the effect of endogenous auxin-induced gene expression, which was the most prominent for the *LBD29* and *GH3.3* genes (Fig. 4a).

Additionally, the effect of compounds on primary root-growth and elongation of hypocotyl segments was evaluated (Fig. 5, Supplementary Figure S2). Nanomolar IAA concentrations trigger primary root-growth inhibition (Woodward and Bartel 2005) which has been demonstrated to happen in less than 30 s after auxin reaches the root surface (Fendrych et al. 2018). In rapid root-growth assay, DNS-labelled compounds **FL5** and **FL6** were able to partially reverse the auxin-induced primary root-growth inhibition, confirming their anti-auxin activity (Fig. 5a, Supplementary Figure S2a). In contrast, NBD-labelled derivative **FL4** was unable to counteract the effect of auxin.

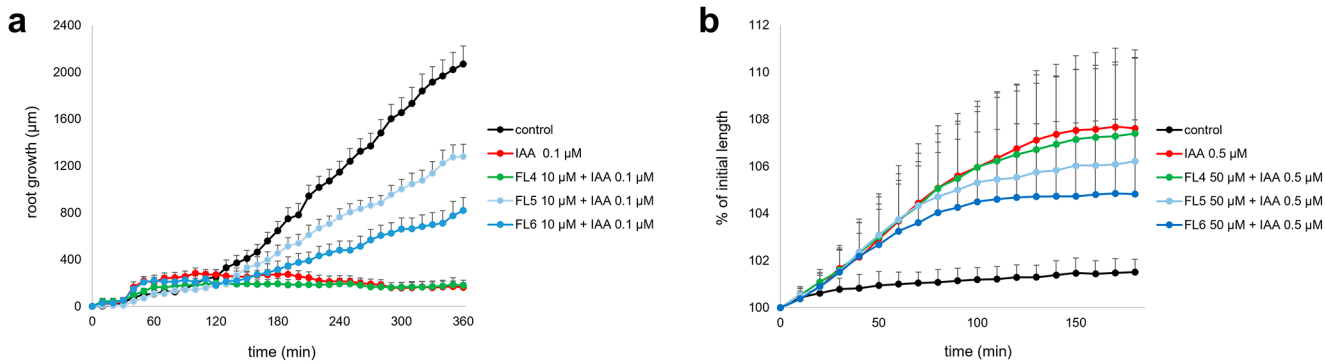

Fig. 5 The effect of compounds **FL4**, **FL5** and **FL6** on primary root growth and elongation of hypocotyl segments in DR5::LUC transgenic plants of *Arabidopsis thaliana*. Five-day-old seedlings were transferred to plates with media containing 0.3% DMSO as a blank control, 0.1 µM IAA as positive control or 10 µM **FL4**, **FL5** and **FL6** with 0.1 µM IAA for 6 h and primary root growth was evaluated (**a**). Hypocotyl segments from three-day-old dark-grown plants were transferred onto a treatment plate with the depletion medium supplemented with 0.3% DMSO as a blank control, 0.5 µM IAA as positive control or 50 µM **FL4**, **FL5** and **FL6** with 0.5 µM IAA for 3 h and elongation of hypocotyl segments was evaluated (**b**). Results are averages from three independent repetitions. Values are means ± S.E.

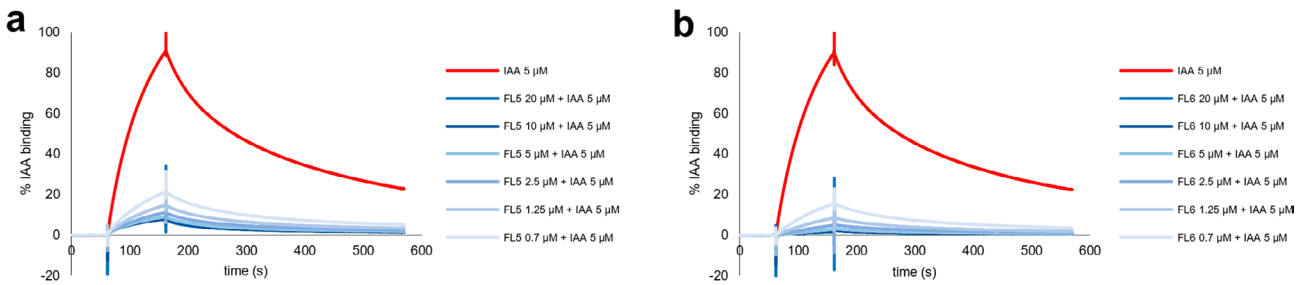

Fig. 6 SPR analysis of the antagonistic effect of compounds **FL5** and **FL6** on auxin-induced interaction between TIR1 protein and IAA7 degron peptide. The sensorgrams show association followed by dissociation in buffer. Results for IAA (5 µM) on TIR1 protein alone (red) and in co-treatment with compounds **FL5** (**a**) and **FL6** (**b**) in a concentration range (0.7, 1.25, 2.5, 5, 10, 20 µM) (shades of blue)

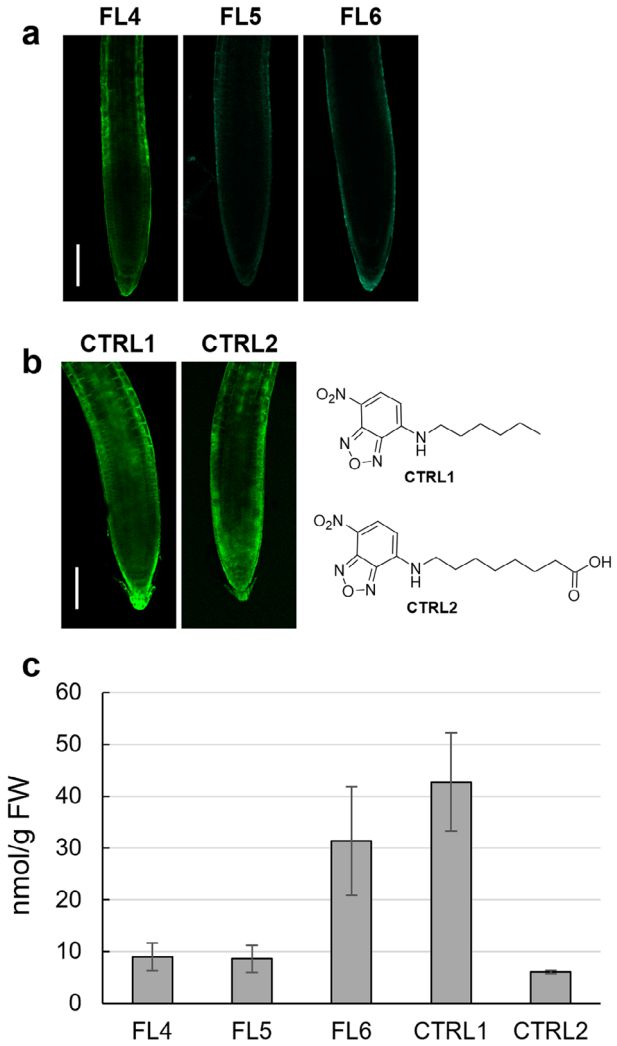

Fig. 7 Uptake of compounds **FL4-6**, **CTRL1** and **CTRL2** in *Arabidopsis thaliana* roots. Five-day-old seedlings were treated with 10 µM **FL4**, **FL5** and **FL6** for 10 min, 10× zoom, scale bar represents 100 µm. (**a**). Five-day-old seedlings were treated with 10 µM **CTRL1** and **CTRL2** for 10 min, 10× zoom, scale bar represents 100 µm; corresponding structures of controls **CTRL1** and **CTRL2** (**b**). Uptake of compounds **FL4-6**, **CTRL1** and **CTRL2** was evaluated in five-day-old *Arabidopsis thaliana* seedlings treated with test compounds at 10 µM concentration and harvested after 30 min (**c**). Results are averages (nmol/g FW) from six biological repetitions. Values are means ± S.D.

Nuclear auxin signalling is believed to be involved in elongation of hypocotyl segments (Fendrych et al. 2016). In etiolated hypocotyls of *Arabidopsis thaliana*, which have been depleted of endogenous auxin by decapitation, compounds **FL5** and, particularly, **FL6** were also able to revert IAA-induced hypocotyl elongation, while **FL4** could not (Fig. 5b, Supplementary Figure S2b).

In vitro determination of anti-auxin activity by SPR binding assay

The capacity of the derivatives to antagonize auxin binding to auxin receptor TIR1 (Dharmasiri et al. 2005a; Kepinski and Leyser 2005) and AUXIN/INDOLE-3-ACETIC ACID7 (IAA7) co-receptor complex (Calderón Villalobos et al. 2012) was studied by SPR analysis (Lee et al. 2014). Similarly, to other anti-auxins (Hayashi et al. 2012; Žukauskaitė et al. 2023), derivatization of the IAA molecule at the α-position resulted in anti-auxin activity of the compounds. In co-treatment with 5 µM IAA, compounds inhibited TIR1 co-receptor assembly with IAA7 degron (Fig. 6) by competing with IAA for its binding site and reducing the signal in a dose dependent manner. Interestingly, DNS-labelled derivatives **FL5** (Fig. 6a) and **FL6** (Fig. 6b) showed stronger anti-auxin activity, outperforming auxinole (Hayashi et al. 2012) (Supplementary Figure S3).

Fluorescence properties and validation of compound uptake *in planta*

To evaluate the suitability of the compounds for microscopy experiments, their fundamental fluorescence properties were evaluated in vitro. As anticipated, in methanol, compound **FL4** had absoption maxima at 467 nm, and emission maxima at 531 nm, resulting in 64 nm Stokes shift typical for NBD-labelled molecules (Lancet and Pecht 1977; Bieleszová et al. 2019). On the other hand, compounds **FL5** and **FL6** had absoption maxima between 331 and 336 nm, and emission maxima at 519–520 nm, resulting in large

Stokes shifts, typical for DNS derivatives (Wei et al. 2023) (Supplementary Figure S4, Supplementary Table S3).

The uptake of compounds **FL4**, **FL5** and **FL6** in *Arabidopsis thaliana* after treatment in liquid medium was evaluated using confocal microscopy and UHPLC-MS/MS (Fig. 7a,c). Due to its superior fluorescence properties, compound **FL4** was the most suitable for confocal experiments. Distribution of **FL4** in *Arabidopsis thaliana* roots was mainly observed in epidermal cells. DNS-labelled compounds **FL5** and **FL6**, which possesed absorption maximas in UV range, could not be properly visualized using the excitation lasers available in our equipment (minimum wavelength of 405 nm), and therefore only low-clarity images could be obtained (Fig. 7a). UHPLC-MS/MS results confirmed the accumulation of compounds **FL4**, **FL5** and **FL6** in plants, indicating that the poor visibility of **FL5** and **FL6** in confocal images is not uptake-related (Fig. 7c). However, compounds **FL5** and **FL6** could probably be used in UV-microscopy experiments, which typically employ microscopes equipped with excitation lasers within the UV spectrum (Maxfield and Wüstner 2012).

Based on the fluorescence measurements in vitro and visualization of compounds in primary roots of *Arabidopsis thaliana*, compound **FL4** was selected to study accumulation patterns *in planta*, alongside of two selected controls **CTRL1** and **CTRL2** (synthesis in Supplementary Information), which are possible degradation products of compound **FL4** (Fig. 7b). The uptake of these control compounds **CTRL1** and **CTRL2** in *Arabidopsis thaliana* after treatment in liquid medium was analogously evaluated using confocal microscopy and UHPLC-MS/MS. From the results, we could see that **CTRL1** accumulated strongly in *Arabidopsis* roots (Fig. 7b,c), which may be caused by its lipophilic nature (Schriever and Lamshoeft 2020). **CTRL2** also showed a uniform accumulation in all root layers, although the uptake was lower than that of **CTRL1** (Fig. 7b,c).

Visualization of subcellular distribution of compound FL4 and its controls

Compound **FL4** and its controls **CTRL1** and **CTRL2** were used to investigate their accumulation patterns at the subcellular level. Both, compound **FL4** and **CTRL1**, displayed strong co-localization with the fluorescent signal of the transgenic marker lines p24δ5-RFP and SYP32-mCherry, revealing their accumulation in endoplasmic reticulum and Golgi apparatus (Fig. 8). The localization of **CTRL1** to both organelles suggests that the auxin part of **FL4** might not be crucial for compound accumulation in endoplasmic reticulum and Golgi apparatus.

To study accumulation in vacuoles, two controls, **CTRL1** and carboxylic acid group bearing **CTRL2**, were used alongside compound **FL4** (Fig. 9). In the case of **FL4**, a co-localization with tonoplast using VAMP711-mCherry marker line could be seen after 3 h (Fig. 9a). Moreover, a partial co-localization with the marker is also visible for carboxylic acid group bearing **CTRL2** (Fig. 9c). On the contrary, **CTRL1** did not show co-localization with the marker (Fig. 9b).

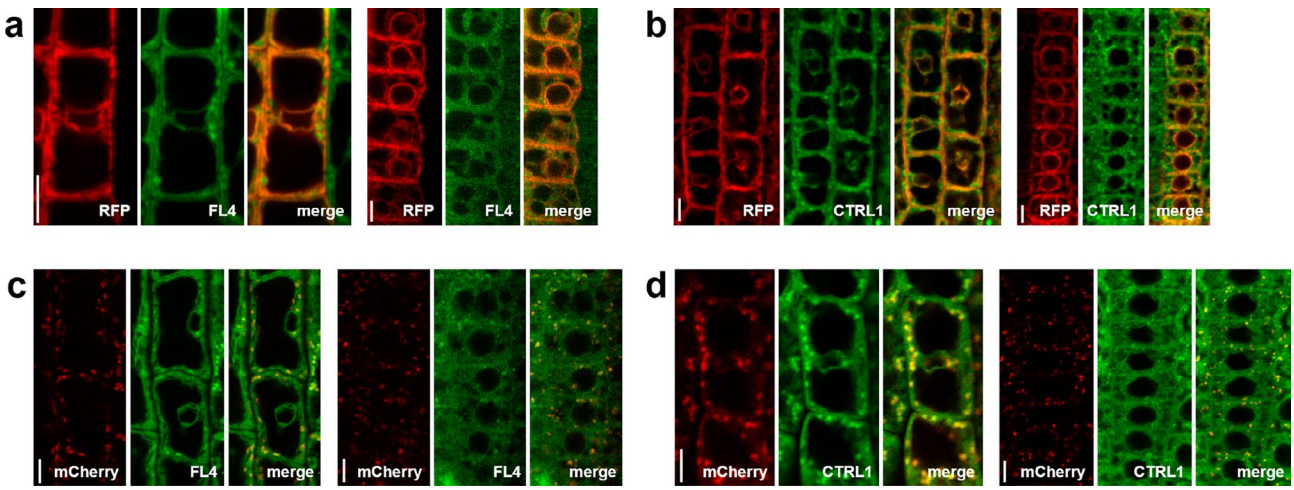

Fig. 8 Uptake of **FL4** and **CTRL1** in epidermal cells of the root meristematic zone of *Arabidopsis thaliana* roots of p24δ5-RFP (**a**,**b**), and SYP32-mCherry (**c**,**d**) lines. Five-day-old seedlings were treated with 10 µM **FL4** (**a**,**c**) and **CTRL1** (**b**,**d**) for 10–20 min. 40× zoom for **CTRL1** or 100× zoom for **FL4**. Scale bars represent 5 µm

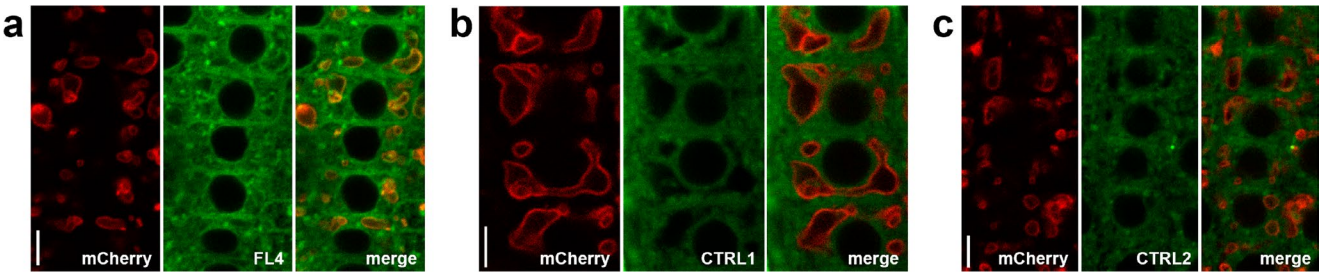

Fig. 9 Uptake of **FL4**, **CTRL1** and **CTRL2** in epidermal cells of the root meristematic zone of *Arabidopsis thaliana* roots of VAMP711-mCherry line. Five-day-old seedlings were treated with **FL4** (**a**), **CTRL1** (**b**), and **CTRL2** (**c**) at 2 µM concentration for 3 h. 40× or 100× zoom. Scale bars represent 5 µm

Conclusions

In this work we have designed and synthesized six new fluorescently labelled IAA derivatives. None of the compounds showcased auxin activity but, on the contrary, acted as anti-auxins at levels of developmental regulation, transcription induction, and binding to receptors.

While NBD-labelled compounds **FL1-4** only possessed weak anti-auxin activity, DNS-labelled compounds **FL5** and **FL6** were able to completely inhibit auxin-induced expression of DR5::GUS transcriptional auxin response reporter. Further testing using another auxin-responsive reporter line, DR5::LUC, revealed stronger anti-auxin activity of **FL5** and **FL6** compounds in roots and hypocotyls in comparison with compound **FL4**. qPCR analysis, performed with the most active compounds **FL5** and **FL6** alone and in co-treatment with IAA, showed decreased expression of early auxin response genes. Anti-auxin activity of compounds was also confirmed by SPR binding assays, where **FL5** and **FL6** showed strong anti-auxin activity, outperforming the established anti-auxin auxinole (Hayashi et al. 2012).

Fluorescence measurements showed that the DNS derivatives are not suitable for most confocal experiments, due to their absorption maxima being around 331–336 nm, which is in the UV part of the spectrum. The compound **FL4**, bearing NBD as a fluorescent label, showed better fluorescent properties and was used for further studies of accumulation patterns *in planta*. Two additional compounds (**CTRL1** and **CTRL2**), which also carried the NBD label in the structures but lacked the auxin molecule, were also prepared to be used as controls. The results from visualization of subcellular localization show that **CTRL1**, despite not having an auxin molecule attached, was able to mimic the accumulation patterns of **FL4**, even at the subcellular level. In the case of the vacuolar marker VAMP711-mCherry, co-localization was visible for compound **FL4** and **CTRL2**, both of which carry a carboxylic acid group in the structure. Due to the relatively strong co-localizations of the **FL4** compound and controls **CTRL1** and **CTRL2**, **FL4** is not suitable for studying auxin accumulation patterns *in planta*. Notably, the strongest anti-auxin activity possessing compounds **FL5** and **FL6** might be used to study mechanism of binding to auxin receptors and for *in planta* manipulations of auxin-regulated processes with potential applications in agriculture.

Supplementary Information The online version contains supplementary material available at https://doi.org/10.1007/s10725-023-01083-0.

Acknowledgements The authors would like to thank Karolína Kubiasová and Iñigo Saiz-Fernández for valuable scientific discussions.

Authors' contributions Conceptualization – AŽ. Methodology – KB, PH, MK, RN, FB, ZG, LF, IK, ON, JF, AŽ. Investigation – KB, PH, MK, RN, AŽ. Formal analysis – KB, PH, MK, RN, FB, JF, AŽ. Visualization – KB, PH, AŽ. Data Curation – KB, MK, RN, ON, AŽ. Resources – AŽ, RN, MS, KD, ON, JF. Writing - Original Draft – KB. Writing - Review & Editing – AŽ, JF. All authors have read and agreed to the published version of the manuscript.

Funding Open access publishing supported by the National Technical Library in Prague. This work was supported by the Palacký University Olomouc Young Researcher Grant Competition (JG_2020_002), by the Internal Grant Agency of Palacký University Olomouc (IGA_PrF_2023_016, IGA_PrF_2023_031), by the Ministry of Education, Youth and Sports of the Czech Republic through the European Regional Development Fund-Project Plants as a tool for sustainable global development (CZ.02.1.01/0.0/0.0/16_019/0000827) and the project Support of mobility at Palacký University Olomouc II. (CZ.02.2.69/0.0/0.0/18_053/0016919). The Biacore T200 SPR instrument was provided by the WISB Research Technology Facility within the School of Life Sciences, University of Warwick.
Open access publishing supported by the National Technical Library in Prague.

Data Availability The data that supports the findings of this study are available from the corresponding authors upon reasonable request.

Declarations

Competing interests On behalf of all authors, the corresponding author states that there is no conflict of interest.

References

Balcerowicz M, Shetty KN, Jones AM (2021) Fluorescent biosensors illuminating plant hormone research. Plant Physiol 187:590–602. https://doi.org/10.1093/plphys/kiab278

Bieleszová K, Pařízková B, Kubeš M et al (2019) New fluorescently labeled auxins exhibit promising anti-auxin activity. N Biotechnol 48:44–52. https://doi.org/10.1016/j.nbt.2018.06.003

Brannon JH, Magde D (1978) Absolute quantum yield determination by thermal blooming. Fluorescein. J Phys Chem 82:705–709. https://doi.org/10.1021/j100495a018

Calderón Villalobos LIA, Lee S, De Oliveira C et al (2012) A combinatorial TIR1/AFB-Aux/IAA co-receptor system for differential sensing of auxin. Nat Chem Biol 8:477–485. https://doi.org/10.1038/nchembio.926

Caumon H, Vernoux T (2023) A matter of time: Auxin signaling dynamics and the regulation of auxin responses during plant development. J Exp Bot erad 132. https://doi.org/10.1093/jxb/erad132

Chen J, Kassenbrock A, Li BX, Xiao X (2013) Discovery of a potent anti-tumor agent through regioselective mono-N-acylation of 7H-pyrrolo[3,2-f]quinazoline-1,3-diamine. Medchemcomm 4:1275–1282. https://doi.org/10.1039/c3md00134b

Dharmasiri N, Dharmasiri S, Estelle M (2005a) The F-box protein TIR1 is an auxin receptor. Nature 435:441–445. https://doi.org/10.1038/nature03543

Dharmasiri N, Dharmasiri S, Weijers D et al (2005b) Plant development is regulated by a family of auxin receptor F box proteins. Dev Cell 9:109–119. https://doi.org/10.1016/j.devcel.2005.05.014

Dindas J, Scherzer S, Roelfsema MRG et al (2018) AUX1-mediated root hair auxin influx governs $SCF^{TIR1/AFB}$-type Ca^{2+} signaling. Nat Commun 9. https://doi.org/10.1038/s41467-018-03582-5

Ensch C, Hesse M (2002) Total syntheses of the spermine alkaloids (-)-(R,R)-hopromine and (±)-homaline. Helv Chim Acta 85:1659–1677. https://doi.org/10.1002/1522-2675(200206)85:6<1659::AID-HLCA1659>3.0.CO;2-D

Fendrych M, Leung J, Friml J (2016) TIR1/AFB-Aux/IAA auxin perception mediates rapid cell wall acidification and growth of Arabidopsis hypocotyls. Elife 5. https://doi.org/10.7554/eLife.19048.001

Fendrych M, Akhmanova M, Merrin J et al (2018) Rapid and reversible root growth inhibition by TIR1 auxin signalling. Nat Plants 4:453–459. https://doi.org/10.1038/s41477-018-0190-1

Friml J (2022) Fourteen stations of auxin. Cold Spring Harb Perspect Biol 14:a039859. https://doi.org/10.1101/cshperspect.a039859

Friml J, Gallei M, Gelová Z et al (2022) ABP1–TMK auxin perception for global phosphorylation and auxin canalization. Nature 609:575–581. https://doi.org/10.1038/s41586-022-05187-x

Geisler M (2018) Seeing is better than believing: visualization of membrane transport in plants. Curr Opin Plant Biol 46:104–112. https://doi.org/10.1016/j.pbi.2018.09.005

Geldner N, Dénervaud-Tendon V, Hyman DL et al (2009) Rapid, combinatorial analysis of membrane compartments in intact plants with a multicolor marker set. Plant J 59:169–178. https://doi.org/10.1111/j.1365-313X.2009.03851.x

Grossmann K (2010) Auxin herbicides: current status of mechanism and mode of action. Pest Manag Sci 66:113–120. https://doi.org/10.1002/ps.1860

Guilfoyle TJ, Hagen G (2007) Auxin response factors. Curr Opin Plant Biol 10:453–460. https://doi.org/10.1016/j.pbi.2007.08.014

Hasegawa J, Sakamoto T, Fujimoto S et al (2018) Auxin decreases chromatin accessibility through the TIR1/AFBs auxin signaling pathway in proliferative cells. Sci Rep 8. https://doi.org/10.1038/s41598-018-25963-y

Hayashi KI, Neve J, Hirose M et al (2012) Rational design of an auxin antagonist of the SCF^{TIR1} auxin receptor complex. ACS Chem Biol 7:590–598. https://doi.org/10.1021/cb200404c

Hemelíková N, Žukauskaitė A, Pospíšil T et al (2021) Caged phytohormones: from chemical inactivation to controlled physiological response. J Agric Food Chem 69:12111–12125. https://doi.org/10.1021/acs.jafc.1c02018

Herud-Sikimić O, Stiel AC, Kolb M et al (2021) A biosensor for the direct visualization of auxin. Nature 592:768–772. https://doi.org/10.1038/s41586-021-03425-2

Jiang K, Asami T (2018) Chemical regulators of plant hormones and their applications in basic research and agriculture. Biosci Biotechnol Biochem 82:1265–1300. https://doi.org/10.1080/09168451.2018.1462693

Kepinski S, Leyser O (2005) The Arabidopsis F-box protein TIR1 is an auxin receptor. Nature 435:446–451. https://doi.org/10.1038/nature03542

Kimura T, Haga K, Shimizu-Mitao Y et al (2018) Asymmetric auxin distribution is not required to establish root phototropism in *Arabidopsis*. Plant Cell Physiol 59:823–835. https://doi.org/10.1093/pcp/pcy018

Lace B, Prandi C (2016) Shaping small bioactive molecules to untangle their biological function: a focus on fluorescent plant hormones. Mol Plant 9:1099–1118. https://doi.org/10.1016/j.molp.2016.06.011

Lancet D, Pecht I (1977) Spectroscopic and immunochemical studies with nitrobenzoxadiazolealanine, a fluorescent dinitrophenyl analog. 16:5150–5157. https://doi.org/10.1021/bi00642a031

Lee S, Sundaram S, Armitage L et al (2014) Defining binding efficiency and specificity of auxins for $SCF^{TIR1/AFB}$-Aux/IAA co-receptor complex formation. ACS Chem Biol 9:673–682. https://doi.org/10.1021/cb400618m

Li L, Krens SFG, Fendrych M, Friml J (2018) Real-time analysis of auxin response, cell wall pH and elongation in *Arabidopsis thaliana* hypocotyls. Bio Protoc 8. https://doi.org/10.21769/bioprotoc.2685

Liang Y, Jiang C, Liu Y et al (2020) Auxin regulates sucrose transport to repress petal abscission in rose (Rosa hybrida). Plant Cell 32:3485–3499. https://doi.org/10.1105/TPC.19.00695

Ma L, Li G, Li S, Jiang S (2020) An improved protocol for whole mount clearing of plant root tip. Chin Bull Bot 55:596–604. https://doi.org/10.11983/CBB20016

Malachowska-Ugarte M, Sperduto C, Ermolovich YV et al (2015) Brassinosteroid-BODIPY conjugates: design, synthesis, and properties. Steroids 102:53–59. https://doi.org/10.1016/j.steroids.2015.07.002

Maxfield FR, Wüstner D (2012) Analysis of cholesterol trafficking with fluorescent probes. Methods Cell Biol 108:367–393. https://doi.org/10.1016/B978-0-12-386487-1.00017-1

Mockaitis K, Estelle M (2008) Auxin receptors and plant development: a new signaling paradigm. Annu Rev Cell Dev Biol 24:55–80. https://doi.org/10.1146/annurev.cellbio.23.090506.123214

Montesinos JC, Sturm S, Langhans M et al (2012) Coupled transport of Arabidopsis p24 proteins at the ER–Golgi interface. J Exp Bot 63:4243–4261. https://doi.org/10.1093/jxb/ers112

Moreno-Risueno MA, Van Norman JM, Moreno A et al (2010) Oscillating gene expression determines competence for periodic Arabidopsis root branching. Science (1979) 329:1306–1311. https://doi.org/10.1126/science.1191937

Okushima Y, Overvoorde PJ, Arima K et al (2005) Functional genomic analysis of the AUXIN RESPONSE FACTOR gene family members in Arabidopsis thaliana: Unique and overlapping functions of ARF7 and ARF19. Plant Cell 17:444–463. https://doi.org/10.1105/tpc.104.028316

Overvoorde PJ, Okushima Y, Alonso JM et al (2005) Functional genomic analysis of the AUXIN/INDOLE-3-ACETIC ACID gene family members in Arabidopsis thaliana. Plant Cell 17:3282–3300. https://doi.org/10.1105/tpc.105.036723

Paponov IA, Paponov M, Teale W et al (2008) Comprehensive transcriptome analysis of auxin responses in *Arabidopsis*. Mol Plant 1:321–337. https://doi.org/10.1093/mp/ssm021

Pařízková B, Pernisová M, Novák O (2017) What has been seen cannot be unseen—detecting auxin in vivo. Int J Mol Sci 18:2736. https://doi.org/10.3390/ijms18122736

Pfaffl MW (2001) A new mathematical model for relative quantification in real-time RT-PCR. Nucleic Acids Res 29:e45. https://doi.org/10.1093/nar/29.9.e45

Prandi C, Ghigo G, Occhiato EG et al (2014) Tailoring fluorescent strigolactones for in vivo investigations: a computational and experimental study. Org Biomol Chem 12:2960–2968. https://doi.org/10.1039/c3ob42592d

Qi L, Kwiatkowski M, Chen H et al (2022) Adenylate cyclase activity of TIR1/AFB auxin receptors in plants. Nature 611:133–138. https://doi.org/10.1038/s41586-022-05369-7

Remington DL, Vision TJ, Guilfoyle TJ, Reed JW (2004) Contrasting modes of diversification in the Aux/IAA and ARF gene families. Plant Physiol 135:1738–1752. https://doi.org/10.1104/pp.104.039669

Rigal A, Ma Q, Robert S (2014) Unraveling plant hormone signaling through the use of small molecules. Front Plant Sci 5. https://doi.org/10.3389/fpls.2014.00373

Santner A, Calderon-Villalobos LIA, Estelle M (2009) Plant hormones are versatile chemical regulators of plant growth. Nat Chem Biol 5:301–307. https://doi.org/10.1038/nchembio.165

Sauer M, Robert S, Kleine-Vehn J (2013) Auxin: simply complicated. J Exp Bot 64:2565–2577. https://doi.org/10.1093/jxb/ert139

Saura AV, Marín MJ, Burguete MI et al (2015) The synthesis of new fluorescent bichromophoric compounds as ratiometric pH probes for intracellular measurements. Org Biomol Chem 13:7736–7749. https://doi.org/10.1039/c5ob00704f

Scheuring D, Löfke C, Krüger F et al (2016) Actin-dependent vacuolar occupancy of the cell determines auxin-induced growth repression. Proc Natl Acad Sci U S A 113:452–457. https://doi.org/10.1073/pnas.1517445113

Schriever C, Lamshoeft M (2020) Lipophilicity matters – a new look at experimental plant uptake data from literature. Sci Total Environ 713. https://doi.org/10.1016/j.scitotenv.2020.136667

Šenkyřík JB, Křivánková T, Kaczorová D, Štefelová N (2023) Investigation of the effect of the auxin antagonist PEO-IAA on cannabinoid gene expression and content in *Cannabis sativa* L. plants under in vitro conditions. Plants 12:1664. https://doi.org/10.3390/plants12081664

Shani E, Weinstain R, Zhang Y et al (2013) Gibberellins accumulate in the elongating endodermal cells of Arabidopsis root. Proc Natl Acad Sci U S A 110:4834–4839. https://doi.org/10.1073/pnas.1300436110

Smýkalová I, Vrbová M, Cvečková M et al (2019) The effects of novel synthetic cytokinin derivatives and endogenous cytokinins on the in vitro growth responses of hemp (Cannabis sativa L.) explants. Plant Cell Tissue Organ Cult 139:381–394. https://doi.org/10.1007/s11240-019-01693-5

Suzuki K, Kobayashi A, Kaneko S et al (2009) Reevaluation of absolute luminescence quantum yields of standard solutions using a spectrometer with an integrating sphere and a back-thinned CCD detector. Phys Chem Chem Phys 11:9850–9860. https://doi.org/10.1039/b912178a

Tamaki H, Reguera M, Abdel-Tawab YM et al (2015) Targeting hormone-related pathways to improve grain yield in rice: a chemical approach. PLoS ONE 10. https://doi.org/10.1371/journal.pone.0131213

Tan X, Calderon-Villalobos LIA, Sharon M et al (2007) Mechanism of auxin perception by the TIR1 ubiquitin ligase. Nature 446:640–645. https://doi.org/10.1038/nature05731

Todd OE, Figueiredo MRA, Morran S et al (2020) Synthetic auxin herbicides: finding the lock and key to weed resistance. Plant Sci 300. https://doi.org/10.1016/j.plantsci.2020.110631

Ulmasov T, Hagen G, Guilfoyle TJ (1997) ARF1, a transcription factor that binds to auxin response elements. Science 276:1865–1868. https://doi.org/10.1126/science.276.5320.1865

Wei P, Xiao L, Gou Y et al (2023) A novel peptide-based relay fluorescent probe with a large Stokes shift for detection of Hg^{2+} and S^{2-} in 100% ueous medium and living cells: visual detection via test strips and smartphone. Spectrochim Acta A Mol Biomol Spectrosc 285. https://doi.org/10.1016/j.saa.2022.121836

Woodward AW, Bartel B (2005) Auxin: Regulation, action, and interaction. Ann Bot 95:707–735. https://doi.org/10.1093/aob/mci083

Žukauskaitė A, Saiz-Fernández I, Bieleszová K et al (2023) New PEO-IAA-inspired anti-auxins: synthesis, biological activity, and possible application in hemp (*Cannabis sativa* L.) micropropagation. https://doi.org/10.1007/s00344-023-11031-x. J Plant Growth Regul

New fluorescent auxin derivatives: anti-auxin activity and accumulation patterns in *Arabidopsis thaliana*

Kristýna Bieleszová,[1] Pavel Hladík,[2] Martin Kubala,[3] Richard Napier,[4] Federica Brunoni,[2] Zuzana Gelová,[5] Lukáš Fiedler,[5] Ivan Kulich,[5] Miroslav Strnad,[2] Karel Doležal,[1,2] Ondřej Novák,[2] Jiří Friml,[5] Asta Žukauskaitė[1*]

[1] Department of Chemical Biology, Faculty of Science, Palacký University, Šlechtitelů 27, CZ-78371 Olomouc, Czech Republic

[2] Laboratory of Growth Regulators, Faculty of Science, Palacký University & Institute of Experimental Botany, The Czech Academy of Sciences, Šlechtitelů 27, CZ-78371 Olomouc, Czech Republic

[3] Department of Experimental Physics, Faculty of Science, Palacký University, 17. listopadu 12, CZ-77146 Olomouc, Czech Republic

[4] School of Life Sciences, University of Warwick, Coventry CV47AL, UK

[5] Institute of Science and Technology Austria, Am Campus 1, 3400 Klosterneuburg, Austria

* Corresponding author.

E-mail address: asta.zukauskaite@upol.cz (A. Žukauskaitė)

Chemicals and general methods

Chemicals were purchased from common commercial suppliers. All reactions were performed in oven-dried glassware. Dimethylformamide was dried over molecular sieves for at least 48 h prior to use. Conversion of starting materials was monitored by thin layer chromatography (TLC) on aluminium plates coated with silica gel 60 F254 (Merck, USA) and the reaction components were visualized by UV light (254 and 365 nm) and staining solutions (vanillin, ninhydrin or potassium permanganate). Reaction mixtures were purified by column chromatography on silica gel (40-63 μm Davisil LC60A, Grace Davison, UK). ^{1}H (500 MHz) and ^{13}C (125 MHz) NMR spectra were recorded in deuterated solvents (acetone-d_6, DMSO-d_6, $CDCl_3$) at room temperature on a Jeol ECA-500 spectrometer equipped with a 5 mm Royal probe. Chemical shifts were calibrated to values of appropriate solvents - ^{1}H 2.50 ppm of residual DMSO-d_6 peak, 7.26 ppm of residual peak of $CDCl_3$, 2.05 ppm of residual peak of acetone-d_6 and ^{13}C 39.50 ppm signal of DMSO-d_6, 77.16 ppm signal of $CDCl_3$, 29.84 and 206.26 ppm signal of acetone-d_6. The LC–MS analyses were performed on an ACQUITY UPLC® H-Class system combined with UPLC® PDA detector and a single-quadrupole mass spectrometer QDa™ (Waters, UK) as described previously (Bieleszová et al. 2019).

Synthesis of compounds

*Synthesis of methyl 3-(2-methoxy-2-oxoethyl)-1H-indole-1-carboxylate **1***

Methyl 3-(2-methoxy-2-oxoethyl)-1*H*-indole-1-carboxylate **1** was prepared from indole-3-acetic acid in accordance with the procedure described by Hayashi *et al.* (Hayashi et al. 2012).

*Synthesis of tert-butyl (iodoalkyl)carbamates **2a-d***

The *tert*-butyl (iodoalkyl)carbamates **2a-d** were prepared from corresponding aliphatic amino alcohols *via* sequential Boc-protection of amino group, followed by iodination of hydroxyl group with slight changes to the procedure described by Ensch *et al.* (Ensch and Hesse 2002).

*General alkylation procedure for the synthesis of methyl 3-((tert-butoxycarbonyl)amino)-1-methoxy-1-oxoalkan-2-yl)-1H-indole-1-carboxylates **3a-d***

Synthesis of methyl 3-(8-((*tert*-butoxycarbonyl)amino)-1-methoxy-1-oxooctan-2-yl)-1*H*-indole-1-carboxylate **3d** is representative. To a solution of methyl 3-(2-methoxy-2-oxoethyl)-1*H*-indole-1-carboxylate **1** (200 mg, 0.81 mmol), dissolved in dry dimethylformamide (2.5

mL), solution of *tert*-butyl (6-iodohexyl)carbamate **2d** (318 mg, 0.97 mmol) in dry dimethylformamide (2.5 mL) was added. Then, sodium hydride (60% in mineral oil) (36 mg, 0.89 mmol) was added at 0 °C and resulting reaction mixture was stirred at room temperature for 3 h under argon. Subsequently, reaction mixture was cooled down to 0 °C, quenched with water (10 mL) and extracted with diethyl ether (3 × 15 mL). The combined organic extracts were washed with brine (2 × 10 mL). Drying with sodium sulfate, filtration and evaporation of the solvent under reduced pressure and purification of the residue by flash chromatography on silica gel (petroleum ether/ethyl acetate 6/1) afforded methyl 3-(8-((*tert*-butoxycarbonyl)amino)-1-methoxy-1-oxooctan-2-yl)-1*H*-indole-1-carboxylate **3d** in 46% yield.

General fluorescent labelling procedure for the synthesis of methyl 3-(1-methoxy-(7-nitrobenzo[c][1,2,5]oxadiazol-4-yl)amino)-1-oxoalkan-2-yl)-1H-indole-1-carboxylates ***4a-d***

Synthesis of methyl 3-(1-methoxy-8-((7-nitrobenzo[*c*][1,2,5]oxadiazol-4-yl)amino)-1-oxooctan-2-yl)-1*H*-indole-1-carboxylate **4d** is representative. Methyl 3-(8-((*tert*-butoxycarbonyl)amino)-1-methoxy-1-oxooctan-2-yl)-1*H*-indole-1-carboxylate **3d** (101 mg, 0.23 mmol) was dissolved in dichloromethane (4 mL) and trifluoroacetic acid (0.58 mL) was added dropwise at 0 °C. Resulting reaction mixture was warmed up to room temperature and stirred for 30 min. Subsequently, reaction mixture was cooled down to 0 °C, quenched by slow addition of aqueous saturated sodium bicarbonate solution until pH = 7 and extracted with ethyl acetate (3 × 10 mL). The combined organic extracts were washed with brine (2 × 5 mL). Drying with sodium sulfate, filtration and evaporation of the solvent under reduced pressure afforded crude methyl 3-(8-amino-1-methoxy-1-oxooctan-2-yl)-1*H*-indole-1-carboxylate, which was used without further purification. Crude methyl 3-(8-amino-1-methoxy-1-oxooctan-2-yl)-1*H*-indole-1-carboxylate (78 mg, 0.23 mmol) was dissolved in acetonitrile (5 mL) and cooled down to 0 °C. To the resulting solution triethylamine (0.06 mL, 0.46 mmol) was added dropwise, followed by addition of 4-chloro-7-nitrobenzofurazan (NBD-Cl) in small portions (45 mg, 0.23 mmol). The reaction mixture was stirred at room temperature for 3 h. Subsequently, reaction mixture was cooled down to 0 °C, quenched with saturated ammonium chloride solution (10 mL) and extracted with ethyl acetate (3 × 20 mL). The combined organic extracts were washed with brine (2 × 10 mL). Drying with sodium sulfate, filtration, evaporation of the solvent under reduced pressure and purification of the residue by flash chromatography on silica gel (dichloromethane/acetone 50/1) afforded methyl 3-(1-methoxy-8-((7-

nitrobenzo[*c*][1,2,5]oxadiazol-4-yl)amino)-1-oxooctan-2-yl)-1*H*-indole-1-carboxylate **4d** in 77% yield.

General fluorescent labelling procedure for the synthesis of methyl 3-(1-methoxy-(3-(5-(dimethylamino)naphthalene)-1-sulfonamido))-1-oxoalkan-2-yl)-1H-indole-1-carboxylates ***4e-f***

Synthesis of methyl 3-(8-((5-(dimethylamino)naphthalene)-1-sulfonamido)-1-methoxy-1-oxooctan-2-yl)-1*H*-indole-1-carboxylate **4f** is representative. 3-(8-((*tert*-Butoxycarbonyl)amino)-1-methoxy-1-oxooctan-2-yl)-1*H*-indole-1-carboxylate **3f** (200 mg, 0.45 mmol) was dissolved in dichloromethane (8 mL) and trifluoroacetic acid (1.13 mL) was added dropwise at 0 °C. Resulting reaction mixture was warmed up to room temperature. After 30 minutes, reaction mixture was cooled down to 0 °C, quenched by slow addition of aqueous saturated sodium bicarbonate solution until pH = 7 and extracted with ethyl acetate (3 × 20 mL). The combined organic extracts were washed with brine (2 × 5 mL). Drying with sodium sulfate, filtration and evaporation of the solvent under reduced pressure afforded crude methyl 3-(8-amino-1-methoxy-1-oxooctan-2-yl)-1*H*-indole-1-carboxylate, which was dissolved in acetonitrile (10 mL) and cooled down to 0 °C. To the resulting solution triethylamine (0.13 mL, 0.90 mmol) was added dropwise, followed by addition of 5-(dimethylamino)naphthalene-1-sulfonyl chloride (DNS-Cl) in small portions (120 mg, 0.45 mmol). The reaction mixture was stirred at room temperature for 3 h. Subsequently, reaction mixture was cooled down to 0 °C, quenched with saturated ammonium chloride solution (20 mL) and extracted with ethyl acetate (3 × 30 mL). The combined organic extracts were washed with brine (2 × 20 mL). Drying with sodium sulfate, filtration, evaporation of the solvent under the reduced pressure and purification of the residue by flash chromatography on silica gel (dichloromethane/acetone 50/1) afforded methyl 3-(8-((5-(dimethylamino)naphthalene)-1-sulfonamido)-1-methoxy-1-oxooctan-2-yl)-1*H*-indole-1-carboxylate **4f** in 31% yield.

General hydrolysis procedure for the synthesis of 2-(1H-indol-3-yl)-(7-nitrobenzo[c][1,2,5]oxadiazol-4-yl)amino)alkanoic acids ***5a-d (FL1-4)***

Synthesis of 2-(1*H*-Indol-3-yl)-8-((7-nitrobenzo[*c*][1,2,5]oxadiazol-4-yl)amino)octanoic acid **5d** (**FL4**) is representative. Methyl 3-(1-methoxy-8-((7-nitrobenzo[*c*][1,2,5]oxadiazol-4-yl)amino)-1-oxooctan-2-yl)-1*H*-indole-1-carboxylate **4d** (148 mg, 0.29 mmol) was dissolved in methanol (12 mL) and 1M lithium hydroxide solution (3 mL) was added at 0 °C. The reaction mixture was warmed up to 50 °C and stirred for 4 h. Subsequently, the reaction mixture was

cooled down to 0 °C, acidified with 1M potassium bisulfate solution to pH = 6 and extracted with ethyl acetate (3 × 20 mL). The combined organic extracts were washed with brine (2 × 10 mL). Drying with sodium sulfate, filtration and evaporation of the solvent under reduced pressure and the purification of the residue by flash chromatography on silica gel (dichloromethane/acetone 50/1), afforded 2-(1*H*-indol-3-yl)-8-((7-nitrobenzo[*c*][1,2,5]oxadiazol-4-yl)amino)octanoic acid **5d** (**FL4**) in 36% yield.

*General hydrolysis procedure for the synthesis of 2-(1H-indol-3-yl)-(5-(dimethylamino)naphthalene)-1-sulfonamido)alkanoic acids **5e-f (FL5-6)***

Synthesis of 8-((5-(dimethylamino)naphthalene)-1-sulfonamido)-2-(1*H*-indol-3-yl)octanoic acid **5f** (**FL6**) is representative. Methyl 3-(8-((5-(dimethylamino)naphthalene)-1-sulfonamido)-1-methoxy-1-oxooctan-2-yl)-1*H*-indole-1-carboxylate **4f** (61 mg, 0.11 mmol) was dissolved in methanol (5 mL) and 1M lithium hydroxide solution (1.1 mL) was added at 0 °C. The reaction mixture was warmed up to 50 °C and stirred for 4 h. Then, the reaction mixture was cooled down to 0 °C and acidified with 1M potassium bisulfate solution to pH = 6. The resulting reaction mixture was extracted with ethyl acetate (3 × 20 mL). The combined organic extracts were washed with brine (2 × 10 mL). Drying with sodium sulfate, filtration and evaporation of the solvent under reduced pressure and the purification of the residue by flash chromatography on silica gel (ethyl acetate/methanol 10/1), afforded 8-((5-(dimethylamino)naphthalene)-1-sulfonamido)-2-(1*H*-indol-3-yl)octanoic acid **5f** (**FL6**) in 43% yield.

*Synthesis of N-hexyl-7-nitrobenzo[c][1,2,5]oxadiazol-4-amine **CTRL1***

Hexan-1-amine (0.13 mL, 0.99 mmol) was dissolved in acetonitrile (16 mL) and cooled down to 0 °C. To the resulting solution triethylamine (0.14 mL, 1.98 mmol) was added dropwise, followed by addition of 4-chloro-7-nitrobenzofurazan in small portions (197 mg, 0.99 mmol). The reaction mixture was stirred at room temperature for 3 h. Subsequently, reaction mixture was cooled down to 0 °C, quenched with saturated ammonium chloride solution (20 mL), extracted with ethyl acetate (3 × 30 mL) and the combined organic extracts were washed with brine (2 × 20 mL). Drying with sodium sulfate, filtration, evaporation of the solvent under the reduced pressure and purification of the residue by flash chromatography on silica gel (petroleum ether/ethyl acetate 3/2) afforded pure compound in 13% yield.

*Synthesis of 8-((7-nitrobenzo[c][1,2,5]oxadiazol-4-yl)amino)octanoic acid **CTRL2***

8-Aminooctanoic acid (100 mg, 0.63 mmol) was dissolved in ethanol (2 mL) and sodium bicarbonate (211 mg, 2.51 mmol) was added. Reaction mixture was stirred in pressure tube at 70 °C for 30 minutes. Subsequently, reaction mixture was cooled down, 4-chloro-7-nitrobenzofurazan (75 mg, 0.38 mmol) was added and stirring was continued at room temperature for 2 h. Subsequently, the reaction mixture was cooled down to 0 °C and acidified with 1 M potassium bisulfate solution to pH = 6. The resulting mixture was extracted with ethyl acetate (3 × 20 mL). The combined organic extracts were washed with brine (2 × 10 mL). Drying with sodium sulfate, filtration and evaporation of the solvent under reduced pressure and the purification of the residue by flash chromatography on silica gel (ethyl acetate/methanol 25/1), afforded pure compound in 12% yield.

*Spectral data of compounds **3a-d**, **4a-f**, **FL1-6** and **CTRL1-2***

Methyl 3-(5-((*tert*-butoxycarbonyl)amino)-1-methoxy-1-oxopentan-2-yl)-1*H*-indole-1-carboxylate **3a**

Colourless oil, yield 44%, R_f = 0.23 (petroleum ether/ethyl acetate 4/1). ^{1}H NMR (500 MHz, $CDCl_3$): δ 1.42 (9H, s, $(CH_3)_3$), 1.52 (2H, p, *J* = 7.4 Hz, CH_2), 1.88-1.97 (1H, m, CH_αH$_\beta$), 2.10-2.17 (1H, m, CH$_\alpha$*H$_\beta$*), 3.00-3.20 (2H, m, CH_2), 3.67 (3H, s, OCH_3), 3.83 (1H, t, *J* = 7.5 Hz, CH), 4.02 (3H, s, OCH_3), 4.40-4.63 (1H, br s, NH), 7.23-7.27 (1H, m, CH), 7.34 (1H, t, *J* = 7.8 Hz, CH), 7.56 (1H, s, CH), 7.61 (1H, d, *J* = 7.9, CH), 8.14-8.21 (1H, br s, CH). ^{13}C NMR (125 MHz, $CDCl_3$): δ 28.1 (CH_2), 28.4 ($(CH_3)_3$), 29.3 (CH_2), 40.1 (CH_2), 42.2 (CH), 52.2 (OCH_3), 53.8 (OCH_3), 79.1 (C), 115.3 (CH), 119.0 (C), 119.4 (CH), 123.0 (CH), 123.2 (CH), 124.9 (CH), 129.3 (C), 135.6 (C), 151.3 (C), 156.0 (C), 173.9 (C). MS (ES, pos. mode): *m/z* (%): 305.19 (M + H^+ - Boc, 100).

Methyl 3-(6-((*tert*-butoxycarbonyl)amino)-1-methoxy-1-oxohexan-2-yl)-1*H*-indole-1-carboxylate **3b**

Colourless oil, yield 19%, R_f = 0.30 (petroleum ether/ethyl acetate 4/1). ^{1}H NMR (500 MHz, $CDCl_3$): δ 1.32-1.45 (11H, m, CH_2, $(CH_3)_3$), 1.51 (2H, p, *J* = 7.4 Hz, CH_2), 1.88-1.97 (1H, m, CH_αH$_\beta$), 2.09-2.18 (1H, m, CH$_\alpha$*H$_\beta$*), 3.05-3.12 (2H, m, CH_2), 3.68 (3H, s, OCH_3), 3.80 (1H, t, *J* = 7.6 Hz, CH), 4.03 (3H, s, OCH_3), 4.40-4.56 (1H, br s, NH), 7.24-7.28 (1H, m, CH), 7.32-7.37 (1H, m, CH), 7.55 (1H, s, CH), 7.60 (1H, d, *J* = 7.6 Hz, CH), 8.18 (1H, s, CH). ^{13}C NMR (125 MHz, $CDCl_3$): δ 25.0 (CH_2), 28.5 ($(CH_3)_3$), 30.0 (CH_2), 32.0 (CH_2), 40.4 (CH_2), 42.7 (CH), 52.3 (OCH_3), 53.9 (OCH_3), 79.1 (C), 115.3 (CH) 119.3 (C), 119.5 (CH), 123.1 (2 × CH), 125.0

(CH), 129.5 (C), 135.6 (C), 151.4 (C), 156.0 (C), 174.1 (C). MS (ES, pos. mode): *m/z* (%): 319.26 ($M + H^+$ - Boc, 100).

Methyl 3-(7-((*tert*-butoxycarbonyl)amino)-1-methoxy-1-oxoheptan-2-yl)-1*H*-indole-1-carboxylate **3c**

Colourless oil, yield 48%, R_f = 0.20 (petroleum ether/ethyl acetate 4/1). ^{1}H NMR (500 MHz, $CDCl_3$): δ 1.31-1.37 (4H, m, 2 × CH_2), 1.40-1.48 (11H, m, CH_2, $(CH_3)_3$), 1.85-1.94 (1H, m, CH_αH$_\beta$), 2.07-2.17 (1H, m, CH$_\alpha$$H_\beta$), 3.07 (2H, t, *J* = 7.0 Hz, CH_2), 3.67 (3H, s, OCH_3), 3.79 (1H, t, *J* = 7.6 Hz, CH), 4.02 (3H, s, OCH_3), 4.38-4.64 (1H, br s, NH), 7.23-7.28 (1H, m, CH), 7.34 (1H, t, *J* = 7.8 Hz, CH), 7.55 (1H, s, CH), 7.60 (1H, d, *J* = 7.9 Hz, CH), 8.17 (1H, s, CH). ^{13}C NMR (125 MHz, $CDCl_3$): δ 26.6 (CH_2), 27.4 (CH_2), 28.5 ($(CH_3)_3$), 30.0 (CH_2), 32.2 (CH_2), 40.6 (CH_2), 42.6 (CH), 52.2 (OCH_3), 53.9 (OCH_3), 79.2 (C), 115.4 (CH), 119.41 (C), 119.43 (CH), 123.1 (2 × CH), 124.9 (CH), 129.5 (C), 135.6 (C), 151.4 (C), 156.1 (C), 174.2 (C). MS (ES, pos. mode): *m/z* (%): 333.26 ($M + H^+$ - Boc, 100).

Methyl 3-(8-((*tert*-butoxycarbonyl)amino)-1-methoxy-1-oxooctan-2-yl)-1*H*-indole-1-carboxylate **3d**

Previously described by Hayashi *et al.* (Hayashi et al. 2012). Obtained spectroscopic data matches published data. Colourless oil, yield 46%, R_f = 0.19 (petroleum ether/ethyl acetate 4/1). MS (ES, pos. mode): *m/z* (%): 347.26 ($M + H^+$ - Boc, 100).

Methyl 3-(1-methoxy-5-((7-nitrobenzo[*c*][1,2,5]oxadiazol-4-yl)amino)-1-oxopentan-2-yl)-1*H*-indole-1-carboxylate **4a**

Red oil, yield 57%, R_f = 0.56 (petroleum ether/ethyl acetate 1/1). ^{1}H NMR (500 MHz, $CDCl_3$): δ 1.82-1.89 (2H, m, CH_2), 2.06-2.15 (1H, m, CH_αH$_\beta$), 2.26-2.35 (1H, m, CH$_\alpha$$H_\beta$), 3.47-3.53 (2H, m, CH_2), 3.69 (3H, s, OCH_3), 3.88 (1H, t, *J* = 7.5 Hz, CH), 4.02 (3H, s, OCH_3), 6.05 (1H, d, *J* = 8.6 Hz, CH), 6.53-6.60 (1H, br s, NH), 7.22 (1H, t, *J* = 7.6 Hz, CH), 7.32 (1H, t, *J* = 7.8 Hz, CH), 7.54-7.58 (2H, m, 2 × CH), 8.12 (1H, s, CH), 8.39 (1H, d, *J* = 8.6 Hz, CH). ^{13}C NMR (125 MHz, $CDCl_3$): δ 26.3 (CH_2), 29.1 (CH_2), 42.2 (CH), 43.7 (CH_2), 52.5 (OCH_3), 54.0 (OCH_3), 98.7 (CH), 115.4 (CH), 118.5 (C), 119.2 (CH), 123.2 (CH), 123.4 (CH), 123.7 (C), 125.1 (CH), 129.1 (C), 135.5 (C), 136.6 (CH), 143.85 (C), 143.94 (C), 144.2 (C), 151.3 (C), 173.7 (C). MS (ES, pos. mode): *m/z* (%): 468.24 ($M + H^+$, 100).

Methyl 3-(1-methoxy-6-((7-nitrobenzo[*c*][1,2,5]oxadiazol-4-yl)amino)-1-oxohexan-2-yl)-1*H*-indole-1-carboxylate **4b**

Red oil, yield 61%, R_f = 0.66 (petroleum ether/ethyl acetate 1/1). ^{1}H NMR (500 MHz, $CDCl_3$): δ 1.48-1.56 (2H, m, CH_2), 1.84 (2H, p, *J* = 7.3 Hz, CH_2), 1.96-2.06 (1H, m, CH_αH$_\beta$), 2.17-2.28 (1H, m, CH$_\alpha$$H_\beta$), 3.43-3.51 (2H, m, CH_2), 3.68 (3H, s, OCH_3), 3.84 (1H, t, *J* = 7.6 Hz, CH), 4.03 (3H, s, OCH_3), 6.10 (1H, d, *J* = 8.6 Hz, CH), 6.25-6.34 (1H, br s, NH), 7.24 (1H, t, *J* = 7.6 Hz, CH), 7.33 (1H, t, *J* = 7.8 Hz, CH), 7.54-7.60 (2H, m, 2 × CH), 8.14 (1H, s, CH), 8.44 (1H, d, *J* = 10.1 Hz, CH). ^{13}C NMR (125 MHz, $CDCl_3$): δ 25.0 (CH_2), 28.2 (CH_2), 31.5 (CH_2), 42.5 (CH), 43.7 (CH_2), 52.4 (OCH_3), 54.0 (OCH_3), 98.7 (CH), 115.5 (CH), 118.8 (C), 119.3 (CH), 123.2 (CH) 123.3 (CH), 124.1 (C), 125.1 (CH), 129.3 (C), 135.6 (C), 136.6 (CH), 143.8 (C), 144.0 (C), 144.3 (C), 151.4 (C), 174.0 (C). MS (ES, pos. mode): *m/z* (%): 482.24 (M + H^+, 100).

Methyl 3-(1-methoxy-7-((7-nitrobenzo[*c*][1,2,5]oxadiazol-4-yl)amino)-1-oxoheptan-2-yl)-1*H*-indole-1-carboxylate **4c**

Red oil, yield 71%, R_f = 0.68 (petroleum ether/ethyl acetate 1/1). ^{1}H NMR (500 MHz, $CDCl_3$): δ 1.39-1.46 (2H, m, CH_2), 1.47-1.55 (2H, m, CH_2), 1.80 (2H, p, *J* = 7.3 Hz, CH_2), 1.90-1.99 (1H, m, CH_αH$_\beta$), 2.12-2.21 (1H, m, CH$_\alpha$$H_\beta$), 3.41-3.49 (2H, m, CH_2), 3.68 (3H, s, OCH_3), 3.81 (1H, t, *J* = 7.0 Hz, CH), 4.02 (3H, s, OCH_3), 6.11 (1H, d, *J* = 8.6 Hz, CH), 6.30-6.43 (1H, br s, NH), 7.22-7.25 (1H, m, CH), 7.33 (1H, t, *J* = 7.6 Hz, CH), 7.55 (1H, s, CH), 7.59 (1H, d, *J* = 7.6, CH), 8.15 (1H, s, CH), 8.43 (1H, d, *J* = 8.6 Hz, CH). ^{13}C NMR (125 MHz, $CDCl_3$): δ 26.7 (CH_2), 27.3 (CH_2), 28.3 (CH_2), 31.9 (CH_2), 42.6 (CH), 43.9 (CH_2), 52.4 (OCH_3), 54.0 (OCH_3), 98.7 (CH), 115.4 (CH), 119.1 (C), 119.4 (CH), 123.1 (CH), 123.2 (CH), 123.9 (C), 125.0 (CH), 129.4 (C), 135.5 (C), 136.7 (CH), 144.0 (C), 144.1 (C), 144.3 (C), 151.4 (C), 174.1 (C). MS (ES, pos. mode): *m/z* (%): 496.24 (M + H^+, 100).

Methyl 3-(1-methoxy-8-((7-nitrobenzo[*c*][1,2,5]oxadiazol-4-yl)amino)-1-oxooctan-2-yl)-1*H*-indole-1-carboxylate **4d**

Red oil, yield 77%, R_f = 0.68 (petroleum ether/ethyl acetate 1/1). ^{1}H NMR (500 MHz, $CDCl_3$): δ 1.32-1.49 (6H, m, 3 × CH_2), 1.77 (2H, p, *J* = 7.2 Hz, CH_2), 1.87-1.96 (1H, m, CH_αH$_\beta$), 2.09-2.17 (1H, m, CH$_\alpha$$H_\beta$), 3.40-3.49 (2H, m, CH_2), 3.67 (3H, s, OCH_3), 3.80 (1H, t, *J* = 7.5 Hz, CH), 4.01 (3H, s, OCH_3), 6.11 (1H, d, *J* = 8.6 Hz, CH), 6.45-6.53 (1H, br s, NH), 7.23 (1H, t, *J* = 7.6 Hz, CH), 7.31 (1H, t, *J* = 7.8 Hz, CH), 7.54 (1H, s, CH), 7.58 (1H, d, *J* = 7.9, CH), 8.13 (1H, s, CH), 8.43 (1H, d, *J* = 8.6 Hz, CH). ^{13}C NMR (125 MHz, $CDCl_3$): δ 26.7 (CH_2), 27.5

(CH_2), 28.4 (CH_2), 29.0 (CH_2), 32.0 (CH_2), 42.6 (CH), 44.0 (CH_2), 52.3 (OCH_3), 54.0 (OCH_3), 98.6 (CH), 115.3 (CH), 119.3 (C), 119.4 (CH), 123.0 (CH), 123.1 (CH), 123.6 (C), 124.9 (CH), 129.5 (C), 135.5 (C), 136.7 (CH), 143.9 (C), 144.1 (C), 144.3 (C), 151.4 (C), 174.2 (C). MS (ES, pos. mode): *m/z* (%): 510.32 ($M + H^+$, 100).

Methyl 3-(6-((5-(dimethylamino)naphthalene)-1-sulfonamido)-1-methoxy-1-oxohexan-2-yl)-1*H*-indole-1-carboxylate **4e**

Light blue oil, yield 27%, R_f = 0.68 (petroleum ether/ethyl acetate 1/1). ^{1}H NMR (500 MHz, DMSO-d_6): δ 1.05-1.13 (2H, m, CH_2), 1.23-1.33 (2H, m, CH_2), 1.56-1.65 (1H, m, CH_αH$_\beta$), 1.74-1.83 (1H, m, CH$_\alpha H_\beta$), 2.73 (2H, q, *J* = 6.4 Hz, CH_2), 2.79 (6H, s, $(CH_3)_2$), 3.56 (3H, s, CH_3), 3.68 (1H, t, *J* = 7.6 Hz, CH), 3.98 (3H, s, CH_3), 7.21-7.28 (2H, m, 2 × CH), 7.35 (1H, t, *J* = 7.3 Hz, CH), 7.52-7.61 (4H, m, 4 × CH), 7.88 (1H, t, *J* = 5.7 Hz, NH), 8.05-8.11 (2H, m, 2 × CH), 8.27 (1H, d, *J* = 8.9 Hz, CH), 8.43 (1H, d, *J* = 8.6 Hz, CH). ^{13}C NMR (125 MHz, DMSO-d_6): δ 24.0 (CH_2), 28.7 (CH_2), 30.9 (CH_2), 41.5 (CH), 42.1 (CH_2), 45.1 (2 × CH_3), 51.9 (CH_3), 54.2 (CH_3), 114.8 (CH), 115.1 (CH), 118.8 (C), 119.2 (CH), 119.6 (CH), 123.0 (CH), 123.1 (CH), 123.6 (CH), 124.8 (CH), 127.8 (CH), 128.3 (CH), 128.9 (C), 129.0 (C), 129.1 (C), 129.4 (CH), 134.8 (C), 136.1 (C), 150.7 (C), 151.3 (C), 173.4 (C). MS (ES, pos. mode): *m/z* (%): 552.42 ($M + H^+$, 100).

Methyl 3-(8-((5-(dimethylamino)naphthalene)-1-sulfonamido)-1-methoxy-1-oxooctan-2-yl)-1*H*-indole-1-carboxylate **4f**

Light blue oil, yield 31%, R_f = 0.75 (petroleum ether/ethyl acetate 1/1). ^{1}H NMR (400 MHz, DMSO-d_6): δ 0.96-1.06 (6H, m, 3 × CH_2), 1.14-1.26 (2H, m, CH_2), 1.63-1.75 (1H, m, CH_αH$_\beta$), 1.82-1.94 (1H, m, CH$_\alpha H_\beta$), 2.74 (2H, q, *J* = 6.2 Hz, CH_2), 2.79 (6H, s, $(CH_3)_2$), 3.58 (3H, s, CH_3), 3.84 (1H, t, *J* = 7.3 Hz, CH), 3.99 (3H, s, CH_3), 7.19 (1H, d, *J* = 7.8 Hz, CH), 7.27 (1H, t, *J* = 7.3 Hz, CH), 7.36 (1H, t, *J* = 7.6 Hz, CH), 7.50-7.63 (4H, m, 4 × CH), 7.85 (1H, t, *J* = 5.4 Hz, NH), 8.04 (2H, m, 2 × CH), 8.28 (1H, d, *J* = 8.8 Hz, CH), 8.42 (1H, d, *J* = 8.3 Hz, CH). ^{13}C NMR (100 MHz, DMSO-d_6): δ 25.6 (CH_2), 26.8 (CH_2), 28.1 (CH_2), 28.9 (CH_2), 31.4 (CH_2), 41.6 (CH), 42.2 (CH_2), 45.0 (2 × CH_3), 51.9 (CH_3), 54.2 (CH_3), 114.8 (CH), 115.0 (CH), 119.0 (C), 119.2 (CH), 119.6 (CH), 123.0 (CH), 123.1 (CH), 123.6 (CH), 124.8 (CH), 127.7 (CH), 128.3 (CH), 128.99 (C), 129.03 (C), 129.1 (C), 129.3 (CH), 134.9 (C), 136.2 (C), 150.7 (C), 151.3 (C), 173.5 (C). MS (ES, pos. mode): *m/z* (%): 580,33 ($M + H^+$, 100).

2-(1*H*-Indol-3-yl)-5-((7-nitrobenzo[*c*][1,2,5]oxadiazol-4-yl)amino)pentanoic acid **FL1**

Red solid, yield 52%, R_f = 0.19 (dichloromethane/acetone 25/1). ^{1}H NMR (500 MHz, DMSO-d_6): δ 1.62-1.73 (2H, m, CH_2), 1.91-2.00 (1H, m, CH_αH$_\beta$), 2.07-2.18 (1H, m, CH$_\alpha$$H_\beta$), 3.42-3.51 (2H, m, CH_2), 3.79 (1H, t, *J* = 7.5 Hz, CH), 6.30 (1H, d, *J* = 8.6 Hz, CH), 6.92 (1H, t, *J* = 7.5 Hz, CH), 7.04 (1H, t, *J* = 7.3 Hz, CH), 7.22 (1H, s, CH), 7.32 (1H, d, *J* = 7.9 Hz, CH), 7.57 (1H, d, *J* = 7.9 Hz, CH), 8.43 (1H, d, *J* = 8.9 Hz, CH), 9.24-10.00 (1H, br s, NH), 10.83-11.05 (1H, br s, NH), 11.78-12.47 (1H, br s, OH). ^{13}C NMR (125 MHz, DMSO-d_6): δ 25.8 (CH_2), 29.2 (CH_2), 42.1 (CH), 43.1 (CH_2), 99.1 (CH), 111.5 (CH), 112.3 (C), 118.4 (CH), 118.9 (CH), 120.5 (C), 121.0 (CH), 123.1 (CH), 126.3 (C), 136.2 (C), 137.8 (CH), 144.2 (C), 144.4 (C), 145.1 (C), 175.3 (C). MS (ES, neg. mode): *m/z* (%): 394.33 (M - H$^-$, 100).

2-(1*H*-Indol-3-yl)-6-((7-nitrobenzo[*c*][1,2,5]oxadiazol-4-yl)amino)hexanoic acid **FL2**
Red solid, yield 28%, R_f = 0.14 (dichloromethane/acetone 5/0.2). ^{1}H NMR (500 MHz, DMSO-d_6): δ 1.33-1.46 (2H, m, CH_2), 1.67-1.76 (2H, m, CH_2), 1.79-1.88 (1H, m, CH_αH$_\beta$), 2.03-2.12 (1H, m, CH$_\alpha$$H_\beta$), 3.39-3.49 (2H, m, CH_2), 3.72 (1H, t, *J* = 7.5 Hz, CH), 6.37 (1H, d, *J* = 8.9 Hz, CH), 6.93 (1H, t, *J* = 7.5 Hz, CH), 7.04 (1H, t, *J* = 7.5 Hz, CH), 7.20 (1H, d, *J* = 2.1 Hz, CH), 7.32 (1H, d, *J* = 7.9 Hz, CH), 7.55 (1H, d, *J* = 7.9 Hz, CH), 8.47 (1H, d, *J* = 8.6 Hz, CH), 9.22-9.97 (1H, br s, NH), 10.89-10.96 (1H, br s, NH), 11.80-12.51 (1H, br s, OH). ^{13}C NMR (125 MHz, DMSO-d_6): δ 24.8 (CH_2), 27.5 (CH_2), 31.8 (CH_2), 42.5 (CH), 43.3 (CH_2), 99.2 (CH), 111.4 (CH), 112.7 (C), 118.4 (CH), 118.8 (CH), 120.4 (C), 121.0 (CH), 122.9 (CH), 126.3 (C), 136.2 (C), 137.9 (CH), 144.2 (C), 144.5 (C), 145.2 (C), 175.5 (C). MS (ES, neg. mode): *m/z* (%): 408.35 (M - H$^-$, 100).

2-(1*H*-Indol-3-yl)-7-((7-nitrobenzo[c][1,2,5]oxadiazol-4-yl)amino)heptanoic acid **FL3**
Red solid, yield 49%, R_f = 0.33 (dichloromethane/acetone 5/0.4). ^{1}H NMR (500 MHz, DMSO-d_6): δ 1.29-1.44 (4H, m, 2 × CH_2), 1.62-1.69 (2H, m, CH_2), 1.74-1.85 (1H, m, CH_αH$_\beta$), 1.97-2.10 (1H, m, CH$_\alpha$$H_\beta$), 3.39-3.49 (2H, m, CH_2), 3.71 (1H, t, *J* = 7.5 Hz, CH), 6.37 (1H, d, *J* = 8.9 Hz, CH), 6.94 (1H, t, *J* = 7.5 Hz, CH), 7.05 (1H, t, *J* = 7.5 Hz, CH), 7.19 (1H, d, *J* = 2.1 Hz, CH), 7.33 (1H, d, *J* = 8.3 Hz, CH), 7.55 (1H, d, *J* = 7.9 Hz, CH), 8.49 (1H, d, *J* = 8.6 Hz, CH), 9.48-9.61 (1H, br s, NH), 10.86-10.97 (1H, br s, NH), 12.02-12.21 (1H, br s, OH). ^{13}C NMR (125 MHz, DMSO-d_6): δ 26.2 (CH_2), 26.9 (CH_2), 27.5 (CH_2), 32.0 (CH_2), 42.4 (CH), 43.3 (CH_2), 99.1 (CH), 111.5 (CH), 112.8 (C), 118.4 (CH), 118.8 (CH), 120.5 (C), 121.0 (CH), 122.8 (CH), 126.3 (C), 136.2 (C), 138.0 (CH), 144.2 (C), 144.4 (C), 145.2 (C), 175.5 (C). MS (ES, neg. mode): *m/z* (%): 422.38 (M - H$^-$, 100).

2-(1*H*-Indol-3-yl)-8-((7-nitrobenzo[*c*][1,2,5]oxadiazol-4-yl)amino)octanoic acid **FL4**
Red solid, yield 36%, R_f = 0.52 (dichloromethane/acetone 4/0.4). ^{1}H NMR (500 MHz, DMSO-d_6): δ 1.23-1.34 (6H, m, 3 × CH_2), 1.60-1.70 (2H, m, CH_2), 1.75-1.82 (1H, m, CH_αH$_\beta$), 1.99-2.06 (1H, m, CH$_\alpha$$H_\beta$), 3.39-3.48 (2H, m, CH_2), 3.70 (1H, t, *J* = 7.5 Hz, CH), 6.38 (1H, d, *J* = 8.9 Hz, CH), 6.95 (1H, t, *J* = 7.5 Hz, CH), 7.05 (1H, t, *J* = 7.3 Hz, CH), 7.19 (1H, d, *J* = 2.1 Hz, CH), 7.33 (1H, d, *J* = 7.9 Hz, CH), 7.56 (1H, d, *J* = 7.9 Hz, CH), 8.49 (1H, d, *J* = 8.9 Hz, CH), 9.49-9.61 (1H, br s, NH), 10.85-10.98 (1H, br s, NH), 12.03-12.15 (1H, br s, OH). ^{13}C NMR (125 MHz, DMSO-d_6): δ 26.3 (CH_2), 27.2 (CH_2), 27.6 (CH_2), 28.5 (CH_2), 32.1 (CH_2), 42.5 (CH), 43.3 (CH_2), 99.1 (CH), 111.5 (CH), 112.9 (C), 118.4 (CH), 118.8 (CH), 120.4 (C), 121.0 (CH), 122.8 (CH), 126.3 (C), 136.2 (C), 138.0 (CH), 144.2 (C), 144.5 (C), 145.2 (C), 175.5 (C). MS (ES, neg. mode): *m/z* (%): 436.31 (M - H^-, 100).

6-((5-(Dimethylamino)naphthalene)-1-sulfonamido)-2-(1*H*-indol-3-yl)hexanoic acid **FL5**
Light blue solid, yield 31%, R_f = 0.23 (dichloromethane/acetone 4.75/0.25). ^{1}H NMR (500 MHz, DMSO-d_6): δ 1.10-1.15 (2H, m, CH_2), 1.24-1.33 (2H, m, CH_2), 1.50-1.59 (1H, m, CH_αH$_\beta$), 1.76-1.85 (1H, m, CH$_\alpha$$H_\beta$), 2.73 (2H, q, *J* = 6.4 Hz, CH_2), 2.80 (6H, s, $(CH_3)_2$), 3.50 (1H, t, *J* = 7.6 Hz, CH), 6.95 (1H, t, *J* = 7.5 Hz, CH), 7.05 (1H, t, *J* = 7.5 Hz, CH), 7.11 (1H, d, *J* = 2.5 Hz, CH), 7.23 (1H, d, *J* = 7.0 Hz, CH), 7.32 (1H, d, *J* = 8.0 Hz, CH), 7.50 (1H, d, *J* = 7.9 Hz, CH), 7.55-7.61 (2H, m, 2 × CH), 7.88 (1H, t, *J* = 5.8 Hz, NH), 8.07 (1H, d, *J* = 7.3 Hz, CH), 8.28 (1H, d, *J* = 8.6 Hz, CH), 8.43 (1H, d, *J* = 8.6 Hz, CH), 10.89-10.92 (1H, br s, NH), 11.89-12.35 (1H, br s, OH). ^{13}C NMR (125 MHz, DMSO-d_6): δ 24.3 (CH_2), 29.0 (CH_2), 31.6 (CH_2), 42.3 (CH_2), 42.4 (CH), 45.0 (2 × CH_3), 111.4 (CH), 112.8 (C), 115.1 (CH), 118.4 (CH), 118.8 (CH), 119.1 (CH), 120.9 (CH), 122.7 (CH), 123.6 (CH), 126.3 (C), 127.7 (CH), 128.2 (CH), 129.0 (C), 129.1 (C), 129.3 (CH), 136.1 (C), 136.2 (C), 151.3 (C), 175.4 (C). MS (ES, pos. mode): *m/z* (%): 480.40 (M + H^+, 100).

8-((5-(Dimethylamino)naphthalene)-1-sulfonamido)-2-(1*H*-indol-3-yl)octanoic acid **FL6**
Light blue solid, yield 43%, R_f = 0.52 (dichloromethane/acetone 10/1). ^{1}H NMR (500 MHz, DMSO-d_6): δ 0.93-1.02 (6H, m, 3 × CH_2), 1.14-1.19 (2H, m, CH_2), 1.58-1.67 (1H, m, CH_αH$_\beta$), 1.83-1.93 (1H, m, CH$_\alpha$$H_\beta$), 2.74 (2H, q, *J* = 6.4 Hz, CH_2), 2.80 (6H, s, $(CH_3)_2$), 3.61 (1H, t, *J* = 7.5 Hz, CH), 6.96 (1H, t, *J* = 7.8 Hz, CH), 7.06 (1H, t, *J* = 7.5 Hz, CH), 7.16 (1H, d, *J* = 2.5 Hz, CH), 7.21 (1H, d, *J* = 7.3 Hz, CH), 7.34 (1H, d, *J* = 8.3 Hz, CH), 7.52-7.61 (3H, m, 3 × CH), 7.85 (1H, t, *J* = 5.7 Hz, NH), 8.08 (1H, d, *J* = 8.6 Hz, CH), 8.28 (1H, d, *J* = 8.9 Hz, CH), 8.43 (1H, d, *J* = 8.6 Hz, CH), 10.90-10.95 (1H, br s, NH), 11.94-12.24 (1H, br s, OH). ^{13}C NMR

(125 MHz, DMSO-d_6): δ 25.8 (CH_2), 27.2 (CH_2), 28.3 (CH_2), 28.9 (CH_2), 32.1 (CH_2), 42.3 (CH_2), 42.6 (CH), 45.1 (2 × CH_3), 111.5 (CH), 112.9 (C), 115.1 (CH), 118.4 (CH), 118.9 (CH), 119.2 (CH), 121.0 (CH), 122.8 (CH), 123.6 (CH), 126.4 (C), 127.8 (CH), 128.3 (CH), 129.0 (C), 129.1 (C), 129.3 (CH), 136.19 (C), 136.21 (C), 151.3 (C), 175.5 (C). MS (ES, pos. mode): *m/z* (%): 508.35 ($M + H^+$, 100).

N-Hexyl-7-nitrobenzo[*c*][1,2,5]oxadiazol-4-amine **CTRL1**

Red solid, yield 13%, R_f = 0.30 (petroleum ether/ethyl acetate 9/1). ^{1}H NMR (500 MHz, DMSO-d_6): δ 0.84-0.90 (3H, m, CH_3), 1.26-1.32 (4H, m, 2 × CH_2), 1.33-1.42 (2H, m, CH_2), 1.67 (2H, p, *J* = 7.3 Hz, CH_2), 3.43-3.50 (2H, m, CH_2), 6.42 (1H, d, *J* = 8.9 Hz, CH), 8.51 (1H, d, *J* = 8.9 Hz, CH), 9.53-9.59 (1H, br s, NH). ^{13}C NMR (125 MHz, DMSO-d_6): δ 13.9 (CH_3), 22.1 (CH_2), 26.1 (CH_2), 27.6 (CH_2), 30.9 (CH_2), 43.4 (CH_2), 99.1 (CH), 120.5 (C), 138.0 (CH), 144.2 (C), 144.5 (C), 145.2 (C). MS (ES, pos. mode): *m/z* (%): 265.14 ($M + H^+$, 100).

8-((7-Nitrobenzo[*c*][1,2,5]oxadiazol-4-yl)amino)octanoic acid **CTRL2**

Red solid, yield 12%, R_f = 0.36 (petroleum ether/ethyl acetate 1/4). ^{1}H NMR (500 MHz, DMSO-d_6): δ 1.19-1.32 (6H, m, 3 × CH_2), 1.48 (2H, p, *J* = 7.3 CH_2), 1.66 (2H, p, *J* = 7.3 Hz, CH_2), 2.15 (2H, t, *J* = 7.3 Hz, CH_2), 3.37-3.47 (2H, m, CH_2), 6.37 (1H, d, *J* = 9.2 Hz, CH), 8.47 (1H, d, *J* = 8.9 Hz, CH), 9.49-9.59 (1H, br s, NH), 11.91-12.01 (1H, br s, OH). ^{13}C NMR (125 MHz, DMSO-d_6): δ 24.4 (CH_2), 26.3 (CH_2), 27.6 (CH_2), 28.4 (CH_2), 28.5 (CH_2), 33.6 (CH_2), 43.4 (CH_2), 99.1 (CH), 120.5 (C), 138.1 (CH), 144.2(C), 144.5 (C), 145.2 (C), 174.6 (C). MS (ES, pos. mode): *m/z* (%): 323.22 ($M + H^+$, 100).

Supplementary Table S1. Conditions of UHPLC-MRM-MS method. Diagnostic MRM transitions and collision energies (CE) were optimised for compounds. In addition, retention time (RT) and limit of detection (LOD) were also measured. Analytes were detected by the triple quadrupole mass spectrometer Xevo™ TQ MS in the positive mode using these optimized conditions: source/desolvation temperature 150/600 °C; cone/desolvation gas flow, 150/1000 L/h; capillary voltage, 1 kV; cone voltage, 20 V; collision gas flow, 0.14 mL/min.

Analyte	**MRM transition**		**CE** (V)	**Retention time** (min)	**LOD** (fmol)	**Linear range** (pmol)
	quantifier	**qualifier**				
CTRL1	265.2 > 118.7	265.2 > 231.0	26	3.9	10	10^{-2} - 100
CTRL2	323.3 > 148.0		20	2.2	1	10^{-3} - 100
FL4	438.1 > 130.2		20	3.5	1	10^{-2} - 100
FL5	480.6 > 184.0	480.6 > 436.0	22	3.5	1	10^{-2} - 100
FL6	508.6 > 462.0	508.6 >234.0	18	4.1	1	10^{-3} - 100

Supplementary Table S2. Liquid-liquid extraction efficiency of fluorescently labeled auxins. To the ≈10 mg of seven-days-old *Arabidopsis thaliana* seedlings, 1 nmol of **FL4-6**, **CTRL1** and **CTRL2** was added and samples were then processed by the LLE. External calibration curve was prepared, recovery factor was calculated from measured analytes levels after LLE, and finally applied for normalization of quantitative determination of each compound shown in Figure 7 and Supplementary Figure S1.

Analyte	**Concentration**		**Recovery**	**Recovery factor**
	(pmol)	MEAN ± S.D. (pmol)	MEAN ± S.D. (%)	
CTRL1	242.97 249.78 264.44	252.40 ± 8.96	25.24 ± 0.90	3.96
CTRL2	461.47 469.41 499.72	476.87 ± 16.48	47.69 ± 1.65	2.10
FL4	699.22 988.25 1002.19	896.55 ± 139.65	89.66 ± 13.97	1.12
FL5	680.77 833.30 840.16	784.74 ± 73.57	78.47 ± 7.36	1.27
FL6	391.42 496.87 549.96	479.41 ± 65.89	47.94 ± 6.59	2.09

Supplementary Table S3. Fundamental absorption and fluorescence characteristics of compounds **FL4-FL6**.

Compound	**λ_{abs} (nm)**	**λ_{em} (nm)**	**SS (nm)**	**ε_{max} ($M^{-1}cm^{-1}$)**	**QY**
FL4	467	531	64	27200	0.291
FL5	336	519	183	4400	0.253
FL6	331	520	189	1700	0.257

SS – Stokes shift, ε_{max} – maximum molar extinction coefficient, QY – fluorescence quantum yield

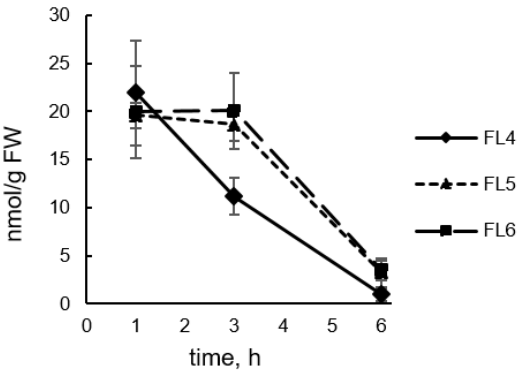

Supplementary Figure S1. Time dependent concentration dynamics of compounds FL4, FL5 and FL6 in *Arabidopsis thaliana* plants. Five-day-old *Arabidopsis thaliana* seedlings were fed with **FL4**, **FL5** or **FL6** at 10 µM concentration. Samples were harvested after 1, 3 and 6 h. Values are means nmol/g FW ± S.D. from five biological replicates.

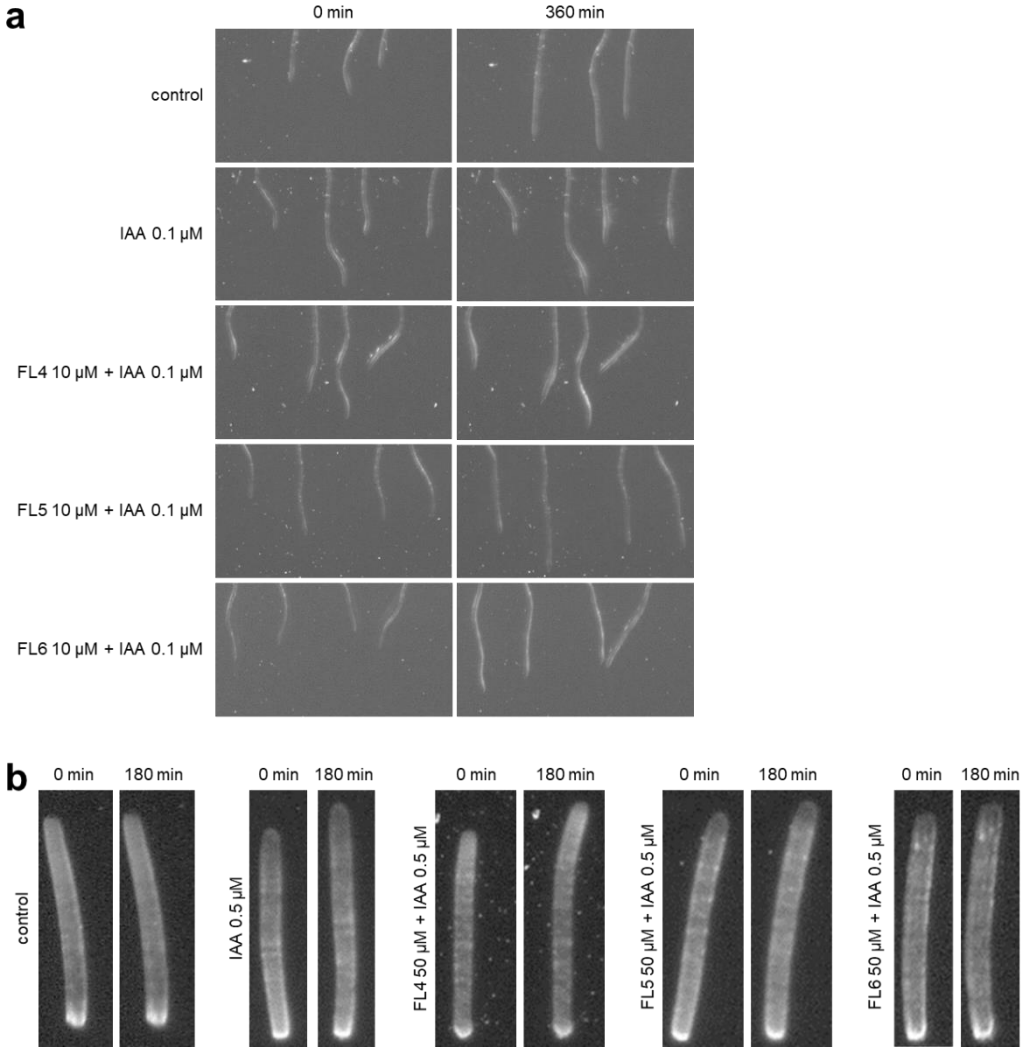

Supplementary Figure S2. The effect of compounds FL4, FL5 and FL6 on primary root growth and elongation of hypocotyl segments in DR5::LUC transgenic plants of *Arabidopsis thaliana*. Five-day-old seedlings were transferred to plates with media containing 0.3% DMSO as a blank control, 0.1 µM IAA as positive control or 10 µM **FL4**, **FL5** and **FL6** with 0.1 µM IAA for 6 h. Pictures were taken every 10 min, displayed pictures represent time points at 0 and 360 min (**a**). Hypocotyl segments from 3-day-old dark-grown plants were transferred onto a treatment plate with the depletion medium supplemented with 0.3% DMSO as a blank control, 0.5 µM IAA as positive control or 50 µM **FL4**, **FL5** and **FL6** with 0.5 µM IAA for 3 h. Pictures were taken every 20 min, displayed pictures represent time points at 0 and 180 min (**b**). Figures were chosen as representatives from three independent biological repetitions.

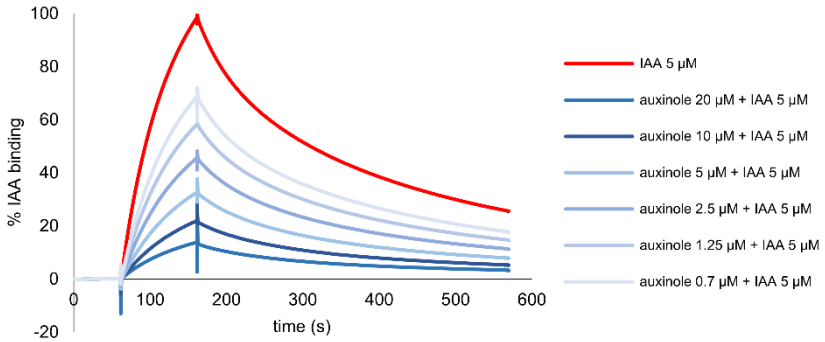

Supplementary Figure S3. SPR analysis of the antagonistic effect of auxinole on auxin-induced interaction between TIR1 protein and IAA7 degron peptide. The sensorgram shows association followed by dissociation in buffer. Results for IAA (5 µM) on TIR1 protein alone (red) and in co-treatment with auxinole in a concentration range (0.7, 1.25, 2.5, 5, 10, 20 µM) (shades of blue).

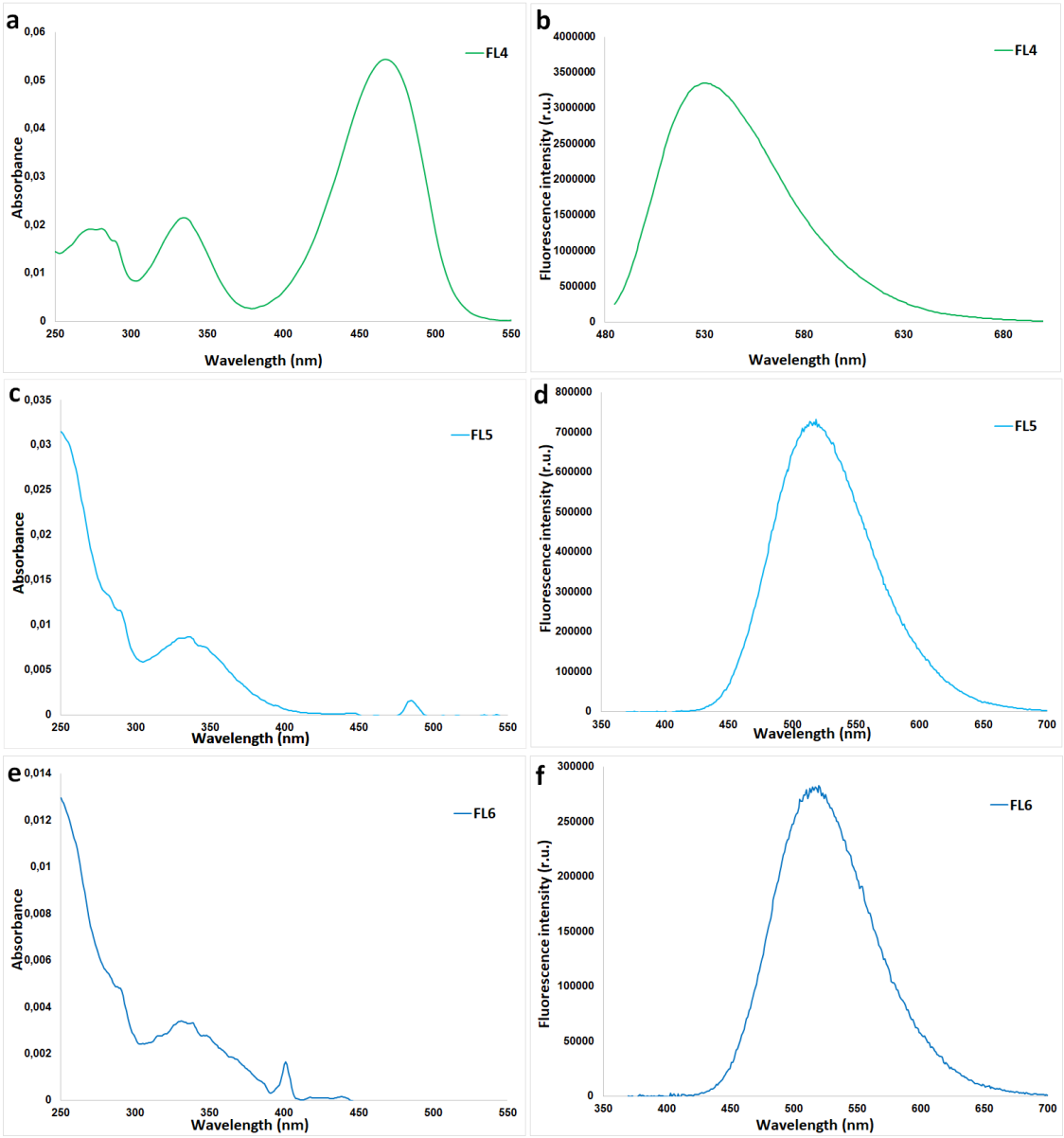

Supplementary Figure S4. Absorption (**a**, **c**, **e**) and emission (**b**, **d**, **f**) spectra of 2 µM solutions of compounds **FL4** (**a**, **b**), **FL5** (**c**, **d**) and **FL6** (**e**, **f**) in methanol.

References

Bieleszová K, Pařízková B, Kubeš M, et al (2019) New fluorescently labeled auxins exhibit promising anti-auxin activity. N Biotechnol 48:44–52. https://doi.org/10.1016/j.nbt.2018.06.003

Ensch C, Hesse M (2002) Total syntheses of the spermine alkaloids (-)-(R,R)-hopromine and (±)-homaline. Helv Chim Acta 85:1659–1677. https://doi.org/10.1002/1522-2675(200206)85:6<1659::AID-HLCA1659>3.0.CO;2-D

Hayashi KI, Neve J, Hirose M, et al (2012) Rational design of an auxin antagonist of the SCF TIR1 auxin receptor complex. ACS Chem Biol 7:590–598. https://doi.org/10.1021/cb200404c

Supplement I

Supplement II

Supplement III

Supplement IV

Zhang C., Bieleszová K., Žukauskaitė A., **Hladík P.**, Grúz J., Novák O., Doležal K. (2024) In situ separation and visualization of isomeric auxin derivatives in Arabidopsis by ion mobility mass spectrometry imaging. *Anal Bioanal Chem*. 416(1), 125-139.

Analytical and Bioanalytical Chemistry (2024) 416:125–139
https://doi.org/10.1007/s00216-023-04996-x

PAPER IN FOREFRONT

In situ separation and visualization of isomeric auxin derivatives in *Arabidopsis* by ion mobility mass spectrometry imaging

Chao Zhang[1] · Kristýna Bieleszová[2] · Asta Žukauskaitė[2] · Pavel Hladík[1] · Jiří Grúz[3] · Ondřej Novák[1] · Karel Doležal[1,2]

Received: 21 August 2023 / Revised: 29 September 2023 / Accepted: 10 October 2023 / Published online: 23 October 2023

Abstract

In situ separation and visualization of synthetic and naturally occurring isomers from heterogeneous plant tissues, especially when they share similar molecular structures, are a challenging task. In this study, we combined the ion mobility separation with desorption electrospray ionization mass spectrometry imaging (DESI-IM-MSI) to achieve a direct separation and visualization of two synthetic auxin derivatives, auxinole and its structural isomer 4pTb-MeIAA, as well as endogenous auxins from *Arabidopsis* samples. Distinct distribution of these synthetic isomers and endogenous auxins in *Arabidopsis* primary roots and hypocotyls was achieved in the same imaging analysis from both individually treated and cotreated samples. We also observed putative metabolites of synthetic auxin derivatives, i.e. auxinole amino acid conjugates and hydrolysed 4pTb-MeIAA product — 4pTb-IAA, based on their unique drifting ion intensity patterns. Furthermore, DESI-IM-MSI-revealed abundance of endogenous auxins and synthetic isomers was validated by liquid chromatography–mass spectrometry (LC-MS). Our results demonstrate that DESI-IM-MSI could be used as a robust technique for detecting endogenous and exogenous isomers and provide a spatiotemporal evaluation of hormonomics profiles in plants.

Keywords Mass spectrometry imaging · Desorption electrospray ionization · Ion mobility · Auxin · Isomer · Metabolite

Introduction

As a group of small-size molecules, phytohormones are widely present in almost all plant tissues and work as regulation centres of plant homeostasis [1]. Since the first phytohormone indole-3-acetic acid (IAA) was discovered, synthetic auxin and other phytohormone derivatives have been developed to mimic their molecular structure and action, which are frequently applied in agriculture and plant physiology studies [2, 3]. Analogously to their natural counterparts, the majority of synthetic plant growth regulators are low-molecular-weight compounds that work in either synergistic or antagonistic ways in complex plant signalling networks [4]. While metabolic pathways of natural plant hormones are extensively studied [5–8], in vivo metabolism of synthetic plant growth regulators or other synthetic compounds of biological relevance, which might aid in understanding and harnessing their potential, is underexplored. For example, auxinole has been developed as an auxin antagonist of TIR1/AFB

✉ Chao Zhang
chao.zhang@upol.cz

✉ Karel Doležal
karel.dolezal@upol.cz

Kristýna Bieleszová
kristyna.bieleszova@upol.cz

Asta Žukauskaitė
asta.zukauskaite@upol.cz

Pavel Hladík
pavel.hladik@upol.cz

Jiří Grúz
jiri.gruz@upol.cz

Ondřej Novák
ondrej.novak@upol.cz

[1] Laboratory of Growth Regulators, Institute of Experimental Botany, The Czech Academy of Sciences & Faculty of Science, Palacký University, Šlechtitelů 27, CZ-78371 Olomouc, Czech Republic

[2] Department of Chemical Biology, Faculty of Science, Palacký University, Šlechtitelů 27, CZ-78371 Olomouc, Czech Republic

[3] Department of Experimental Biology, Faculty of Science, Palacký University, Šlechtitelů 27, CZ-78371 Olomouc, Czech Republic

receptors and is frequently used in auxin-related experiments and other phytohormone research [9]. However, direct in situ visualization of auxinole or other synthetic auxin derivatives from plant tissues is hardly achieved due to limited tracking methods. Currently, the use of reporter lines, chemical staining, or labelling are the most prevalent methods with advantages of high sensitivity and specificity for tracing endogenous and synthetic compounds within plant tissues [10, 11]. However, these methods do not allow tracking of multiple targets from the same sample or distinguishing them after in vivo modifications.

Mass spectrometry (MS) is a high-throughput analytical tool used for the identification and quantification of various analytes, including peptides, proteins, lipids, polysaccharides, and synthetic drugs from biological samples [12, 13]. In the field of plant research, accurate quantification of auxins and other phytohormone species based on liquid chromatography–mass spectrometry (LC-MS) has been established, which can distinguish different amounts of endogenous phytohormones and related metabolites from various plants, plant organs, and at the level of organelles [14–18]. Even more so than in the case of endogenous phytohormones, the characterization of synthetic plant growth regulators using chromatography or fragmentation ions can be challenging due to very similar elemental composition and isomeric structures of the compounds. Additionally, in vivo spatial distribution of targeted compounds cannot be preserved during LC-MS sample preparation, which makes it hard to distinguish analyte origins in plant tissues [19].

Mass spectrometry imaging (MSI) is a staple in lipidomics and metabolomics analysis in mammalian or medical research and has recently emerged as an advanced method to map biomolecules and their metabolites in plants [20, 21]. The desorption electrospray ionization mass spectrometry imaging (DESI-MSI) is an ambient ionization technique which enables analysis of heterogeneous tissues without destructive sample preparation. Compared with other MSI sources, such as matrix-assisted laser desorption/ionization (MALDI) and secondary ion mass spectrometry (SIMS), DESI overcomes limitations associated with signal variation and ion suppression caused by the coating of the matrix before MSI analysis [22]. Recently, we employed DESI-MSI to successfully visualize arguably the most extensively used auxin antagonist auxinole and other new anti-auxins from individually treated plant samples [23]. However, separation, visualization, and quantification of two or more isomeric plant growth regulators or their derivatives from cotreated samples have not yet been achieved. Ion mobility (IM) applies an extra analytical dimension to separate compounds based on their 3D structure using drifting gas which allows accurate evaluation of synthetic and endogenous analytes of interest from plant tissues and their separation from other structural isomers [24]. For instance, Hou et al. employed IM-MSI to reveal unique spatial distribution of lipidomes in different nut species [25].

In the present study, travelling wave (T-Wave) ion mobility was coupled with DESI-MSI analysis to carry out the separation of auxinole and its structural isomer, methyl 2-(1*H*-indol-3-yl)-4-oxo-4-*p*-tolyl-butanoate (4pTb-MeIAA), from both individually treated and cotreated 10-day-old *Arabidopsis* (Col-0) seedlings. We achieved accurate separation of auxinole, 4pTb-MeIAA and endogenous IAA from their intact positions in *Arabidopsis* root and hypocotyl and further revealed putative auxinole and 4pTb-MeIAA metabolites, auxinole-Asp and auxinole-Glu as well as hydrolysed product 4pTb-IAA. Identification of isomers and their metabolites was further confirmed using in situ MS/MS fragmentation ions with collision cross-section (CCS) value. DESI-IM-MSI detected target abundance in different treated groups which was also in agreement with LC-MS quantification. These results prove that DESI-IM-MSI is an advanced label-free technique which can be used for the in situ separation, visualization, and characterization of phytohormone derivatives and their metabolites in planta.

Materials and methods

Chemicals and analytical standards

4-(2,4-Dimethylphenyl)-2-(1*H*-indol-3-yl)-4-oxo butanoic acid (auxinole) and 2-(1*H*-indol-3-yl)-4-oxo-4-(*p*-tolyl)butanoic acid (4pTb-IAA) were prepared in accordance to the procedure described by Hayashi *et al.* implementing minor modifications described by Žukauskaitė *et al.* [9, 23]. Synthesis and spectral data of (4-(2,4-dimethylphenyl)-2-(1*H*-indol-3-yl)-4-oxobutanoyl)-L-aspartic acid (auxinole-Asp), (4-(2,4-dimethylphenyl)-2-(1*H*-indol-3-yl)-4-oxobutanoyl)-L-glutamic acid (auxinole-Glu) and methyl 2-(1*H*-indol-3-yl)-4-oxo-4-(*p*-tolyl)butanoate (4pTb-MeIAA) are described in Supplementary Information (Method S1). Auxin standards, indole-3-acetic acid (IAA), indole-3-acetyl-L-aspartic acid (IAA-Asp), indole-3-acetyl-L-glutamic acid (IAA-Glu), oxindole-3-acetic acid (oxIAA), oxindole-3-acetyl-L-aspartic acid (oxIAA-Asp), oxindole-3-acetyl-L-glutamic acid (oxIAA-Glu) and oxindole-3-acetyl-β-1-D-glucoside (oxIAA-Glc) were obtained from OlChemIm s.r.o. Isotopically labelled auxin standards were purchased from Cambridge Isotope Laboratories, Inc (Tewksbury, MA). HPLC-grade acetonitrile (ACN) and ammonia were obtained from Merck (Dusseldorf, Germany). HPLC-grade water was obtained from a Milli-Q water purification system (Millipore, Watford, UK).

Preparation of plant samples

Arabidopsis thaliana wild-type ecotype Col-0 seeds were sterilized with 70% EtOH with 0.1% Tween-20 solution for 10 min (2×) and rinsed with 96% EtOH for 10 min. After 2 days of stratification (4 °C in the dark), seeds were germinated on sterile ½ MS medium (2.2 g/L Murashige and Skoog medium, 1% sucrose, 0.7% agar and 0.5 g/L MES PUFFERAN, pH 5.6) in long-day light conditions (22 °C/20 °C, 16 h light/8 h dark, 100 µmol/s/m^2). Ten-day-old seedlings were transferred to horizontally divided heterogeneous media plates containing ½ MS (1.5% agar) medium supplemented with 0.05% dimethyl sulfoxide (DMSO) and 0.25% acetonitrile (ACN). Synthetic isomers were added individually (10 µM auxinole or 10 µM 4pTb-MeIAA) or in cotreatment (10 µM auxinole + 10 µM 4pTb-MeIAA) to the bottom half of the medium, while the upper part of the medium was kept untreated (Fig. 1). Plates were covered with aluminium foil and kept in a growth chamber with long-day light conditions (22 °C/20 °C, 16 h light/8 h dark, 100 µmol/s/m^2) in a vertical position. After 24 h, *Arabidopsis* plants with roughly 5-cm-long roots were freshly collected and rapidly washed in ultrapure water for 10 s to remove the surface medium, mounted on Superfrost glass slides (Thermo Fisher Scientific, Waltham, MA, USA) using non-conductive double-sided tape (Plano GmbH, Wetzlar, Germany) and stored in −80 ℃ freezer. Sample slides were dried in a vacuum desiccator (Merck), scanned and subjected to DESI-IM-MSI acquisition.

Standard infusion

Analytical standards were diluted at 0.1–100 pmol/µL, submitted to the DESI source (Waters, Milford, MA, USA) and infused at a flow rate of 3µL/min to Synapt G2-Si MS instrument (Waters, Milford, MA, USA). The MS and MS/MS spectra of all standards were acquired using a Synapt G2-Si MS instrument coupled to T-wave Ion Mobility (Waters). The ion mobility collision cell was optimized in negative mode for small analytes ranging from 100 to 600 Da and calibrated with poly-DL-alanine (Sigma-Aldrich). Molecular structures of standard and major fragment ions of the standard compounds were identified using MassLynx™ software (v4.1, Waters) where targets' standard masses, drift time and major fragmentation ions were recorded. The DriftScope (v3.0, Waters) was employed to calibrate drift time (dt) and calculate collision cross-section (CCS) values [26].

DESI-IM-MSI and DESI-IM-MS/MS

The DESI-IM-MSI analysis was achieved by the Synapt G2-Si MS coupled with a 2D-DESI source (Waters). The spray solvent was delivered at 3 µL/min (80% ACN with 0.1% ammonia), nebulized with 5–6 Mbps ultrapure nitrogen; the DESI source was optimized with an incidence angle of 55°, 4 kV capillary voltage, 30 eV cone voltage, scanned in 90-µm spatial resolution and 100–600 Da mass range in negative mode. Travelling wave ion mobility derived target analyte collision cross in N_2 with IMS wave velocity 750 m/s and transfer wave velocity 350 m/s. Acquired ion masses

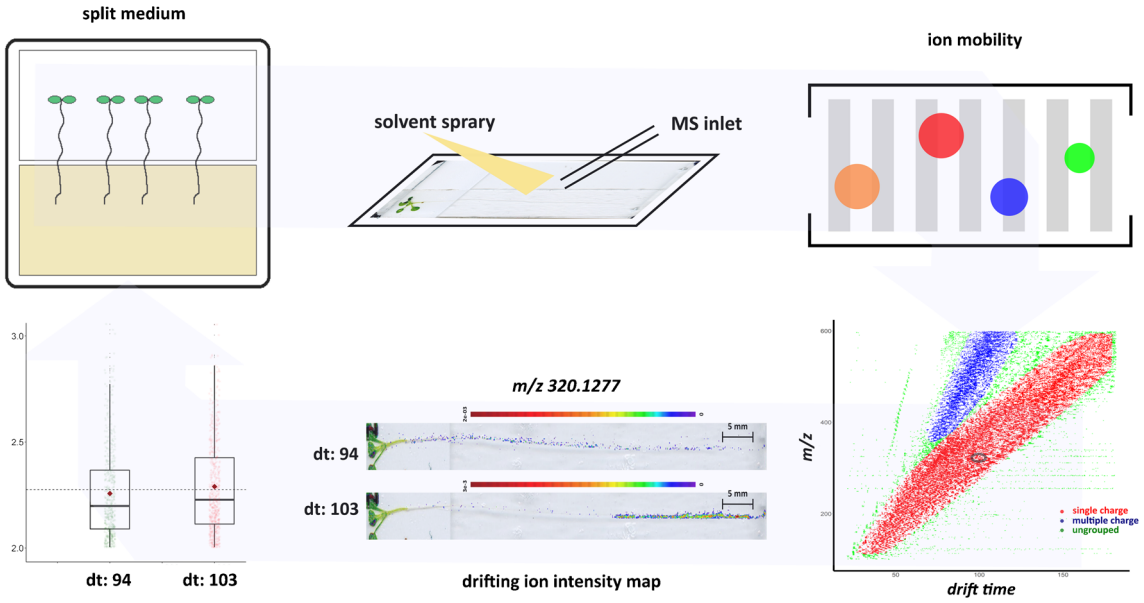

Fig. 1 Analytical workflow for in situ separation and visualization of structural isomers (auxinole and 4pTb-MeIAA) from individually and cotreated *Arabidopsis* via DESI-IM-MSI

were recalibrated with palmitic acid ([M-H]$^-$ 255.2324) using MassLynx™ software (v4.1), and their CCS values were calibrated using previous infusion standard reference in DriftScope v3.0 (Waters). To validate target metabolites, in situ IM-MS/MS was performed on the same *Arabidopsis* samples with 5–20 eV collision energy scanning throughout the regions with high parent ion intensities. The unique fragmented ions were picked from standard infusion spectra according to their unique masses and drift times.

LC–MS/MS

Arabidopsis samples were prepared as described above. After 24 h, treated *Arabidopsis* plants were rapidly washed in ultrapure water for 10 s to remove the surface medium and collected into Eppendorf tubes, each of them containing roughly 10 mg of roots and hypocotyls mixture (10–12 plants per biological replicate, 5 biological replicates). The samples were flash frozen in liquid nitrogen and then stored at −80 ℃ before the quantification of isomeric compounds and auxin metabolites. For the auxin profiling, the samples were extracted in 1 mL of ice-cold Na-phosphate buffer (50 mM, pH 7.0, 4 °C, 0.1% diethyldithiocarbamic acid sodium salt) containing a cocktail of labelled standards and then homogenized in a vibration mill (MM400, Retsch GmbH & Co. KG, Haan, Germany). The homogenized sample solution was purified using in-tip micro solid-phase extraction (in-tip µSPE) as described in Pěnčík et al. (2018) [27] with modifications from Hladík et al. (2023) [28]. For HPLC-MS/MS analysis, 1290 Infinity LC system (Agilent Technologies, Santa Clara, CA, USA) and a 6490 Triple Quadrupole LC-MS system (Agilent Technologies) were used. All chromatogpraphic data were then processed by Mass Hunter software (Agilent Technologies) where the area under the curve (AUC) of the targeted analytes was normalized by the weight of the sample and AUC of the internal standard and displayed as intensity ratio. Auxinole and 4pTb-MeIAA were processed and analysed according to the method described in Method S2.

Data analysis

The acquired spectra were recalibrated using the exact mass of palmitic acid (*m/z* 255.2324, dt: 90.0) and peaks within 20–180 ms drift bins were processed into a peaklist with 20000 FWHM resolution using HDImaging (Waters). Subsequent analysis was performed using an *in house* R script, where the data were processed for low-intensity removal, total ion count (TIC) normalization, drift time alignment and raw ion intensity map creation. Tissue-specific regions of interest (ROI) and single-charged ions were selected and exported from ImageJ (NIH, USA). Peak groups repeatedly detected from triplicated datasets were picked for further analysis. Peak intensities among different treatments were analysed using an unpaired Student's *t*-test, which provided the mean, standard deviation and statistical significance in the bar plots [29]. Ion intensity maps for the peaks of interest were generated using the HDImaging (Waters).

Results and discussion

Standard library construction

Deprotonated masses and drift times for targeted isomeric compounds (auxinole and 4pTb-MeIAA) and endogenous auxin metabolites were acquired by dissolved standard infusion in DESI source. Initially, spectra of auxinole and 4pTb-MeIAA were acquired in both positive and negative modes. Isomeric ions acquired in positive ion mobility mode showed high noise levels, high limit of detection and inseparable drift times in the infusion test. Considering low abundance of endogenous auxins and auxin derivatives in a single *Arabidopsis* sample, the following DESI-IM-MSI and MS/MS analyses were performed in the negative mode that provided significantly higher signal qualities of target analytes than in the positive mode. Due to the different ionization efficiency of target analytes, 80% ACN with 0.1% ammonia was chosen as the most suitable spray solvent. Normalized intensities in the infusion were linearly correlated with analyte concentrations in the range of 0.1–100 pmol/µL (Fig. S1). Standard compounds, spotted on a glass slide, were introduced into MS for the establishment of a standard library with ion masses, drift time and CCS values in DriftScope (v3.0). In summary, deprotonated ions of isomeric compounds auxinole and 4pTb-MeIAA in spray solvent were detected at *m/z* 320.1288, within ± 0.01 Da range from the common calculated mass (*m/z* 320.1292), and their drift time (dt) was separated into bins 103.7 and 95.3, respectively (Table 1). Meanwhile, polyalanine calibrated CCS values for auxinole and 4pTb-MeIAA were 188.0 Å^2 and 179.5 Å^2, respectively. The drifting ion information of IAA (*m/z* 174.0557, dt 48.4, CCS 126.5 Å^2) and its metabolites oxIAA, IAA-Asp, IAA-Glu, oxIAA-Asp, oxIAA-Glu and oxIAA-Glc are also listed in Table 1. Besides, expected metabolites of isomeric derivatives, namely, auxinole-aspartate (auxinole-Asp), auxinole-glutamate (auxinole-Glu) and 4pTb-IAA, i.e. hydrolysed form of 4pTb-MeIAA, were also measured with detected masses of *m/z* 435.1578, 449.1763 and 306.1078 in infusion test, respectively, and their unique ion drift times and CCSs are also highlighted in Table 1.

DESI-IM-MSI

DESI-IM-MSI was performed on 24-h treated *Arabidopsis thaliana* (Col-0, 10 days old) plants with 60–70-mm-long

Table 1 Molecular structures and experiment properties of isomeric compounds (auxinole and 4pTb-MeIAA), their modification products and auxins detected in DESI-IM-MS analysis

Targets	Molecular formula	Calculated mass[1] $[M-H]^-$	Measured mass[2] $[M-H]^-$	Drift time[3] (bins)	Collision cross Sect.[4] ($Å^2$)
auxinole	$C_{20}H_{19}NO_3$	320.1292	320.1288	103.7	188.0
4pTb-MeIAA	$C_{20}H_{19}NO_3$	320.1292	320.1288	95.3	179.5
auxinole-Asp	$C_{24}H_{24}N_2O_6$	435.1562	435.1578	131.0	212.1
auxinole-Glu	$C_{25}H_{26}N_2O_6$	449.1718	449.1763	141.4	221.2
4pTb-IAA	$C_{19}H_{17}NO_3$	306.1136	306.1078	98.8	183.6
IAA	$C_{10}H_9NO_2$	174.0557	174.0516	48.4	126.5
oxIAA	$C_{10}H_9NO_3$	190.0510	190.0491	53.2	132.8
IAA-Asp	$C_{14}H_{14}N_2O_5$	289.0830	289.0740	80.8	164.1
IAA-Glu	$C_{15}H_{16}N_2O_5$	303.0935	303.0993	88.6	172.6
oxIAA-Asp	$C_{15}H_{18}N_2O_5$	305.0779	305.0757	88.1	172.0
oxIAA-Glu	$C_{16}H_{20}N_2O_5$	319.0936	319.1009	92.0	176.0
oxIAA-Glc	$C_{16}H_{19}NO_8$	352.1038	352.1111	99.1	182.9

[1]Deprotonated masses of the compounds were calculated based on their molecular formulas using ACD/ChemSketch (v2018.12.1)

[2]The measured mass of targeted compounds was summarized from the mean intensities collected from compound infusion in DESI-IM-MSI analysis

[3]The drift time of infusion standards was measured in ion mobility separated using nitrogen gas

[4]CCS values of the infusion standards were calibrated with poly-DL-alanine

sampling regions, consisting of primary root and hypocotyl with the leaves excluded. Isomeric auxin derivatives, auxinole and 4pTb-MeIAA (Fig. 2), together with selected endogenous auxins were acquired at the *m/z* 100–600 mass range in ion mobility separation.

Raw spectra acquired from control (blank medium), 10 µM auxinole, 10 µM 4pTb-MeIAA and 10 µM auxinole + 10 µM 4pTb-MeIAA cotreated samples were processed into peaks in HDImaging (Waters). Detected peaks were recalibrated with their measured masses and drift times according to palmitic acid (*m/z* 255.2324, dt 90.0). Peaks with similar *m/z* values, potentially ionized from the same or isomeric compounds, were grouped using density-based clustering (DBSCAN with an epsilon of 0.003 Da and a minimum of 4 ion peaks per group) [30]. Additionally, singly charged drift ions were manually selected from the drift time *vs* mass plotting results using an *in house* R script. In total, 487 of 5025 peak groups could be detected from all triplicated datasets in each treatment group with a minimum intensity over 100 arbitrary units, within which 347 peaks demonstrated singly charged conditions in the drift time plotting separation (Fig. 3a). The abundance weighted mean (AWM) of singly charged peak group was calculated as the common mass of all peaks grouped inside and maximum *m/z* value difference of peak groups was set below 0.01 Da (Table S3). Peak groups with more than 4 bin differences in peak drift times were assigned as isomeric ions. In total, 435 peak groups showed significant differences in peak drift times, including the peak group (AWM 320.1273 ± 0.0071) where standard masses of auxinole and 4pTb-MeIAA are located (Fig. 3b, c). The peak difference of target isomers (auxinole and 4pTb-MeIAA), based on mass and drift time grouping, is displayed in Table 2.

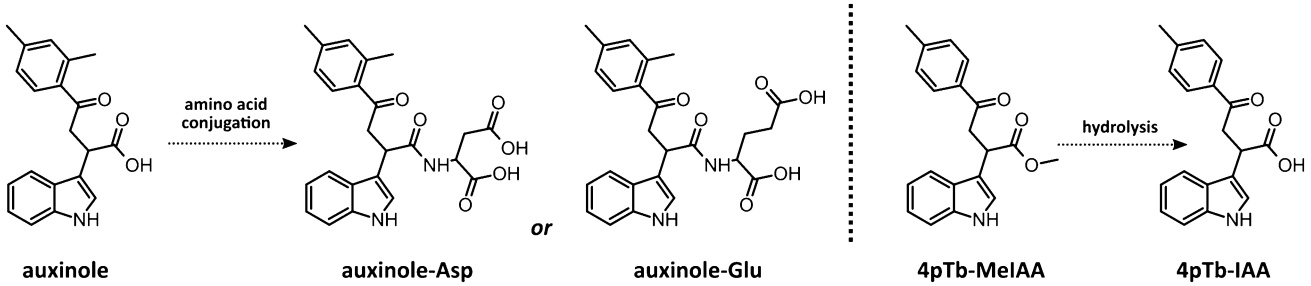

Fig. 2 Structures of auxinole, 4pTb-MeIAA and their metabolites, namely, auxinole-Asp, auxinole-Glu and 4pTb-IAA

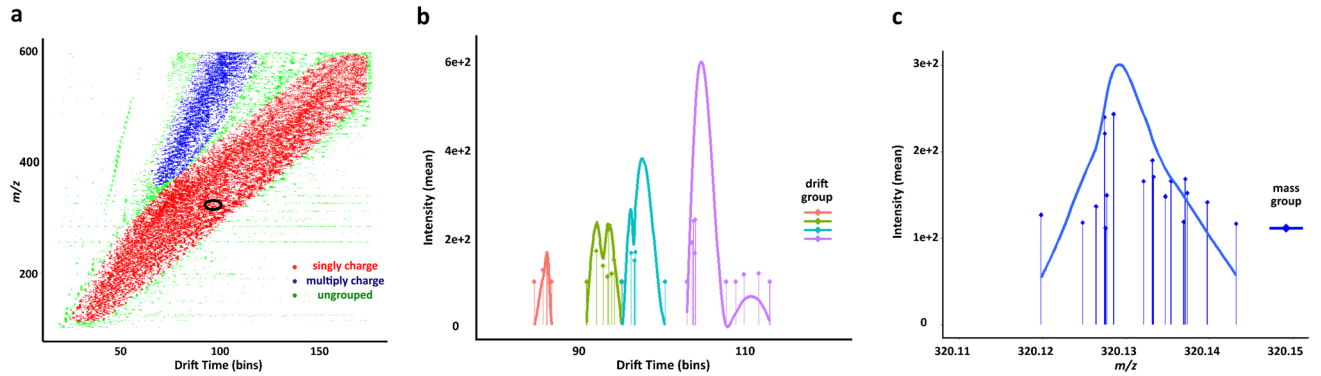

Fig. 3 Ion mobility mass spectrometry for in situ small-molecule separation of isomeric compound (auxinole and 4pTb-MeIAA) cotreated *Arabidopsis* samples. **a** Visualization of drift time plotting of singly and multiply charged ions acquired from DESI-IM-MSI, targeted isomeric compounds (AWM 320.1273) are circled. **b** Drift time of isomer peaks identified inside the same peak group and **c** peak grouping using *m/z* value only

Table 2 Drifting ion peak groups containing targeted compounds in the DESI-IM-MSI analysis of isomer cotreated *Arabidopsis* samples

Standard mass[1]	Group AWM[2]	Minimum *m/z*	Maximum *m/z*	Mass range (R)[2]	Minimum drift time	Maximum drift time	Gap of drift time[3]
320.1288	320.1273	320.1239	320.1310	0.0071	68.6	103.4	34.8
435.1578	435.1589	435.1501	435.1670	0.0017	81.2	146.0	64.8
449.1763	449.1767	449.1670	449.1856	0.0019	84.9	140.9	56.0
306.1078	306.1113	306.1048	306.1162	0.0118	65.0	99.9	34.9
174.0516	174.0530	174.0457	174.0643	0.0186	50.9	57.7	6.8
190.0491	190.0467	190.0426	190.0507	0.0081	54.1	58.4	4.2
289.0740	289.0736	289.0704	289.0770	0.0066	80.7	86.2	5.5
303.0993	303.0995	303.0973	303.1013	0.0040	87.1	87.6	0.5
305.0757	305.0701	305.0647	305.0760	0.0113	60.8	85.3	24.5
319.1009	319.1059	319.1004	319.1085	0.0081	66.5	111.0	44.5
352.1111	352.1110	352.1081	352.1134	0.0053	67.5	102.7	35.2

[1]The standard mass of targeted compounds was acquired from the measurement of 1 pmol/µL standard directly infusion into DESI source

[2]Abundant weight mean (AWM) and mass range (R) of each peak group was calculated according to peak mass distribution using *in house* R script

[3]Drift time gaps were used to identify peak groups the presenting isomeric ions

Visualization of synthetic auxin derivatives and endogenous auxins

Split media has been used for decades to study long- and short-distance transport and signalling in plants [23, 31, 32]. Aiming to characterize targeted isomers within a plant, bottom parts of *Arabidopsis* roots were cultivated in an agar medium containing auxinole and 4pTb-MeIAA for 24 h to ensure their uptake, transport and metabolism. The primary roots and hypocotyls of samples were scanned with 90-µm spatial resolution. Established drifting ion intensity maps were co-registered with optical images of sample slides *via* HDImaging (Waters). The spatial distribution of auxinole, its isomer 4pTb-MeIAA and endogenous IAA from the representative sample is displayed in Fig. 4. In situ measured drift times and calculated CCS values of the analytes are also shown. In treated plants, drift peaks at AWM 320.1273, dt 103.2 matched auxinole standard drift time and were only displayed in the lower half of the primary root grown in auxinole-treated and auxinole + 4pTb-MeIAA cotreated medium, which is in agreement with our previously published findings [23]. As anticipated, auxinole drifting ion peaks were not detected in the roots and hypocotyls harvested from control and 4pTb-MeIAA-treated plants (Fig. 4a). Although isomeric target 4pTb-MeIAA was grouped with auxinole in the same molecular weight, 4pTb-MeIAA (dt 95.2) signal was present not only at the bottom part of the primary root but also in the upper

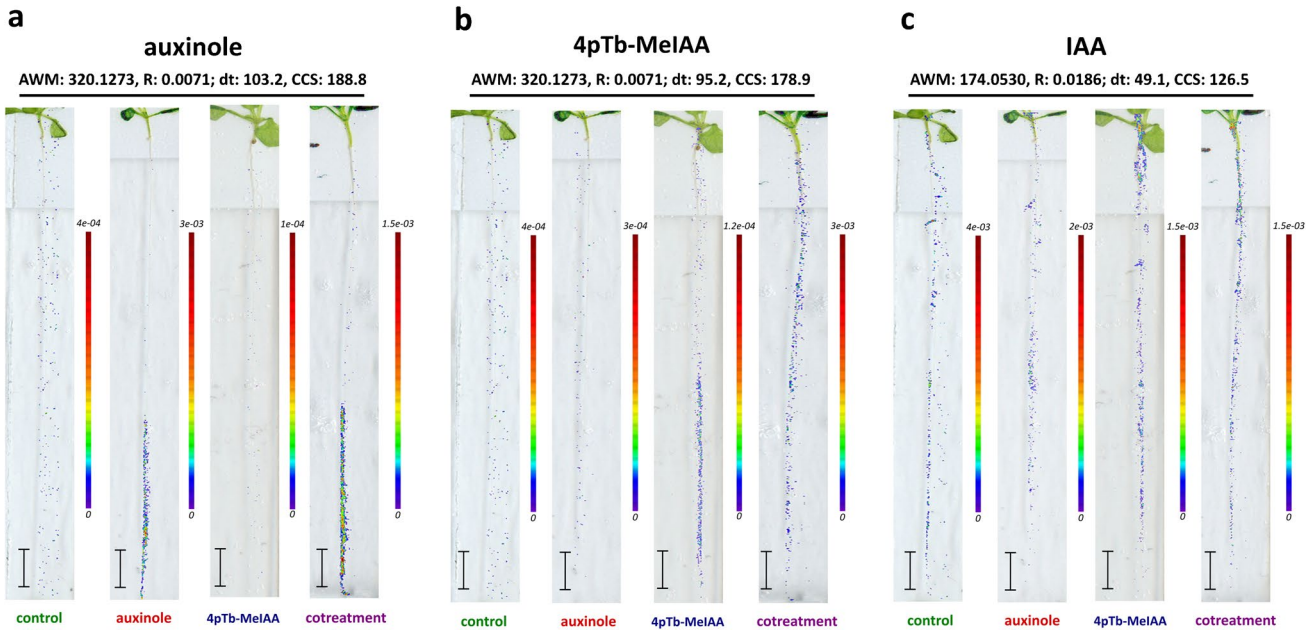

Fig. 4 Drift ion intensity maps of auxinole, its isomer 4pTb-MeIAA and endogenous IAA in 24-h treated *Arabidopsis* using DESI-IM-MSI. The AWM (Da), R (Da), dt (bin) and CCS (Å^2) of target ions are also shown. **a** Spatial distribution of auxinole ions in the primary root of 10-µM auxinole-treated and 10 µM auxinole + 10 µM 4pTb-MeIAA cotreated samples. **b** Spatial distribution of 4pTb-MeIAA ions in root and hypocotyl of 10 µM 4pTb-MeIAA-treated and 10 µM auxinole + 10 µM 4pTb-MeIAA cotreated samples. **c** Endogenous IAA ion distribution in control, 10 µM auxinole, 10 µM 4pTb-MeIAA and 10 µM auxinole + 10 µM 4pTb-MeIAA-treated plant samples. Scale bar = 5 mm

part of root and hypocotyl (Fig. 4b), suggesting that unlike auxinole, it is transported to the upper parts of the plant. The higher abundance of 4pTb-MeIAA peaks in the upper root and hypocotyl was also found in auxinole + 4pTb-MeIAA cotreated samples, which might be influenced by auxinole overaccumulation in the lower parts of the root, in turn resulting in a substantial amount of 4pTb-MeIAA to be transported and/or passively diffused to the upper parts of the plant. Peaks of endogenous phytohormone IAA (assigned as AWM 174.0530) were also found in the primary root of *Arabidopsis* samples (Fig. 4c). Distinct spatial distributions of auxinole and its isomer 4pTb-MeIAA were repeatedly observed in triplicated experiments that indicated their unique and independent movement within cotreated *Arabidopsis* plants (Fig. S2).

Metabolite visualization

To investigate whether synthetic auxin derivatives, auxinole and 4pTb-MeIAA, could be potentially metabolized in 24-h treated *Arabidopsis* plants, unlabelled auxinole-Asp, auxinole-Glu and 4pTb-IAA standards were synthesized as predicted conjugation and hydrolysis products. In situ visualization of predicted metabolites in DESI-IM-MSI was performed using peak groups containing their standard masses which were used to establish drifting ion intensity maps in 10 µM auxinole or 10 µM 4pTb-MeIAA-treated and 10 µM auxinole + 10 µM 4pTb-MeIAA cotreated samples. Furthermore, peaks assigned as amino acid-conjugated analogues, auxinole-Asp (AWM 435.1589; dt 131.2) and auxinole-Glu (AWM 449.1767; dt 141.0) were highlighted in the entire primary root from root tip to mature region after auxinole feeding; a similar distribution was also reported in the cotreated plant sample (Fig. 5a, b), revealing that while auxinole does not get transported to the upper plant parts, after conjugation with amino acids, it can be observed throughout the entire root. The hydrolysed product of 4pTb-MeIAA, namely, 4pTb-IAA (*m/z* 306.1113; dt 99.6), showed a high-intensity level across the acquired region from root tip to hypocotyl, analogously to its precursor, in 4pTb-MeIAA-treated plants. On the other hand, 4pTb-IAA peaks were barely detectable in the upper plant when cultivated together with auxinole (Fig. 5c).

Using infusion standards, primary and secondary metabolites of endogenous IAA, namely, oxIAA, IAA-Asp, IAA-Glu, oxIAA-Asp, oxIAA-Glu and oxIAA-Glc, were also separated from unrelated isomeric background peaks and established into drift ion intensity maps. IAA metabolites showed different distribution in *Arabidopsis* root and hypocotyl (Fig. 6). For instance, oxIAA (AWM 190.0467, dt 53.4) demonstrated a relatively high-intensity level in both, hypocotyl and primary root of control and auxinole-treated

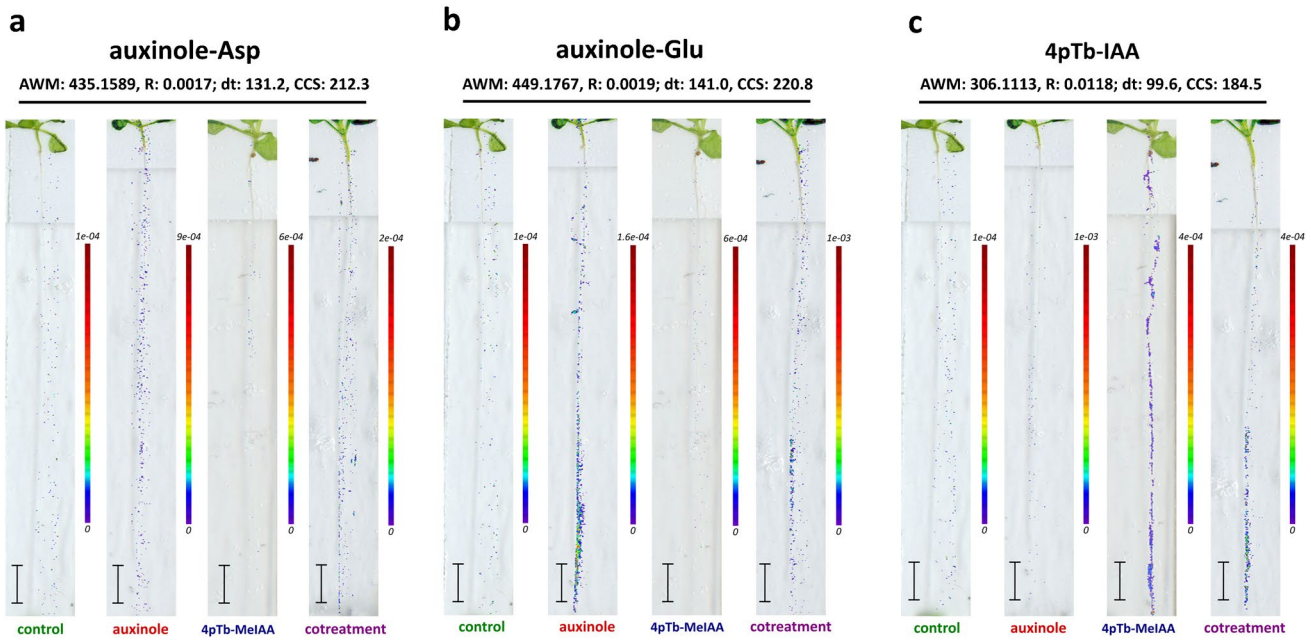

Fig. 5 In situ visualization of predicted auxin derivative modifications from auxinole and 4pTb-MeIAA-treated and cotreated samples. Spatial distributions of auxinole-related metabolites, **a** auxinole-Asp, **b** auxinole-Glu and 4pTb-MeIAA hydrolysed product **c** 4pTb-IAA are revealed by DESI-IM-MSI analysis of 10-µM auxinole-treated and 10 µM auxinole + 10 µM 4pTb-MeIAA cotreated samples. Scale bar = 5 mm. Their AWM (Da), R (Da), dt (bin) and CCS (Å^2) of target ions are also shown

plants, in contrast to very low signal in the hypocotyls collected from 4pTb-MeIAA-treated and auxinole + 4pTb-MeIAA cotreated plants (Fig. 6a). In case of auxin metabolites, namely, IAA-Asp, IAA-Glu, oxIAA-Asp, oxIAA-Glu and oxIAA-Glc (AWM of 289.0736, 303.0995, 305.0701, 319.1059 and 352.1110 and drift time 79.7, 90.4, 88.1, 93.2 and 101.0, respectively), their peaks were widely present in primary roots of untreated *Arabidopsis*, but their intensity levels were significantly decreased in comparison to control plants (Fig. 6c–f). Chemical inhibition of the auxin inactivation pathway was reported for kakeimide (KKI), which specifically inhibits auxin-conjugating GH3 enzymes [33]. It is yet to be investigated if auxinole and/or 4pTb-MeIAA to some extent possess such effect. Drifting ion intensity maps of replicate samples are shown in Figure S2.

Overall, the application of IM on DESI-MSI analysis provided an additional dimension to separate both synthetic isomers and auxin metabolites from the interferences of endogenous compounds and background peaks, while the presence of drift time and CCS values of detected molecules provides confident molecular identifications in the MSI data.

In situ IM-MS/MS validation

To validate the drifting ions of auxinole, 4pTb-MeIAA and their metabolites detected in DESI-IM-MSI analysis, ion mobility separated ions were further sent to tandem MS/MS for the precursor ion fragmentation and drifting tube separation, which allows to distinguish low-intensity fragmentation ions from isomeric backgrounds. In situ DESI-IM-MS/MS was carried out on the treated plant samples, and the collision energy was optimized as described above. The AWM 320.1273 was manually picked as the common in situ parent mass of both isomeric compounds, yet their precursor ions could be separated in the IM-MS/MS *via* their drift times of fragmentation ions. The collision energy of the two isomers was optimized at 15 eV; both precursor ions of auxinole (dt 104.0) and 4pTb-MeIAA (dt 95.0) as well as their respective fragmentation ions could be observed in the in situ IM-MS/MS spectrum acquired from cotreated samples. Ions of *m/z* 116.05 ± 0.1 Da (dt 37.5 ± 1 bin), assigned as deprotonated indole group, were detected in MS/MS spectra of auxinole-treated *Arabidopsis* roots (Fig. 7a, c). Other fragmentation peaks, such as the *m/z* 276.15 ± 0.1 Da and *m/z* 147.08 ± 0.1 Da, were also detected in IM-MS/MS analysis. The *p*-acetyl toluene fragment (*m/z* 133.06 ± 0.1 Da; dt 45.4 ± 1 bin) was identified as the unique fragmentation ion in the MS/MS spectra of 4pTb-MeIAA-treated samples (Fig. 7b). Although drifting ions of *p*-acetyl toluene displayed lower intensities than auxinole fragments in the cotreated samples, they could still be detected from fragmentation products of 4pTb-MeIAA using unique drift time (Fig. 7c). Detected masses of predicted metabolites were also validated using the in situ IM-MS/MS with collision energy optimized in

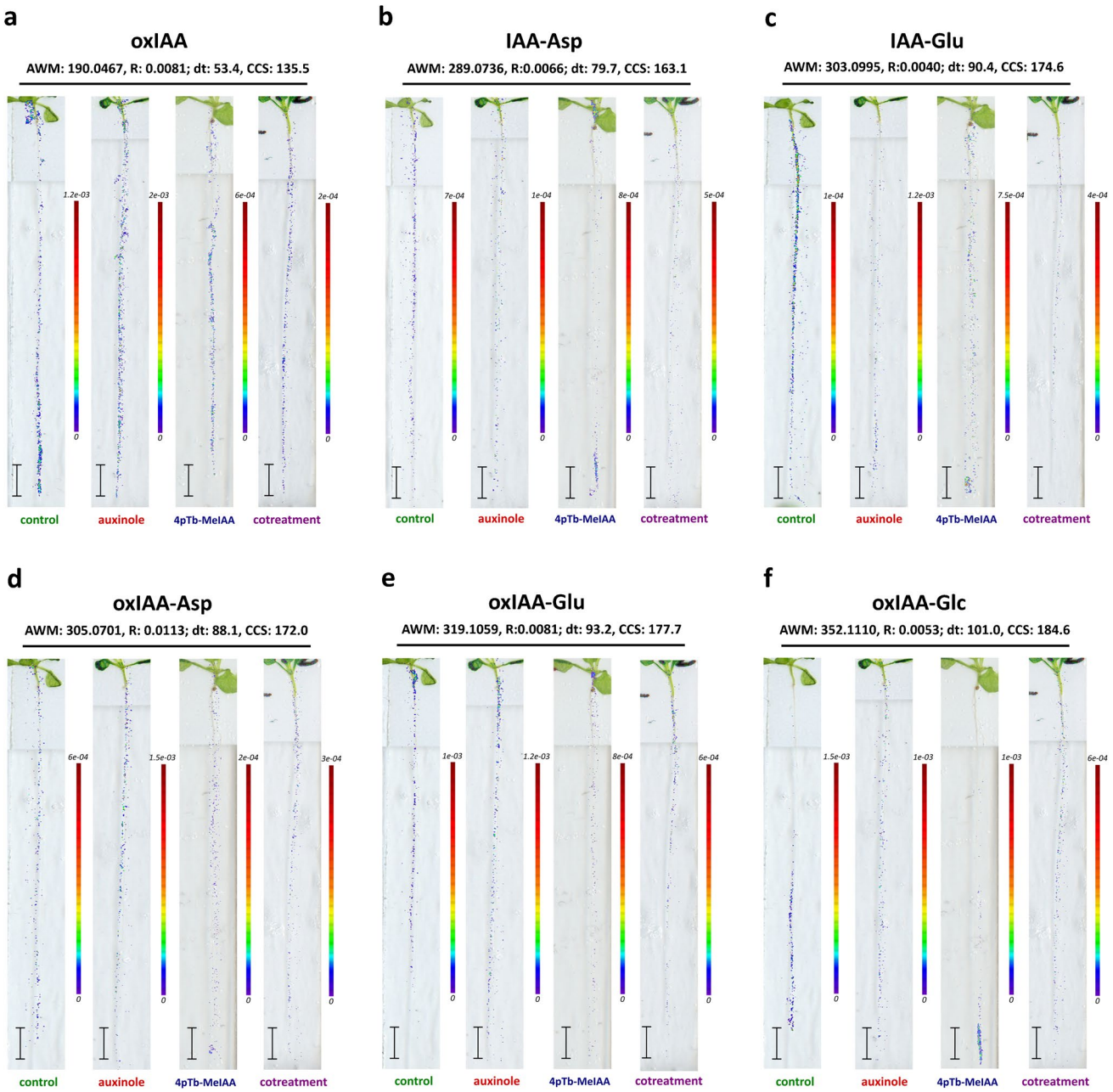

Fig. 6 Spatial distributions of primary and secondary IAA metabolites revealed by DESI-IM-MSI analysis of auxinole, 4pTb-MeIAA and auxinole + 4pTb-MeIAA cotreated *Arabidopsis*. Peaks assigned as **a** oxIAA, **b** IAA-Asp, **c** IAA-Glu, **d** oxIAA-Asp, **e** oxIAA-Glu and **f** oxIAA-Glc standard profiles are shown with their AWM (Da), R (Da), drift time (bin) and CCSs ($Å^2$) in all four types of plant treatments. Scale bar = 5 mm

standard infusion. The indole group (*m/z* 116.05 ± 0.1 Da; dt 37.5 ± 1 bin), as a common fragmentation product of auxinole-Asp, auxinole-Glu and 4pTb-IAA, could be detected in their spectra acquired from auxinole and 4pTb-MeIAA cotreated *Arabidopsis* samples (Fig. 8a–c). Besides, unique fragmentation ions matching aspartate (*m/z* 131.1163; dt 42.0), glutamate (*m/z* 146.1020; dt 42.30) and 4pTb-IAA decarboxylated residue (*m/z* 262.1319, dt 85.4) were also detected. Precursor ions of IAA and its metabolites were selected and submitted to in situ IM-MS/MS for validation; spectra of their drift ion and major product ions are shown in Figure S3. In comparison with classical MSI, very low signal intensities of synthetic compound fragmentation ions were observed after filtering with an IM trap, which made it impossible to collect enough peaks for imaging establishment.

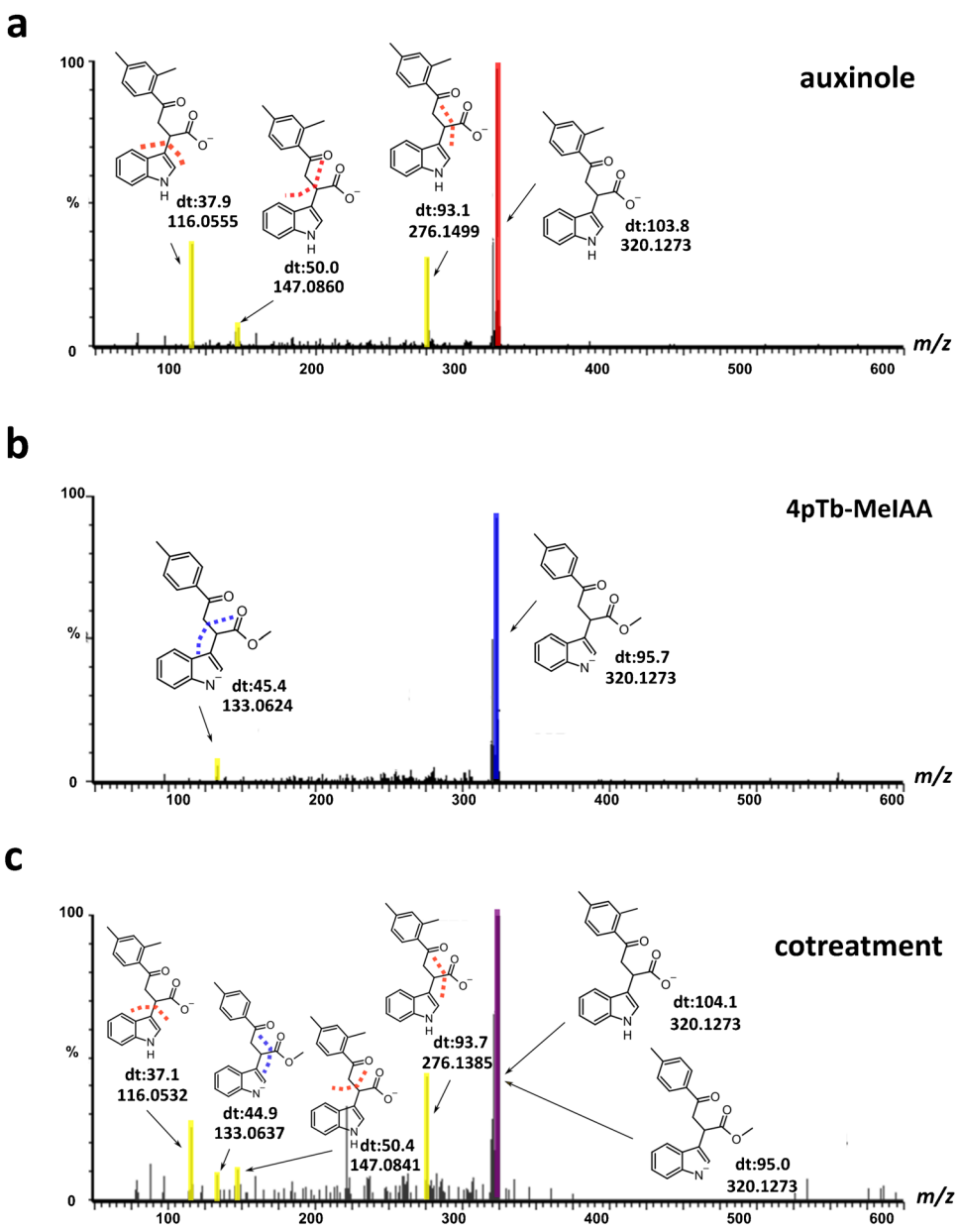

Fig. 7 In situ DESI-IM-MS/MS spectra of auxinole and 4pTb-MeIAA from treated *Arabidopsis* sample roots. **a** Fragmentation spectrum of targeted mass *m/z* 320.1273 in 10-µM auxinole-treated root. **b** IM-MS/MS spectrum of targeted mass *m/z* 320.1273 in 10 µM 4pTb-MeIAA-treated root. **c** IM-MS/MS spectrum of common precursor mass *m/z* 320.1273 of two isomeric compounds (dt 104.0 as auxinole and dt 95.0 as 4pTb-MeIAA) in the cotreated root

Target evaluation using DESI-IM-MSI and LC-MS

To evaluate the abundance changes of synthetic and endogenous compounds established using DESI-IM-MSI, classical LC-MS analysis was performed as a quantification reference on root and hypocotyl samples of auxinole and 4pTb-MeIAA treated and cotreated *Arabidopsis* plants. Compound abundances calculated from MSI results were processed with drift time and intensity thresholds and averaged from group-wide intensities (TIC normalized) collected from all data points in the *in house* R script. The LC-MS analysis method was modified from the published protocols, and intensities of target analytes were summarized from the peak area under curve (AUC) in liquid chromatography [27, 28]. Sample quantification results were further compared using Student's *t*-test to determine whether targeted abundances among four sample groups (control *vs* 10 µM auxinole, 10 µM 4pTb-MeIAA and 10 µM auxinole + 10 µM 4pTb-MeIAA) were different with and without drift time filtering (Fig. 9a). In DESI-IM-MSI results of TIC intensity quantification of isomeric auxin derivatives (*m/z* 320.1273), peak intensities acquired from auxinole (dt 103.2) and 4pTb-MeIAA (dt 95.2) were convoluted together. Drift time filtering allowed the discrimination of targeted ions generated from two isomeric derivates and endogenous compounds. In contrast to similar amount of auxinole in both treated and cotreated samples, a significant decrease of 4pTb-MeIAA intake was detected in plants once cotreated with auxinole (Fig. 9b). In

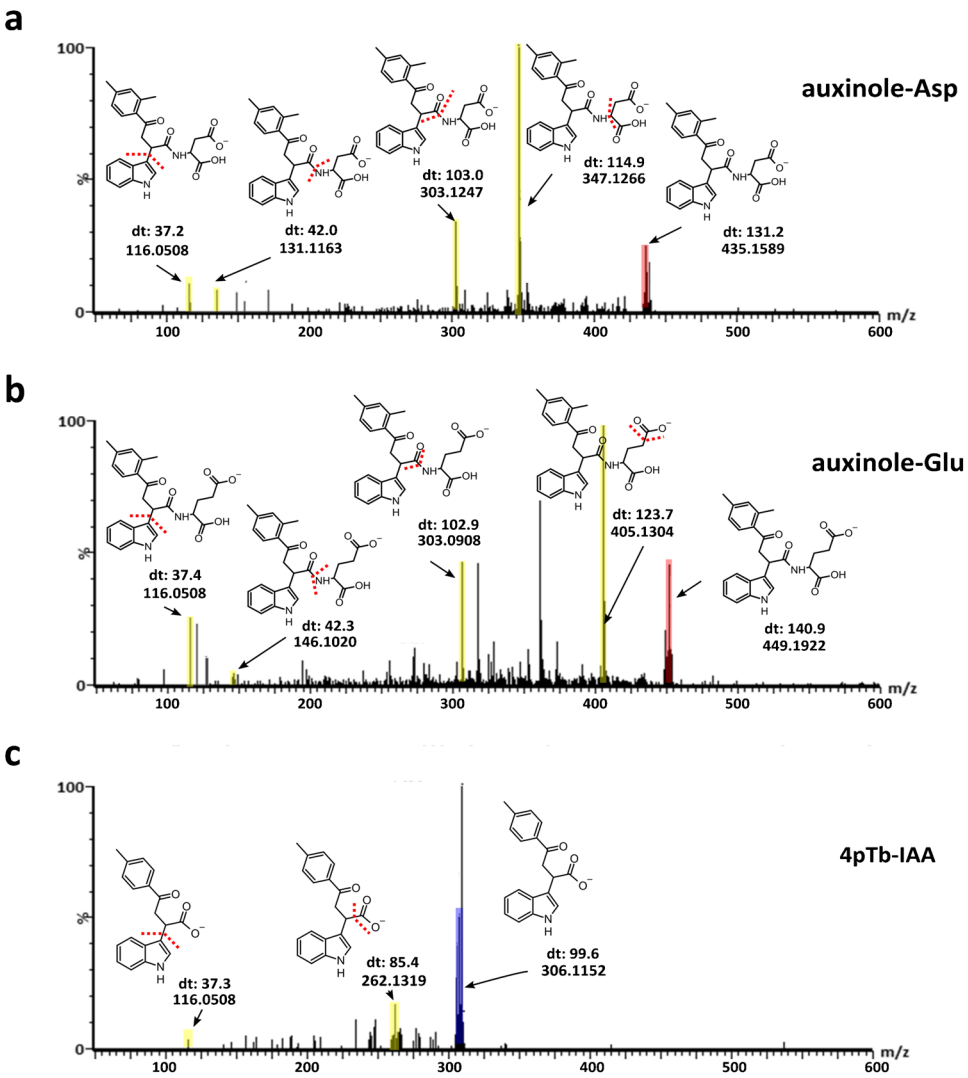

Fig. 8 In situ DESI-IM-MS/MS spectra of auxinole and 4pTb-MeIAA metabolites from cotreated *Arabidopsis* sample roots. DESI-IM-MS analysis of **a** auxinole-Asp, **b** auxinole-Glu and **c** 4pTb-IAA, from auxinole and 4pTb-MeIAA-treated and cotreated samples reveals their common and unique fragmentation ions from 24-h cotreatment

the LC-MS analysis, an average auxinole AUC intensity of 91.72 ± 35.35 was detected from 10-µM auxinole-treated samples and 113.18 ± 32.35 from 10 µM auxinole + 10 µM 4pTb-MeIAA cotreated samples (Fig. 9c). A higher AUC intensity level of 4pTb-MeIAA (41.52 ± 21.15) was detected in 10 µM 4pTb-MeIAA-treated samples, while its intensity was roughly 26.30 ± 8.77 in the cotreated samples. Besides synthetic isomers, all targeted auxin metabolites were quantified in LC-MS analysis (Table S4). IAA was further interrogated for tissue-wise abundance in auxinole and 4pTb-MeIAA treated and cotreated samples. As anticipated, unfiltered DESI-MSI results misevaluated abundance of targeted analytes within plant samples (Fig. 9a). On the other hand, analysis using DESI-IM-MSI with drift time selection demonstrated high compatibility with the AUC intensities using highly sensitive LC-MS method (Fig. 9b, c). Moreover, quantification of endogenous auxin metabolites in response to isomeric compound treatment and cotreatment by both classical LC-MS and DESI-IM-MSI analysis is shown in Figure S4. Upon filtering grouped peaks acquired from ambient DESI source using standard drift time, DESI-IM-MSI provided robust evaluation of low-abundant small molecules from heterogeneous plant tissues, comparable to the classical quantification approach LC-MS (Fig. 9).

Conclusion

Ambient DESI-MSI, which offers easy sample preparation and high-throughput analysis, has been employed in numerous studies as a tool to reveal spatial distribution of both known and unknown compounds. Currently, accurate identification of low-abundant compounds in DESI-MSI is convoluted by low quality of MS/MS fragmentation [25]. Besides, MSI typically utilizes only mass-to-charge ratio for analyte visualization, while in situ validation using MS/MS imaging is challenged when studying derivatives with similar molecular backbones leading to the same fragmentation

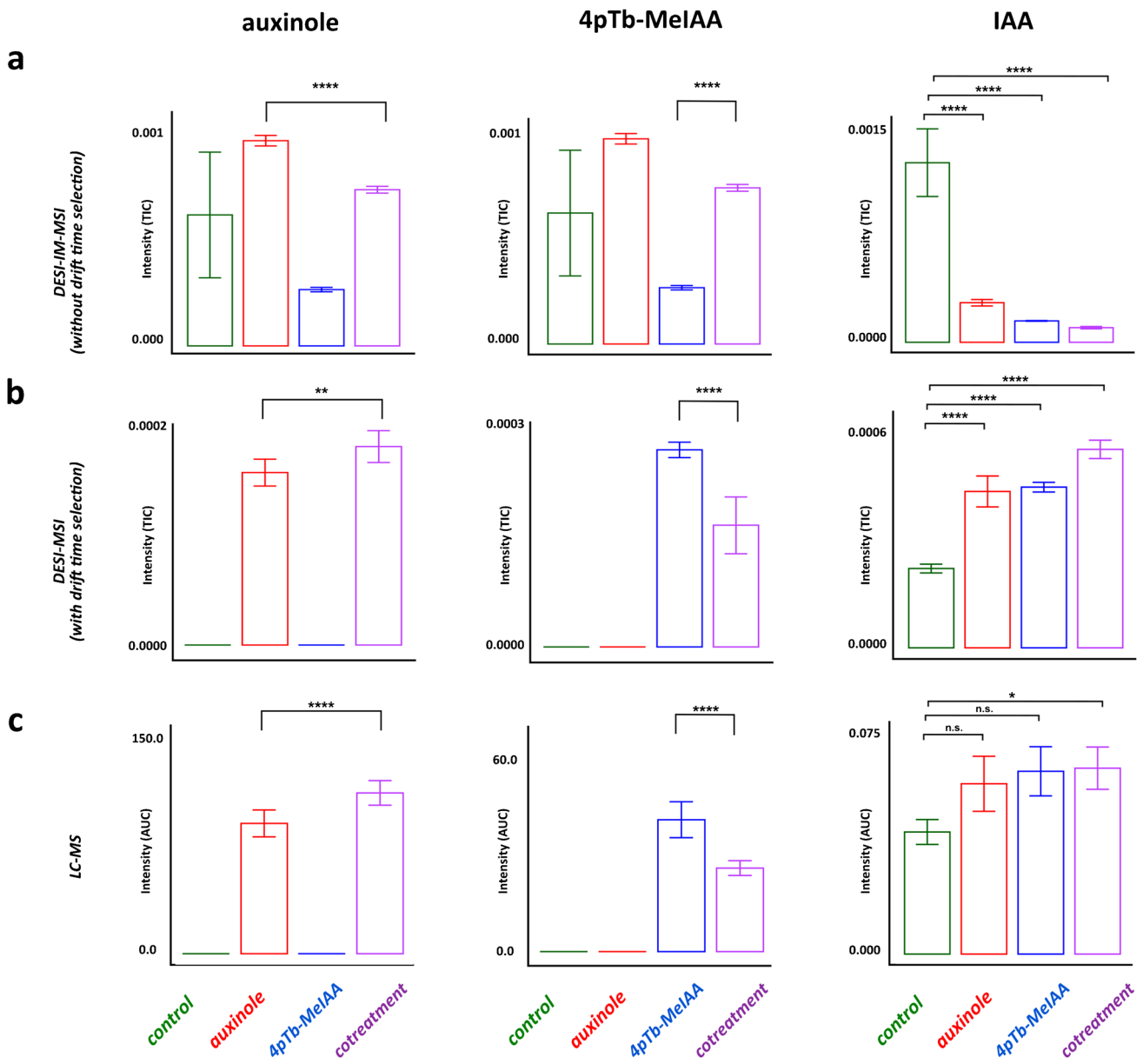

Fig. 9 Mass spectrometry analysis of auxinole and 4pTb-MeIAA abundance in control compared to 10 µM auxinole, 10 µM 4pTb-MeIAA and 10 µM auxinole + 10 µM 4pTb-MeIAA cotreated samples. **a** Boxplots of unfiltered auxinole and 4pTb-MeIAA intensities using all unfiltered DESI-MSI data points collected from triplicated experiments. **b** Evaluation of isomeric compound intensities using selected mass group processed from triplicated DESI-IM-MSI analysis. **c** Quantification of isomeric auxin derivatives and IAA using AUC intensities from parallel LC-MS analysis of control and treated *Arabidopsis* ($n = 5$). n.s. not significant, $*p \leq 0.05$, $**p \leq 0.01$, $***p \leq 0.001$, $****p \leq 0.001$

products. Therefore, it is almost impossible to establish correct spatial distribution of isomeric compounds without the assistance of additional analytical parameters. On the other hand, rapid IM analysis, which separates ions in milliseconds, makes coupling with DESI-MSI technology possible for in situ isomer imaging and identification.

To the best of our knowledge, we are for the first time presenting visualization of two isomeric auxin derivatives and endogenous auxins from cotreated plants using ion mobility coupled DESI-MSI. In this proof of concept analysis, DESI-IM-MSI was utilized to reveal unique distributions of auxinole and 4pTb-MeIAA in *Arabidopsis* upon individual and combined treatment (Fig. 4). Furthermore, we provide direct evidence of *in planta* metabolism of targeted derivatives to auxinole-Asp, auxinole-Glu and 4pTb-IAA, after 24-h treatment.

In summary, our study reveals the unique advantages of in situ low-molecular-weight isomeric compound separation,

CCS value-aided metabolite identification and improved target evaluation using IM coupled ambient DESI-MSI. Besides, DESI-IM-MSI enables high spatial resolution imaging of endogenous and exogenous compounds from small plant tissue such as *Arabidopsis* root and hypocotyl which does not require complex sample preparation. These advances allow further monitoring of isomeric compounds and their metabolites from the same plant sample in a single run.

Supplementary Information The online version contains supplementary material available at https://doi.org/10.1007/s00216-023-04996-x.

Acknowledgements The authors are thankful to Tomáš Pospíšil for valuable scientific discussions and Alexander Muck from Analytical Professional Services Group (Waters Corporation) for technical solutions.

Author contribution C.Z.: conceptualization; methodology; investigation; software; visualization; and writing, original draft. K.B.: investigation and formal analysis. A.Ž.: investigation; formal analysis; visualization; and writing, review and editing. P.H.: investigation and formal analysis. J.G.: resources. O.N.: funding acquisition; supervision; and writing, review and editing. K.D.: funding acquisition; supervision; and writing, review and editing.

Funding This work was supported by the Internal Grant Agency of Palacký University Olomouc (IGA_PrF_2023_016, IGA_PrF_2023_031).

Data availability The data that supports the findings of this study are available from the corresponding author upon reasonable request.

Code availability Not applicable.

Declarations

Ethics approval Not applicable.

Statement on animal welfare Not applicable.

Source of biological material Not applicable.

Consent to participate Not applicable.

Consent for publication Not applicable.

Conflict of interest The authors declare no competing interests.

References

1. Davies PJ. The plant hormones: their nature, occurrence, and functions. In: Davies PJ, editor. Plant hormones: biosynthesis, signal transduction, action! Dordrecht: Springer Netherlands; 2010. p. 1-15.
2. Jiang K, Asami T. Chemical regulators of plant hormones and their applications in basic research and agriculture. Biosci Biotechnol Biochem. 2018;82(8):1265–300. https://doi.org/10.1080/09168451.2018.1462693.
3. Prusinska J, Uzunova V, Schmitzer P, Weimer M, Bell J, Napier RM. The differential binding and biological efficacy of auxin herbicides. Pest Manag Sci. 2023;79(4):1305–15. https://doi.org/10.1002/ps.7294.
4. Nambara E, Van Wees SCM. Plant hormone functions and interactions in biological systems. Plant J. 2021;105(2):287–9. https://doi.org/10.1111/tpj.15151.
5. Pokorná E, Hluska T, Galuszka P, Hallmark HT, Dobrev PI, Záveská Drábková L, et al. Cytokinin N-glucosides: occurrence, metabolism and biological activities in plants. Biomolecules. 2021;11(1):24. https://doi.org/10.3390/biom11010024.
6. Balarynová J, Klčová B, Tarkowská D, Turečková V, Trněný O, Špundová M, et al. Domestication has altered the ABA and gibberellin profiles in developing pea seeds. Planta. 2023;258(2):25. https://doi.org/10.1007/s00425-023-04184-2.
7. Hayashi K-i, Arai K, Aoi Y, Tanaka Y, Hira H, Guo R, et al. The main oxidative inactivation pathway of the plant hormone auxin. Nat Commun. 2021;12(1):6752. https://doi.org/10.1038/s41467-021-27020-1.
8. Brunoni F, Pěnčík A, Žukauskaitė A, Ament A, Kopečná M, Collani S, et al. Amino acid conjugation of oxIAA is a secondary metabolic regulation involved in auxin homeostasis. New Phytol. 2023;238(6):2264–70. https://doi.org/10.1111/nph.18887.
9. Hayashi K, Neve J, Hirose M, Kuboki A, Shimada Y, Kepinski S, et al. Rational design of an auxin antagonist of the SCF(TIR1) auxin receptor complex. ACS Chem Biol. 2012;7(3):590–8. https://doi.org/10.1021/cb200404c.
10. Isoda R, Yoshinari A, Ishikawa Y, Sadoine M, Simon R, Frommer WB, et al. Sensors for the quantification, localization and analysis of the dynamics of plant hormones. Plant J. 2021;105(2):542–57. https://doi.org/10.1111/tpj.15096.
11. Wells DM, Laplaze L, Bennett MJ, Vernoux T. Biosensors for phytohormone quantification: challenges, solutions, and opportunities. Trends Plant Sci. 2013;18(5):244–9. https://doi.org/10.1016/j.tplants.2012.12.005.
12. Gika HG, Theodoridis GA, Plumb RS, Wilson ID. Current practice of liquid chromatography–mass spectrometry in metabolomics and metabonomics. J Pharm Biomed Anal. 2014;87:12–25. https://doi.org/10.1016/j.jpba.2013.06.032.
13. Durgbanshi A, Arbona V, Pozo O, Miersch O, Sancho JV, Gómez-Cadenas A. Simultaneous determination of multiple phytohormones in plant extracts by liquid chromatography–electrospray tandem mass spectrometry. J Agric Food Chem. 2005;53(22):8437–42. https://doi.org/10.1021/jf050884b.
14. Skalický V, Antoniadi I, Pěnčík A, Chamrád I, Lenobel R, Kubeš MF, et al. Fluorescence-activated multi-organelle mapping of subcellular plant hormone distribution. Plant J. 2023;n/a(n/a). https://doi.org/10.1111/tpj.16456.
15. Široká J, Brunoni F, Pěnčík A, Mik V, Žukauskaitė A, Strnad M, et al. High-throughput interspecies profiling of acidic plant hormones using miniaturised sample processing. Plant Methods. 2022;18(1):122. https://doi.org/10.1186/s13007-022-00954-3.
16. Urbanová T, Tarkowská D, Novák O, Hedden P, Strnad M. Analysis of gibberellins as free acids by ultra performance liquid chromatography–tandem mass spectrometry. Talanta. 2013;112:85–94. https://doi.org/10.1016/j.talanta.2013.03.068.
17. Šimura J, Antoniadi I, Široká J, Tarkowská De, Strnad M, Ljung K, et al. Plant hormonomics: multiple phytohormone profiling by targeted metabolomics. Plant Physiol. 2018;177(2):476–89. https://doi.org/10.1104/pp.18.00293.
18. Včelařová L, Skalický V, Chamrád I, Lenobel R, Kubeš MF, Pěnčík A, et al. Auxin metabolome profiling in the Arabidopsis endoplasmic reticulum using an optimised organelle isolation protocol. Int J Mol Sci. 2021;22(17):9370. https://doi.org/10.3390/ijms22179370.
19. Yan Z, Maher N, Torres R, Cotto C, Hastings B, Dasgupta M, et al. Isobaric metabolite interferences and the requirement for

close examination of raw data in addition to stringent chromatographic separations in liquid chromatography/tandem mass spectrometric analysis of drugs in biological matrix. Rapid Commun Mass Spectrom RCM. 2008;22(13):2021–8. https://doi.org/10.1002/rcm.3577.
20. Boughton BA, Thinagaran D, Sarabia D, Bacic A, Roessner U. Mass spectrometry imaging for plant biology: a review. Phytochem Rev. 2016;15(3):445–88. https://doi.org/10.1007/s11101-015-9440-2.
21. Bjarnholt N, Li B, D'Alvise J, Janfelt C. Mass spectrometry imaging of plant metabolites – principles and possibilities. Nat Prod Rep. 2014;31(6):818–37. https://doi.org/10.1039/C3NP70100J.
22. Parrot D, Papazian S, Foil D, Tasdemir D. Imaging the unimaginable: desorption electrospray ionization – imaging mass spectrometry (DESI-IMS) in natural product research. Planta Med. 2018;84(09/10):584–93. https://doi.org/10.1055/s-0044-100188.
23. Žukauskaitė A, Saiz-Fernández I, Bieleszová K, Iškauskienė M, Zhang C, Smýkalová I, et al. New PEO-IAA-inspired anti-auxins: synthesis, biological activity, and possible application in hemp (Cannabis sativa L.) Micropropagation. J Plant Growth Regul. 2023. https://doi.org/10.1007/s00344-023-11031-x.
24. Kanu AB, Dwivedi P, Tam M, Matz L, Hill HH Jr. Ion mobility–mass spectrometry. J Mass Spectrom. 2008;43(1):1–22. https://doi.org/10.1002/jms.1383.
25. Hou J, Zhang Z, Zhang L, Wu W, Huang Y, Jia Z, et al. Spatial lipidomics of eight edible nuts by desorption electrospray ionization with ion mobility mass spectrometry imaging. Food Chem. 2022;371: 130893. https://doi.org/10.1016/j.foodchem.2021.130893.
26. Hinnenkamp V, Klein J, Meckelmann SW, Balsaa P, Schmidt TC, Schmitz OJ. Comparison of CCS values determined by traveling wave ion mobility mass spectrometry and drift tube ion mobility mass spectrometry. Anal Chem. 2018;90(20):12042–50. https://doi.org/10.1021/acs.analchem.8b02711.
27. Pěnčík A, Casanova-Sáez R, Pilařová V, Žukauskaitė A, Pinto R, Micol JL, et al. Ultra-rapid auxin metabolite profiling for high-throughput mutant screening in Arabidopsis. J Exp Bot. 2018;69(10):2569–79. https://doi.org/10.1093/jxb/ery084.
28. Hladík P, Petřík I, Žukauskaitė A, Novák O, Pěnčík A. Metabolic profiles of 2-oxindole-3-acetyl-amino acid conjugates differ in various plant species. Front Plant Sci. 2023;14:1217421. https://doi.org/10.3389/fpls.2023.1217421.
29. Guo R, Zhou L, Chen X. Desorption electrospray ionization (DESI) source coupling ion mobility mass spectrometry for imaging fluoropezil (DC20) distribution in rat brain. Anal Bioanal Chem. 2021;413(23):5835–47. https://doi.org/10.1007/s00216-021-03563-6.
30. Hahsler M, Piekenbrock M, Doran D. dbscan: fast density-based clustering with R. J Stat Softw. 2019;91(1):1–30. https://doi.org/10.18637/jss.v091.i01.
31. Yu B, Zheng W, Persson S, Zhao Y. Protocol for analyzing root halotropism using split-agar system in Arabidopsis thaliana. STAR Protoc. 2023;4(2): 102157. https://doi.org/10.1016/j.xpro.2023.102157.
32. Saiz-Fernández I, Černý M, Skalák J, Brzobohatý B. Split-root systems: detailed methodology, alternative applications, and implications at leaf proteome level. Plant Methods. 2021;17:1–19. https://doi.org/10.1186/s13007-020-00706-1.
33. Fukui K, Arai K, Tanaka Y, Aoi Y, Kukshal V, Jez JM, et al. Chemical inhibition of the auxin inactivation pathway uncovers the roles of metabolic turnover in auxin homeostasis. Proc Natl Acad Sci. 2022;119(32):e2206869119. https://doi.org/10.1073/pnas.2206869119.

Chao Zhang is a junior researcher at the Laboratory of Growth Regulators, Faculty of Science, Palacký University Olomouc. His research mainly focuses on developing mass spectrometry imaging methods for high-resolution analysis and related applications in hormonomics, metabolomics, lipidomics and proteomics.

Kristýna Bieleszová is a Ph.D. student in experimental biology at the Faculty of Science, Palacký University Olomouc. Her work is focused on the synthesis of new auxin derivatives and evaluation of their biological activity.

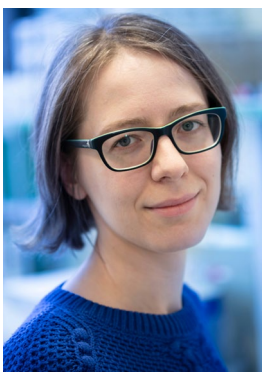

Asta Žukauskaitė is a leader of application-oriented organic synthesis group at the Department of Chemical Biology, Faculty of Science, Palacký University Olomouc. Her primary research focus is on the synthesis and application of phytohormones, particularly auxins. This encompasses the synthesis of both, their known and putative metabolites, the creation of synthetic derivatives and the investigation of their biological functions and practical implications.

Pavel Hladík is a Ph.D. student at University Palacký Olomouc in Prof. Ondřej Novák's group. His research focuses on the identification of novel auxin metabolites and the exploration of metabolic pathways operating at both the organ and cellular levels in plants. Another part of his work is the development of LC–MS methods tailored for synthesized auxin-like compounds.

Jiri Gruz is an assistant professor at the Department of Experimental Biology at Palacký University Olomouc, Czech Republic. His research interests focus on metabolomics, pharmacognosy and the discovery of biologically active compounds.

Ondřej Novák is currently a professor at the Faculty of Science of the Palacký University Olomouc and a senior researcher at the Institute of Experimental Botany of the Czech Academy of Sciences. His research is focused on the study of the metabolism of biologically active compounds (e.g. plant hormones) and the discovery of their role in plant growth and development using biochemical and molecular biological tools. He also has experience with modern analytical techniques, such as new miniaturized isolation and purification protocols or the development of highly sensitive LC-MS methods.

Karel Doležal is a senior researcher at the Faculty of Science, Palacký University Olomouc and the Institute of Experimental Botany of the Czech Academy of Sciences. His research is focused on the study of different aspects of chemistry and biology of plant hormones, namely, their organic synthesis and structure–activity relationship(s), as well as their endogenous identification and quantification using different mass spectrometry approaches.

Supplementary Information

In situ separation and visualization of isomeric auxin derivatives in *Arabidopsis* by ion mobility mass spectrometry imaging

Chao Zhang[1*], Kristýna Bieleszová[2], Asta Žukauskaitė[2], Pavel Hladík[1], Jiří Grúz[3], Ondřej Novák[1] and Karel Doležal[1,2*]

[1] Laboratory of Growth Regulators, Institute of Experimental Botany, The Czech Academy of Sciences & Faculty of Science, Palacký University, Šlechtitelů 27, CZ-78371 Olomouc, Czech Republic

[2] Department of Chemical Biology, Faculty of Science, Palacký University, Šlechtitelů 27, CZ-78371 Olomouc, Czech Republic

[3] Department of Experimental Biology, Faculty of Science, Palacký University, Šlechtitelů 27, CZ-78371 Olomouc, Czech Republic

*Corresponding authors
E-mails: chao.zhang@upol.cz; karel.dolezal@upol.cz

Method S1: Synthesis

Method S1.1: Chemicals and general methods

Chemicals were purchased from common commercial suppliers. All reactions were performed in oven-dried glassware. Dimethylformamide was kept over molecular sieves at least 48 h prior to use. Conversion of starting materials was monitored by thin layer chromatography (TLC) on aluminium plates coated with silica gel 60 F254 (Merck, USA) and visualized by UV light (254 and 365 nm) and staining solutions (vanillin or potassium permanganate). Purification of reaction mixtures was done by column chromatography on silica gel (40-63 μm Davisil LC60A, Grace Davison, UK). ^{1}H (500 MHz) and ^{13}C (125 MHz) NMR spectra were recorded in deuterated dimethyl sulfoxide (DMSO-d_6) at room temperature on a Jeol ECA-500 spectrometer equipped with a 5 mm Royal probe. Chemical shifts were calibrated to ^{1}H 2.50 ppm and ^{13}C 39.52 ppm signals of DMSO-d_6. The LC–MS analyses were performed on an ACQUITY UPLC® H-Class system combined with UPLC® PDA detector and a single-quadrupole mass spectrometer QDa™ (Waters, UK) as described previously (1).

Method S1.2: 2,5-Dioxopyrrolidin-1-yl 4-(2,4-dimethylphenyl)-2-(1*H*-indol-3-yl)-4-oxobutanoate

4-(2,4-Dimethylphenyl)-2-(1*H*-indol-3-yl)-4-oxobutanoic acid (auxinole) (50 mg, 0.16 mmol) and *N*-hydroxysuccinimide (17.9 mg, 0.16 mmol) were dissolved in dioxane (4.5 ml) and ethyl acetate (2.1 ml) mixture to which *N*,*N'*-dicyclohexylcarbodiimide (32 mg, 0.16 mmol) was added at 0 °C. Resulting mixture was warmed up to room temperature and stirred for 18 h. Subsequently, the reaction mixture was filtered over celite and the filter cake was washed with dioxane (3 × 5 ml). Evaporation of the solvent under reduced pressure afforded crude 2,5-dioxopyrrolidin-1-yl 4-(2,4-dimethylphenyl)-2-(1*H*-indol-3-yl)-4-oxobutanoate which was used in the next step without purification. Yield 88%, white solid, R_f = 0.65 (petroleum ether/ethyl acetate 4/1). ^{1}H NMR (500 MHz, DMSO-d_6): δ 2.31 (3H, s, CH_3), 2.39 (3H, s, CH_3), 2.65-2.76 (4H, br s, 2 × CH_2), 3.55 (1H, dd, *J* = 18.0, 4.6 Hz, $CH_\alpha H_\beta$), 3.92 (1H, dd, *J* = 18.0, 10.1 Hz, $CH_\alpha H_\beta$), 4.76 (1H, dd, *J* = 10.1, 4.3 Hz, CH), 7.02 (1H, ddd, *J* = 8.0, 7.0, 0.9 Hz, CH), 7.09-7.13 (3H, m, 3 × CH), 7.38 (1H, d, *J* = 8.3 Hz, CH), 7.46 (1H, d, *J* = 2.4 Hz, CH), 7.65 (1H, d, *J* = 7.9 Hz, CH), 7.82 (1H, d, *J* = 7.9 Hz, CH), 11.17 (1H, br d, *J* = 2.1 Hz, NH). ^{13}C NMR (125 MHz, DMSO-d_6): δ 20.9, 21.0, 25.4, 35.6, 43.7, 109.3, 111.6, 118.6, 118.9, 121.4, 123.9, 125.9, 126.4, 129.6, 132.4, 133.9, 136.1, 137.9, 141.8, 156.6, 169.3, 169.9, 199.7. MS (ES, neg. mode): *m/z* (%): 417.17 ($M - H^-$, 100).

Method S1.3: Dimethyl (4-(2,4-dimethylphenyl)-2-(1*H*-indol-3-yl)-4-oxobutanoyl)aspartate

2,5-Dioxopyrrolidin-1-yl 4-(2,4-dimethylphenyl)-2-(1*H*-indol-3-yl)-4-oxobutanoate (200 mg, 0.48 mmol) was dissolved in dry dimethylformamide (2 ml) and the resulting mixture was cooled down to 0 °C. Subsequently, solution of dimethyl L-aspartate hydrochloride (189 mg, 0.96 mmol) in dry dimethylformamide (2.5 ml) was added, followed by triethylamine (199 μl, 1.43 mmol) and the resulting mixture was stirred at room temperature for 3 h. Subsequently, reaction mixture was cooled down to 0 °C, quenched with water (10 ml) and extracted with diethyl ether (3 × 15 ml). The combined organic extracts were washed with brine (2 × 10 ml). Drying with sodium sulfate, filtration and evaporation of the solvent under reduced pressure and purification of the residue by flash chromatography on silica gel (petroleum ether/ethyl acetate 2/3 to 1/4) afforded dimethyl (4-(2,4-dimethylphenyl)-2-(1*H*-indol-3-yl)-4-oxobutanoyl)aspartate as a mixture of diastereomers. Yield 73%, white-yellowish solid, R_f = 0.20 (petroleum ether/ethyl acetate/methanol 10/10/1). ^{1}H NMR (500 MHz, DMSO-d_6): δ 2.30 (6H, s, 2 × CH_3 or 2 × CH_3* or CH_3 and CH_3*), 2.31 (3H, s, CH_3 or CH_3*), 2.32 (3H, s, CH_3 or CH_3*), 2.57 (1H, dd, *J* = 16.4, 7.0 Hz, $CH_\alpha H_\beta$ or $CH_\alpha H_\beta$*), 2.64 (1H, dd, *J* = 16.5, 6.7 Hz, $CH_\alpha H_\beta$ or $CH_\alpha H_\beta$*), 2.74 (1H, dd, *J* = 16.4, 6.4 Hz, $CH_\alpha H_\beta$ or $CH_\alpha H_\beta$*),2.78 (1H, dd, *J* = 16.4, 6.4 Hz, $CH_\alpha H_\beta$ or $CH_\alpha H_\beta$*), 3.16-3.22 (2H, m, $CH_\alpha H_\beta$ and $CH_\alpha H_\beta$*), 3.41 (3H, s, OCH_3 or OCH_3*), 3.46 (3H, s, OCH_3 or OCH_3*), 3.53 (3H, s, OCH_3 or OCH_3*), 3.54 (3H, s, OCH_3 or OCH_3*), 3.68-3.74 (2H, m, $CH_\alpha H_\beta$ and $CH_\alpha H_\beta$*), 4.34-4.38 (2H, m, CH and CH*),4.55 (1H, ddd, *J* = 7.6, 7.0, 6.7 Hz, -*CH*-NH- or -*CH**-NH-), 4.61 (1H, ddd, *J* = 7.9, 6.9, 6.7 Hz, -*CH*-NH- or -*CH**-NH-), 6.94-6.98 (2H, m, CH and CH*), 7.04-7.11 (6H, m, 3 × CH and 3 × CH*), 7.15 (1H, d, *J* = 2.1 Hz, CH or CH*), 7.17 (1H, d, *J* = 2.1 Hz, CH or CH*), 7.31-7.34 (2H, m, CH and CH*), 7.61 (1H, d, *J* = 8.0 Hz, CH or CH*), 7.63 (1H, d, *J* = 8.0 Hz, CH or CH*), 7.70-7.72 (2H, m, CH and CH*), 8.45-8.48 (2H, m, NH and NH*), 10.90-10.92 (2H, m, NH and NH*). ^{13}C NMR (125 MHz, DMSO-d_6): δ 20.6, 20.7, 20.9, 35.5, 38.66, 38.75, 43.9, 44.0, 48.6, 48.8, 51.5, 51.6, 51.9, 52.0, 111.30, 111.36, 112.89, 112.94, 118.38, 118.41, 118.97, 119.04, 121.0, 123.0, 126.1, 126.2, 126.4, 129.0, 129.1, 132.2, 135.1, 135.2, 136.2, 137.3, 141.19, 141.21, 170.4, 170.5, 171.12, 171.14, 172.7, 172.8, 201.6, 201.7. MS (ES, pos. mode): *m/z* (%): 465.44 ($M + H^+$, 100).

Method S1.4: (4-(2,4-Dimethylphenyl)-2-(1*H*-indol-3-yl)-4-oxobutanoyl)aspartic acid (auxinole-Asp)

Dimethyl (4-(2,4-dimethylphenyl)-2-(1*H*-indol-3-yl)-4-oxobutanoyl)aspartate (163 mg, 0.35 mmol) was dissolved in methanol (16 ml) and 1M lithium hydroxide solution (3.84 ml) was added at 0 °C. The reaction mixture was warmed up to 50 °C and stirred for 4 h. Subsequently, the reaction mixture was cooled down to 0 °C, acidified with 1M potassium bisulfate solution to pH = 6 and extracted with ethyl acetate (3 × 10 ml). The combined organic extracts were washed with brine (2 × 5 ml). Drying with sodium sulfate, filtration and evaporation of the solvent under reduced pressure and the purification of the residue by flash chromatography on silica gel (ethyl acetate/methanol 50/3), afforded (4-(2,4-dimethylphenyl)-2-(1*H*-indol-3-yl)-4-oxobutanoyl)aspartic acid as a mixture of diastereomers. Yield 59%, white-yellowish solid, R_f = 0.17 (ethyl acetate/methanol 10/1). ^{1}H NMR (500 MHz, DMSO-*d*$_6$): δ 2.29 (3H, s, CH_3 or CH_3*), 2.30 (6H, s, CH_3 or CH_3* and 2 × CH_3 or 2 × CH_3*), 2.42 (1H, dd, *J* = 16.8, 6.0 Hz, C*H*$_\alpha$H$_\beta$ or C*H*$_\alpha$H$_\beta$*), 2.50-2.53 (1H, m, C*H*$_\alpha$H$_\beta$ or C*H*$_\alpha$H$_\beta$*), 2.59 (1H, dd, *J* = 16.8, 6.7 Hz, CH$_\alpha$*H*$_\beta$ or CH$_\alpha$*H*$_\beta$*), 2.66 (1H, dd, *J* = 16.5, 7.3 Hz, CH$_\alpha$*H*$_\beta$ or CH$_\alpha$*H*$_\beta$*), 3.17-3.24 (1H, m, C*H*$_\alpha$H$_\beta$ or C*H*$_\alpha$H$_\beta$*), 3.65-3.72 (1H, m, CH$_\alpha$*H*$_\beta$ or CH$_\alpha$*H*$_\beta$*), 4.37-4.42 (2H, m, CH and CH*), 4.44-4.53 (2H, m, -*CH*-NH- and -*CH**-NH-), 6.96 (2H, t, *J* = 7.6 Hz, CH and CH*), 7.03-7.10 (6H, m, 3× CH and 3 × CH*), 7.16 (1H, d, *J* = 2.1 Hz, CH or CH*), 7.19 (1H, d, *J* = 2.1 Hz, CH or CH*), 7.30-7.33 (2H, m, CH and CH*), 7.62 (1H, d, *J* = 7.6 Hz, CH or CH*), 7.65 (1H, d, *J* = 8.0 Hz, CH or CH*), 7.70 (2H, d, *J* = 8.0 Hz, CH and CH*), 8.22-8.29 (2H, br s, NH and NH*), 10.88-10.91 (2H, m, NH and NH*), 12.22-12.66 (4H, m, 2 × OH and 2 × OH*). ^{13}C NMR (125 MHz, DMSO-*d*$_6$): δ 20.6, 20.7, 20.9, 35.95, 36.06, 38.6, 38.7, 44.1, 44.3, 48.6, 48.7, 111.3, 113.0, 118.35, 118.38, 118.9, 119.0, 120.9, 122.98, 123.01, 126.17, 126.24, 126.3, 128.96, 128.99, 132.2, 135.1, 135.2, 136.1, 137.2, 141.07, 141.10, 171.67, 171.71, 172.3, 172.5, 201.6, 201.8. MS (ES, neg. mode): *m/z* (%): 435.38 (M – H$^-$, 100).

Method S1.5: Dimethyl (4-(2,4-dimethylphenyl)-2-(1*H*-indol-3-yl)-4-oxobutanoyl)glutamate

2,5-Dioxopyrrolidin-1-yl 4-(2,4-dimethylphenyl)-2-(1*H*-indol-3-yl)-4-oxobutanoate (100 mg, 0.24 mmol) was dissolved in dry dimethylformamide (1 ml) and the reaction mixture was cooled down to 0 °C. Subsequently, solution of dimethyl L-glutamate hydrochloride (101 mg, 0.48 mmol) in dry dimethylformamide (1 ml) was added, followed by triethylamine (99 µl, 0.72 mmol) and resulting reaction mixture was stirred at room temperature for 3 h. Subsequently, reaction mixture was cooled down to 0 °C, quenched with water (10 ml) and extracted with diethyl ether (3 × 15 ml). The combined organic extracts were washed with brine (2 × 10 ml). Drying with sodium sulfate, filtration and evaporation of the solvent under reduced pressure and purification of the residue by flash chromatography on silica gel (petroleum ether/ethyl acetate 2/3 to 1/4) afforded dimethyl (4-(2,4-dimethylphenyl)-2-(1*H*-indol-3-yl)-4-oxobutanoyl)glutamate as a mixture of diastereomers. Yield 53%, white-yellowish solid, R_f = 0.26 (petroleum ether/ethyl acetate/methanol 10/10/1). ^{1}H NMR (500 MHz, DMSO-*d*$_6$): δ 1.73-1.86 (2H, m, C*H*$_\alpha$H$_\beta$ and C*H*$_\alpha$H$_\beta$*), 1.87-2.02 (2H, m, CH$_\alpha$*H*$_\beta$ and CH$_\alpha$*H*$_\beta$*), 2.17-2.22 (2H, m, C*H*$_\alpha$H$_\beta$ and C*H*$_\alpha$H$_\beta$*), 2.29 (3H, s, CH_3 or CH_3*), 2.30 (6H, s, 2 × CH_3 or 2 × CH_3* or CH_3 and CH_3*), 2.33 (3H, s, CH_3 or CH_3*), 2.36-2.45 (2H, m, CH$_\alpha$*H*$_\beta$ and CH$_\alpha$*H*$_\beta$*), 3.21 (2H, dd, *J* = 17.4, 4.5 Hz, C*H*$_\alpha$H$_\beta$ and C*H*$_\alpha$H$_\beta$*), 3.47 (3H, s, OCH_3 or OCH_3*), 3.50 (3H, s, OCH_3 or OCH_3*), 3.55 (3H, s, OCH_3 or OCH_3*), 3.56 (3H, s, OCH_3 or OCH_3*), 3.69-3.76 (2H, m, CH$_\alpha$*H*$_\beta$ and CH$_\alpha$*H*$_\beta$*), 4.13-4.18 (1H, m, -*CH*-NH- or -*CH**-NH-), 4.29-4.34 (1H, m, -*CH*-NH- or -*CH**-NH-), 4.37-4.42 (2H, m, CH and CH*), 6.93-6.99 (2H, m, CH and CH*), 7.03-7.11 (6H, m, 3 × CH and 3 × CH*), 7.17 (1H, d, *J* = 2.1 Hz, CH or CH*), 7.18 (1H, d, *J* = 2.1 Hz, CH or CH*), 7.31-7.34 (2H, m, CH and CH*), 7.68 (1H, d, *J* = 8.0 Hz, CH or CH*), 7.69 (1H, d, *J* = 8.0 Hz, CH or CH*), 7.72 (1H, d, *J* = 8.0 Hz, CH or CH*), 7.74 (1H, d, *J* = 8.0 Hz, CH or CH*), 8.44-8.47 (2H, m, NH and NH*), 10.89-10.93 (2H, br s, NH and NH*). ^{13}C NMR (125 MHz, DMSO-*d*$_6$): δ 20.7, 20.8, 20.9, 25.9, 26.3, 29.36, 29.39, 38.5, 38.7, 43.8, 44.1, 51.0, 51.28, 51.32, 51.68, 51.70, 111.3, 111.4, 113.1, 113.2, 118.3, 118.4, 119.0, 119.2, 121.0, 122.9, 123.0, 126.1, 126.2, 126.3, 129.1, 129.2, 132.2, 132.3, 134.9, 135.1, 136.2, 137.3, 137.4, 141.2, 141.3, 172.07, 172.09, 172.6, 172.8, 172.95, 173.03, 201.6, 201.8. MS (ES, pos. mode): *m/z* (%): 479.45 (M + H$^+$, 100).

Method S1.6: (4-(2,4-Dimethylphenyl)-2-(1*H*-indol-3-yl)-4-oxobutanoyl)glutamic acid (auxinole-Glu)

Dimethyl (4-(2,4-dimethylphenyl)-2-(1*H*-indol-3-yl)-4-oxobutanoyl)glutamate (60 mg, 0.13 mmol) was dissolved in methanol (4 ml) and 1M lithium hydroxide solution (1.05 ml) was added at 0 °C. The reaction mixture was warmed up to 50 °C and stirred for 4 h. Subsequently, the reaction mixture was cooled down to 0 °C, acidified with 1M potassium bisulfate solution to pH = 6 and extracted with ethyl acetate (3 × 10 ml). The combined organic extracts were washed with brine (2 × 5 ml). Drying with sodium sulfate, filtration and evaporation of the solvent under reduced pressure and the purification of the residue by flash chromatography on silica gel (ethyl acetate/methanol 50/3), afforded (4-(2,4-dimethylphenyl)-2-(1*H*-indol-3-yl)-4-oxobutanoyl)glutamic acid as a mixture of diastereomers. Yield 75%, white-yellowish solid, R_f = 0.17 (ethyl acetate/methanol 10/1). ^{1}H NMR (500 MHz, DMSO-*d*$_6$): δ 1.66-1.74 (1H, m, C*H*$_\alpha$H$_\beta$*), 1.75-1.81 (1H, m, C*H*$_\alpha$H$_\beta$), 1.82-1.89 (1H, m, CH$_\alpha$*H*$_\beta$*), 1.90-1.98 (1H, m, CH$_\alpha$*H*$_\beta$), 2.07-2.11 (2H, m, C*H*$_\alpha$H$_\beta$ and C*H*$_\alpha$H$_\beta$*), 2.27-2.36 (8H, m, CH$_\alpha$*H*$_\beta$ and CH$_\alpha$*H*$_\beta$*, 2 × CH_3 and 2 × CH_3*), 3.18-3.24 (2H, m,

CH_{α}H$_{\beta}$ and CH_{α}H$_{\beta}$*), 3.69 (1H, dd, *J* = 17.6, 8.6 Hz, CH$_{\alpha}H_{\beta}$*), 3.72 (1H, dd, *J* = 17.4, 9.5 Hz, CH$_{\alpha}H_{\beta}$), 4.11 (1H, ddd, *J* = 8.8, 7.6, 5.5 Hz, -*CH**-NH-), 4.23 (1H, ddd, *J* = 9.0, 7.6, 4.9 Hz, -*CH*-NH-), 4.39-4.44 (2H, m, CH and CH*), 6.95 (1H, t, *J* = 7.3 Hz, CH*), 6.96 (1H, t, *J* = 8.0 Hz, CH), 7.02-7.11 (6H, m, 3 × CH and 3 × CH*), 7.17 (1H, d, *J* = 2.1 Hz, CH), 7.19 (1H, d, *J* = 2.1 Hz, CH*), 7.31 (1H, d, *J* = 8.0 Hz, CH*), 7.32 (1H, d, *J* = 8.3 Hz, CH), 7.67-7.74 (4H, m, 2 × CH and 2 × CH*), 8.26 (1H, d, *J* = 7.6 Hz, NH*), 8.28 (1H, d, *J* = 7.6 Hz, NH), 10.88-10.94 (2H, br s, NH and NH*), 12.20-12.48 (4H, br s, 2 × OH and 2 × OH*). ^{13}C NMR (125 MHz, DMSO-d_6): δ 20.7, 20.8, 20.9, 26.4, 26.8, 29.9, 38.5, 38.7, 43.9, 44.3, 51.2, 51.4, 111.3, 111.4, 113.3, 113.4, 118.3, 118.4, 119.0, 119.2, 120.95, 120.98, 122.89, 122.92, 126.2, 126.28, 126.33, 129.0, 129.1, 132.2, 132.3, 135.0, 135.2, 136.1, 137.3, 137.4, 141.1, 141.2, 172.7, 172.8, 173.3, 173.8, 174.0, 201.7, 201.8. MS (ES, neg. mode): *m/z* (%): 449.33 (M – H$^-$, 100).

Method S1.7: Methyl 2-(1*H*-indol-3-yl)-4-oxo-4-(*p*-tolyl)butanoate (4pTb-MeIAA)

To a solution of 2-(1*H*-indol-3-yl)-4-oxo-4-(*p*-tolyl)butanoic acid (4pTb-IAA) (307 mg, 1.00 mmol) in methanol (10 ml), acetyl chloride (171 µl, 2.4 mmol) was added dropwise at 0 °C and the reaction mixture was stirred at room temperature for 2 h. The resulting reaction mixture was cooled down to 0 °C and quenched with saturated sodium hydrogencarbonate solution (10 ml) and extracted with ethyl acetate (3 × 10 ml). The combined organic extracts were washed with brine (10 ml). Drying with sodium sulfate, filtration and evaporation of the solvent under reduced pressure and the purification of the residue by flash chromatography on silica gel (petroleum ether/ethyl acetate 4/1 to 3/1), afforded methyl 2-(1*H*-indol-3-yl)-4-oxo-4-(*p*-tolyl)butanoate (4pTb-MeIAA). Yield 89%, light brown solid, R_f = 0.19 (petroleum ether/ethyl acetate 4/1). ^{1}H NMR (500 MHz, DMSO-d_6): δ 2.38 (3H, s, CH$_3$), 3.41 (1H, dd, *J* = 18.3, 4.0 Hz, CH_{α}H$_{\beta}$), 3.55 (3H, s, CH$_3$), 4.04 (1H, dd, *J* = 18.2, 10.9 Hz, CH$_{\alpha}H_{\beta}$), 4.40 (1H, dd, *J* = 10.9, 3.8 Hz, CH), 7.01 (1H, t, *J* = 7.5 Hz, CH), 7.09 (1H, t, *J* = 7.5 Hz, CH), 7.32-7.39 (4H, m, 4 × CH), 7.65 (1H, d, *J* = 7.9 Hz, CH), 7.94 (2H, d, *J* = 7.9 Hz, 2 × CH), 11.06-11.10 (1H, br s, NH). ^{13}C NMR (125 MHz, DMSO-d_6): δ 21.2, 37.4, 41.1, 51.7, 111.2, 111.6, 118.8, 121.3, 123.4, 126.1, 128.2, 129.3, 133.8, 136.2, 143.8, 173.9, 197.8. MS (ES, pos. mode): m/z (%): 322.46 (M + H$^+$, 100).

Method S2: LC-MS quantification method

For the auxinole and 4pTb-MeIAA quantification, the samples were purified by liquid-liquid extraction. A combination of methanol:H_2O:hexane (1:1:1) was used as the extraction solvent in a total volume of 900 µl. Three ceria-stabilized zirconium oxide beads were added and samples were homogenized by MixerMill MM 400 bead mill (Retsch GmBH, Haan, DE) at a frequency 27 Hz for 10 min. Following homogenization, the samples were then incubated at 4 °C with continuous shaking for 15 min and centrifuged (15 min, 23 000 g, 4 °C). After the extraction, the methanol/H_2O phase was transferred to MicroSpin tubes (0.2 µm, nylon; Chromservis s.r.o.®, Prague, CZ), centrifuged for an additional 10 min (12 000 g, 4 °C) and the flow-through fraction was then evaporated to dryness under vacuum.

The prepared samples were then dissolved in 50 µl of 10 % methanol, and 2 µl were injected into 1290 Infinity LC system coupled with a 6490 Triple Quadrupole LC/MS system equipped with Jet Stream and Dual Ion Funnel systems (Agilent Technologies, CA, USA). The HPLC separation was performed using a chromatographic reverse-phase column (Kinetex C18 100A, length 50 mm, diameter 2.1 mm, particle size 1.7 µm; Phenomenex, CA, USA). During the HPLC analysis, the samples were stored at 4 °C, and the column was tempered to 40 °C. Time of each analysis was 13 minutes, flow rate 0.3 mL/min, and the mobile phase consisted of deionized water (A) and methanol (B), both with the addition of 0.1 % acetic acid. The gradient elution was set as follows: 0 min – 60% A, 9 min – 5% A, 9.25 min – 1 % A, 10 min – 1 % A, 10.50 min – 60% A.

Following the separation step, samples were ionized by the electrospray ion source of a tandem MS analyzer operating in positive mode (ESI+) using these optimized conditions: drying gas flow and temperature, 11 L/min and 150°C; nebulizer pressure, 20 psi; sheath gas flow and temperature, 12 L/min and 325°C; capillary voltage, 2.8 kV; nozzle voltage, 0 V; collision energy, 15 V. The analytes were quantified using multiple reaction monitoring (MRM) mode with optimized conditions as described in Table S1. The acquired raw data were then interpreted by Mass Hunter software (Agilent Technologies, Santa Clara, CA, USA). For quantification, analytes peak areas (AUC) were normalized on the sample weight and their intensity ratio displayed.

To determine the compound's concentration in pmol/g FW, samples with addition of known amount of auxinole and 4pTb-MeIAA were prepared, and the method recovery factor was calculated. Three replicates of seven-day-old

Arabidopsis thaliana plants were harvested, with each sample weighing approximately 10 mg, and rapidly frozen in liquid nitrogen. To each sample, 1 nmol of auxinole and 4pTb-MeIAA were added, and samples were processed by LLE as described above. To account for matrix effects and analyte losses during extraction, six points external calibration curve ranging from 1 fmol to 100 pmol was prepared in 10% methanol. From these measurements, the recovery factor was calculated using the response of calibration and analyte levels after LLE (Table S2). For real samples, concentration was calculated from an external calibration curve after the application of dilution and recovery factors.

Table S1: Conditions of HPLC-MRM-MS method for auxinole and 4pTb-MeIAA. Diagnostic MRM transitions, for quantification and confirmation of the analytes, as well as collision energies were optimized.

Analyte	**MRM transition**		**CE**	**Retention times**	**ESI polarity**
	quantifier	qualifier	(V)	(min)	
auxinole	322 > 133	322 > 174	15	5.85	+
4pTb-MeIAA	322 > 262	322 > 188	15	6.03	+

Table S2: Liquid-liquid extraction efficiency of auxinole and 4pTb-MeIAA. Three replicates of ≈10 mg of seven-days-old *Arabidopsis thaliana* roots were prepared, 1 nmol of auxinole and 4pTb-MeIAA was added and samples were then processed by the LLE using methanol:H_2O:hexane (1:1:1). For quantification of the compounds, external calibration curve was prepared, and recovery factor was calculated from measured analytes levels after LLE.

	Concentration				**Recovery**			**Recovery**
Analyte		**MEAN**	**±**	**SD**	**MEAN**	**±**	**SD**	**factor**
	(pmol)		(pmol)			(%)		
auxinole	304.78 332.62 348.87	328.76	±	18.20	0.33	±	0.02	3.04
4pTb-MeIAA	30.90 12.61 25.97	23.16	±	7.73	0.02	±	0.01	43.17

Table S3: Summary of selected peakgroups presented in DESI-IM-MSI analysis

Abundant weight means (AWM)	m.z minimum	m.z maximum	mass group range (R)	Drift time minimum	Drift time maximum	drift_time_group_range	Number of detected treatments	Grouped charge condition
255.3631	255.3586	255.3678	0.0092	89.92	89.98	0.06	4	singly
220.2659	220.2614	220.2695	0.0081	73.09	73.21	0.12	2	singly
341.835	341.8343	341.8361	0.0018	72.82	72.99	0.17	1	singly
256.3661	256.3617	256.371	0.0093	89.81	89.99	0.18	4	singly
286.2708	286.2665	286.2758	0.0093	98.86	99.08	0.22	4	singly
298.0451	298.0414	298.0496	0.0082	84.53	84.84	0.31	4	singly
297.3639	297.3621	297.3662	0.0041	101.37	101.72	0.35	2	singly
306.8979	306.8954	306.8995	0.0041	67.54	67.9	0.36	2	singly
278.1788	278.1755	278.1833	0.0078	91.62	92	0.38	4	singly
436.8406	436.8368	436.8441	0.0073	81.57	81.95	0.38	3	singly
277.2145	277.211	277.2184	0.0074	93.9	94.32	0.42	4	singly
321.2904	321.2878	321.293	0.0052	114.52	114.95	0.43	3	singly
273.9925	273.988	273.9973	0.0093	69.65	70.09	0.44	4	singly
275.9952	275.992	275.9995	0.0075	74.73	75.17	0.44	4	singly
349.0631	349.0611	349.0651	0.004	88.02	88.47	0.45	2	singly
296.9478	296.944	296.9516	0.0076	64.45	64.92	0.47	4	singly
303.0995	303.0973	303.1013	0.004	87.1	87.6	0.5	3	singly
313.9397	313.9366	313.9433	0.0067	68.39	68.91	0.52	4	singly
276.6086	276.6039	276.613	0.0091	65.92	66.45	0.53	4	singly
278.2179	278.2141	278.2218	0.0077	93.77	94.36	0.59	4	singly
261.1443	261.1397	261.1491	0.0094	85.27	85.87	0.6	4	singly
263.1974	263.1923	263.2016	0.0093	91.29	91.93	0.64	4	singly
308.796	308.7924	308.7992	0.0068	67.23	67.87	0.64	4	singly
328.1841	328.1802	328.1876	0.0074	110.66	111.3	0.64	4	singly
313.9983	313.9947	314.0017	0.007	81.17	81.89	0.72	4	singly
311.5929	311.5902	311.5965	0.0063	106.71	107.44	0.73	3	singly
261.1299	261.1262	261.1343	0.0081	75.1	75.85	0.75	4	singly
302.2188	302.215	302.223	0.008	100.8	101.55	0.75	4	singly
302.0965	302.0947	302.0994	0.0047	61.96	62.76	0.8	2	singly
346.2329	346.2314	346.2346	0.0032	103.76	104.59	0.83	2	singly
301.2155	301.2115	301.2194	0.0079	100.65	101.49	0.84	4	singly
304.2347	304.2311	304.2394	0.0083	105.08	105.94	0.86	4	singly
305.2471	305.2432	305.2516	0.0084	104.06	104.93	0.87	4	singly
300.2032	300.1995	300.2078	0.0083	103.76	104.69	0.93	4	singly
342.4053	342.4046	342.4056	0.001	83.23	84.18	0.95	1	singly
316.2563	316.252	316.2608	0.0088	103.74	104.78	1.04	4	singly
303.2315	303.2279	303.2363	0.0084	104.85	105.92	1.07	4	singly
290.9089	290.9074	290.9107	0.0033	64.91	66.07	1.16	2	singly
458.6838	458.6828	458.6858	0.003	87.55	88.73	1.18	2	singly

313.2372	313.2334	313.2413	0.0079	101.76	103.19	1.43	4	singly
314.2409	314.2367	314.2453	0.0086	101.84	103.3	1.46	4	singly
273.1678	273.1647	273.172	0.0073	81.89	83.38	1.49	4	singly
310.404	310.403	310.4056	0.0026	74.39	75.88	1.49	1	singly
347.1332	347.1297	347.1367	0.007	98.77	100.59	1.82	4	singly
335.297	335.2933	335.3021	0.0088	114.99	117.3	2.31	3	singly
326.2737	326.2699	326.2775	0.0076	109.25	111.95	2.7	4	singly
530.7133	530.7123	530.7142	0.0019	99.44	102.47	3.03	1	singly
261.1676	261.1653	261.1703	0.005	78.16	81.31	3.15	2	singly
269.4618	269.4576	269.4656	0.008	91.17	94.44	3.27	4	singly
158.0747	158.0682	158.0786	0.0104	50.99	54.8	3.81	4	singly
263.1602	263.1558	263.1651	0.0093	84.67	88.7	4.03	4	singly
265.9887	265.984	265.9944	0.0104	66.58	70.79	4.21	4	singly
190.0467	190.0426	190.0507	0.0081	54.1	58.4	4.2	4	singly
223.1281	223.1225	223.1329	0.0104	70.44	74.71	4.27	4	singly
210.0341	210.0263	210.0405	0.0142	59.73	64.05	4.32	4	singly
342.6688	342.666	342.6717	0.0057	81.03	85.36	4.33	2	singly
266.89	266.8873	266.8927	0.0054	55.74	60.16	4.42	2	singly
271.1871	271.1825	271.1919	0.0094	84.73	89.18	4.45	3	singly
232.9802	232.9788	232.9817	0.0029	57.51	62.02	4.51	1	singly
126.9827	126.9778	126.9884	0.0106	33.03	37.7	4.67	4	singly
204.1102	204.1061	204.1144	0.0083	62.09	66.92	4.83	4	singly
291.1567	291.152	291.1608	0.0088	90.96	95.82	4.86	4	singly
196.0138	196.008	196.0198	0.0118	53.08	58.15	5.07	4	singly
305.104	305.0994	305.1079	0.0085	88.23	93.36	5.13	4	singly
300.2599	300.2559	300.2645	0.0086	100.46	105.62	5.16	4	singly
330.2374	330.2334	330.2414	0.008	100.24	105.49	5.25	4	singly
270.1744	270.1702	270.1778	0.0076	82.72	88.14	5.42	4	singly
225.1061	225.0989	225.1119	0.013	67.73	73.2	5.47	4	singly
286.207	286.2035	286.2113	0.0078	90.03	95.51	5.48	4	singly
261.2178	261.2123	261.2219	0.0096	89.05	94.56	5.51	4	singly
291.1931	291.1901	291.1976	0.0075	96.17	101.86	5.69	4	singly
255.9789	255.9725	255.9839	0.0114	59.85	65.61	5.76	4	singly
376.9505	376.946	376.9541	0.0081	84.14	89.94	5.8	3	singly
271.1533	271.1489	271.1583	0.0094	80.52	86.4	5.88	4	singly
307.009	307.0053	307.0118	0.0065	70.81	76.71	5.9	4	singly
256.1582	256.153	256.1629	0.0099	77.44	83.39	5.95	4	singly
257.1717	257.1658	257.1771	0.0113	79.74	85.69	5.95	4	singly
374.0474	374.0432	374.0529	0.0097	101.36	107.33	5.97	4	singly
229.1393	229.1342	229.1435	0.0093	70.23	76.37	6.14	4	singly
258.1739	258.1688	258.1791	0.0103	79.26	85.83	6.57	4	singly
272.1512	272.1488	272.1526	0.0038	79.64	86.28	6.64	2	singly
354.9961	354.9942	354.9987	0.0045	78.28	84.94	6.66	3	singly

240.1189	240.1081	240.1301	0.022	73.71	80.45	6.74	4	singly
335.2236	335.2186	335.2275	0.0089	106.99	113.77	6.78	4	singly
307.0782	307.0743	307.0814	0.0071	80.9	87.77	6.87	4	singly
214.0421	214.036	214.0466	0.0106	60.36	67.23	6.87	4	singly
257.1378	257.132	257.1419	0.0099	75.98	82.96	6.98	4	singly
226.1793	226.1735	226.1873	0.0138	72.79	79.84	7.05	4	singly
388.1727	388.1673	388.1781	0.0108	117.56	124.67	7.11	4	singly
336.2261	336.2202	336.2317	0.0115	106.87	114.01	7.14	4	singly
343.1154	343.1131	343.1188	0.0057	88.17	95.39	7.22	4	singly
273.0031	272.9972	273.0093	0.0121	64.65	71.89	7.24	4	singly
327.564	327.5615	327.5673	0.0058	76.47	83.74	7.27	2	singly
215.1206	215.1145	215.1261	0.0116	65.4	72.69	7.29	4	singly
265.0412	265.0358	265.0456	0.0098	62.53	70.03	7.5	4	singly
390.238	390.2364	390.2393	0.0029	123.31	130.82	7.51	2	singly
215.0859	215.0806	215.0919	0.0113	62.18	69.72	7.54	4	singly
259.1157	259.1098	259.1219	0.0121	73	80.7	7.7	4	singly
280.9264	280.9227	280.9318	0.0091	62.71	70.43	7.72	4	singly
213.1058	213.1002	213.1114	0.0112	64.65	72.38	7.73	4	singly
217.069	217.0621	217.076	0.0139	59.72	67.61	7.89	4	singly
206.0731	206.0667	206.0777	0.011	55.53	63.51	7.98	4	singly
196.0416	196.0344	196.0511	0.0167	51.63	59.75	8.12	4	singly
202.1436	202.1361	202.1502	0.0141	64.88	73.08	8.2	4	singly
333.6796	333.6758	333.6845	0.0087	75.85	84.14	8.29	3	singly
288.978	288.9724	288.9842	0.0118	67.5	75.86	8.36	4	singly
274.0996	274.0957	274.1028	0.0071	74.51	83.05	8.54	4	singly
281.1375	281.133	281.1415	0.0085	77.2	85.77	8.57	4	singly
239.1589	239.1539	239.1635	0.0096	77.15	85.75	8.6	4	singly
264.0832	264.0791	264.0881	0.009	71.91	80.52	8.61	4	singly
199.0729	199.0717	199.0741	0.0024	55.82	64.47	8.65	1	singly
246.0678	246.0599	246.0744	0.0145	63.13	71.82	8.69	4	singly
270.0386	270.0344	270.0426	0.0082	73.04	81.89	8.85	2	singly
294.9984	294.9945	295.0028	0.0083	71.79	80.68	8.89	4	singly
224.02	224.015	224.0263	0.0113	57.74	66.7	8.96	4	singly
273.2292	273.2251	273.234	0.0089	89.62	98.72	9.1	4	singly
229.1029	229.0979	229.1085	0.0106	66.73	76.09	9.36	4	singly
272.2271	272.2227	272.2318	0.0091	89.31	98.78	9.47	4	singly
245.1373	245.1316	245.1422	0.0106	72.29	81.77	9.48	4	singly
287.2192	287.2137	287.2239	0.0102	90.86	100.41	9.55	4	singly
256.1053	256.0996	256.11	0.0104	76.3	85.89	9.59	4	singly
202.0609	202.0533	202.0682	0.0149	49.8	59.59	9.79	4	singly
321.2101	321.2056	321.215	0.0094	95.54	105.51	9.97	4	singly
213.1435	213.1384	213.1481	0.0097	62.22	72.23	10.01	4	singly
283.1886	283.1833	283.1923	0.009	88.66	98.83	10.17	4	singly

311.223	311.218	311.2268	0.0088	98.37	108.56	10.19	4	singly
381.9929	381.9907	381.9948	0.0041	92.34	102.58	10.24	4	singly
274.0695	274.0636	274.0759	0.0123	67.38	77.67	10.29	4	singly
199.1211	199.1143	199.1253	0.011	55.61	65.97	10.36	3	singly
365.2739	365.27	365.2791	0.0091	118.47	128.96	10.49	4	singly
182.9143	182.9091	182.9197	0.0106	38.69	49.21	10.52	4	singly
310.9681	310.9621	310.9731	0.011	72.24	82.93	10.69	4	singly
262.1369	262.1295	262.1456	0.0161	75.05	85.89	10.84	4	singly
210.9851	210.9798	210.9959	0.0161	49.71	60.56	10.85	4	singly
280.0017	279.9962	280.0075	0.0113	66.76	77.72	10.96	4	singly
291.0876	291.0831	291.0919	0.0088	77.74	88.74	11	4	singly
267.051	267.0442	267.0574	0.0132	65.01	76.18	11.17	4	singly
286.0801	286.0769	286.0846	0.0077	76.61	87.82	11.21	3	singly
273.091	273.0862	273.0959	0.0097	71.87	83.14	11.27	4	singly
199.0176	199.0104	199.0246	0.0142	48.76	60.05	11.29	4	singly
283.5677	283.5631	283.5718	0.0087	67.45	78.76	11.31	2	singly
446.0567	446.0523	446.0611	0.0088	112.68	124.11	11.43	4	singly
296.5575	296.5536	296.5616	0.008	68.46	79.96	11.5	2	singly
209.0179	209.0094	209.0254	0.016	51.94	63.59	11.65	4	singly
242.9089	242.9072	242.9099	0.0027	55.96	67.64	11.68	1	singly
385.0802	385.0744	385.0837	0.0093	92.48	104.35	11.87	4	singly
227.1272	227.1186	227.1328	0.0142	68.89	81.35	12.46	4	singly
193.0137	193.0031	193.0237	0.0206	47.89	60.38	12.49	4	singly
279.0504	279.0465	279.0551	0.0086	64.72	77.48	12.76	4	singly
281.0833	281.0793	281.0876	0.0083	75.63	88.4	12.77	3	singly
287.1287	287.1242	287.134	0.0098	80.96	93.99	13.03	4	singly
205.112	205.1014	205.1207	0.0193	61.59	74.64	13.05	4	singly
249.0725	249.0656	249.0813	0.0157	60.2	73.32	13.12	4	singly
180.9995	180.9939	181.0056	0.0117	41.49	54.7	13.21	4	singly
269.0509	269.0474	269.0551	0.0077	67.6	80.82	13.22	4	singly
224.9995	224.9929	225.0051	0.0122	50.36	63.6	13.24	4	singly
249.0398	249.0343	249.0453	0.011	54.78	68.05	13.27	3	singly
218.0542	218.0445	218.0613	0.0168	51.19	64.48	13.29	3	singly
293.0313	293.0282	293.0356	0.0074	61.66	75.07	13.41	3	singly
257.2345	257.2301	257.2396	0.0095	76.62	90.1	13.48	4	singly
277.1397	277.1344	277.1448	0.0104	87.15	100.75	13.6	4	singly
315.1801	315.1758	315.1835	0.0077	93.96	107.79	13.83	4	singly
375.0433	375.0384	375.0476	0.0092	93.61	107.49	13.88	4	singly
442.2606	442.2576	442.265	0.0074	129.68	143.76	14.08	4	singly
313.1669	313.1628	313.1709	0.0081	93.91	108.03	14.12	4	singly
261.0891	261.0836	261.0967	0.0131	63.22	77.4	14.18	4	singly
278.1421	278.1372	278.1471	0.0099	86.14	100.34	14.2	4	singly
271.1158	271.1112	271.1215	0.0103	77.84	92.46	14.62	4	singly

212.0411	212.035	212.05	0.015	52.03	66.94	14.91	4	singly
403.2234	403.2165	403.2298	0.0133	125.99	140.9	14.91	4	singly
325.1678	325.164	325.1717	0.0077	76.53	91.63	15.1	3	singly
243.0212	243.0153	243.0253	0.01	56.67	71.85	15.18	4	singly
299.0747	299.0685	299.0792	0.0107	71.92	87.11	15.19	4	singly
258.2372	258.2326	258.2423	0.0097	74.88	90.12	15.24	4	singly
289.1614	289.1563	289.1669	0.0106	83.91	99.18	15.27	4	singly
241.0022	240.9921	241.0103	0.0182	54.87	70.19	15.32	4	singly
337.0465	337.0422	337.0515	0.0093	83.83	99.4	15.57	4	singly
470.2935	470.2885	470.2993	0.0108	140.35	156.03	15.68	4	singly
272.1176	272.1124	272.1238	0.0114	76.89	92.69	15.8	4	singly
263.0695	263.0646	263.0744	0.0098	68.67	84.51	15.84	4	singly
269.0998	269.0948	269.1046	0.0098	63.61	79.46	15.85	4	singly
184.1315	184.1194	184.1421	0.0227	53.07	68.98	15.91	4	singly
170.1131	170.1021	170.1217	0.0196	48.06	63.99	15.93	4	singly
273.1319	273.1276	273.1369	0.0093	75.53	91.54	16.01	4	singly
314.1675	314.1639	314.1714	0.0075	92.16	108.21	16.05	4	singly
425.2973	425.2927	425.3025	0.0098	133.73	149.89	16.16	4	singly
227.0246	227.0113	227.0368	0.0255	53.15	69.36	16.21	4	singly
288.1502	288.1461	288.1549	0.0088	83.26	99.55	16.29	4	singly
287.148	287.143	287.1518	0.0088	83.1	99.49	16.39	4	singly
317.1227	317.1183	317.1267	0.0084	92.61	109.01	16.4	4	singly
286.1343	286.1301	286.1395	0.0094	80.52	97.14	16.62	4	singly
341.3341	341.3305	341.3384	0.0079	102.71	119.51	16.8	4	singly
301.108	301.1037	301.113	0.0093	79.8	96.61	16.81	3	singly
259.0183	259.0099	259.0263	0.0164	58.31	75.19	16.88	4	singly
285.1306	285.1253	285.1362	0.0109	80.32	97.2	16.88	4	singly
332.1724	332.1683	332.1782	0.0099	77.81	94.85	17.04	4	singly
471.3031	471.2951	471.3103	0.0152	140.39	157.52	17.13	4	singly
325.0919	325.0866	325.096	0.0094	83.16	100.34	17.18	4	singly
237.051	237.0405	237.0576	0.0171	59.91	77.1	17.19	4	singly
411.1673	411.1617	411.1725	0.0108	121.09	138.34	17.25	4	singly
297.0444	297.0411	297.0492	0.0081	84.49	101.82	17.33	4	singly
299.1496	299.1452	299.1538	0.0086	85.95	103.41	17.46	4	singly
124.9463	124.9436	124.9485	0.0049	28.37	45.84	17.47	1	singly
433.2517	433.2484	433.2539	0.0055	122.09	139.72	17.63	1	singly
255.0817	255.076	255.0864	0.0104	61.66	79.45	17.79	4	singly
276.1127	276.1021	276.1206	0.0185	65.93	83.78	17.85	4	singly
300.1507	300.1465	300.1548	0.0083	85.47	103.53	18.06	4	singly
348.0125	348.0102	348.0149	0.0047	81.19	99.66	18.47	1	singly
235.0369	235.0328	235.0411	0.0083	53.44	72.04	18.6	4	singly
288.0581	288.0527	288.0635	0.0108	69.04	87.65	18.61	4	singly
503.2257	503.2191	503.2316	0.0125	137.9	156.73	18.83	3	singly

335.126	335.1245	335.128	0.0035	91.89	110.76	18.87	2	singly
336.054	336.0471	336.0591	0.012	76.72	95.81	19.09	4	singly
288.1309	288.1252	288.1358	0.0106	74.89	94.11	19.22	4	singly
317.1606	317.1551	317.167	0.0119	80.84	100.24	19.4	4	singly
196.9735	196.964	196.9831	0.0191	40.31	59.81	19.5	4	singly
270.102	270.0967	270.1077	0.011	59.95	79.55	19.6	4	singly
312.1532	312.1491	312.1575	0.0084	71.11	90.75	19.64	3	singly
234.0372	234.0312	234.0434	0.0122	50.42	70.07	19.65	4	singly
394.1751	394.1703	394.1804	0.0101	111.86	131.68	19.82	4	singly
401.2246	401.2188	401.2332	0.0144	121.21	141.15	19.94	4	singly
319.0584	319.0531	319.0672	0.0141	74.8	94.8	20	4	singly
586.6271	586.6256	586.6287	0.0031	126.46	146.58	20.12	1	singly
339.0736	339.0682	339.0788	0.0106	89.66	109.87	20.21	3	singly
226.933	226.932	226.9343	0.0023	52.49	72.75	20.26	1	singly
321.0587	321.0496	321.0683	0.0187	74.93	95.23	20.3	4	singly
231.0814	231.0756	231.0878	0.0122	51.64	71.99	20.35	4	singly
242.0471	242.0411	242.053	0.0119	55.01	75.37	20.36	4	singly
254.0438	254.036	254.0519	0.0159	58.11	78.62	20.51	3	singly
255.155	255.1493	255.1596	0.0103	62.35	83.33	20.98	4	singly
242.0744	242.0673	242.0798	0.0125	58.83	79.92	21.09	4	singly
577.6215	577.6209	577.622	0.0011	127.11	148.2	21.09	1	singly
494.5856	494.5852	494.5864	0.0012	126.52	147.93	21.41	1	singly
335.0522	335.0471	335.056	0.0089	77.82	99.35	21.53	4	singly
245.0973	245.0918	245.1021	0.0103	54.45	76.22	21.77	4	singly
282.9882	282.9832	282.9933	0.0101	77.12	98.99	21.87	4	singly
355.3217	355.3176	355.3262	0.0086	102.99	124.92	21.93	4	singly
344.0382	344.0312	344.0459	0.0147	77.72	99.79	22.07	4	singly
233.9957	233.99	234.0024	0.0124	49.53	71.78	22.25	4	singly
263.0463	263.0383	263.0529	0.0146	56.64	79.12	22.48	3	singly
224.0536	224.046	224.0615	0.0155	53.07	75.66	22.59	4	singly
275.073	275.0666	275.0805	0.0139	66.79	89.48	22.69	4	singly
289.1288	289.1233	289.1363	0.013	71.85	94.58	22.73	4	singly
277.114	277.1031	277.1254	0.0223	61.78	84.59	22.81	4	singly
281.1181	281.114	281.123	0.009	71.91	94.82	22.91	4	singly
339.8239	339.8212	339.829	0.0078	46.65	69.89	23.24	3	singly
270.1208	270.1164	270.1255	0.0091	68.52	92.37	23.85	4	singly
287.1076	287.1027	287.1121	0.0094	61.97	85.99	24.02	4	singly
255.0424	255.0377	255.047	0.0093	65.95	90.03	24.08	4	singly
329.1493	329.1454	329.1523	0.0069	79.52	104.92	25.4	3	singly
267.1014	267.0971	267.1059	0.0088	64.6	90.41	25.81	4	singly
275.1136	275.1043	275.1222	0.0179	65.64	91.57	25.93	4	singly
337.6059	337.6023	337.6109	0.0086	87.6	113.9	26.3	4	singly
321.0974	321.0936	321.1031	0.0095	84.84	111.25	26.41	4	singly

325.1153	325.1083	325.1228	0.0145	86.8	113.26	26.46	4	singly
283.6164	283.6141	283.6183	0.0042	72.57	99.04	26.47	2	singly
371.6044	371.6026	371.606	0.0034	82.55	109.27	26.72	1	singly
296.1388	296.1339	296.1441	0.0102	73.72	100.83	27.11	4	singly
341.2693	341.2635	341.2754	0.0119	87.89	115.04	27.15	4	singly
376.1893	376.1838	376.1952	0.0114	106.8	134.48	27.68	4	singly
282.1226	282.1175	282.128	0.0105	68.04	95.75	27.71	4	singly
471.0822	471.0813	471.083	0.0017	128.64	156.37	27.73	2	singly
268.1071	268.1003	268.113	0.0127	64.72	92.49	27.77	4	singly
259.1891	259.1828	259.1984	0.0156	64.74	92.63	27.89	4	singly
342.5844	342.5805	342.5877	0.0072	72.86	100.92	28.06	2	singly
318.1605	318.1547	318.1668	0.0121	72.82	100.92	28.1	4	singly
351.201	351.1965	351.2057	0.0092	97.11	125.26	28.15	4	singly
277.0688	277.0552	277.0775	0.0223	55.98	84.38	28.4	4	singly
326.0976	326.0943	326.1021	0.0078	83.44	111.86	28.42	4	singly
295.1349	295.1306	295.1394	0.0088	72.36	100.89	28.53	4	singly
463.1112	463.1027	463.119	0.0163	125.59	155.62	30.03	4	singly
272.0861	272.0799	272.0933	0.0134	57.16	87.3	30.14	4	singly
367.1064	367.1017	367.1117	0.01	87.15	117.53	30.38	4	singly
290.1259	290.1205	290.1298	0.0093	65.01	95.41	30.4	4	singly
284.4036	284.3993	284.4094	0.0101	68.49	99.03	30.54	4	singly
322.1589	322.1495	322.168	0.0185	79.64	110.19	30.55	4	singly
325.5594	325.5546	325.5645	0.0099	81.21	111.91	30.7	4	singly
337.1844	337.1805	337.1883	0.0078	88.58	119.34	30.76	4	singly
283.4017	283.3943	283.4062	0.0119	68	98.99	30.99	4	singly
309.1512	309.147	309.1563	0.0093	75.68	106.78	31.1	4	singly
310.1553	310.1506	310.1598	0.0092	75.74	106.95	31.21	4	singly
319.2265	319.2225	319.231	0.0085	74.83	106.39	31.56	4	singly
265.0839	265.0792	265.0895	0.0103	56.17	87.74	31.57	4	singly
257.0414	257.0343	257.0487	0.0144	58.58	90.19	31.61	4	singly
226.0557	226.0498	226.0617	0.0119	50.87	82.51	31.64	4	singly
338.1869	338.1827	338.1917	0.009	88.06	120.03	31.97	4	singly
334.1697	334.163	334.1766	0.0136	74.88	107.47	32.59	4	singly
285.0338	285.0288	285.0392	0.0104	65.74	98.84	33.1	4	singly
324.1718	324.1672	324.1764	0.0092	79.07	112.65	33.58	4	singly
391.101	391.0931	391.1113	0.0182	100.28	133.89	33.61	4	singly
320.1273	320.1239	320.131	0.0071	68.64	103.4	34.76	4	singly
306.1113	306.1048	306.1162	0.0118	65	99.9	34.9	3	singly
306.1113	306.1048	306.1162	0.0118	65	99.9	34.9	3	singly
357.3326	357.3267	357.3371	0.0104	89.82	125.48	35.66	4	singly
306.0751	306.0715	306.0792	0.0077	65.03	103	37.97	4	singly
341.1779	341.1714	341.1827	0.0113	75.17	113.14	37.97	3	singly
298.8872	298.8858	298.8888	0.003	62.91	101.57	38.66	2	singly

331.1728	331.1639	331.1784	0.0145	77.42	116.26	38.84	4	singly
342.1817	342.1771	342.1854	0.0083	74.19	113.27	39.08	3	singly
343.1653	343.1564	343.1732	0.0168	74.04	113.18	39.14	4	singly
256.0371	256.0324	256.0425	0.0101	50.68	90.01	39.33	4	singly
296.9966	296.9914	297.0025	0.0111	63.77	103.37	39.6	4	singly
321.1483	321.1351	321.1561	0.021	69.88	109.95	40.07	4	singly
310.8765	310.8708	310.8812	0.0104	66.56	107.87	41.31	4	singly
297.0857	297.0766	297.0913	0.0147	61.22	103.91	42.69	4	singly
337.1455	337.1398	337.1514	0.0116	71.55	114.41	42.86	4	singly
326.8527	326.8487	326.8565	0.0078	69.42	112.34	42.92	4	singly
319.1059	319.1004	319.1085	0.0081	66.5	111	44.5	4	singly
319.1173	319.1058	319.1273	0.0215	66.48	110.99	44.51	4	singly
335.1676	335.1572	335.175	0.0178	73.07	117.7	44.63	4	singly
349.1824	349.1621	349.2006	0.0385	75.03	122.64	47.61	4	singly
449.1767	449.167	449.1856	0.0019	84.9	140.9	56	2	singly
435.1589	435.1501	435.167	0.0017	81.2	146	64.8	2	singly
251.2372	251.2357	251.239	0.0033	88.66	92.53	3.87	1	doubly
366.7618	366.7589	366.7654	0.0065	75.84	81.06	5.22	3	doubly
277.1766	277.1731	277.1802	0.0071	91.62	101.67	10.05	4	doubly
340.2032	340.1997	340.2073	0.0076	113.62	123.69	10.07	4	doubly
258.2113	258.2069	258.2154	0.0085	83.68	96.03	12.35	4	doubly
243.1905	243.1849	243.195	0.0101	79.08	92.21	13.13	4	doubly
368.2367	368.2319	368.2412	0.0093	123.05	136.69	13.64	4	doubly
168.9867	168.9781	168.9937	0.0156	33.98	47.98	14	4	doubly
275.1608	275.1564	275.1661	0.0097	86.8	101.54	14.74	4	doubly
211.0892	211.0831	211.0957	0.0126	63.31	79.51	16.2	4	doubly
276.1352	276.1327	276.1383	0.0056	86.67	103.18	16.51	2	doubly
333.8477	333.8442	333.8518	0.0076	69.94	86.68	16.74	3	doubly
239.1226	239.119	239.1276	0.0086	74.01	91.69	17.68	4	doubly
181.0596	181.0587	181.0611	0.0024	53.91	71.75	17.84	1	doubly
202.1009	202.0946	202.1078	0.0132	60.92	80.11	19.19	4	doubly
369.2311	369.2256	369.2363	0.0107	117.58	136.84	19.26	4	doubly
267.0103	267.0064	267.0137	0.0073	50.8	70.85	20.05	3	doubly
323.2569	323.2528	323.2616	0.0088	108.53	128.98	20.45	4	doubly
295.2246	295.2197	295.2299	0.0102	97.59	118.31	20.72	4	doubly
296.2275	296.2228	296.2334	0.0106	97.5	118.24	20.74	4	doubly
365.2171	365.2138	365.2208	0.007	110.01	131.38	21.37	3	doubly
364.8467	364.8419	364.8501	0.0082	73.81	95.37	21.56	4	doubly
183.1291	183.1175	183.1406	0.0231	46.73	69.03	22.3	4	doubly
218.9863	218.9756	218.9943	0.0187	41.11	63.56	22.45	4	doubly
292.0514	292.0468	292.0562	0.0094	56.42	79.79	23.37	4	doubly
311.9717	311.9676	311.9772	0.0096	59.13	82.52	23.39	4	doubly
352.0901	352.0874	352.0926	0.0052	74.21	97.91	23.7	2	doubly

362.5976	362.596	362.599	0.003	77.99	102.11	24.12	1	doubly
280.9852	280.9815	280.9898	0.0083	52.69	77.76	25.07	4	doubly
378.0909	378.0862	378.0957	0.0095	78.95	104.25	25.3	4	doubly
514.5844	514.5831	514.5854	0.0023	128.77	154.09	25.32	1	doubly
165.0312	165.0238	165.0381	0.0143	45.01	70.48	25.47	4	doubly
377.0891	377.083	377.0933	0.0103	67.16	93.13	25.97	4	doubly
441.0569	441.0549	441.0601	0.0052	84.67	112.69	28.02	1	doubly
200.9524	200.9509	200.9537	0.0028	47.13	75.41	28.28	1	doubly
526.081	526.0803	526.082	0.0017	129.22	157.56	28.34	1	doubly
526.5822	526.5804	526.5836	0.0032	128.98	157.55	28.57	1	doubly
329.1255	329.1202	329.1299	0.0097	67.83	96.55	28.72	4	doubly
408.07	408.0623	408.0812	0.0189	88.73	117.5	28.77	4	doubly
239.1086	239.1036	239.1129	0.0093	67.57	96.36	28.79	3	doubly
148.9607	148.9584	148.9628	0.0044	36.38	65.93	29.55	1	doubly
210.0016	209.9948	210.0071	0.0123	51.04	81.16	30.12	4	doubly
501.3233	501.3181	501.3273	0.0092	146.96	177.15	30.19	3	doubly
227.1025	227.0956	227.1087	0.0131	76.35	106.69	30.34	4	doubly
257.0985	257.093	257.1025	0.0095	72.85	104.71	31.86	4	doubly
349.0905	349.0843	349.0973	0.013	67.05	99.48	32.43	4	doubly
330.762	330.7574	330.7662	0.0088	55.25	88.2	32.95	4	doubly
400.1726	400.1687	400.1763	0.0076	81.82	114.88	33.06	3	doubly
338.0997	338.0951	338.1046	0.0095	64.05	97.63	33.58	4	doubly
283.1351	283.1306	283.1415	0.0109	97.17	131.69	34.52	4	doubly
564.1282	564.1255	564.1316	0.0061	124.91	159.93	35.02	1	doubly
355.0848	355.0746	355.0925	0.0179	66.45	102.1	35.65	4	doubly
476.5734	476.5707	476.5747	0.004	106.47	142.92	36.45	1	doubly
476.2983	476.2876	476.3079	0.0203	130.57	167.07	36.5	4	doubly
285.2679	285.2637	285.273	0.0093	98.83	136.54	37.71	4	doubly
401.149	401.1443	401.1538	0.0095	77.79	116.5	38.71	4	doubly
223.0176	223.0093	223.024	0.0147	54.05	93.04	38.99	4	doubly
350.8698	350.8662	350.8729	0.0067	47.77	86.85	39.08	3	doubly
421.1661	421.1577	421.1736	0.0159	82.36	121.73	39.37	4	doubly
430.1626	430.1604	430.1651	0.0047	82.75	122.34	39.59	2	doubly
312.1719	312.1675	312.1752	0.0077	107.37	148.21	40.84	4	doubly
422.1715	422.1627	422.1775	0.0148	82.92	123.81	40.89	4	doubly
248.9689	248.9621	248.9737	0.0116	26.7	68.57	41.87	4	doubly
307.1265	307.1115	307.1398	0.0283	61.95	103.92	41.97	4	doubly
211.0351	211.0271	211.0417	0.0146	55.72	98.47	42.75	4	doubly
365.1742	365.1663	365.1814	0.0151	78.87	122.97	44.1	4	doubly
355.1603	355.1495	355.1709	0.0214	75.76	120.06	44.3	4	doubly
401.0902	401.0875	401.0938	0.0063	69.64	114.52	44.88	3	doubly
352.3604	352.3571	352.3628	0.0057	126.16	171.66	45.5	3	doubly
416.094	416.0867	416.1003	0.0136	90.49	136.15	45.66	4	doubly

366.1794	366.1742	366.1844	0.0102	76.72	122.75	46.03	4	doubly
313.0751	313.0669	313.0816	0.0147	61.21	107.62	46.41	4	doubly
511.2658	511.2597	511.2717	0.012	119.82	166.25	46.43	4	doubly
345.1669	345.1628	345.1714	0.0086	72.6	119.89	47.29	4	doubly
421.3378	421.3282	421.3443	0.0161	103.41	150.98	47.57	4	doubly
183.0015	182.9927	183.0099	0.0172	45.97	93.55	47.58	4	doubly
429.1827	429.1765	429.1879	0.0114	86.42	134	47.58	4	doubly
327.1837	327.1796	327.1881	0.0085	110.49	158.37	47.88	4	doubly
441.0936	441.0859	441.0995	0.0136	103.61	152.05	48.44	3	doubly
453.1477	453.1402	453.1544	0.0142	82.98	131.55	48.57	4	doubly
194.0428	194.0343	194.0501	0.0158	59.13	108.54	49.41	4	doubly
353.3081	353.3039	353.3126	0.0087	82.55	132.42	49.87	4	doubly
477.1232	477.1133	477.1325	0.0192	130.58	180.46	49.88	4	doubly
409.1396	409.1366	409.1448	0.0082	77.8	128.05	50.25	3	doubly
363.0965	363.0882	363.1078	0.0196	67.58	118.04	50.46	4	doubly
456.2035	456.1977	456.2094	0.0117	91.29	141.82	50.53	4	doubly
371.0685	371.0634	371.0728	0.0094	67.23	117.91	50.68	4	doubly
393.1689	393.1577	393.1781	0.0204	81.11	131.85	50.74	4	doubly
472.2042	472.1996	472.2075	0.0079	92.96	144.29	51.33	4	doubly
402.0877	402.0744	402.1008	0.0264	87.36	138.88	51.52	4	doubly
433.2028	433.1961	433.2101	0.014	84.04	135.72	51.68	4	doubly
471.2008	471.1979	471.2035	0.0056	92.56	144.26	51.7	3	doubly
225.0521	225.0457	225.0587	0.013	51.01	103.04	52.03	4	doubly
366.2225	366.2183	366.2277	0.0094	81.08	133.39	52.31	4	doubly
496.6094	496.6073	496.6121	0.0048	105.18	158.46	53.28	1	doubly
473.2112	473.2051	473.2169	0.0118	92.3	145.96	53.66	4	doubly
355.1054	355.0979	355.1149	0.017	67.78	121.49	53.71	4	doubly
381.1578	381.1534	381.1659	0.0125	78.11	133.39	55.28	4	doubly
514.2103	514.2005	514.2186	0.0181	97.11	155.71	58.6	4	doubly
415.2381	415.2331	415.2422	0.0091	83.43	142.49	59.06	4	doubly
198.0292	198.0167	198.039	0.0223	50.88	110.19	59.31	4	doubly
385.1015	385.0983	385.1062	0.0079	71.61	131.05	59.44	4	doubly
339.2017	339.1965	339.2075	0.011	113.62	173.27	59.65	4	doubly
323.1678	323.163	323.1731	0.0101	77.32	137.3	59.98	4	doubly
375.1864	375.1822	375.1919	0.0097	107.46	167.58	60.12	4	doubly
498.1762	498.1678	498.1815	0.0137	91.22	152.31	61.09	4	doubly
389.1288	389.1226	389.1351	0.0125	73.51	135.08	61.57	4	doubly
447.1359	447.1274	447.1462	0.0188	84.59	146.58	61.99	4	doubly
436.0939	436.0887	436.0997	0.011	73.64	135.69	62.05	4	doubly
435.0894	435.083	435.0944	0.0114	73.02	135.74	62.72	4	doubly
440.1606	440.1555	440.1661	0.0106	84.79	147.6	62.81	4	doubly
425.1479	425.1397	425.1569	0.0172	78.35	142.42	64.07	4	doubly
197.0198	197.005	197.0288	0.0238	50.82	115	64.18	4	doubly

427.1453	427.1409	427.1489	0.008	81.14	145.39	64.25	4	doubly
297.1512	297.1469	297.1561	0.0092	103.04	168.46	65.42	4	doubly
421.1132	421.1048	421.1219	0.0171	75.28	141.13	65.85	4	doubly
553.1862	553.1841	553.1874	0.0033	98.04	164.63	66.59	1	doubly
347.1043	347.0959	347.111	0.0151	69.05	136.45	67.4	4	doubly
488.1965	488.1853	488.208	0.0227	94.67	162.6	67.93	4	doubly
468.1224	468.1149	468.1286	0.0137	81.38	151.44	70.06	4	doubly
541.1938	541.1873	541.1992	0.0119	89.68	161.69	72.01	3	doubly
449.1076	449.1029	449.1125	0.0096	76.8	150.13	73.33	4	doubly
540.1962	540.1842	540.2094	0.0252	98.87	175.8	76.93	4	doubly
457.1271	457.1208	457.134	0.0132	80.7	157.72	77.02	4	doubly
473.1732	473.1644	473.1798	0.0154	87.31	164.58	77.27	4	doubly
271.224	271.2192	271.2281	0.0089	89.35	166.89	77.54	4	doubly
509.2231	509.2137	509.23	0.0163	99.32	179.56	80.24	4	doubly
367.234	367.2295	367.2392	0.0097	80.98	162.15	81.17	4	doubly
270.2078	270.2041	270.2138	0.0097	88.69	174.85	86.16	4	doubly
265.1455	265.1396	265.1499	0.0103	29.54	129.72	100.18	4	doubly
120.965	120.9625	120.9686	0.0061	31.26	152.92	121.66	1	doubly
326.1883	326.184	326.1926	0.0086	29.46	175.65	146.19	4	doubly
293.1744	293.1697	293.1779	0.0082	22.88	169.84	146.96	4	doubly
299.2574	299.252	299.2601	0.0081	23.81	170.85	147.04	4	doubly
284.2658	284.261	284.2705	0.0095	31.87	180.89	149.02	4	doubly
256.2329	256.2273	256.2375	0.0102	29.61	179.84	150.23	4	doubly
311.1688	311.1638	311.173	0.0092	28.88	180.84	151.96	4	doubly
325.185	325.1801	325.1917	0.0116	24.7	179.4	154.7	4	doubly
283.2619	283.258	283.2682	0.0102	22.46	180.69	158.23	4	doubly
255.2294	255.2248	255.2342	0.0094	21.22	179.59	158.37	4	doubly
289.0736	289.0704	289.077	0.0066	80.7	86.2	5.5	4	multiply
174.053	174.0457	174.0643	0.0186	50.9	57.7	6.8	4	multiply
305.0701	305.0647	305.076	0.0113	60.8	85.3	24.5	4	multiply
364.1652	364.1596	364.1716	0.012	76.24	106.53	30.29	3	multiply
352.111	352.1081	352.1134	0.0053	67.5	102.7	35.2	4	multiply
426.0884	426.0815	426.0956	0.0141	94.98	131.69	36.71	4	multiply
364.0766	364.067	364.0844	0.0174	64.77	106.56	41.79	4	multiply
417.1754	417.1699	417.1803	0.0104	84.37	127.28	42.91	4	multiply
403.0916	403.0807	403.1049	0.0242	88.64	131.92	43.28	4	multiply
363.1602	363.1491	363.1688	0.0197	75.95	123.16	47.21	4	multiply
540.6025	540.6011	540.6041	0.003	114.98	168.98	54	1	multiply
509.6004	509.5988	509.6018	0.003	106.36	160.49	54.13	1	multiply
439.2518	439.2493	439.2549	0.0056	92.98	148.5	55.52	3	multiply
460.0899	460.0851	460.0956	0.0105	77.71	134.06	56.35	3	multiply
377.1688	377.1657	377.1744	0.0087	79.73	136.65	56.92	4	multiply
562.5985	562.5972	562.601	0.0038	115.26	174.55	59.29	1	multiply

387.1499	387.1457	387.153	0.0073	76.94	140.53	63.59	3	multiply
379.1559	379.1464	379.1659	0.0195	76.77	140.87	64.1	4	multiply
437.2006	437.1906	437.213	0.0224	89.53	155.58	66.05	4	multiply
459.1055	459.1013	459.111	0.0097	99.24	166.28	67.04	2	multiply
503.0993	503.0932	503.1057	0.0125	81.3	150.95	69.65	4	multiply
481.1677	481.1586	481.1778	0.0192	87.04	160.16	73.12	4	multiply
405.1162	405.1093	405.1258	0.0165	74.07	150.12	76.05	4	multiply
545.0968	545.0861	545.1078	0.0217	98.86	176.16	77.3	4	multiply
410.1679	410.1636	410.1729	0.0093	83.23	161.09	77.86	4	multiply
433.1218	433.1101	433.1302	0.0201	76.74	154.9	78.16	4	multiply
487.1931	487.1863	487.2028	0.0165	93.05	171.81	78.76	4	multiply
471.1543	471.142	471.1651	0.0231	85.01	165.21	80.2	4	multiply
437.1626	437.1534	437.1697	0.0163	82.32	162.94	80.62	4	multiply
448.1296	448.1142	448.1412	0.027	78.66	159.5	80.84	4	multiply
495.2016	495.1919	495.2082	0.0163	93.08	174.07	80.99	4	multiply
449.1269	449.1223	449.1317	0.0094	79.66	160.94	81.28	4	multiply
452.145	452.1397	452.1546	0.0149	81.7	165.63	83.93	4	multiply
478.1192	478.1124	478.1249	0.0125	79.86	180.27	100.41	4	multiply

Table S4: Liquid chromatography mass spectrometry analysis of auxin metabolites

Table S4.1: Quantification of the auxinole, 4pTb-MeIAA and IAA determined through isotopically labelled LC-MS/MS analysis. *Arabidopsis thaliana* samples (10 mg FW) were extracted, purified using the in-tip µSPE (IAA) or LLE (auxinole, 4pTb-MeIAA) procedure and analysed by LC–MS/MS. The standard curves with regression equations were also shown below.

Analytes	auxinole					4pTb-MeIAA					IAA				
	AUC	pmol/g FW ± SD; RSD [%]				AUC	pmol/g FW ± SD; RSD [%]				AUC	pmol/g FW ± SD; RSD [%]			
control	0.000	0.00	0.00	±	0.00	0.000	0.00	0.00	±	0.00	0.037	49.71	56.96	±	4.38
control	0.000	0.00			0.00%	0.000	0.00			0.00%	0.039	55.58			7.69%
control	0.000	0.00				0.000	0.00				0.055	57.32			
control	0.000	0.00				0.000	0.00				0.037	59.24			
control	0.000	0.00				0.000	0.00				0.037	62.96			
10 µM auxinole	67.494	16.09	26.61	±	10.48	0.000	0.00	0.00	±	0.00	0.082	100.43	69.57	±	22.74
10 µM auxinole	74.437	21.59			39.40%	0.000	0.00			0.00%	0.024	29.60			32.69%
10 µM auxinole	69.351	23.12				0.000	0.00				0.063	71.28			
10 µM auxinole	86.861	25.63				0.000	0.00				0.060	71.57			
10 µM auxinole	160.479	46.62				0.000	0.00				0.062	74.98			
10 µM 4pTb-MeIAA	0.000	0.000				21.223	20.45	43.31	±	32.61	0.062	75.19	76.80	±	20.79
10 µM 4pTb-MeIAA	0.000	0.000				48.452	32.98			75.29%	0.092	113.99			27.07%
10 µM 4pTb-MeIAA	0.000	0.000				25.261	90.99				0.041	50.83			
10 µM 4pTb-MeIAA	0.000	0.000				40.569	2.09				0.065	77.22			
10 µM 4pTb-MeIAA	0.000	0.000				79.547	70.05				0.054	66.78			
10 µM auxinole + 10 µM 4pTb-MeIAA	116.361	42.10	31.52	±	8.48	26.346	4.20	1.94	±	1.30	0.055	67.06	77.46	±	16.67
10 µM auxinole + 10 µM 4pTb-MeIAA	171.032	37.69			26.92%	38.851	1.11			66.96%	0.088	104.98			21.52%
10 µM auxinole + 10 µM 4pTb-MeIAA	99.278	33.30				23.989	2.22				0.047	58.58			
10 µM auxinole + 10 µM 4pTb-MeIAA	94.564	51.13				23.764	0.35				0.072	87.46			
10 µM auxinole + 10 µM 4pTb-MeIAA	84.684	36.04				21.360	1.81				0.056	69.25			
Standard curve	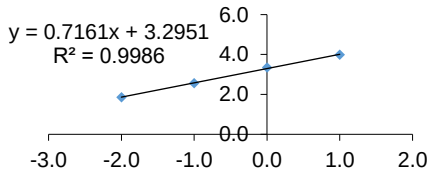					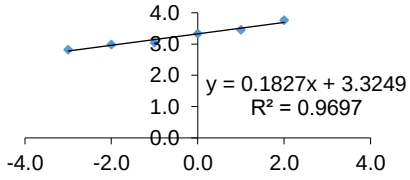					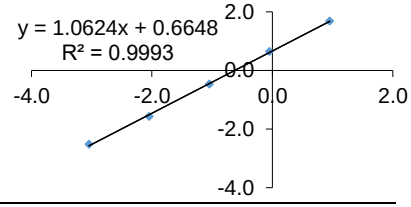				

Table S4.2: Quantification of the auxin metabolites through isotopically labelled LC-MS/MS analysis. *Arabidopsis thaliana* samples (10 mg FW) were extracted, purified using the in-tip µSPE procedure and analysed by LC–MS/MS. The standard curves with regression equations were also shown below.

Analytes	oxIAA					IAA-Asp					IAA-Glu				
	AUC	pmol/g FW ± SD; RSD [%]				AUC	pmol/g FW ± SD; RSD [%]				AUC	pmol/g FW ± SD; RSD [%]			
control	0.191	652.50	510.00	±	91.45	0.045	6.56	8.00	±	1.55	0.247	85.81	49.54	±	21.54
control	0.087	542.14			17.93%	0.029	6.66			19.35%	0.119	58.51			43.48%
control	0.245	496.01				0.062	7.15				0.373	46.48			
control	0.376	490.40				0.066	9.19				0.285	31.91			
control	0.191	368.96				0.045	10.44				0.247	24.98			
10 µM auxinole	0.332	924.07	541.15	±	206.64	0.076	37.55	21.09	±	8.31	0.342	170.98	99.26	±	37.97
10 µM auxinole	0.174	373.96			38.19%	0.034	16.33			39.38%	0.144	70.39			38.25%
10 µM auxinole	0.191	344.84				0.038	18.40				0.153	74.55			
10 µM auxinole	0.152	541.53				0.036	17.94				0.212	105.29			
10 µM auxinole	0.137	521.37				0.031	15.25				0.148	75.10			
10 µM 4pTb-MeIAA	0.187	494.93	549.51	±	97.64	0.043	21.07	18.83	±	4.73	0.139	71.24	81.86	±	19.22
10 µM 4pTb-MeIAA	0.208	713.61			17.77%	0.048	24.28			25.14%	0.200	104.85			23.48%
10 µM 4pTb-MeIAA	0.195	463.24				0.043	21.32				0.141	72.13			
10 µM 4pTb-MeIAA	0.137	608.75				0.034	16.87				0.210	104.09			
10 µM 4pTb-MeIAA	0.076	467.00				0.021	10.62				0.109	57.00			
10 µM auxinole + 10µM 4pTb-MeIAA	0.289	511.79	507.91	±	13.45	0.054	26.44	21.37	±	5.91	0.238	119.28	102.94	±	13.42
10 µM auxinole + 10µM 4pTb-MeIAA	0.059	517.61			2.65%	0.020	10.11			27.65%	0.160	81.99			13.04%
10 µM auxinole + 10µM 4pTb-MeIAA	0.194	481.85				0.049	24.20				0.231	115.69			
10 µM auxinole + 10µM 4pTb-MeIAA	0.156	518.51				0.042	21.02				0.194	98.77			
10 µM auxinole + 10µM 4pTb-MeIAA	0.212	509.77				0.051	25.10				0.195	99.00			
Standard curve	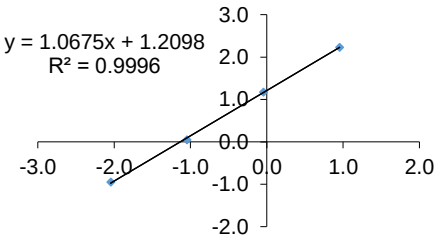					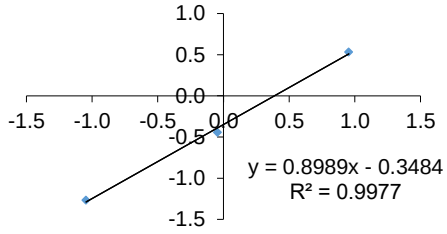					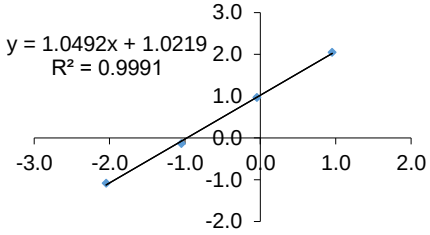				

(continued)

Analytes	oxIAA-Asp					oxIAA-Glu					oxIAA-Glc				
	AUC	pmol/g FW ± SD; RSD [%]				AUC	pmol/g FW ± SD; RSD [%]				AUC	pmol/g FW ± SD; RSD [%]			
control	0.191	3.62	20.87	±	13.13	0.264	79.64	90.64	±	9.70	2.750	3094.42	2763.22	±	249.77
control	0.087	10.47			62.94%	0.146	79.76			10.70%	1.711	2985.36			9.04%
control	0.245	22.31				0.310	93.20				3.452	2747.11			
control	0.376	26.52				0.361	95.93				3.604	2559.04			
control	0.191	41.43				0.264	104.67				2.750	2430.17			
10 µM auxinole	0.332	77.23	43.67	±	17.22	0.401	207.64	132.74	±	39.54	3.788	3455.51	2415.59	±	525.73
10 µM auxinole	0.174	36.91			39.43%	0.194	90.91			29.79%	2.457	2021.04			21.76%
10 µM auxinole	0.191	41.49				0.238	114.23				2.703	2201.70			
10 µM auxinole	0.152	32.68				0.250	127.71				2.399	2145.03			
10 µM auxinole	0.137	30.05				0.250	123.22				2.501	2254.68			
10 µM 4pTb-MeIAA	0.187	41.77	37.98	±	11.56	0.291	133.10	133.96	±	45.88	2.768	2507.55	2571.99	±	393.38
10 µM 4pTb-MeIAA	0.208	51.10			30.44%	0.396	218.84			34.25%	2.998	2977.83			15.29%
10 µM 4pTb-MeIAA	0.195	46.05				0.260	122.21				3.449	3059.02			
10 µM 4pTb-MeIAA	0.137	32.73				0.254	114.70				2.552	2268.50			
10 µM 4pTb-MeIAA	0.076	18.25				0.175	80.96				2.138	2047.06			
10 µM auxinole + 10µM 4pTb-MeIAA	0.289	63.20	39.01	±	16.46	0.277	136.00	129.08	±	9.36	2.542	2331.21	2693.59	±	549.10
10 µM auxinole + 10µM 4pTb-MeIAA	0.059	12.78			42.20%	0.309	139.87			7.25%	1.986	1913.60			20.39%
10 µM auxinole + 10µM 4pTb-MeIAA	0.194	41.81				0.288	130.84				3.330	2972.54			
10 µM auxinole + 10µM 4pTb-MeIAA	0.156	32.54				0.271	125.74				2.963	2726.97			
10 µM auxinole + 10µM 4pTb-MeIAA	0.212	44.69				0.244	112.96				3.986	3523.62			
Standard curve	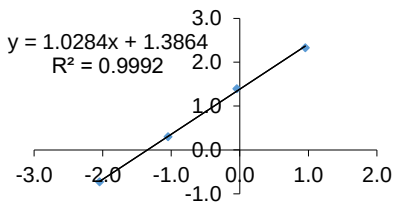					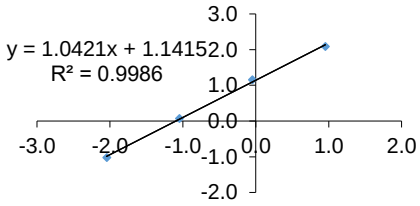					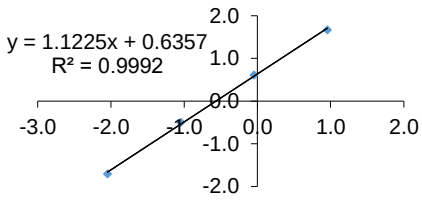				

Fig. S1: Standard curves of auxinole and 4pTb-MeIAA in DESI-MS infusion

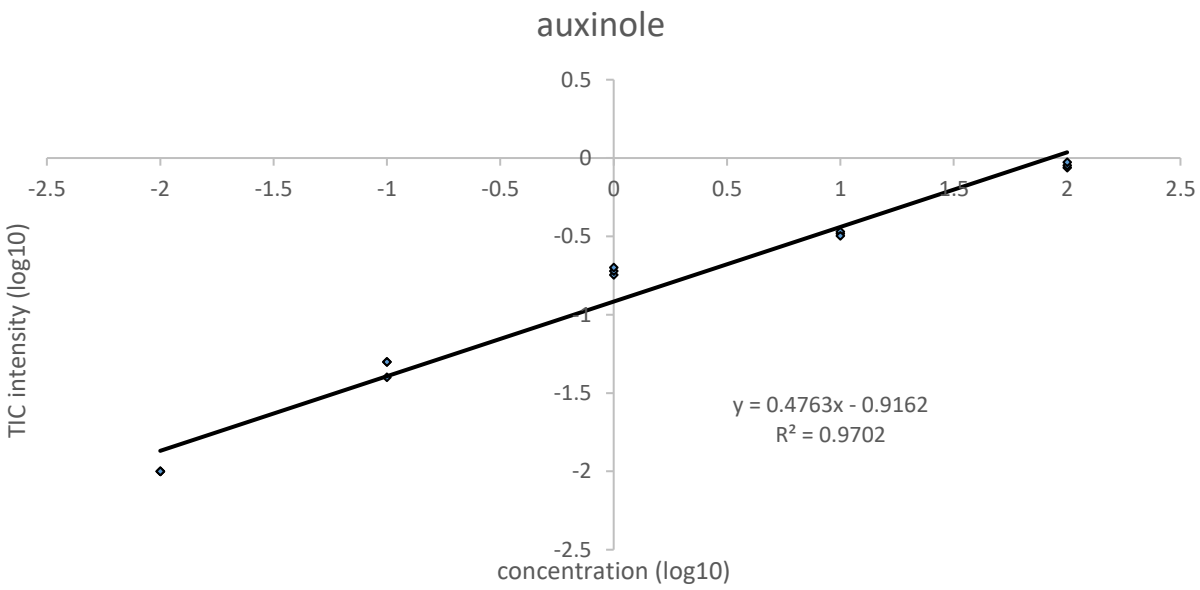

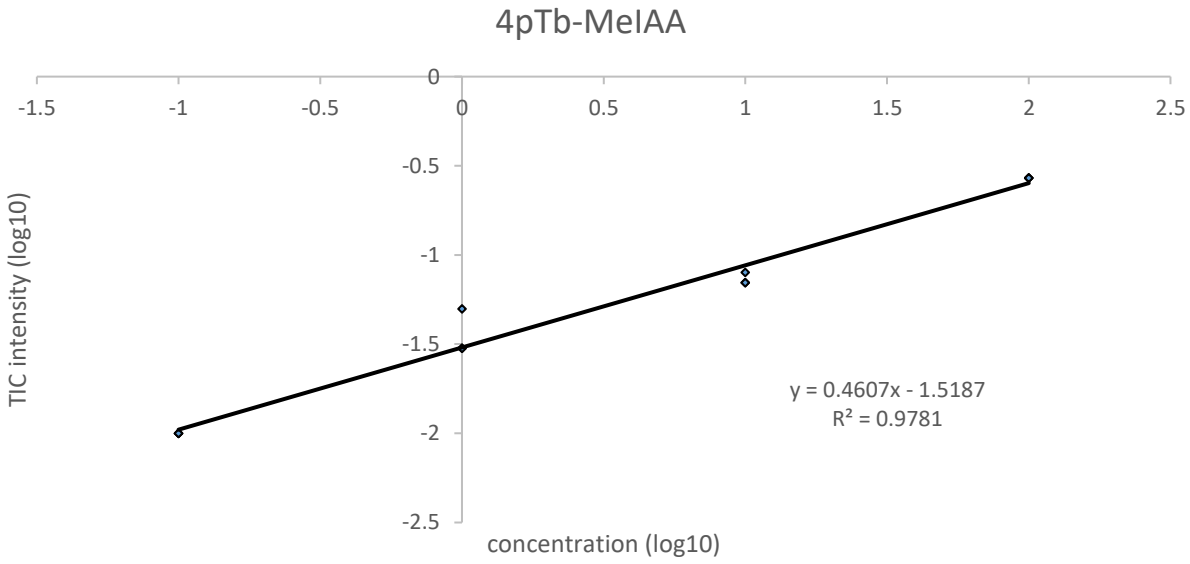

Fig. S2: Drift ion intensity maps of replicated samples

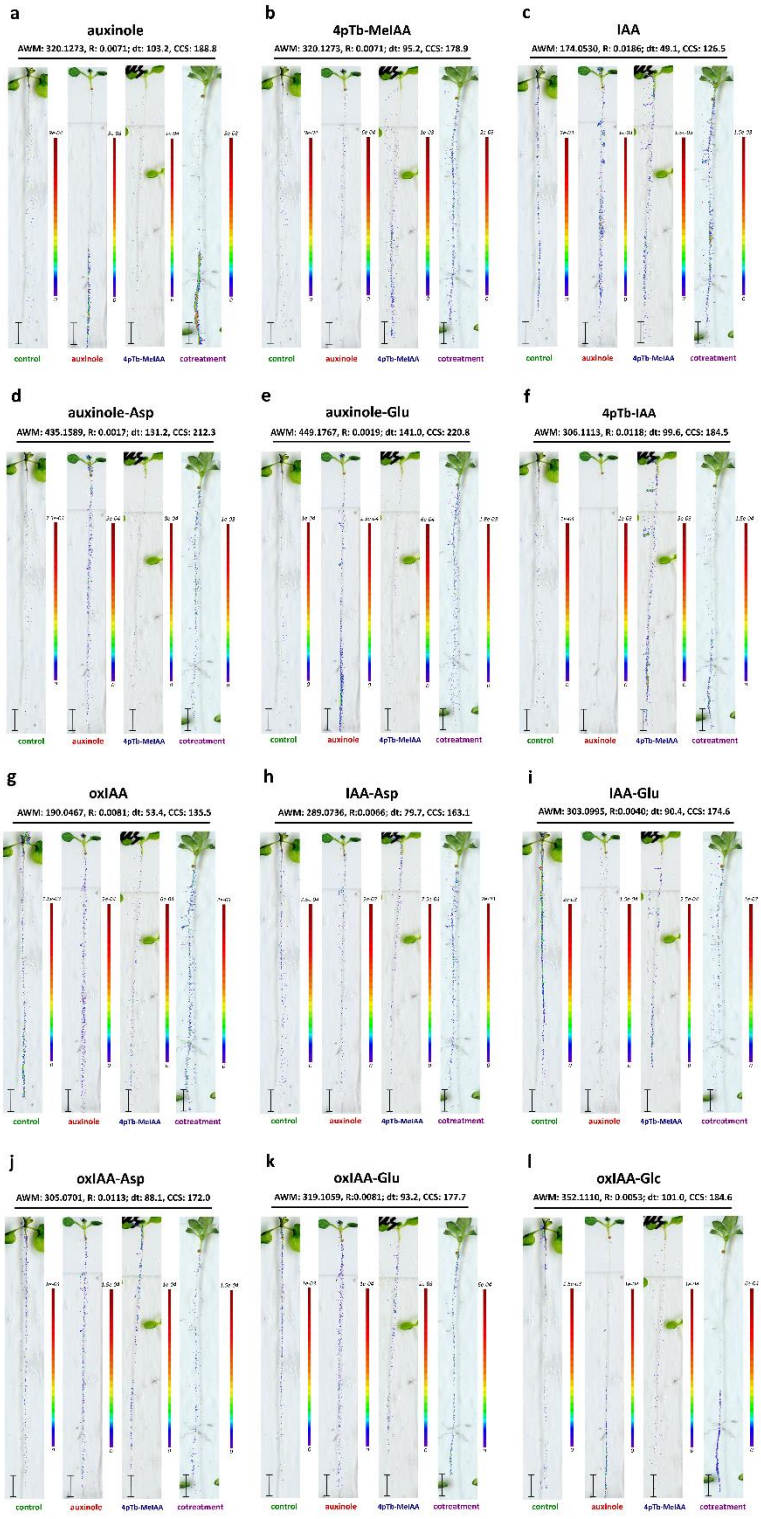

(continued)

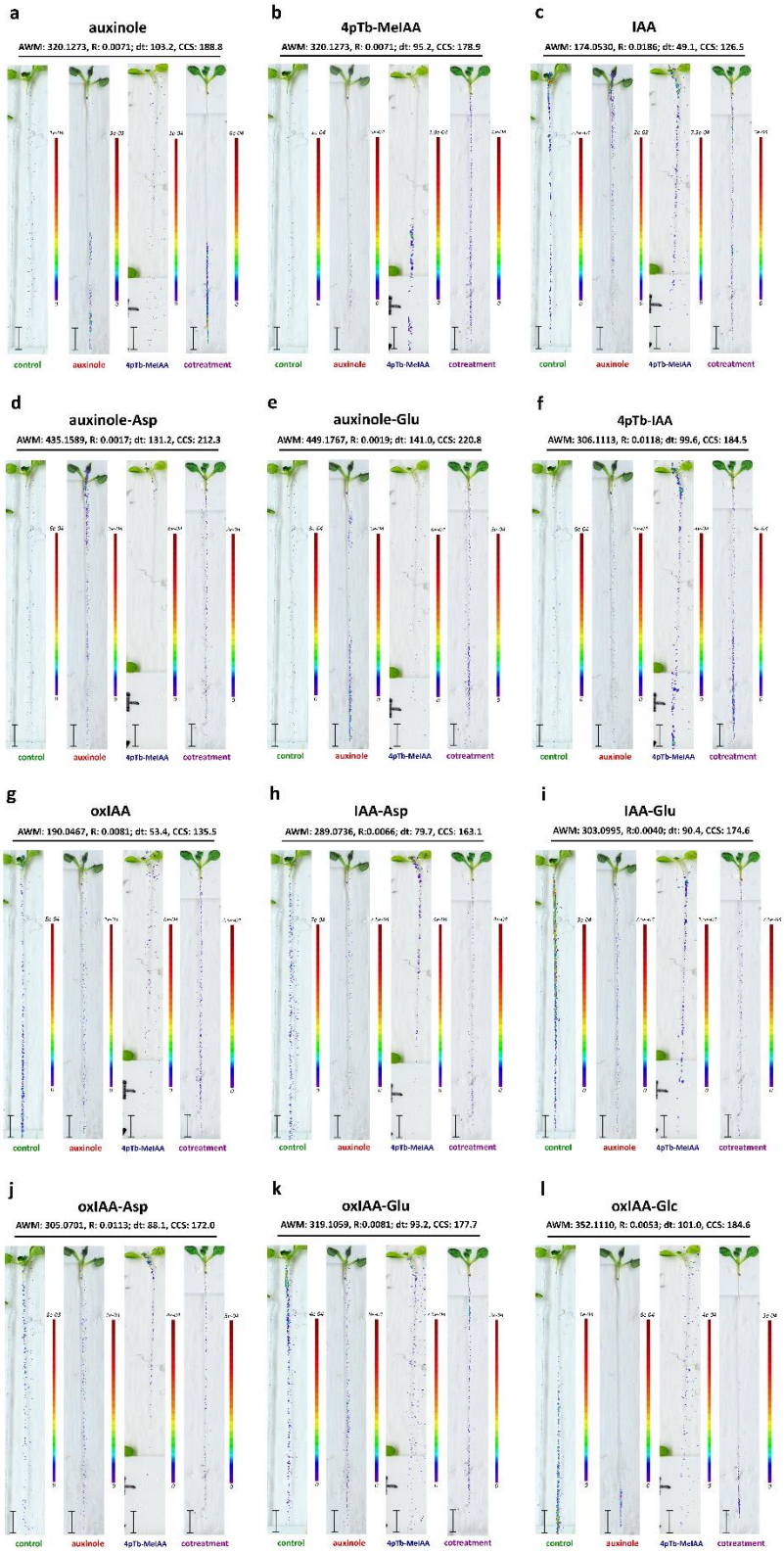
a
auxinole
AWM: 320.1273, R: 0.0071; dt: 103.2, CCS: 188.8
b
4pTb-MeIAA
AWM: 320.1273, R: 0.0071; dt: 95.2, CCS: 178.9
c
IAA
AWM: 174.0530, R: 0.0186; dt: 49.1, CCS: 126.5
d
auxinole-Asp
AWM: 435.1589, R: 0.0017; dt: 131.2, CCS: 212.3
e
auxinole-Glu
AWM: 449.1767, R: 0.0019; dt: 141.0, CCS: 220.8
f
4pTb-IAA
AWM: 306.1113, R: 0.0118; dt: 99.6, CCS: 184.5
g
oxIAA
AWM: 190.0467, R: 0.0081; dt: 53.4, CCS: 135.5
h
IAA-Asp
AWM: 289.0736, R:0.0066; dt: 79.7, CCS: 163.1
i
IAA-Glu
AWM: 303.0995, R:0.0040; dt: 90.4, CCS: 174.6
j
oxIAA-Asp
AWM: 305.0701, R: 0.0113; dt: 88.1, CCS: 172.0
k
oxIAA-Glu
AWM: 319.1059, R:0.0081; dt: 93.2, CCS: 177.7
l
oxIAA-Glc
AWM: 352.1110, R: 0.0053; dt: 101.0, CCS: 184.6
control
auxinole
4pTb-MeIAA
cotreatment

Fig. S3: *In situ* DESI-IM-MS/MS spectra of auxins

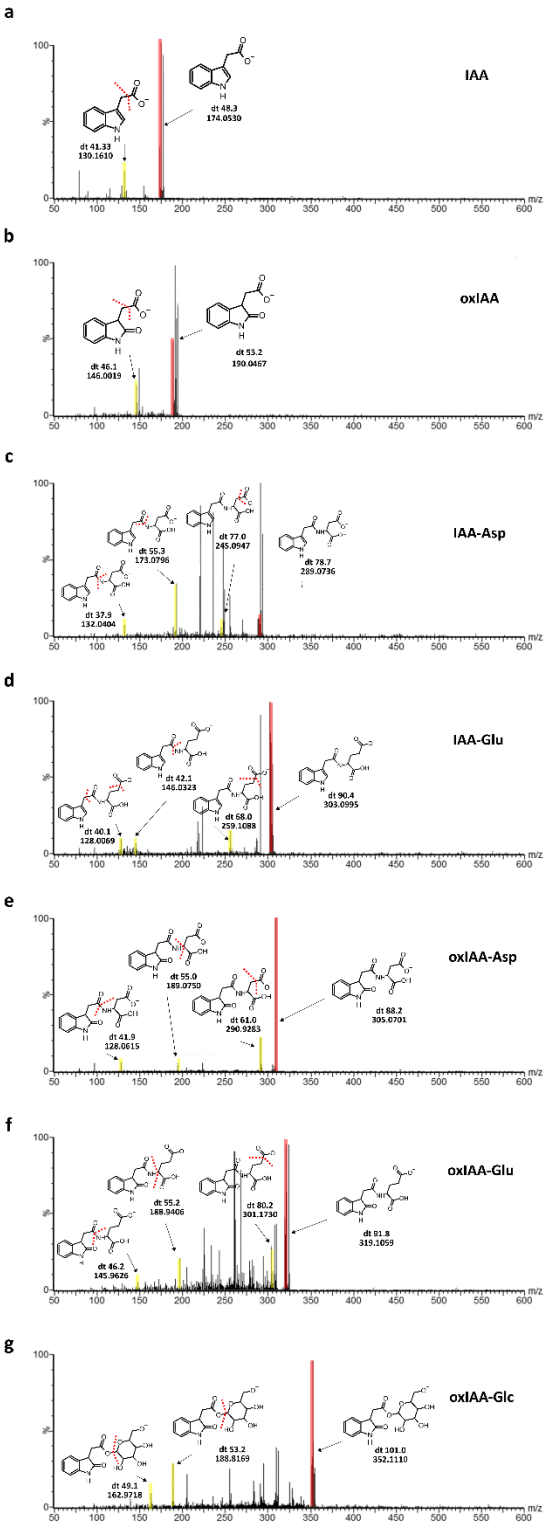

Fig. S4: Mass spectrometry analysis of auxin metabolites abundance in control compared to 10 μM auxinole, 10 μM 4pTb-MeIAA and 10 μM auxinole + 10 μM 4pTb-MeIAA cotreated samples. n.s. not significant, *p ≤ 0.05, **p ≤ 0.01, ***p ≤ 0.001, ****p ≤ 0.001.

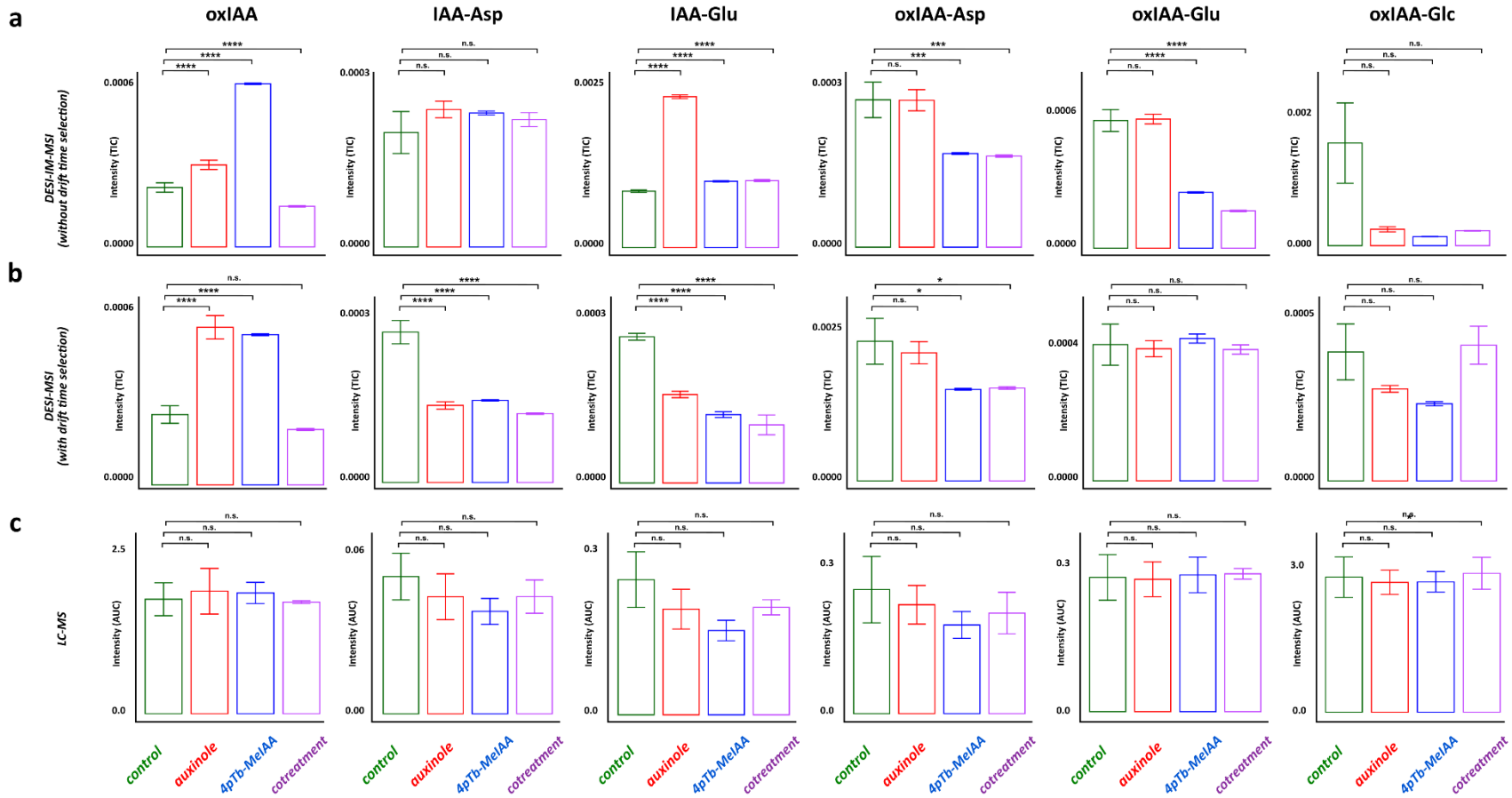

Reference

1. Bieleszová K, Pařízková B, Kubeš M, Husičková A, Kubala M, Ma Q, et al. New fluorescently labeled auxins exhibit promising anti-auxin activity. New Biotechnology. 2019;48:44-52.

PALACKÝ UNIVERSITY IN OLOMOUC

FACULTY OF SCIENCE

Laboratory of Growth Regulators

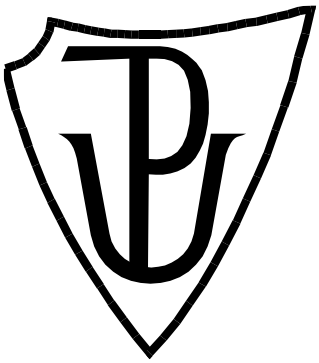

Summary of the Doctoral Thesis

Study of auxin metabolism at the organ level

Mgr. Pavel Hladík

P0511D030004 - Experimental biology

Supervisor

Prof. Mgr. Ondřej Novák, Ph.D.

Olomouc

2024

This Ph.D. thesis was realized in the Laboratory of Growth Regulators within the framework of internal Ph.D. Study of Experimental Biology, guaranteed by the Laboratory of Growth Regulators, Faculty of Science, Palacký University in Olomouc, between the years 2020 – 2024.

Ph. D. candidate:	**Mgr. Pavel Hladík**
Supervisor:	**Prof. Mgr. Ondřej Novák, Ph.D.** Laboratory of Growth Regulators, Institute of Experimental Botany, The Czech Academy of Sciences & Faculty of Science, Palacký University, Olomouc, Czech Republic.
Consultant:	**Mgr. Aleš Pěnčík, Ph.D.** Laboratory of Growth Regulators, Institute of Experimental Botany, The Czech Academy of Sciences & Faculty of Science, Palacký University, Olomouc, Czech Republic.
Opponents:	**Dr. Branka Salopek Sondi** Department for Molecular Biology, Ruđer Bošković Institut, Zagreb, Croatia.
	Ing. Karel Müller, Ph.D. Laboratory of Hormonal Regulations in Plants, Institute of Experimental Botany, The Czech Academy of Sciences, Prague, Czech Republic.

The evaluation of this Ph.D. thesis was written by **Prof. Ing. Miroslav Strnad, CSc. DSc.**, Laboratory of Growth Regulators, Institute of Experimental Botany, The Czech Academy of Sciences & Faculty of Science, Palacký University, Olomouc, Czech Republic.

The oral defence will take place on 20. 6. 2024 before the Commission for the Ph.D. thesis of the Study programme Experimental biology, **Seminary room – Building No. 52**, Šlechtitelů 27, Olomouc – Holice.

The Ph.D. thesis and expert reviews will be available 14 days before the defence in the Study Department of Faculty of Science (Mgr. M. Karásková), Palacký University in Olomouc, 17. Listopadu 12, Olomouc.

After the defence, the Ph.D. thesis will be stored in the Library of the Biological Departments of Faculty of Science, Palacký University, Šlechtitelů 27, Olomouc – Holice.

Prof. Ing. Miroslav Strnad, CSc. DSc.

Chairman of the Commission for the Ph.D. thesis,

Study programme Experimental Biology,

Faculty of Science, Palacký University in Olomouc

Content

1 Introduction 4

2 Aims and scopes 5

3 Material and Methods 6

4 Survey of results 9

5 Conclusion and future perspectives 15

6 References 16

7 List of author's publications 18

8 Souhrn (Summary in Czech) 20

1 Introduction

Proper plant growth and development are intricately regulated by a group of bioactive compounds known as plant hormones (phytohormones). These substances function optimally within a narrow concentration range, necessitating strict regulation of their levels in plant cells and organs. This regulation primarily occurs through biosynthesis, metabolism and transport mechanisms.

Among the diverse groups of phytohormones, auxins were the first to be identified owing to their profound effects on plant tropisms. Two essential endogenous auxins are indole-3-acetic acid (IAA) and phenylacetic acid (PAA). These compounds exhibit biological active only in their free, unconjugated form. Enzymatic reactions produce metabolites that serve as temporary storage and transport forms, as well as degradation products. This conversion occurs either through irreversible oxidation of IAA to 2-oxo-indole-3-acetic acid (oxIAA) or reversible conjugation with amino acids and sugars. In the presence of GRETCHEN HAGEN 3 (GH3) family enzymes, IAA and oxIAA form amides, primarily (ox)IAA-aspartate and glutamate. Another important pathway involves reversible glycosylation by the uridine diphosphate glucosyltransferases, UGT84B1 and UGT74D1, resulting in indole-3-acetyl-1-O-ß-d-glucose (IAA-glc) and its oxidised form 2-oxindole-3-acetyl-1-O-ß-d-glucose (oxIAA-glc), respectively.

In most plant species, the auxin PAA is found at higher levels than IAA. However, the concentration required to induce an auxin response is significantly higher for PAA. Consequently, PAA has received less research attention, and its metabolism remains relatively unexplored. So far, the metabolism of PAA and IAA appears quite similar, as the same enzymes catalyse the synthesis of identical conjugates. Currently, only three metabolites (PAA-aspartate, PAA-glutamate and PAA-tryptophan) have been identified in plants. Although *in vitro* studies have demonstrated the conjugation of PAA with glucose by the enzyme UGT84B1, this compound has not yet been found *in planta*.

Delving deeper into the complex world of phytohormones can uncover their role in plant growth and development. Therefore, this doctoral thesis aims to broaden our understanding of auxin metabolic pathways across various plant species and their organs by sensitive mass spectrometry methods.

2 Aims and scopes

In recent years, many new discoveries have been made in the field of auxin metabolism, expanding our knowledge about conjugates and catalysing enzymes. However, most of this research is connected to IAA and *Arabidopsis thaliana* as a model plant. Therefore, this doctoral thesis aims to broaden the understanding of these processes in two endogenous auxins (IAA and PAA) across various land plant species and their organs.

The main aims described in this thesis are as follows:

- Identification of novel IAA and PAA metabolites in plants by liquid chromatography coupled with tandem mass spectrometry (LC-MS/MS).

- Complex IAA and PAA metabolite profiling in various land plant species and their organs by previously developed LC-MS/MS methods.

- Understanding the regulatory mechanism of PAA metabolism by elucidating catalysing enzymes and pathways complementarity.

- Developing extraction and detection methods for newly synthesized synthetic auxins with anti-auxin activity and utilizing this method to measure the uptake and stability of these compounds in plants.

3 Material and Methods

Chemicals

- Plant agar and Murashige & Skoog media were purchased from Duchefa (Haarlem, Netherlands); hypergrade purity methanol and acetonitrile for LC-MS/MS analysis and all other chemicals were purchased from Merck (Darmstadt, Germany), Sigma-Aldrich (MA, USA), and Lach-Ner (Neratovice, Czech Republic).
- Auxin standards and analogues were purchased from OlChemIm (Olomouc, Czech Republic) or synthesized by colleagues from Department of Chemical biology (Faculty of Science, Palacký University in Olomouc). Isotopically labelled auxin standards were purchased from Cambridge Isotope Laboratories, Inc (MA, USA).

Plant material and growth conditions

- *Arabidopsis thaliana* seeds ecotype Columbia-0 (Col-0) were used as a wild type (WT) in all experiments.
- Arabidopsis knockout mutant lines with alterations in auxin metabolism - GH3 sextuple *gh3.1,2,3,4,5,6* (Porco et al., 2016); GH3 octuple *gh3.1,2,3,4,5,6,9,17* (Casanova-Saéz et al., 2022); *ugt74d1* and *ugt84b1* (Mateo-Bonmatí et al., 2021).
- Other cultivated plant species: maize (*Zea mays* L.), pea (*Pisum sativum arvense* L.), wheat (*Triticum aestivum* L.), moss (*Physcomitrella patens*), and spruce (*Picea abies* L. Karst).
- Arabidopsis seeds were sterilized in 70% ethanol with the addition of 0.1% Tween 20 for 5 min, sown on Murashige & Skoog medium in square agar plates (10 g sucrose, 2.2 g MS medium, 10 g agar, pH 5.7, all amounts are per litre), and cold treated for 4 days prior to germination. The plates were then transferred to a cultivation chamber and vertically placed under long-day conditions (16 h light/8 h dark) at 22 ± 1°C under cool white fluorescent light (maximum irradiance 550 µmol m^{-2} s^{-1}).
- Pea, wheat, and maize seeds were left germinating in wet conditions in the dark for 2, 3, and 4 days, respectively, selected according to their uniformity from a large population, transferred to hydroponic boxes, watered with Hoagland's solution and left growing in the cultivation room (16 h light/8 h dark) at 22 ± 2°C, while changing the solution every 3 days.
- Spruce seeds were soaked in the tap water for 24 h at 4°C and sown in a wet vermiculite. Germination and seedling growth occurred in a growth chamber under long-day conditions (16 h light/8 h dark) at 22 ± 2°C.

- Gametophores from *P. patens* were cultured on round Petri plates (Knop medium, pH 5.8, 1.5% plant agar). The plates with gametophores were transferred to a cultivation chamber and vertically placed under long-day conditions (16 h light/8 h dark) at 22 ± 1°C. Each 3 weeks, gametophores were moved to a fresh medium.
- For auxin metabolite profiling, all plant species were harvested in the growth stage 1.0 according to *Biologische Bundesanstalt, Bundessortenamt und Chemische Industrie* (BBCH) scale (Tottman, 1987; Lancashire et al., 1991; Boyes et al., 2001), except for *P. patens* which was harvested 3 weeks after the last transfer and moved to the fresh medium.

Methods

Extraction and purification

- For auxin metabolite profiling, ≈ 10 mg FW of plant tissues was harvested and extracted in 1 mL of sodium-phosphate buffer (50 mM, pH 7.0, 4°C) containing 0.1% diethyldithiocarbamic acid sodium salt. The extracts were then purified by in-tip micro solid-phase extraction (in-tip µSPE) (Pěnčík et al., 2018; Hladík, 2020) and evaporated to dryness *in vacuo*. To cover analytes lost during sample preparation, a mixture of isotopically labelled standards was added prior to extraction.
- Plant extracts from Arabidopsis tissues for all measured auxin analogues were prepared by an one-step liquid-liquid extraction (LLE) utilizing a water:methanol/acetonitrile:hexane (1:1:1) solution. The water:methanol/acetonitrile fraction was filtered through MicroSpin tubes (0.2 µm, nylon, Chromservis, Czech Republic) and flow-through fraction was then evaporated *in vacuo*.

LC-MS/MS

- For measurement of IAA, PAA and their metabolic profiles, a high-performance liquid chromatography (HPLC) 1260 Infinity II system and a 6495B Triple Quadrupole LC/MS system equipped with Jet Stream and Dual Ion Funnel systems (Agilent Technologies, CA, USA) were employed. A reverse-phase column (Kinetex C18 100 Å, 50 x 2.1 mm, 1.7 µm; Phenomenex, CA, USA) was used to separate the compounds. The time of each analysis was 18 min, the flow rate was 0.3 mL/min, and metabolites were eluted with a linear gradient as follows: 0 min – 10% B, 11.5 min – 60% B, 11.75 min – 100% B, 14.75 min – 100% B, 15 min – 10% B. Analytes were detected and quantified using diagnostic multiple reaction monitoring (MRM) transitions of precursor and appropriate product ions. The concentrations of all compounds were then calculated by the isotopic dilution method using corresponding stable isotope labelled standards. LC-MS/MS analysis as well as data processing were performed using Mass Hunter software (Agilent Technologies, CA, USA).

- Development of LC-MS/MS method for the analysis of newly synthesized nitrobenzoxadiazole (NBD) or 5-(dimethylamino)naphthalene-1-sulfonyl (DNS) labelled auxin analogues was performed on an Acquity UPLC® I-Class System (Waters, USA) coupled to a triple quadrupole mass spectrometer Xevo™ TQ-S MS (Waters MS Technologies, UK). A reverse-phase column (Kinetex C18 100 Å, 50 x 2.1 mm, 1.7 µm; Phenomenex, CA, USA) was used for LC compound separation. The mobile phase consisted of acetonitrile (A) and deionized water (B), both with the addition of 0.1% acetic acid. The duration of each analysis was 5.5 min, flow rate 0.3 mL/min and gradient elution as follows: 0 min – 60% B, 3.0 min – 30% B, 4.25 min – 99% B, 4.5 min – 99% B, 5.5 – 60% B. For compound quantification, Arabidopsis extracts were spiked with 1 nmol of NBD- or DNS-labelled conjugates and samples were processed by LLE as described above. To calculate analytes losses and matrix effects, a six-point external calibration curve ranging from 1 fmol to 100 pmol in 10% acetonitrile was measured and the recovery factor of each analyte was calculated. For samples with unknown conjugates levels, dilution and recovery factors were applied and concentration was calculated from an external calibration curve.
- 4-(2,4-dimethylphenyl)-2-(1H-indol-3-yl)-4-oxobutanoic acid (auxinole) and methyl 2-(1H-indol-3-yl)-4-oxo-4-p-tolyl-butanoate (4pTb-MeIAA) were measured on a HPLC 1260 Infinity II system and a 6495B Triple Quadrupole LC/MS system (Agilent Technologies, CA, USA). The chromatographic reverse-phase column (Kinetex C18 100 Å, 50 x 2.1 mm, 1.7 µm; Phenomenex, CA, USA) was employed for analytes separation. The analysis time was 13 min, the flow rate was 0.3 mL/min, and the mobile phase consisted of deionized water (A) and methanol (B), both with the addition of 0.1% acetic acid. Gradient elution was set as follows: 0 min – 40% B, 9 min – 95% B, 9.25 min – 99% B, 10 min – 99% B, 10.50 min – 40% B. For metabolites quantification, the same method as described in the previous paragraph was applied.

4 Survey of results

The methodical part of this work builds upon the results obtained in the master's thesis, where the LC-MS/MS method was developed for measuring the IAA and PAA metabolic profiles (Hladík, 2020). By utilizing this method, we made a groundbreaking discovery: two new oxIAA conjugates, namely oxIAA-leucine (oxIAA-Leu) and oxIAA-phenylalanine (oxIAA-Phe), were identified in plants for the first time. We further measured low-molecular-weight IAA metabolites, with a specific focus on oxIAA conjugates, in the organs of four representative monocotyledonous and dicotyledonous plants at different developmental stages. This investigation aimed to enhance our understanding of auxin metabolism during plant growth.

In our exploration of PAA metabolites, we identified four new conjugates: phenylacetyl-leucine (PAA-Leu), phenylacetyl-phenylalanine (PAA-Phe), phenylacetyl-valine (PAA-Val) and phenylacetyl-1-O-ß-d-glucose (PAA-glc). The concentrations of these new conjugates with other known PAA metabolites were then screened at the organ level in various plants species. To gain insights into novel PAA metabolic pathways, we concluded feeding experiments with PAA using Arabidopsis mutant lines defective in auxin metabolic regulation. Additionally, we employed kakeimide (KKI), a selective inhibitor of GH3 proteins (Fukui et al., 2022), in conjunction with PAA treatments in Arabidopsis, spruce and moss. These experiments allowed us to monitor metabolic redundancy in other plant species where mutant lines were not available.

Synthetic auxins play a crucial role in auxin homeostasis research. Many of these molecules have anti-auxin activity by binding to the TRANSPORT INHIBITOR RESPONSE 1/AUXIN SIGNALING F-BOX receptor, yet they do not trigger typical auxin responses (Hayashi et al., 2012). This group of synthetic auxins includes compounds such as auxinole and its analogues, as well as fluorescently labelled synthetic anti-auxins. Notably, these molecules have different chemical structures compared to endogenous auxins, necessitating the development and optimization of novel extraction and MS-based methods. This task was particularly challenging task due to their varying polarity, size and stability. Importantly, the newly developed methods have enabled us to study the stability and uptake of selected synthetic auxins in treated plants.

2-oxindole-3-acetyl-amino acids are important auxin metabolites in plants

Recently, many studies describing the synthesis and hydrolysis of 2-oxindole-3-acetyl-amino acids (oxIAA-AAs) have been published (Hayashi et al., 2021; Müller et al., 2021; Isobe and Miyagawa, 2022). However, their distribution and importance in auxin metabolism have not been determined. Therefore, we employed a previously developed in-tip µSPE purification method (Pěnčík et al., 2018)

and subsequent LC-MS/MS analysis, to quantify oxIAA-AAs in multiple plant species and their organs and compare their levels with other IAA metabolites. This method was subsequently optimised and validated for full IAA metabolite profiling, including oxIAA-AAs (Hladík, 2020). Due to the low detection limit of the LC-MS/MS method, optimised MRM transitions for oxIAA-Leu and oxIAA-Phe were added and their occurrence screened in organs of different plant species. Their endogenous concentrations were observed in pea cotyledons and oxIAA-Phe also in maize cotyledons, however both at low levels, corresponding to low abundance of their IAA counterparts (Kowalczyk and Sandberg, 2001; Pěnčík et al., 2009).

Employing the LC-MS/MS method, we performed profiling of IAA metabolite in roots, shoots and cotyledons of pea, wheat and maize, and only in roots and shoots of Arabidopsis due to the large amount of plant material required and the technical difficulties of cotyledon harvesting. To make the metabolic profile of various species as comparable as possible, we harvested plants at growth stage 1.0, according to the BBCH scale, which was developed to compare between species according to their phenotype (Tottman, 1987; Lancashire et al., 1991; Boyes et al., 2001). All of indole-3-acetyl-amino acids (IAA-AAs) and oxIAA-AAs were combined into an appropriate group and their relative (%) abundance to the total IAA pool was calculated. This profiling revealed significant difference in dominant conjugates and metabolic pathways between plant species and even their tissues. In Arabidopsis organs, most of the IAA was found in the form of oxIAA-glc, followed by oxIAA, demonstrating the importance of this pathway. On the other hand, in pea, oxIAA-AAs were completely dominant, as in cotyledons, oxIAA-aspartate (oxIAA-Asp) forms > 99% of the total IAA pool. Furthermore, we quantified the IAA metabolome in seeds of the same species, which were allowed to germinate for 24 hours under wet conditions (Tab. 1). Interestingly, our results indicate higher levels of free IAA in these seeds compared to cotyledons at growth stage 1.0, suggesting a potential contribution of free IAA to seed germination. Conversely, levels of IAA conjugates were lower in seeds, implying that cotyledons may serve as a reservoir for auxin during later developmental stages.

In plants, auxin metabolism is an ever-changing process depending on the development and environmental conditions. To address these changes during plant development, we measured plants and their tissues in the three growth stages 1.0, 1.1 and 1.2 according to BBCH scale. These stages show early seedling development from the first leaf emergence to two fully developed leaves in stage 1.2. In all crop species, higher auxin concentrations were found in roots compared to shoots at all growth stages. Amide-linked conjugates were more prevailed in earlier stages and steadily decreased, in contrast to oxIAA-glc in monocots roots, which increased during growth. In conclusion, IAA metabolites levels are strongly dependent on plant development, which contributes to the proper auxin balance.

Tab. 1: IAA metabolite profiles in seeds of maize, wheat, and pea. Levels (pmol/g FW) of IAA, oxIAA and their conjugates with amino acids and glucose were determined in seeds of maize, wheat and pea after being left to germinate in moist conditions for 24 hours. The levels of IAA and oxIAA conjugates with individual amino acids (Asp, Glu, Leu and Phe) were summed up into two corresponding groups IAA-AA and oxIAA-AA, respectively. The distribution (%) of different conjugate classes was calculated as their relative abundance to the total measured IAA metabolite pool (%). All samples were measured in five biological replicates. <LOD, under the limit of detection.

	Maize		**Wheat**		**Pea**	
	(pmol/g)	(%)	(pmol/g)	(%)	(pmol/g)	(%)
IAA	6,858.6	27.31	119.5	63.14	19.2	0.01
IAA-AA	287.8	0.00	30.7	16.24	710.2	0.30
IAA-glc	<LOD	-	<LOD	-	<LOD	-
oxIAA	17,311.9	68.94	39.0	20.62	170.0	0.07
oxIAA-AA	297.0	1.18	<LOD	-	238,191.5	99.62
oxIAA-glc	356.5	1.42	<LOD	-	<LOD	-

All data are summarized in: **Hladík P.**, Petřík I., Žukauskaitė A., Novák O., Pěnčík A. (2023) Metabolic profiles of 2-oxindole-3-acetyl-amino acid conjugates differ in various plant species. *Front. Plant Sci.* **14**, 1217421.

Unravelling novel metabolic pathways in PAA metabolism

In the field of auxin research, most attention has been dedicated to studying IAA owing to its high activity in auxin bioassays. Nevertheless, emerging evidence suggests that other auxins, such as PAA, which exhibits approximately 10% of the activity of IAA in these tests, may also play crucial roles in plant development. Numerous studies suggest that PAA contributes to processes such as lateral root development, antimicrobial activity and auxin crosstalk (reviewed in Perez et al., 2023). Despite sharing similarities in conjugation pathways with IAA, including involvement of the same enzymes, information regarding PAA metabolism remains limited (Sugawara et al., 2015; Westfall et al., 2017). We therefore aimed to elucidate novel conjugates and metabolic pathways associated with PAA metabolism.

The extraction and LC-MS/MS methods developed for the profiling of IAA metabolites were also optimized and validated also for PAA metabolite profile (Hladík, 2020). Utilizing this method, we identified four new PAA conjugates: PAA-Leu, PAA-Phe, PAA-Val and PAA-glc. Although *in vitro* synthesis of PAA-glc has been reported previously (Aoi et al., 2020c), we provide the first evidence of its presence in Arabidopsis and spruce tissues. Furthermore, we conducted bacterial enzymatic assays with AtUGT84B1 and AtUGT74D1 expressed in *Escherichia coli* to investigate their conjugation activity towards PAA. Our findings demonstrate that both enzymes are capable of forming PAA-glc *in vitro*.

Finally, this was also confirmed in Arabidopsis *ugt74d1* and *ugt84b1* knockout lines, which exhibited reduced concentrations of PAA-glc compared to WT Col-0.

Similar experiments were also performed for the newly identified phenylacetyl-amino acids (PAA-AAs). These metabolites were detected in all pea tissues and also in wheat cotyledons, although at concentrations not surpassing 8 picomoles per gram fresh weight (pmol/g FW). These low concentrations mirror those of their IAA and oxIAA relatives. The potential for their synthesis in Arabidopsis was examined through PAA treatment, revealing their formation even after 30 minutes. However, their levels did not show significant increases over time, indicating rapid turnover. While the involvement of GH3 enzymes in PAA-Glu and PAA-Asp synthesis has been previously published (Sugawara et al., 2015; Staswick et al., 2017), our study demonstrates that these enzymes also form other PAA-AAs. Although the hydrolysis of IAA-AAs back to IAA has been documented (Bartel and Fink, 1995; Hayashi et al., 2021), such a process has not been investigated for PAA-AAs. Utilizing bacterial enzyme assays with IAA-ALANINE RESISTANT 3 (AtIAR3), IAA-LEUCINE RESISTANT 1 (AtILR1), ILR1-LIKE 2 (AtILL2), and ILR1-LIKE 6 (AtILL6) enzymes cloned in *E. coli*, we confirmed that PAA-Glu, PAA-Leu, PAA-Trp and PAA-Val can serve as substrates for these enzymes and then release free PAA. Overall, our findings confirm that PAA undergoes metabolic processes similar to IAA.

Previous studies have extensively measured PAA levels in diverse plant species and their tissues (reviewed in Perez et al., 2023), however our understanding of PAA metabolism is largely restricted to Arabidopsis. Therefore, we conducted a comprehensive analysis of known PAA metabolites across six species spanning from Eudicots to Bryophyta. Our findings showed that PAA-AA formation is the dominant metabolic pathway in all species except spruce. Conversely, in spruce, PAA glycosylation emerges as the preferred metabolic pathway.

To further elucidate the complementarity of these two metabolic pathways, we utilised Arabidopsis knockout lines *gh3.1,2,3,4,5,6* and gh3.*1,2,3,4,5,6,9,17*, which lack the formation of amino acid conjugates depending on GH3 activity. It was hypothesised that a metabolic shift towards other conjugates would be induced after PAA treatment. This was successfully observed by blocking PAA-Asp synthesis in both lines, as there was no significant increase after PAA treatment. However, higher levels of PAA-Glu were detected in *gh3* mutant lines compared to WT Col-0. This indicates GH3-independent synthesis of PAA-AA conjugates or the potential that these mutant lines are not null expressing lines, which is consistent with findings regarding IAA conjugates (Casanova-Sáez et al., 2022). Despite the increases in PAA levels, PAA-glc concentrations remained unaltered compared to WT Col-0, suggesting no compensation in Arabidopsis. To validate this lack of complementarity in other species, we employed the selective GH3 inhibitor KKI (Fukui et al., 2022). Our results demonstrated a similar trend in spruce and Arabidopsis, with significant differences observed in PAA-AAs levels between PAA alone or PAA+KKI treatments. Interestingly, no difference in PAA-glc levels was noted.

On the other hand, KKI did not prevent PAA-Asp synthesis in *P. patens*, raising questions about species-specific differences in GH3 enzymes. Moreover, PAA-glc was not detected in the moss even after PAA treatment, suggesting the inability to synthesize this conjugate. In conclusion, our data contribute to a better understanding of PAA metabolism in plants, but also highlight the potential significance of other as-yet-undiscovered metabolic pathways.

All data are summarized in: **Hladík P.**, Brunoni F., Žukauskaitė A., Zatloukal M., Novák O., Pěnčík A. (2023) Phenylacetic acid metabolism in plants: unravelling novel pathways and metabolites by liquid chromatography-mass spectrometry analysis. (In preparation)

Method development for novel synthetic auxin derivatives

Over the past decades, numerous synthetic hormone analogues, encompassing agonists, antagonists, or fluorescently labelled compounds, have been utilized (Jiang and Asami, 2018). These analogues serve as invaluable tools for investigating auxin distribution and signalling pathways. To facilitate these studies, several novel NBD- or DNS-labelled IAA derivatives were prepared. Remarkably, DNS-labelled molecules exhibited the capacity to impede IAA signalling by downregulating the expression of early responsive auxin genes. To validate the uptake of these compounds and their stability *in planta*, an extraction protocol and an LC-MS/MS method were developed.

The chosen extraction protocol employed LLE with a solvent mixture of water:acetonitrile:hexane (1:1:1). This extraction method, previously proven to be effective for the extraction of fluorescently labelled auxin analogues (Pařízková et al., 2021), was adapted and optimized for the current study. Subsequently, an LC-MS/MS method was developed involving the optimization of LC and MS conditions for each compound. The efficacy of this method was then demonstrated by measuring the uptake of new fluorescent auxin derivatives by Arabidopsis plants after a 30-min treatment. Similarly, their stability was assessed after 1, 3 and 6 h of treatment. Overall, these studies revealed a good uptake of all compounds by Arabidopsis roots, albeit with poor stability observed over longer treatment durations, suggesting their suitability for short-term experimental applications.

All data are summarized in: Bieleszová K., **Hladík P.**, Kubala M., Napier R., Brunoni F., Gelová Z., Fiedler L., Kulich L., Strnad M., Doležal K., Novák O., Friml J., Žukauskaitė A. (2024) New fluorescent auxin derivatives: anti-auxin activity and accumulation patterns in *Arabidopsis thaliana*. Plant Growth Regul. 102, 589-602.

The structural similarity of synthetic auxin analogues poses a challenge for their separation and highlights the need for innovative analytical approaches. To address this, we employed desorption electrospray ionization coupled with ion mobility mass spectrometry imaging (DESI-IM-MSI) to visualize and separate selected isomers. Specifically, two isomers, auxinole and 4pTb-MeIAA, were administered to Arabidopsis plants, quantified using DESI-IM-MSI and LC-MS/MS techniques, and the results obtained were compared.

Therefore, we developed and optimized LLE protocols and LC-MS/MS methods for both compounds. Subsequently, administered to Arabidopsis plants were treated with auxinole and 4pTb-MeIAA, and their levels were measured using LC-MS/MS or DESI-MSI with or without ion mobility separation. Additionally, IAA metabolic profiles were also analysed using these MS-based techniques, with quantification performed either pmol/g FW or by calculating the area under the curve for the chromatographic peaks of each analyte. These quantitative data were then compared across all three MS methods. Ultimately, DESI-IM-MSI emerged as a promising technique for isomer separation that offers high spatial resolution imaging of low-molecular-weight compounds from tissues such as Arabidopsis roots.

All data are summarized in: Zhang C., Bieleszová K., Žukauskaitė A., **Hladík P.**, Grúz J., Novák O., Doležal K. (2024) In situ separation and visualization of isomeric auxin derivatives in Arabidopsis by ion mobility mass spectrometry imaging. Anal Bioanal Chem. 416(1), 125-139.

5 Conclusion and future perspectives

This doctoral thesis aims to broaden our understanding of auxin metabolism in various plant species and their organs. Through the application of LC-MS/MS methods, several novel conjugates of two auxins, IAA and PAA, together with their metabolic pathways, were identified. Additionally, the development of extraction and detection methods for newly synthesized synthetic auxins with anti-auxin activity enabled the measurement of their uptake and stability *in planta*.

The key results obtained in this thesis include the following:

- Utilizing the LC-MS/MS detection methods, novel oxIAA and PAA amino acid conjugates were identified for the first time *in planta*.
- Analysis of auxin metabolic profiles in organs of various plant species at different growth stages facilitated the elucidation of dominant metabolic pathways during seedlings development.
- The enzymes responsible for PAA conjugation with amino acids and glucose *in planta* have been characterised. Moreover, the interrelationship of these metabolic pathways was explored in Arabidopsis, spruce and moss, indicating the potential existence of additional unexplored pathways.
- New extraction and LC-MS/MS methods were developed for NBD- and DNS-labelled auxins with anti-auxins activity and employed to measure their stability and uptake by Arabidopsis roots.
- A new DESI-IM-MSI method was developed for *in situ* imaging of two synthetic auxin isomers, auxinole and 4pTb-MeIAA. Quantitative results were then compared with a conventional LC-MS/MS approach, highlighting the potential of high spatial resolution imaging of low-molecular-weight compounds by the DESI-IM-MSI.

In summary, the results presented in this thesis should help to understand auxin homeostasis in plants as well as their organs and cells. In the future, follow-up experiments could explore whether these novel metabolites and biosynthetic pathways play roles in plant responses to environmental stimuli, such as biotic or abiotic stresses. Additionally, considering the insights gained from measuring PAA metabolism complementarity, further screening for additional PAA conjugates should be performed.

6 References

Aoi Y., Hira H., Hayakawa Y., Liu H., Fukui K., Dai X., Tanaka K., Hayashi K., Zhao Y., Kasahara H. (2020) UDP-glucosyltransferase UGT84B1 regulates the levels of indole-3-acetic acid and phenylacetic acid in Arabidopsis. *Biochem Bioph Res Co*. **532**(2), 244–250.

Bartel B., Fink G. R. (1995) ILR1, an amidohydrolase that releases active indole-3-acetic acid from conjugates. *Science*. **268**(5218), 1745–1748.

Boyes D. C., Zayed A. M., Ascenzi R., McCaskill A. J., Hoffman N. E., Davis K. R., Görlach J. (2001) Growth stage-based phenotypic analysis of Arabidopsis: a model for high throughput functional genomics in plants. *Plant Cell*. **13**(7), 1499–1510.

Casanova-Sáez R., Mateo-Bonmatí E., Šimura J., Pěnčík A., Novák O., Staswick P., Ljung K. (2022) Inactivation of the entire Arabidopsis group II GH3s confers tolerance to salinity and water deficit. *New Phytol*. **235**, 263–275.

Fukui K., Arai K., Tanaka Y., Aoi Y., Kukshal V., Jez J. M., Kubeš M. F., Napier R., Zhao Y., Kasahara H., Hayashi K. (2022) Chemical inhibition of the auxin inactivation pathway uncovers the roles of metabolic turnover in auxin homeostasis. *P Natl Acad Sci USA*. **119**, e2206869119.

Hayashi K., Neve J., Hirose M., Kuboki A., Shimada Y., Kepinski S., Nozaki H. (2012) Rational Design of an Auxin Antagonist of the SCFTIR1 Auxin Receptor Complex. *ACS Chem Biol*. **7**(3), 590–598.

Hayashi K., Arai K., Aoi Y., Tanaka Y., Hira H., Guo R., Hu Y., Ge C., Zhao Y., Kasahara H., Fukui K. (2021) The main oxidative inactivation pathway of the plant hormone auxin. *Nat Commun*. **12**(1), 6752.

Hladík P. (2020) Studium nových metabolických drah auxinů v rostlinách. Master thesis. University of Palacký in Olomouc, Faculty of Science. Available from: https://theses.cz/id/a44ieq/.

Isobe T., Miyagawa H. (2022) Facilitation of auxin biosynthesis and metabolism by salt stress in rice plants. *Biosci Biotech Bioch*. **86**(7), 824–831.

Jiang K, Asami T. (2018) Chemical regulators of plant hormones and their applications in basic research and agriculture. *Biosci Biotech Bioch*. **82**(8), 1265–1300.

Kowalczyk M., Sandberg G. (2001) Quantitative analysis of indole-3-acetic acid metabolites in Arabidopsis. *Plant Physiol*. **127**(4), 1845–1853.

Lancashire P. D., Bleiholder H., Boom P. V. D., Langeluddeke P., Stauss R., Weber E., Witzenberger A. (1991) A uniform decimal code for growth stages of crops and weeds. *Ann Appl Biol*. **11**, 561–601.

Mateo-Bonmatí E., Casanova-Sáez R., Šimura J., Ljung K. (2021) Broadening the roles of UDP-glycosyltransferases in auxin homeostasis and plant development. *New Phytol*. **232**(2), 642–654.

Müller K., Dobrev P. I., Pěnčík A., Hošek P., Vondráková Z., Filepová R., Malínská K., Brunoni F., Helusová L., Moravec T., Retzer K., Harant K., Novák O., Hoyerová K., Petrášek J. (2021) DIOXYGENASE FOR AUXIN OXIDATION 1 catalyzes the oxidation of IAA amino acid conjugates. *Plant Physiol*. **187**(1), 103–115.

Pařízková B., Žukauskaitė A., Vain T., Grones P., Raggi S., Kubeš M. F., Kieffer M., Doyle S. M., Strnad M., Kepinski S., Napier R., Doležal K., Robert S., Novák O. (2021) New fluorescent auxin probes visualise tissue-specific and subcellular distributions of auxin in Arabidopsis. *New Phytol*. **230**(2), 535–549.

Pěnčík A., Rolčík J., Novák O., Magnus V., Barták P., Buchtík R., Salopek-Sondi B., Strnad M. (2009) Isolation of novel indole-3-acetic acid conjugates by immunoaffinity extraction. *Talanta*. **80**(2), 651–655.

Pěnčík A., Casanova-Sáez R., Pilarová V., Žukauskaite A., Pinto R., Micol J. L., Ljung K., Novák O. (2018) Ultra-rapid auxin metabolite profiling for high-throughput mutant screening in Arabidopsis. *J Exp Bot*. **69**, 2569–2579.

Perez V. C., Zhao H., Lin M., Kim J. (2023) Occurrence, Function, and Biosynthesis of the Natural Auxin Phenylacetic Acid (PAA) in Plants. *Plants (Basel)*. **12**(2), 266.

Porco S., Pěnčík A., Rashed A., Voß U., Casanova-Sáez R., Bishopp A., Golebiowska A., Bhosale R., Swarup R., Swarup K., Peňáková P., Novák O., Staswick P., Hedden P., Phillips A. L., Vissenberg K., Bennett M. J., Ljung K. (2016) Dioxygenase-encoding AtDAO1 gene controls IAA oxidation and homeostasis in Arabidopsis. *P Natl Acad Sci USA*. **113**(39), 11016–11021.

Staswick P., Rowe M., Spalding E. P., Splitt B. L. (2017) Jasmonoyl-L-Tryptophan Disrupts IAA Activity through the AUX1 Auxin Permease. *Front Plant Sci*. **8**, 736.

Sugawara S., Mashiguchi K., Tanaka K., Hishiyama S., Sakai T., Hanada K., Kinoshita-Tsujimura K., Yu H., Dai X., Takebayashi Y., Takeda-Kamiya N., Kakimoto T., Kawaide H., Natsume M., Estelle M., Zhao Y., Hayashi K., Kamiya Y., Kasahara H. (2015) Distinct Characteristics of Indole-3-Acetic Acid and Phenylacetic Acid, Two Common Auxins in Plants. *Plant Cell Physiol*. **56**(8), 1641–1654.

Tottman D. R. (1987) The decimal code for the growth stages of cereals, with illustrations. *Ann Appl Biol*. **110**, 441–454.

Westfall C. S., Sherp A. M., Zubieta C., Alvarez S., Schraft E., Marcellin R., Ramirez L., Jez, J. M. (2017) Arabidopsis thaliana GH3.5 acyl acid amido synthetase mediates metabolic crosstalk in auxin and salicylic acid homeostasis. *P Natl Acad Sci USA*. **113**(48), 13917–13922.

7 List of author's publications

Papers published in scientific journals:

Hladík P., Petřík I., Žukauskaitė A., Novák O., Pěnčík A. (2023) Metabolic profiles of 2-oxindole-3-acetyl-amino acid conjugates differ in various plant species. *Front. Plant Sci.* 14, 1217421.

Bieleszová K., **Hladík P.**, Kubala M., Napier R., Brunoni F., Gelová Z., Fiedler L., Kulich L., Strnad M., Doležal K., Novák O., Friml J., Žukauskaitė A. (2024) New fluorescent auxin derivatives: anti-auxin activity and accumulation patterns in *Arabidopsis thaliana*. *Plant Growth Regul.* 102, 589-602.

Zhang C., Bieleszová K., Žukauskaitė A., **Hladík P.**, Grúz J., Novák O., Doležal K. (2024) In situ separation and visualization of isomeric auxin derivatives in Arabidopsis by ion mobility mass spectrometry imaging. *Anal Bioanal Chem*. 416(1), 125-139.

Karady M., **Hladík P.**, Cermanová K., Jiroutová P., Antoniadi I., Casanova-Sáez R., Ljung K., Novák O. (2024) Profiling of 1-aminocyclopropane-1-carboxylic acid and selected phytohormones in Arabidopsis using liquid chromatography-tandem mass spectrometry. *Plant Methods* 20(1), 41.

Papers in preparation:

Hladík P., Brunoni F., Žukauskaitė A., Zatloukal M., Novák O., Pěnčík A. (2024) Phenylacetic acid metabolism in plants: unravelling novel pathways and metabolites by liquid chromatography-mass spectrometry analysis. (In preparation)

Petřík I., **Hladík P.**, Zhang C., Pěnčík A., Novák O. (2024) Spatio-temporal plant hormonomics: From tissue to subcellular resolution. *J. Exp. Bot.* (under review)

Published abstracts:

Hladík P., Pěnčík A., Žukauskaitė A., Zatloukal M., Novák O. Quantitative analysis of IAA, oxIAA and PAA amino acids conjugates in various plant species. *21. škola hmotnostní spektrometrie*, Srní, Czech Republic, 2020, poster presentation.

Hladík P., Pěnčík A., Novák O., Žukauskaitė A. Characterisation of newly discovered indole compounds in various plant species. *22. škola hmotnostní spektrometrie*, Srní, Czech Republic, 2021, poster presentation.

Hladík P., Pěnčík A., Žukauskaitė A., Zatloukal M., Novák O. Quantitative analysis of IAA and PAA conjugates in various plant species. *Chemistry and biology of phytohormones and related substances 2021 (CBPRS)*, Malenovice, Czech Republic, 2020, oral presentation.

Hladík P., Pěnčík A., Petřík I., Žukauskaitė A., Zatloukal M., Novák O. Quantitative analysis of IAA and PAA conjugates in various plant species. *Chemistry and biology of phytohormones and related substances 2022 (CBPRS)*, Bystřice nad Pernštejnem, Czech Republic, 2022, oral presentation.

Hladík P., Petřík I., Novák O., Žukauskaitė A., Pěnčík A. Characterisation of newly discovered indole compounds in various plant species. *Advances in Chromatography and Electrophoresis & Chiranal 2022*, Olomouc, Czech Republic, 2022, poster presentation.

Hladík P., Petřík I., Novák O., Žukauskaitė A., Pěnčík A. Characterisation of newly discovered indole compounds in various plant species. *23. škola hmotnostní spektrometrie*, Milovy, Czech Republic, 2022, poster presentation.

Hladík P., Pěnčík A., Zatloukal M., Novák O. Quantitative analysis of PAA amino acid conjugates in various plant species. *6th international conference on auxin research – Auxin 2022*, Cavtat, Croatia, 2022, poster presentation.

Hladík P., Pěnčík A., Petřík I., Žukauskaitė A., Zatloukal M., Brunoni F., Novák O. Metabolic profiles of auxin conjugates differ in various plant species. *Chemistry and biology of phytohormones and related substances 2023 (CBPRS)*, Velké Losiny, Czech Republic, 2023, oral presentation.

Hladík P., Pěnčík A., Žukauskaitė A., Zatloukal M., Novák O. Quantitative analysis of phenylacetic acid conjugates in various plant species. *Auxins and Cytokinins in Plant Development (ACPD 2023)*, Prague, Czech Republic, 2023, poster presentation.

Hladík P., Žukauskaitė A., Zatloukal M., Novák O., Pěnčík A. Metabolic profiles of phenylacetic acid conjugates differ in various plant species. *17th Student Days of Plant Biology CS 2023*, Srní, Czech Republic, 2023, oral presentation.

8 Souhrn (Summary in Czech)

Název disertační práce:

Studium metabolismu auxinů na orgánové úrovni

V posledních letech bylo učiněno velké množství objevů objasňujících metabolismus auxinů, které rozšířili informace o jejich konjugátech a katalyzujících enzymech. Nicméně většina tohoto výzkumu je spojena pouze s jedním auxinem – IAA a *Arabidopsis thaliana* jako modelovou rostlinou. Proto se tato dizertační práce zaměřuje na metabolismus dvou endogenních auxinů (IAA a PAA) napříč vyššími rostlinami a jejich orgány.

Pomocí LC-MS/MS metody byly v rostlinách poprvé identifikovány nové konjugáty oxIAA a PAA (oxIAA-Leu, oxIAA-Phe, PAA-Leu, PAA-Phe, PAA-Val a PAA-glc), a následně bylo provedeno metabolické profilování těchto dvou auxinů v orgánech několika druhů rostlin od krytosemenných (*Magnoliophyta*) po mechy (*Briopsida*), a to v několika vývojových stádiích. Toto měření ukázalo dominantní metabolické dráhy během raného vývoje a prokázalo, že hladiny IAA konjugátů jsou silně závislé na vývojovém stádiu.

Během výzkumu PAA metabolismu byly charakterizovány enzymy zodpovědné za konjugaci PAA s aminokyselinami a glukózou. Stejně jako u IAA, jsou za katalýzu syntézy PAA-AA zodpovědné enzymy z rodiny GH3, a tyto konjugáty jsou poté zpětně hydrolyzovatelné na aktivní PAA pomocí enzymů AtIAR3, AtILL2, AtILL6 a AtILR1. Přestože syntéza PAA-glc byla již prokázána *in vitro* (Aoi et al., 2020), naše výsledky poprvé ukázaly její přítomnost v rostlinách. Bakteriální enzymatické testy a studium hladiny PAA-glc v mutantních liniích Arabidopsis poukázali na její syntézu pomocí enzymů UGT84B1 a UGT74D1, které jsou také zodpovědné za glykosylaci IAA a oxIAA. Při měření komplementarity těchto dvou metabolických drah bylo zjištěno, že při blokování jedné z nich nedochází ke kompenzaci druhou, což naznačuje potencionální existenci dalších neprozkoumaných drah.

Další částí této práce byl vývoj extrakčních a detekčních metod pro nově syntetizované fluorescenčně značené auxiny s anti-auxinovou aktivitou, které umožnily měření jejich příjmu kořenem a stability v rostlině. Tyto extrakční a LC-MS/MS metody byly také vyvinuty pro isomery auxinů (auxinole a 4pTb-MeIAA) a použity pro měření jejich koncentrace v rostlinách po ošetření těmito látkami. Tyto tradiční metody byly poté porovnány s DESI-IM-MSI měřením a prokázaly potenciál tohoto nového přístupu pro měření nízkomolekulárních látek ve vysokém prostorovém rozlišení.

V souhrnu by tyto výsledky měly vést k lepšímu porozumění homeostáze auxinu ve vyšších rostlinách a jejich orgánech. V budoucnu by mohly být provedeny experimenty, které by určily, zda tyto nové metabolity a dráhy hrají roli v reakcích rostlin na environmentální podněty, včetně biotického nebo abiotického stresu. Dále, jak naznačují výsledky získané měřením komplementarity metabolismu PAA, by měl být proveden screening potenciálních nových konjugátů.